Bruno André Cunha de Vallêra Jacques Pedras

SYNTHESIS, CHARACTERIZATION AND APPLICATIONS OF NEW SCHIFF BASE FLUORESCENT CHEMOSENSORS FOR METAL AND DNA INTERACTIONS: CONVENTIONAL AND "GREEN" APPROACHES

Lisboa

2011

- nº de arquivo

- “copyright”

UNIVERSIDADE NOVA DE LISBOA

Faculdade de Ciências e Tecnologia

SYNTHESIS, CHARACTERIZATION AND APPLICATIONS OF NEW SCHIFF BASE FLUORESCENT CHEMOSENSORS FOR METAL AND DNA INTERACTIONS: CONVENTIONAL AND "GREEN" APPROACHES

BRUNO ANDRÉ CUNHA DE VALLÊRA J. PEDRAS

Dissertação apresentada para a obtenção do Grau de Doutor em Química Sustentável, especialidade de Química-Física Inorgânica, pela Universidade Nova de Lisboa, Faculdade de Ciências e Tecnologia

Supervisor: Prof. Dr. Carlos Lodeiro Espiño

Co-supervisores: Prof. Dr. Teresa Avilés e Prof. Dr. José Luís Capelo

LISBOA

2011

“What we don’t understand, we explain to each other”

J. Robert Oppenheimer

“Se podes olhar, vê. Se podes ver, repara”

José Saramago

Dedicado aos meus pais.

Agradecimentos

Começo por agradecer ao meu orientador principal, o Professor Doutor Carlos Lodeiro Espiño. Foi ele a pessoa que apostou em mim desde o princípio e me motivou para o mundo dos sensores e da fluorescência; transmitindo-me os seus conhecimentos, contribuiu para o meu processo de formação científica e pessoal, sempre tendo em mente que um Doutor não deve ser um especialista numa só área, mas sim um cientista polivalente e com condições de encarar qualquer desafio no futuro. Soube compreender a minha forma de trabalhar, não deixando de me chamar a atenção para os meus erros, mas sempre de uma forma construtiva e apoiando-me nos momentos menos bons. Por tudo isto, o meu enorme obrigado!

Simultaneamente, quero agradecer aos meus co-orientadores. À Professora Doutora Teresa Avilés Perea, pela forma como me recebeu e me tratou ao longo destes anos, proporcionando-me as melhores condições para desenvolver o meu trabalho e pelos seus muitos e bons conselhos durante a síntese de grande parte dos compostos desta tese. Ao Professor Doutor José Luís Capelo, pelo seu espírito sempre optimista e motivador em todas as etapas desta tese e por tudo o que me transmitiu na área da Química Analítica.

À Fundação para a Ciência e a Tecnologia, agradeço o financiamento através da bolsa de doutoramento SFRH/BD/27786/2006.

Aos membros do BIOSCOPE (Lisboa) e restantes companheiros de laboratório, nomeadamente Elisabete, Vítor, Tiago, Carla, Marco, Hugo, Gonçalo, Ricardo, Mário e Luz. A los miembros del BIOSCOPE (Ourense) y demás compañeros de la Facultad de Ciencias de Ourense, que han hecho que mi estancia allí fuese inolvidable: Cristina, Javier, Jorge, Júlio, Profesor Juan Carlos Mejuto, Gonzalo, Óscar, Iago, Serxio, Antonio, Marta, Rosi y Vittorio.

Ao Grupo de Fotoquímica, representado na pessoa do Professor Doutor Fernando Pina, pela forma como me acolheu durante períodos importantes do meu doutoramento. Um agradecimento especial ao Professor Doutor Jorge Parola, pela preciosa ajuda nas sínteses em micro-ondas, ao Professor Doutor João Carlos Lima, pela sua constante disponibilidade para esclarecimento de dúvidas pontuais e excelente disposição para abordar os mais variados temas (lembrando que a vida não é só ciência!) e ao Doutor César Laia pela amizade e interessantes discussões científicas (e musicais, entre outras!).

Quiero agradecer al Profesor Dr. Guillermo Orellana Moraleda, por darme la oportunidad de trabajar en el GSOLFA, y por su valiosa colaboración en mi trabajo. A todos los miembros del Grupo, en particular a la Dra. Laura Tormo por su apoyo en los estudios con DNA, y a todos los que hicieron que mi primera estancia en un país extranjero fuera una de las experiencias más apasionantes de mi vida: David, Aurélien, Pilar, Ruymán, Sofia, Niko, Clara, Juan, y porque hay amistades que se quedan para siempre, Paco, Kássio, André e Irene. Muchas gracias a todos!

Aos meu grandes amigos Filipe Folgosa e Filipe Agapito, pelos pilares que têm sido ao longo dos anos, com as suas enormes amizade e generosidade e pelo apoio incondicional no dia-a-dia. Sem o primeiro, esta “aventura” não teria sequer começado, e sem o último esta nunca teria chegado a bom porto.

Agradeço à Cris todo o apoio que me deu durante os primeiros anos.

Ao Bruno Rosíndio, agradeço os mais de 20 anos de amizade.

A Manoli, te agradezco todo lo que eres y lo que significas en mi vida. Sin ti nada de esto tendría la mitad del sentido. Gracias por tu comprensión, sobre todo durante este período largo de escrita, y por tu amor incondicional!

Por último, o agradecimento mais especial: aos meus pais, Nelma e Manuel José, e à minha irmã Daniela. Sem eles nada teria sido alcançado e foi graças ao seu apoio ilimitado e à Família que somos que este trabalho se concluiu com êxito. Obrigado por tudo, desde sempre!

Abstract

The work presented in this thesis, which has as its central subject the synthesis and applications of new fluorescent chemosensors and probes, can be divided in two major groups. The first one deals with Schiff base-derived fluorescent chemosensors, with application in the detection of metal cations, and the second group concerns the development of new Ru(II) polypyridyl luminescent molecular probes for DNA.

Before the description and discussion of the performed work, a general introduction is presented in **Chapter I**, where emphasis is put on the applications of molecular fluorescence to chemical sensing, in order to obtain a better understanding of the photophysical processes that underlie molecular recognition. This connection is made by defining concepts and giving examples when necessary. A brief mention to the studied analytes and the instrumental methods used both in developing the chemosensors and in their applications is also made.

In **Chapter II**, two new chemosensors possessing crown ether moieties linked through a Schiff base to a bithiophene group are presented. These systems were synthesized and fully characterized, and their application in the sensing of Ni(II), Pd(II), Hg(II) and Na(I) was tested by absorption and emission spectroscopies, and MALDI-TOF MS.

Chapter III describes two new pincer-type ligands, in which a thiophene unit is linked through a Schiff base either to pyrene or naphthalene chromophores. Sensing applications for Ni(II) and Pd(II) were investigated by different techniques, and solid complexes with the aforementioned metals were also synthesized.

A new tripodal ligand derived from indole and containing three Schiff base groups is introduced in **Chapter IV**, and its complexes with Zn(II), Cu(II), Ni(II), Hg(II) and Pd(II) are also described. Metal ion titrations of the free ligand with the respective metal salts have been performed, helped by DFT calculations, in order to investigate the role of the central tertiary amine in metal coordination.

The search for new luminescent molecular probes to be used in DNA binding is the subject of **Chapter V**, in which a new family of six Ru(II) polypyridyl complexes is synthesized. The relation between their structure and the binding mode to DNA is studied by absorption and steady-state emission spectroscopies, as well as by time-resolved experiments.

Chapter VI returns to cation sensing, but it is included in the end of the thesis because this work is still in progress. It reports the synthesis of three new quinoline-derived chemosensors for Zn(II) and Cu(II), and a dinuclear Zn(II) complex with potential application as water sensor by fluorescence quenching. With this last compound, only preliminary studies have been performed.

The general conclusions of this work are collected in **Chapter VII**.

It is noteworthy that sustainable synthetic methodologies were employed throughout this thesis in parallel with conventional techniques, namely microwave and ultrasound-assisted synthesis (inorganic and organic).

Resumo

O trabalho apresentado nesta tese, que tem como tema principal a síntese e aplicações de novos quimiossensores e sondas fluorescentes, pode dividir-se em dois grupos principais. O primeiro diz respeito a quimiossensores fluorescentes derivados de bases de Schiff, com aplicação na detecção de catiões metálicos, e o segundo grupo trata do desenvolvimento de novos complexos de Ru(II) polipiridilo como sondas moleculares luminescentes para ADN.

Antes da descrição e discussão do trabalho efectuado, é apresentada uma introdução geral no **Capítulo I**, onde se dá ênfase às aplicações da fluorescência molecular em química de sensores, de modo a obter um melhor conhecimento dos processos fotofísicos subjacentes ao reconhecimento molecular. Esta ligação é feita definindo conceitos e exemplificando sempre que necessário. Faz-se também uma breve menção aos analitos estudados e aos métodos instrumentais utilizados, quer no desenvolvimento dos quimiossensores, quer na sua aplicação.

No **Capítulo II** são apresentados dois novos quimiossensores dotados de unidades éter-coroa ligadas através de uma base de Schiff a um grupo bitiofeno. Estes sistemas foram sintetizados e completamente caracterizados, e a sua aplicação na detecção de Ni(II), Pd(II), Hg(II) e Na(I) foi testada por espectroscopias de absorção e emissão, e MALDI-TOF MS.

O **Capítulo III** descreve dois novos ligandos do tipo pinça, nos quais uma unidade de tiofeno está ligada através de uma base de Schiff a cromóforos pireno ou naftaleno. Aplicações como sensores de Ni(II) e Pd(II) foram investigadas por diferentes técnicas, e foram também sintetizados complexos sólidos com os metais supracitados.

Um novo ligando tripodal derivado de indol e contendo três grupos base de Schiff é introduzido no **Capítulo IV**, e os seus complexos com Zn(II), Cu(II), Ni(II), Hg(II) e Pd(II) são também descritos. Foram ainda realizadas titulações do ligando livre com os respectivos sais metálicos, e com a ajuda de cálculos DFT, investigou-se o papel da amina terciária central na coordenação de metais.

A procura de novas sondas moleculares luminescentes para aplicações em estudos de união ao ADN é o tema do **Capítulo V**, onde uma família de seis complexos de Ru(II) polipiridilo é sintetizada. A relação entre a sua estrutura e o modo de união ao ADN foi estudada por espectroscopias de absorção e de emissão em estado-estacionário, bem como por experiências com resolução temporal.

O **Capítulo VI** aborda novamente o tema dos sensores de catiões, mas vem incluído no final da tese pois este trabalho ainda se encontra em fase de realização. É descrita a síntese de três novos quimiossensores para Zn(II) e Cu(II) derivados de quinolina, bem como um complexo dinuclear de Zn(II) com potencial aplicação como sensor de água através da supressão de fluorescência. Com este último, apenas foram realizados estudos preliminares.

As conclusões gerais deste trabalho são apresentadas no **Capítulo VII**.

É de salientar que ao longo desta tese foram utilizadas metodologias sustentáveis de síntese, em paralelo com técnicas convencionais, nomeadamente síntese assistida por micro-ondas e ultra-sons (inorgânica e orgânica).

List of Symbols and Abbreviations

A	Absorbance
	Acceptor
a.u.	Arbitrary units
bpy	2,2'-Bipyridine
CHEF	Chelation Enhancement of Fluorescence
CHEQ	Chelation Enhancement of Quenching
CT	Calf thymus
	Charge transfer
d	Doublet
D	Donor
DMF	Dimethylformamide
DMSO	Dimethyl sulfoxide
DNA	Deoxyribonucleic acid
dppz	Dipyrido[3,2-a:2',3'-c]phenazine
ds	double-stranded
δ	Chemical shift
ETBr	Ethidium bromide
EI	Electronic impact
ESI	Electrospray ionization
ESIPT	Excited-State Intramolecular Proton Transfer
ε	Molar absorption coefficient
Φ_F	Fluorescence Quantum Yield
FRET	Förster Resonance Energy Transfer
HOMO	Highest Occupied Molecular Orbital
^{1}H-NMR	Proton Nuclear Magnetic Resonance
Hz	Hertz
I	Intensity of emission
IR	Infrared
IUPAC	International Union of Pure and Applied Chemistry
K_b	Intrinsic DNA binding constant
k_q	Quenching rate constant
K_{SV}	Stern-Volmer constant
LC	Ligand Centered

LMCT	Ligand to Metal Charge Transfer
LUMO	Lowest Unoccupied Molecular Orbital
λ	Wavelength
λ_{em}	Emission wavelength
λ_{exc}	Excitation wavelength
λ_{max}	Wavelength of maximum emission or absorption
m	Multiplet
MALDI-TOF	Matrix Assisted Laser Desorption/Ionization Time of Flight
MC	Metal Centered
MS	Mass Spectrometry
MV^{2+}	Methyl Viologen
MLCT	Metal to Ligand Charge Transfer
m/z	Mass-to-charge ratio
OS	Oscillator strengths
PET	Photoinduced Electron Transfer
PCT	Photoinduced Charge Transfer
PPT	Photoinduced Proton Transfer
phen	1,10-Phenanthroline
RNA	Ribonucleic acid
s	Singlet
SPT	Single-photon timing
t	Triplet
TD-DFT	Time-Dependent Density Functional Theory
THF	Tetrahydrofuran
τ	Emission lifetime
τ_m	Pre-exponential weighted emission lifetime
TREN	Tris(2-aminoethyl)amine
TRIS	Tris(hydroxymethyl)aminomethane
UV-Vis	Ultraviolet-Visible

General Index

Index of Figures

Index of Schemes

Index of Tables

Chapter I

Introduction

In this chapter are presented and explained some definitions and concepts that serve as a complement for the introductions of the remaining chapters. Throughout this thesis, molecular fluorescence is used as a tool for chemical sensing; as a consequence, the approach for this chapter is to make a bridge between photophysics and its applications in sensing, instead of an exhaustive and detailed description of the basic principles of photophysics and photochemistry.

I.1 Concept of chemosensor.

The desire and need to monitor everything that surrounds us have led to a growing effort of developing something that can receive information and turn it into a form which is compatible with our perception, knowledge and understanding. This would be the simplest and most common definition of what a sensor, in general, might be. Sensors are not only man-made; our body, for example, is provided with a vast number of sensors that respond to *stimuli* such as light, heat, odor, etc. Unfortunately, these intrinsic sensors are not sufficiently capable of providing us with objective knowledge about what happens inside and outside of our body and what benefits or threats us as individuals, or the society as a whole. Being able to tell the difference between useful and harmful compounds, or to monitor the environment by searching for heavy metal pollutants in waters or the presence of bacteria in drinking water, are achievements only accomplishable with the help of man-made sensors.

Among the great variety of sensors synthesized by man, there are those which allow us to detect chemical species. This particular type is called a chemical sensor, and is defined by IUPAC as “a device that transforms chemical information, ranging from the concentration of a specific sample component to total composition analysis, into an analytically useful signal”.[1] This device can be either macroscopic (e.g. a pH measuring electrode) or microscopic, which leads us to the next definition. In a strict sense, a chemosensor is a molecule (or an assembled supra-molecular unit) that can selectively bind the target analyte and furnish information about this binding, and thus act as a microscopic chemical sensor.

Due to the two different processes that take place in chemical sensing through analyte detection, i.e. molecular recognition and signal transduction, there are usually three parts that constitute a chemosensor (Figure I.1): a receptor (which is responsible for the selective analyte binding), an active unit (whose properties should change upon the aforementioned binding) and, in some cases, a spacer that is able

to modify the geometry of the system and tune the electronic interaction between the two other components.[2]

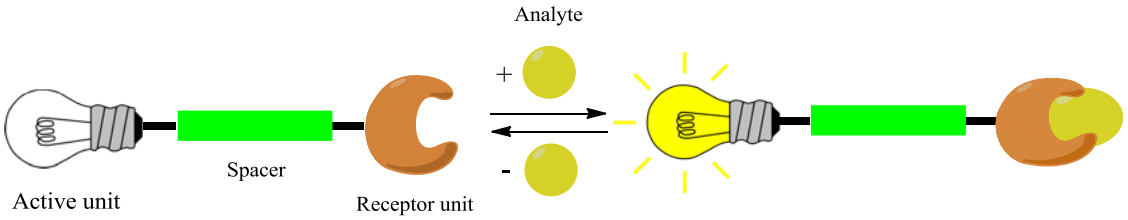

Figure I.1 – Schematic representation of a chemosensor.

Chemosensors can be classified according to the nature of the signal emitted by the active unit. They can be, for example, electrochemical, optical or calorimetric. In optical sensors, a spectroscopic measurement is associated with the recognition process, e.g. absorbance, reflectance or luminescence measurements.

I.2 Fluorescent chemosensors. Advantages and general classification.

One of the most commonly used types of chemosensors is fluorescent chemosensors.[3,4,5,6,7] The success of this group of sensors may be explained by the several characteristics that distinguish fluorescence from all other methods used in chemical sensing.[8,9,10] Firstly, there is its ultra-high sensitivity, which is particularly required whenever the analyte to be studied is present in trace amounts. By choosing the appropriate dye and experimental conditions, sensitivity may even reach the limit of single molecules. High response time is the second important feature of fluorescence, which can be as fast as 10^{-8}–10^{-10} s and is limited by fluorescence lifetime and the speed of the photophysical event that furnishes the response. Also noteworthy are the very high spatial resolution that can be achieved with fluorescence (e.g. in detecting cellular images), and the non-destructive and non-invasive character of fluorescence sensing (which allows biological and medical applications). Finally, the most important advantage of fluorescence sensing is its versatility, which allows its accomplishment in solid, liquid and gaseous media.

Recalling the general representation of a chemosensor given in Section I.1, the active unit in the case of fluorescent chemosensors is called a fluorophore, and it is responsible for converting the information (presence of an analyte) into an optical signal which is then expressed through changes in the photophysical properties of the fluorophores.

Three types of fluorescent chemosensors[8] can be distinguished (Figure I.2):

- Type 1: fluorophores that experience fluorescence quenching motivated by collision with an analyte (e.g. O_2).

- Type 2: fluorophores able to bind the analyte in a reversible manner. In the case of the analyte being a proton, the term “fluorescent pH indicator” is employed. If it is an ion, the term “fluorescent chelating agent” is normally used. Two processes can occur upon analyte binding: Chelation Enhancement of Quenching (CHEQ), which means that the fluorescence emission is quenched, and Chelation Enhancement of Fluorescence (CHEF), where an increase in the emission intensity is observed. These compounds, in which the fluorophore is simultaneously responsible for binding and signaling, are usually called fluorogenic (in the case of CHEF).

- Type 3: fluorophores connected, with or without spacer, to a receptor unit. The bound analyte causes perturbations of photoinduced processes like electron transfer, charge transfer, energy transfer, excimer or exciplex formation or disappearance, etc. (see section I.3), which bring about changes in the photophysical properties of the fluorophore. When the analyte is an ion, the receptor is called an ionophore, and the whole chemosensor is called a fluoroionophore. Also in this case, CHEQ and CHEF effects can be observed.

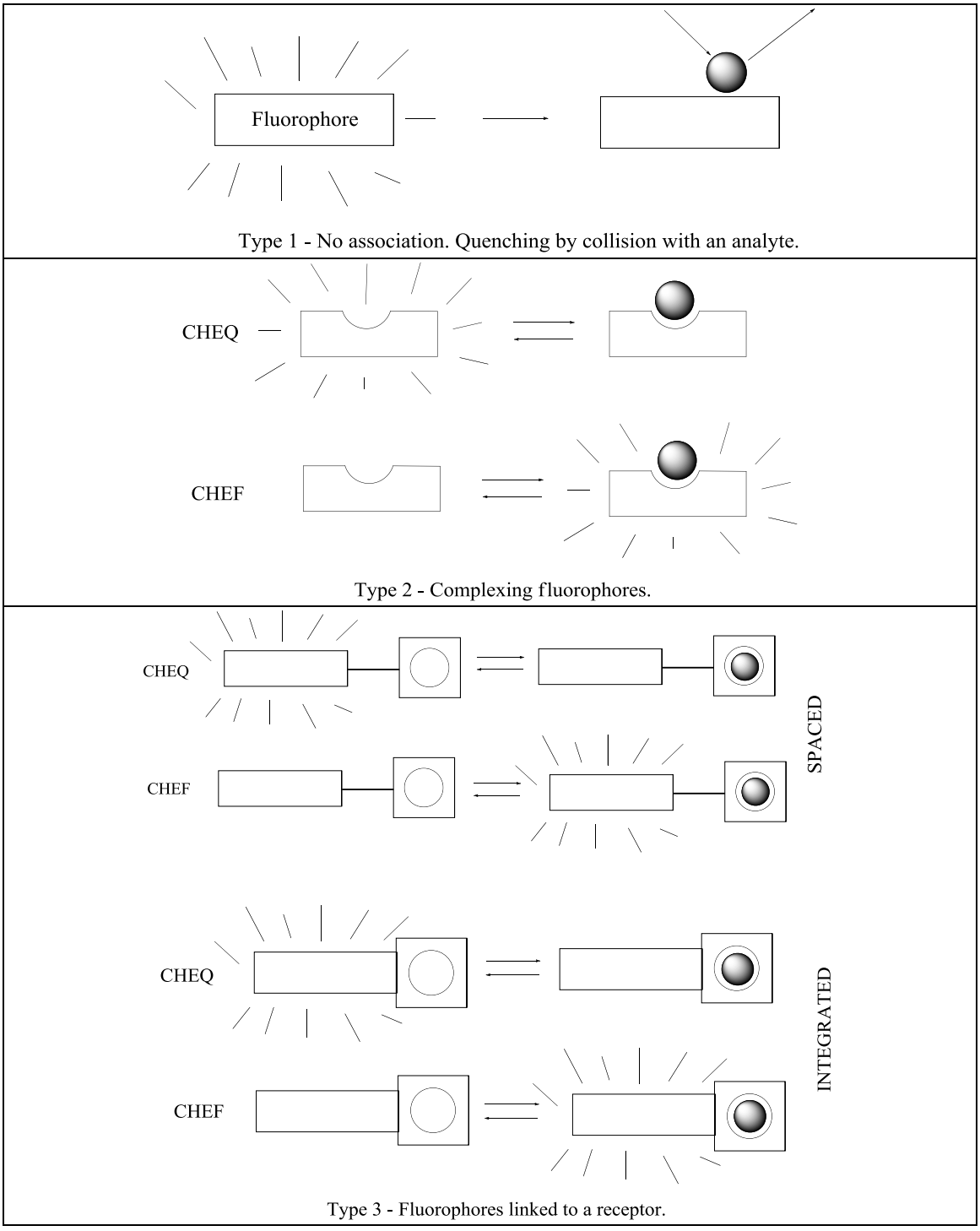

Figure I.2 – Main types of fluorescent molecular sensors of ions or molecules.

I.3 Mechanisms of transduction: PET, ESIPT, ET, excimer and exciplex formation, PCT.

Fluorescence emission takes place from the electronic excited states of molecules. However, given the high reactivity of the electrons in these states,

reactions that usually do not occur in the ground states are able to take place. From the point of view of chemical sensing, some of these reactions are found to be interesting, since they enable a one-step deactivation of the excited state (quenching) and, sometimes, formation of new emission bands corresponding to the products of these reactions. Upon analyte binding to chemosensors, it is possible to modulate some of these reactions (since they depend on the interaction of reaction sites with enhancers or quenchers of their emission), and thus take advantage of the different mechanisms for signal transduction.

I.3.1 Photoinduced electron transfer (PET).

Absorption of light changes dramatically the redox properties of molecules. As an electron is promoted to a higher energy level, the molecule becomes simultaneously a better electron donor (reducing agent) and a better electron acceptor (oxidizing agent) than it was in its ground state.[11] Photoinduced electron transfer (PET) is the process by which an electron is transferred between an excited-state species and a ground-state species. The direction of electron transfer is determined by the oxidation and reduction potential of the ground and excited states, which means that the excited fluorophore can be either the electron donor or the acceptor. This process requires closeness in space of the two species and the matching of their redox potentials. Thus, the distances for this process are much shorter than for FRET (see section I.3.3), since it needs the overlapping of electronic wave functions of both species. Covalent bonding between donor and acceptor via a short spacer can make the process easier to occur.

This process finds vast application in the design of pH indicators and cation sensors. Since the former are out of the scope of this thesis, although the principle is the same for both types, only a brief description of the latter is given.

In a typical cation sensing fluoroionophore,[5,8] two electronic systems, one involved in ion recognition and the other used for signaling, are connected by a short spacer (Figure I.3). The cation receptor is an electron donor (e.g. an amino group) and the fluorophore is the acceptor. When the fluorophore absorbs a photon, an electron is promoted from the highest occupied molecular orbital (HOMO) to the lowest unoccupied molecular orbital (LUMO), which leaves a hole in the former orbital, that can be filled via PET from the HOMO of the donor (cation receptor in its

free form) to that of the fluorophore. This new electron inhibits the decay of the previously excited one, and in this way fluorescence is quenched. Cation binding raises the redox potential of the donor, and the HOMO that was involved in the PET process has now a lower energy (stabilization arising from the dative covalent bonding between the donor and the metal ion, which requires both electrons). As a consequence, PET becomes impossible, and fluorescence intensity is enhanced.

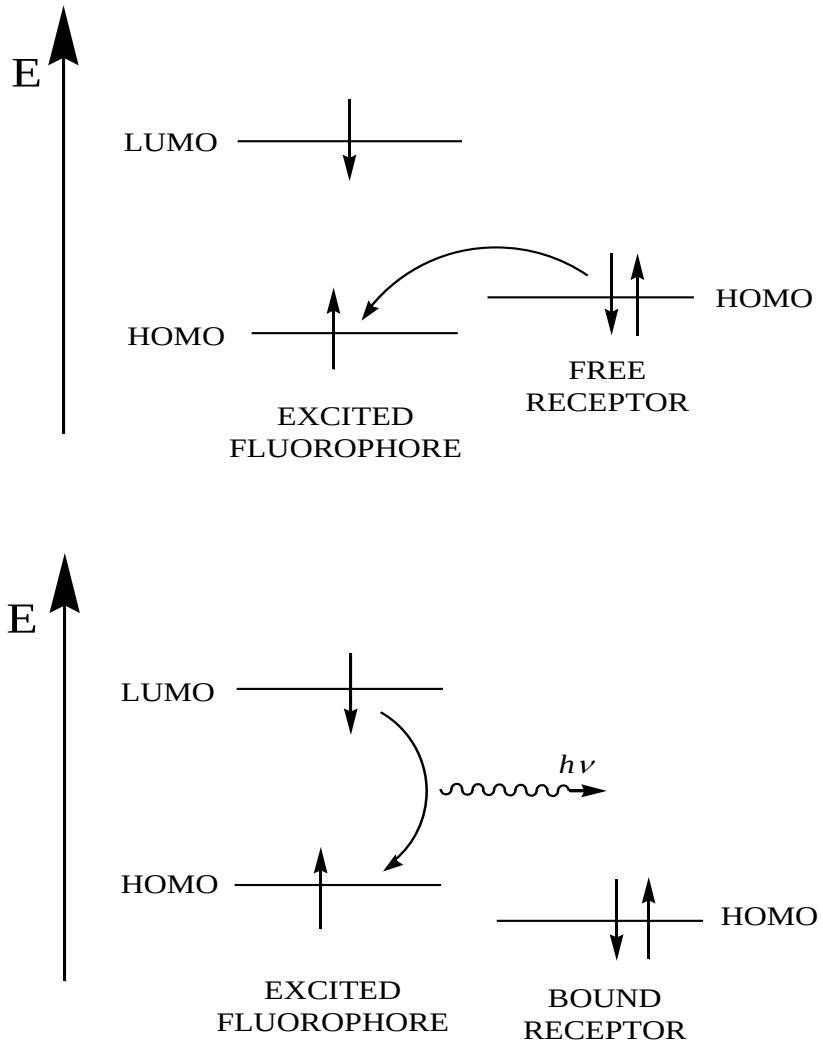

Figure I.3 – Principle of cation recognition by PET-based sensors.

I.3.2 Excited state proton transfer.

In the excited state, the acidic or basic properties of dye molecules differ from correspondent ground states, one of the causes being the redistribution of electronic

density after light absorption. Molecules that are more acidic or basic in the excited state than in the ground state (photo-acids and photo-bases, respectively) are able to undergo excited state proton transfer upon excitation.

The two excited-state forms can reach an equilibrium on a very short time scale and, in aqueous solution, this equilibrium can be shifted by changing, for example, the solvent pH.

When the same molecule contains both proton-donor and proton-acceptor groups in a close proximity, the solvent loses influence, since the proton can be transferred directly from the acidic site to the basic site. This process is named excited-state intramolecular proton transfer (ESIPT).[9] The proton-donor group is commonly a hydroxyl and the basic proton acceptor should be either a heterocyclic nitrogen atom or a carbonyl oxygen. These two groups normally form hydrogen bonds in the ground state, and this bond in the excited state facilitates proton transfer.

I.3.3 Excited state energy transfer.

Two molecules with similar excited-state energies can exchange their energies under certain conditions and through different mechanisms. When the emission spectrum of a fluorophore (donor, D) overlaps with the absorption spectrum of another molecule (acceptor, A), energy transfer occurs. For the sake of simplicity, only non-radiative energy transfer mechanisms will be described.

When the molecules are separated by long distances, an interaction through space occurs, via a transition dipole vector. The electron in the LUMO of the excited donor (D*) returns to the ground state, causing the simultaneous promotion of an electron in the acceptor (A) to a higher excited-state orbital (Figure I.4). The mechanism is analogous to that of electronic excitation produced by the electric vector of a light wave, but in this case the excitation is produced by a transition dipole vector, originated in the relaxation of D* to D. For this reason, the mechanism is designed as Coulombic (dipole-dipole) energy transfer, or resonance energy transfer.[10,11] A detailed theory of this mechanism was developed by Förster, so the name Förster resonance energy transfer is also used. This acronym is frequently presented as “Fluorescence Resonance Energy Transfer”, which is not correct, since the mechanism does not necessarily involve fluorescence. The FRET effect has a strong dependence on the distance between donor and acceptor. Its efficiency is

inversely proportional to the sixth power of the distance between both molecules. As a consequence, FRET can be used to determine distances between donor and acceptor fluorophores (the so called “molecular ruler”).[11]

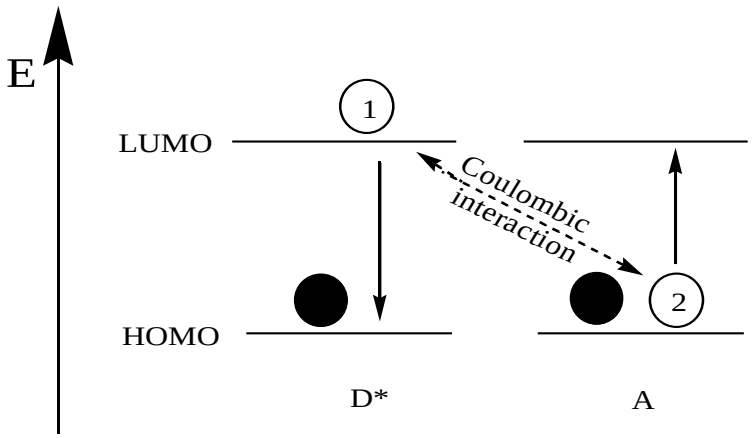

Figure I.4 – Electron movements taking place in long-range Coulombic energy transfer.

In addition to the previously mentioned mechanism, there is another one that involves close approach between the two molecules. The so called exchange mechanism of transfer, or Dexter mechanism, requires overlap between regions of electron density, so that electrons are exchanged between the two molecules. It represents a “double” electron substitution reaction, which means that an electron initially located on D* is transferred to A, simultaneously with an electron transfer from A to D* (Figure I.5), unlike the Förster mechanism, where the electrons initially on D* stay on D and the electrons initially on A stay on A*.[12]

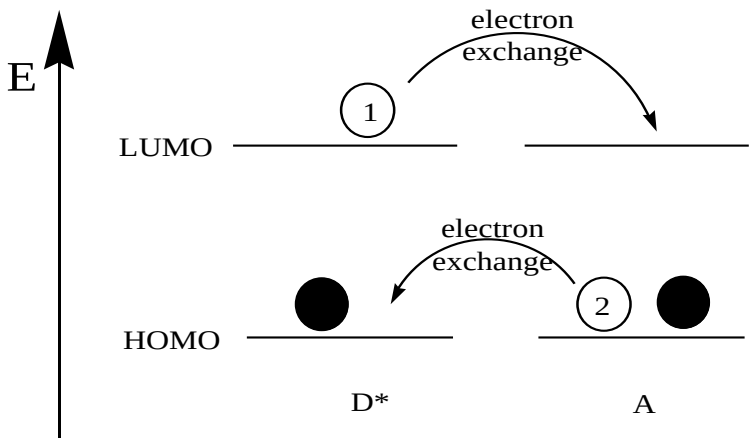

Figure I.5 – Electron movements taking place in short-range energy transfer by the exchange mechanism.

It is important to note that, while in PET the excited state can be an electron donor or an acceptor, in energy transfer it is exclusively an energy donor.

I.3.4 Excimer and exciplex formation

A molecule in the excited state can associate with an unexcited molecule like itself, giving rise to a dimer in the excited state,[8,9] which is called excimer (from “excited dimer”). The excimer emission spectrum differs substantially from that of monomers; it is normally broad, shifted to longer wavelengths and does not show vibrational resolution. One famous example is the excimer of pyrene (see Chapter III).

If the collision takes place between molecules that differ in structure (e.g. an electron donor and an acceptor), an excited state complex is formed, and is named exciplex (from “excited complex”).

The formation of excimers and exciplexes is reversible (after emission they separate and are free to form again upon excitation), and requires close location and adequate orientation of the two molecules involved (in the case of excimers, usually two heterocycles rich in π-electrons are required, which form two parallel planes through π- π stacking).

I.3.5 Photoinduced charge transfer (PCT)

This process is, in principle, also an electron transfer. The two (PET and PCT) phenomena are easily distinguished by their absorption and emission spectra.[8] In PET, strong quenching takes place and no spectral shifts are observed. On the other hand, the PCT states are usually fluorescent but exhibit a Stokes shift, caused by the change in the dipole moment that results from PCT from an electron-donating group (usually an amino group) to an electron-withdrawing group (conjugated to the former).

In terms of cation sensing, it is predictable that a complexed cation will diminish the electron-donating character of the electron donor, causing a reduction in conjugation and a consequent blue-shift of the absorption spectrum. Oppositely, if the acceptor group (e.g. a carbonyl group) interacts with a cation, its electron-withdrawing character is enhanced, the conjugation is increased, and a red-shift in the absorption spectrum is observed. The fluorescence spectra are usually shifted in the same way as the absorption spectra.

I.4 Cation sensing

Cations are extremely important in fields such as biology, chemistry, medicine and environment. Metal cation roles in biological processes range from maintaining potentials across cell membranes to triggering muscle contraction, among other functions. They also have catalytic functions at the active sites of many enzymes. On the other hand, pollutant metals like lead, mercury or cadmium show the undesirable side of the coin, in environmental terms.

Due to their importance in so many areas, the chemistry of cation complexation has played an important role in the origin of the field of molecular recognition. A great range of selective receptors for cationic species has been prepared and, by coupling those receptors (ionophores) to the adequate fluorophores, powerful chemosensors have been developed.[13,14] The characteristics of the ionophore in terms of the ligand topology and the number and nature of the complexing atoms must be adequate to the type of cation being studied.

According to the scope of the present thesis, emphasis will be given to two distinct types of receptors for metal cation sensors: crown ethers and Schiff bases.

I.4.1. Crown ethers

The crown ethers are simultaneously some of the simplest and most attractive macrocyclic (constituted by a large ring) ligands, and can be applied both in the sensing of metal ions or neutral molecules. These compounds are constituted by a cyclic array of ether oxygen atoms linked by organic spacers, normally —CH_2CH_2— groups.[15] Comparing the metal coordinating ability of simple ethers (e.g. diethyl ether) with crown ethers, it is observed that the latter bind much more effectively, due to the simultaneous chelate and macrocyclic effects.[16] The chelate effect states that bidentate ligands (e.g. ethylenediamine) form more stable complexes than the corresponding unidentate ligands. The macrocyclic effect has to do not only with the chelation of the metal by multiple binding sites, but also with a certain "pre-organization" or arrangement of the binding sites in space, which require less energy to perform the chelation.

Crown ethers have been firstly discovered by Pedersen,[17] in the mid-1960s, when he accidentally synthesized the compound dibenzo-18-crown-6 (Figure I.6). This nomenclature was suggested by Pedersen in his pioneering papers, not only because the systematic names to these compounds were extremely long, but also due to their "crown-like" conformation in molecular models. In this particular case, "18" refers to the total number of atoms in the macrocycle and "6" to the number of oxygen atoms in the ring.

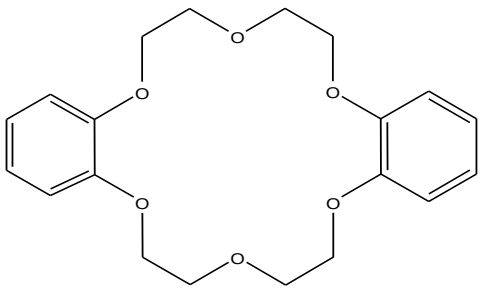

Figure I.6 – Dibenzo-18-crown-6.

In sensing of alkali metals by crown ethers, there is a relationship between the size of the cavity, cationic radius and stability of the formed complex (Table I.1).[18] Stronger complexes are formed when the cation fits perfectly into the cavity, in such

a way that if the cavity is too large (e.g. 18-crown-6) for a very small cation (e.g. Na^+), the crown ether becomes distorted, “wrapping” itself around the metal in order to maximize the electrostatic interactions, but simultaneously increasing the ring strain and, consequently, its stability.

Cation	Diameter (Å)	Crown Ether	Cavity Diameter (Å)
Li^+	1.36	12-crown-4	1.2 – 1.5
Na^+	1.94	15-crown-5	1.7 – 2.2
K^+	2.66	18-crown-6	2.6 – 3.2
Cs^+	3.34	21-crown-7	3.4 – 4.3

Table I.1 – Cation diameters for alkali metals and crown ether cavity sizes.

If oxygen atoms in the crown moiety are replaced with softer donor atoms, like nitrogen or sulfur, transition metals can also be sensed, according to Pearson’s rules for hard and soft acids and bases.[19]

Many crown-containing sensors are based in PET sensing mechanism, like the ones developed by de Silva and coworkers.[4] One such example is shown in Figure I.7,[20] where the complexing of K^+ hinders the photoinduced electron transfer from the crown donor atoms to the anthracene fluorophore, resulting in a strong CHEF effect.

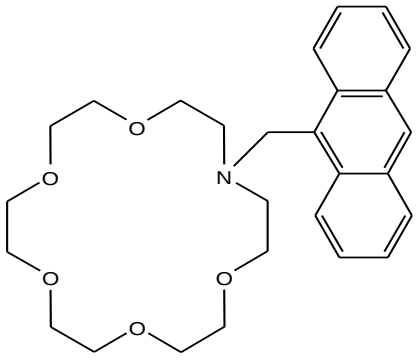

Figure I.7 – Crown-containing PET sensor.

There are also crown-containing sensors whose mechanism is based on PCT, e.g. those where a nitrogen atom contained in an azacrown moiety is conjugated to an electron-withdrawing group. In the case of the sensor represented in Figure I.8,[21] upon complexation by alkaline-earth metal cations the absorption and emission spectra experienced hypsochromic shifts, following the mechanism explained in section I.3.5.

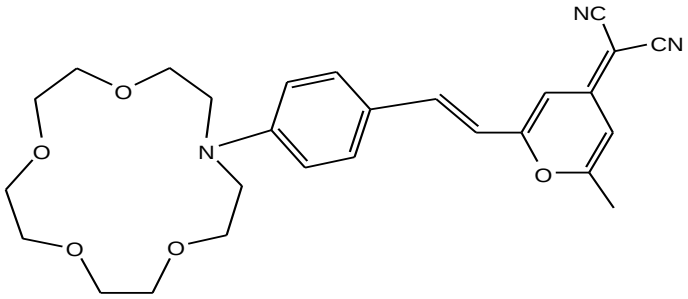

Figure I.8 – Crown-containing PCT sensor.

Since Pedersen's pioneer work in this field, an enormous variety of functionalized and derivatized crown ethers have been developed as sensors for ions.[22,23] Some very interesting systems include simultaneous recognition of a transition metal ion and an alkali or alkaline earth metal ion,[24,25,26,27] which is very useful to modulate different interesting properties.

Other useful applications of crown ethers include their uses as artificial membranes[28] (ionic channels), new smart materials,[29] active components of molecular machines[30] and biomedical applications as potential antitumor agents.[31]

I.4.2. Schiff bases

A Schiff base (also called imine, or azomethine) is a functional group with general formula RR'C=N-R'', where the nitrogen atom is never connected to a hydrogen. The synthesis of this type of compounds is relatively simple, by reaction between an amine and a carbonyl group (Scheme I.1). Since the reaction involves a

dehydration, the presence of dehydrating agents (such as $MgSO_4$) usually favours the formation of the desired product. During the purification step, however, some precautions must be taken in order to avoid degradation. Silica gel chromatography columns can cause hydrolysis of the imine; the alternative purification method is crystallization.[32]

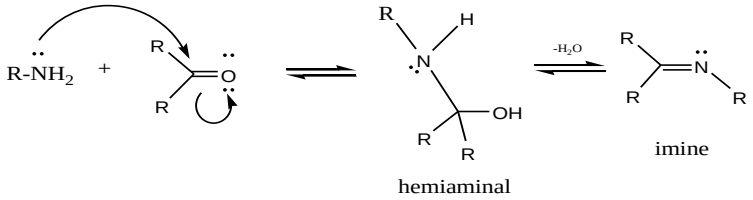

Scheme I.1 – Imine synthesis.

Schiff bases have been very important in the development of coordination chemistry,[33,34] in part due to their capability to form stable complexes[35,36,37] with the majority of the transition metals. The ability to stabilize most metals in different oxidation states also enhances their performance in catalytic processes.[32] In the field of bioinorganic chemistry, Schiff base complexes have received careful attention, due to their role in providing synthetic models for the metal-containing sites in metallo-proteins and enzymes.

Regarding their applications in chemical sensing, more specifically in cation detection, Schiff bases offer the advantage of possessing a good electron-donating group, the nitrogen atom, that with its lone electron pair can easily coordinate metal ions.[38] Upon coordination, the properties of the system can be modulated, accordingly to the type of cation and its oxidation state.[39,40] Two different behaviors can be observed, for example, for Zn(II) and Cu(II) upon coordination to two PET based systems.

In Figure I.9 is represented a new Zn(II) chemosensor derived from a hydrazone-pyrene moiety.[41,42]

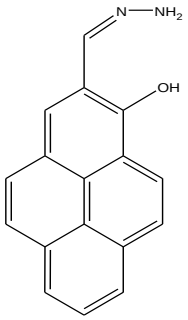

Figure I.9 – Hydrazone PET chemosensor for Zn(II).

The compound is weakly fluorescent in the absence of Zn(II), probably due to PET of the nitrogen lone pair to the pyrene fluorophore. After complexation, it experiences a large fluorescence enhancement, which can be assigned to blocking of the PET process. This is a typical case of an “OFF-ON” system, which means it experiences a CHEF effect upon cation binding. It is noteworthy that this particular system was applied in monitoring the level of Zn^{2+} in pancreatic cells, offering a very important biological application.

A different situation has been verified in the system depicted in Scheme I.2,[43,44] applied in Cu(II) sensing:

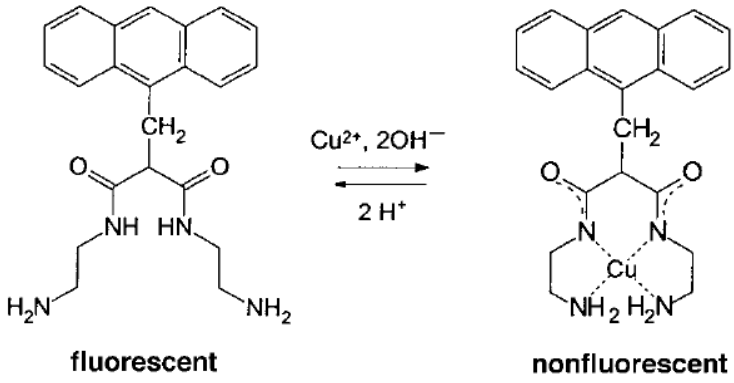

Scheme I.2 – Dioxotetraaza PET sensor for Cu(II).[43]

In this case, the compound is initially fluorescent, and after complexation with Cu(II) the fluorescence is quenched. Two mechanisms were proposed in this case: electron transfer or energy transfer (Dexter type). The former is likely to occur due to the possible oxidation of Cu(II) to Cu(III) by transferring an electron to the anthracene

moiety. It is worth noting that this ligand is not a Schiff base, but shows a similar behavior, since all the nitrogen atoms are involved in the coordination.

The fusion between Schiff bases and other coordinating entities (e.g. a crown-ether moiety)[45] expands the number of metal ions that can be detected by the same molecule simultaneously. Moreover, if the molecule is functionalized with a group that can contribute at the same time with coordinating atoms and intrinsic fluorescence, the possibilities are enhanced. An example of such groups is thiophene and its oligomers (oligothiophenes).[46] These compounds offer many advantages as fluorescent markers, since their fluorescence frequencies can be tuned in the whole visible range,[47] and their applications include recognition events in biological systems and ion sensing.[48]

Many interesting Schiff base systems can be found in the development of ion selective membrane sensors,[49] among other applications.

The possible instability of Schiff bases and their tendency to hydrolysis, which could be considered as drawbacks, are easily overcome by treating the imine with adequate reducing agents, with the consequent formation of the corresponding amine derivative, which is less sensitive to hydrolysis, more flexible and has an increased water solubility. However, upon reduction of the imine, the interaction with metals will become weaker, because the back-bonding interactions with the C=N π* orbital will be lost.[16]

I.5 Ruthenium(II) polypyridyl complexes as luminescent probes for DNA.

Among the numerous classes of luminescent metal complexes, ruthenium(II) polypyridyl complexes are probably the ones that deserved the most attention throughout the last decades. Their unique properties in terms of chemical stability, excited-state reactivity, redox potentials, luminescence emission and excited-state lifetimes turned these complexes into subject of thorough investigation. These complexes are good visible light absorbers, exhibit relatively intense and long-lived luminescence, and have a reversible redox behavior both in the ground and excited states. A better understanding of some of these properties requires a brief

introduction to its electronic configuration and photophysical processes upon excitation by light.

Ru^{2+} is a d^6 metal ion, and the polypyridine ligands possess σ donor orbitals localized on the nitrogen atoms and π donor and π^* acceptor orbitals more or less delocalized on aromatic rings. In a simplified molecular orbital diagram for this type of complexes (Figure I.10) are represented the types of transitions that can take place after irradiation. Promotion of an electron from a π_M metal orbital to the π_L^* ligand orbitals originates the singlet metal-to-ligand charge transfer (^{1}MLCT) excited state, that then experiences intersystem crossing and populates the triplet ^{3}MLCT state.[50,51] The complex can then follow

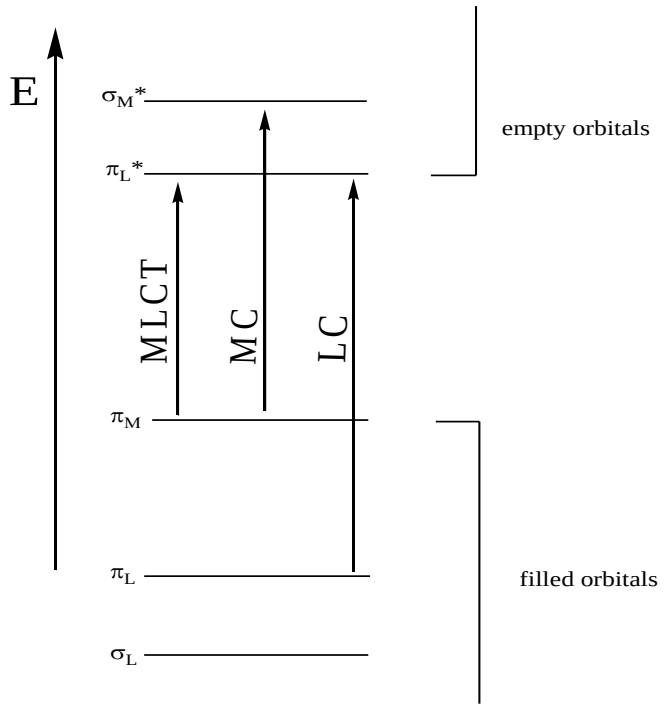

Figure I.10 – Simplified molecular orbital diagram for Ru(II) polypyridyl complexes in octahedral symmetry.

different pathways: it can either deactivate by radiative or radiationless processes back to the ground state, or reach the upper triplet metal-centered (^{3}MC) state by thermal activation (this process depends on the energy difference between the two triplet states).[52] Usually, from the ^{3}MLCT state, the complex reacts by redox processes, while from the ^{3}MC state, a rupture of a Ru-N bond occurs. For the majority of Ru(II) polypyridine complexes, the lowest excited state is the ^{3}MLCT level (more precisely, a cluster of closely spaced ^{3}MLCT levels),[53] which suffers relatively

slow radiationless transitions and for this reason exhibits relatively long lifetime and intense luminescence emission.

Adding to the aforementioned properties, the great stability and flexibility of these complexes when compared to other metallic compounds is enormous, which opened the door to a vast synthetic chemistry. Due to all these extraordinary features, Ru(II) polypyridyl complexes have found applications in a great number of areas, such as solar energy applications,[54] molecular devices,[55,56] optical sensing,[57] polymer modified electrodes,[58] electroluminescent displays, and interactions with nucleic acids and other biomolecules.

Concerning their use as optical chemosensors, the most common applications are sensing of oxygen,[59] carbon dioxide[60] and pH.[61,57] Also frequent are applications in anion sensing,[62] by functionalizing the polypyridyl ligands with anion receptors, and cation sensing,[63] by inserting recognition units such as crown ethers. Figure I.11 shows an example of a chemosensor in which one of the bipyridyl ligands is functionalized with a large macrocyclic receptor unit containing five amine groups:[64]

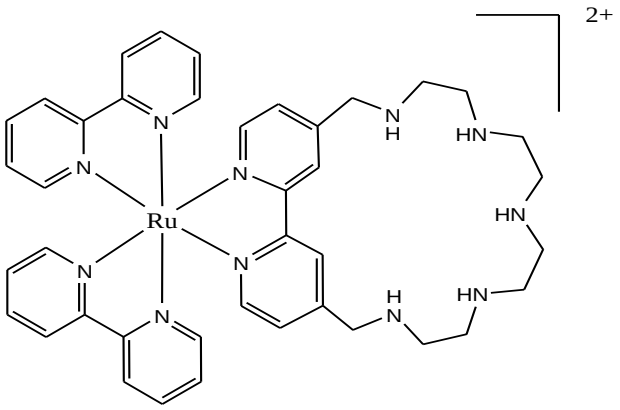

Figure I.11 – Ru(II) polypyridyl chemosensor functionalized with a macrocyclic polyamine.

This polyamine unit is capable of complexing cationic or anionic substrates, depending on its level of protonation.

Interaction of Ru(II) polypyridyl complexes with DNA, which is the application investigated in this thesis, started to be studied more than twenty years

ago.[65,66,67,68,69] The principle of interaction between Ru(II) polypyridyl complexes with DNA has been a very discussed topic,[70,71] since complexes are positively charged and can interact with the negatively charged phosphate backbone (for details on DNA structure, see section I.6.2) and can also bind through intercalation of a planar portion of the molecule into the stacking of bases (provided that at least one of the ligands has a large planar heteroaromatic system).[72] Figure I.12 shows a simplified illustration of an intercalating complex with respect to the DNA double helix:[65]

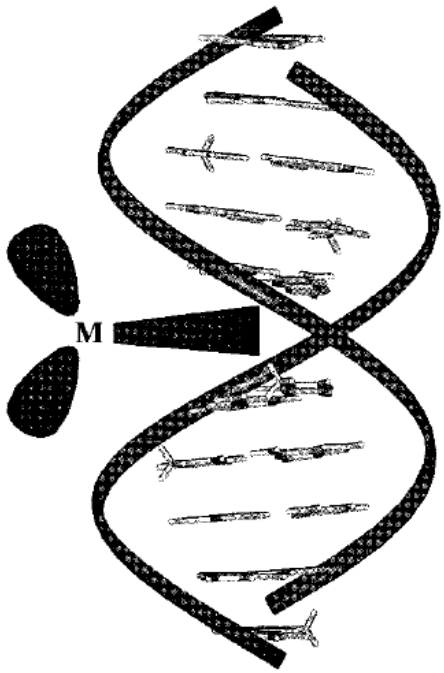

Figure I.12 – Simplified representation of an intercalating complex oriented with respect to the DNA double helix.[65]

One of the most remarkable examples of how increasing the size of one of the ligands affected intercalation (and consequently, photophysical properties, as it will be explained below) was the complex $[Ru(bpy)_2(dppz)]^{2+}$ (Figure I.13):

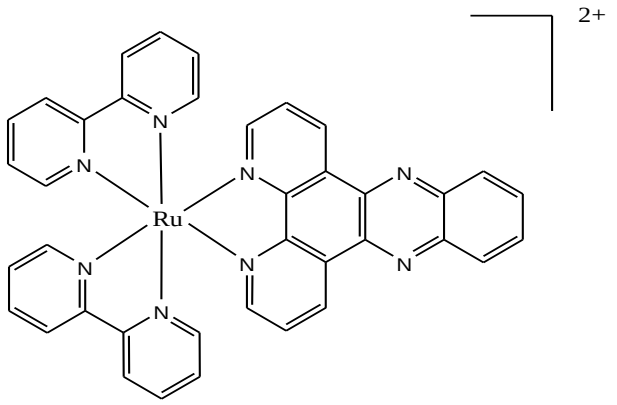

Figure I.13 – Structure of $[Ru(bpy)_2(dppz)]^{2+}$.

This particular complex behaves as a “light-switch” for DNA in aqueous solution,[73] since it is practically non-emissive in its free form, but strongly enhances its fluorescence emission upon binding to DNA. The explanation for this behavior lies in the lowest-lying excited state swap that takes place in protic solvents (when the complex is not bound to DNA, the polarity of the solvent prompts the formation of a new MLCT species, which decays non-radiatively),[74] combined with the intercalative binding mode to DNA of Ru(II)-dppz and related complexes,[75,76,77] that protects them from quenching by oxygen and solvent molecules. Very recently, these complexes have been studied as multifunctional biological agents for direct DNA imaging in living cells.[78] Absorption MLCT bands in the visible region of the spectrum allow a wide range of biological applications. Through DNA binding it is possible to develop new chemotherapeutic agents, as an alternative to the more toxic and long time used Pt(II) compounds.

Binding of a Ru(II) polypyridyl complex to double stranded DNA through intercalation usually produces hypochromism and bathochromism of its MLCT visible absorption band, and the extent of hypochromism is normally proportional to the intercalative binding strength of the complex.[79] In this way, absorption spectroscopy proves to be a very useful technique in these studies. At the same time, enhancements of luminescence intensity and lifetime of the complexes upon binding are also frequently observed (for the reasons described in the aforementioned paragraph in the example of Ru(II)-dppz derived complexes), which turns luminescence spectroscopy and single-photon timing measurements into valuable techniques as well (see section I.7 for details on the instrumental methods).

I.6 Sensing targets: metal ions and DNA.

After having described the types of chemosensors and probes related to the scope of this thesis, attention will now be given to the analytes or subjects of this sensing.

I.6.1 Metal ions

The importance of metal sensing has been briefly addressed in section I.4. In the present section are introduced most of the metals studied in this thesis, in order to better understand their coordinating properties, and consequently, their effects upon recognition.

Sometimes, fluorescence enhancement upon metal coordination may be misleading. There is a natural tendency of d block metals to quench the emission of a nearby fluorophore, either via electron transfer or energy transfer mechanism (or both). However, most of the times fluorescence enhancement is observed upon d block metal complexation. This apparent paradox can be explained taking as an example a nitrogen donor chemosensor. Before coordination, a very efficient quenching mechanism takes place (electron transfer from a nitrogen atom to the fluorophore), and almost no light emission is observed. After metal coordination to the nitrogen atoms, this mechanism of quenching is replaced by another one (from the metal, either electron transfer or energy transfer in nature), but this new quenching process involves a more distant metal centre, and is definitely less efficient. Hence, after metal binding, what is observed is not a full enhancement of the fluorescence, but simply a less efficient quenching of the fluorophore (which results in a net enhancement of light emission).[80]

I.6.1.1 Sodium

Sodium is the sixth most abundant element in the Earth's crust, and its compounds play a vital role in nature.

Metal ions such as Na^+ that have a closed shell electronic configuration and absence of any redox activity (which prevent energy transfer and electron transfer,

respectively), are photophysically inactive.[80] For this reason, most of their sensors are of the type “OFF-ON”, or CHEF. A classic example was given in Figure I.7, with the crown ether derived sensor designed by de Silva and coworkers[20] that was used to sense potassium, but the principle is the same as for sodium (in this case a 15-crown-5 bearing only oxygen atoms as donors would be the adequate receptor).

I.6.1.2 Nickel

Nickel is rarely found in its pure form on the Earth’s surface, although it is believed that a significant amount is present at the core. Its most stable oxidation state is +2, while +1 and 0 are only found in organometallic chemistry. It has a very rich coordination chemistry, and can form complexes with different geometries (octahedral, trigonal bipyramidal, tetrahedral, square-based pyramidal and square planar)

Divalent cations of the 3d series are considered “intermediate” in the hard and soft classification of metal centers,[19] and therefore have great affinity towards the “intermediate” nitrogen donor atom, either sp^3 (amine) or sp^2 (imine) hybridized. The ligand field stabilization energy predicts a preferable tetragonal stereochemistry, for what a tetraamine chelating agent would be an adequate receptor.

I.6.1.3 Copper

Copper is one of the most well-known metals, and finds application in many areas of everyday life. It is also the least reactive of the first row transition metals. It can be found in a great number of metalloproteins. This metal is the only first row d-block metal that exhibits a stable +1 oxidation state, even though the most stable one is +2 (copper(I) is easily oxidized and copper(III) is very difficult to obtain). Like nickel, it also forms complexes with a great variety of geometries.

In terms of molecular recognition, Cu(II) usually quenches the emission of fluorophores (see the example given in section I.4.2, Scheme I.2) because it is a d^9 ion, and can undergo electron transfer or energy transfer processes.

I.6.1.4 Zinc

When compared to copper, zinc is not an abundant element, and trace amounts are present in the Earth's crust. Due to its high reactivity it is rarely found pure in nature.

The Zn(II) ion has a $3d^{10}$ electronic configuration, and it cannot be strictly considered as a transition metal ion. Due to this electronic configuration, its compounds are colorless and diamagnetic and there is no ligand-field stabilization energy associated with this ion, for what no particular geometry is preferred in the formation of complexes.

Regarding its sensing, Zn(II) is not a redox active centre, and for this reason cannot participate in electron-transfer processes. Plus, it is a hard metal center[19] and has affinity for nitrogen and oxygen donors. After complexation it usually enhances the fluorescence of the system (see section I.4.2, Figure I.9), by blocking PET from the donor atoms to the fluorophore.

I.6.1.5 Palladium

Palladium is a relatively abundant metal on earth. Its most known applications are in catalysis, e.g. the Pd/C catalyst. The most stable oxidation state for this element is II, although Pd(IV) compounds are also common.

In sensing applications, Pd(II) is a d^8 ion and is a soft metal center, according to Pearson's rules.[19] The combination of these two factors predicts that Pd(II) is more likely to be coordinated by soft donors, like sulfur, and that it can undergo electron-transfer processes (because it does not have a closed-shell configuration). For this reason, chemosensors that increase the emission intensity upon palladium(II) coordination are very appealing and necessary.

I.6.1.6 Mercury

Mercury has unique properties, for it is the only metallic element that exists in liquid form at room temperature. Another unusual property for a metal is its poor heat conductivity (even though it is a good conductor of electricity). It has many practical uses (e.g. barometers, electrodes, etc.), but it is extremely toxic to humans. Both I

and II oxidation states are stable, but in terms of sensing it was chosen in this thesis to detect Hg(II).

The d^{10} configuration of Hg(II) should, in principle, predict a similar behavior to Zn(II) in terms of CHEF effect, with the difference that mercury(II) is a soft metal centre,[19] and in this case, like in palladium(II), coordination to sulfur donors is especially favored.

I.6.2 DNA

DNA (deoxyribonucleic acid) is the molecule that carries all the genetic information that is needed for a living organism. All eukaryotic organisms contain DNA in its cell nuclei, and each one of the cells contains the genetic code that is necessary to build the entire organism and make it work as a whole.[16] Due to the great quantity of information that is processed, the individual strands have to be quite long (each cell contains ca. 3 cm of DNA), and they are able to fit within the cell because of their very small diameter (2 nm).

The structure of the DNA molecule, as proposed by Watson and Crick, consists of a double helical structure, where two identical strands are linked via hydrogen bonding and π-π stacking interactions (Figure I.14):[81]

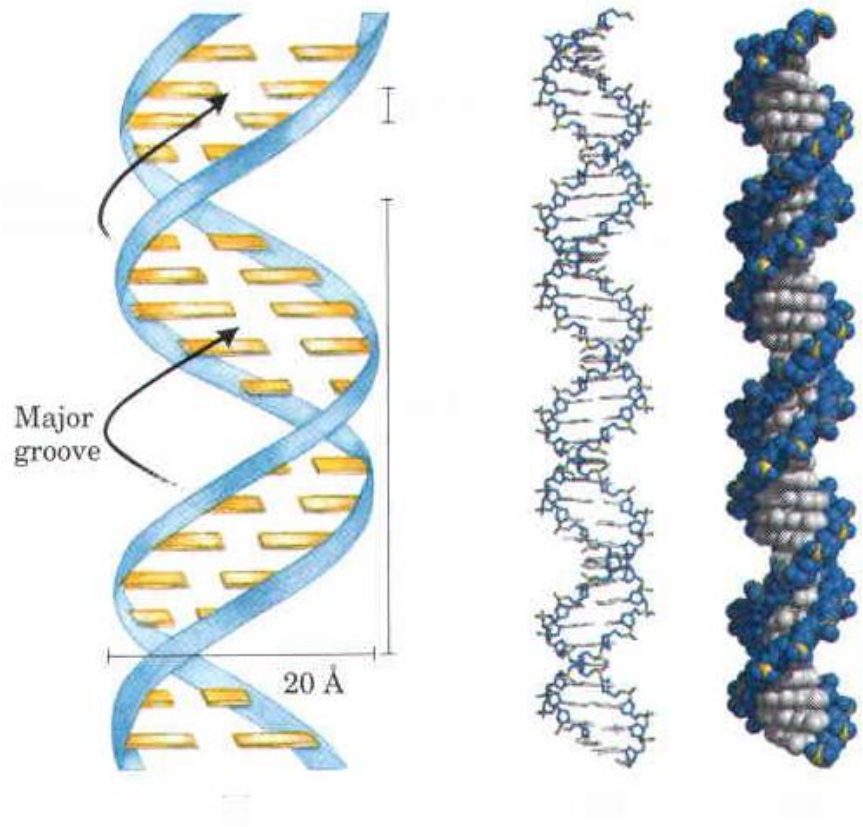

Figure I.14 – Watson-Crick model for the structure of DNA. (a) Schematic representation, showing dimensions of the helix. (b) Stick representation showing the backbone and stacking of the bases. (c) Space-filling model.[81]

The pairing of the two strands creates a major groove and a minor groove. This assembly is achieved probably because this double helical structure allows the hydrophobic part of the molecule (the nucleobases, Figure I.15) to avoid the contact with water, by stacking inside the helix.

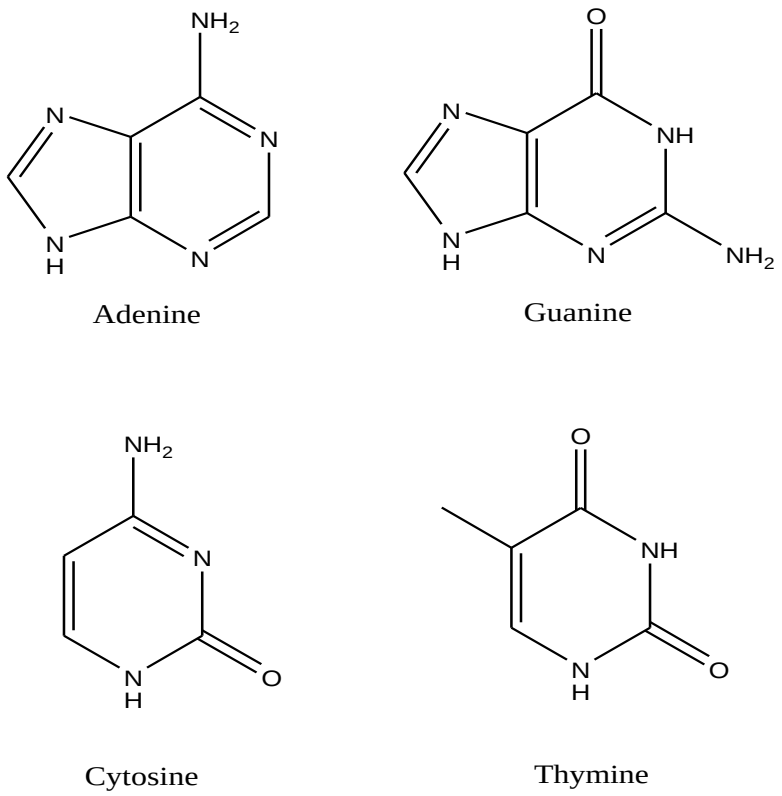

Figure I.15 – DNA nucleobases.

Each nucleobase is linked to a sugar and a phosphate tail, to form the nucleotides, which are the monomers that constitute DNA. Bases are paired through hydrogen bonds, in a unique fashion, that is mutually complementary (adenine with thymine; guanine with cytosine). It is this combination of base pairs that governs the replication of DNA and the passing of the genetic code to transfer RNA.

I.7 Scope of the present thesis

In the previous sections, some important notions related to this work were introduced. By putting together some of these concepts it is possible to define the objective of this thesis. It can be theoretically divided in two parts: one that deals with cation sensing and other with the search for DNA probes.

In the first part, fluorescent chemosensors derived from Schiff bases were developed for detection of metal ions by fluorescence spectroscopy. Molecules were

designed having in mind Pearson's rules of hard and soft donors and acceptors, and the photophysical mechanisms of recognition inherent to cation binding. In this way, functionalization with different donor atoms was carried out in some cases (crown ethers, thiophene units), while in others the driving force was a search for enhancement of chelation effects by increasing the number of nitrogen atoms (poly-imines, quinolines). A varied choice of fluorophores was performed, some of them including donor atoms, others looking for different photophysical properties (pyrene, with excimer emission).

In the second part, concerning DNA luminescent probes, different ruthenium(II) polypyridyl complexes were developed in order to study the relation between their structure and binding mode to calf thymus DNA, and thus use this feature to the future design of new molecular probes for this polynucleotide, based on the obtained results.

Although chapter VI concerns cation sensing, it is included in the end because this work is still in progress.

I.8 Instrumental methods

In this section is given a brief introduction to some of the experimental techniques and procedures used in this thesis.

I.8.1 UV-Vis and steady-state fluorescence spectroscopies.

Cation sensing in this thesis was simultaneously followed by absorption and emission spectroscopies. These two techniques are closely related, and usually are used together, when fluorescence sensing is involved (if the chemosensors are not fluorescent, but are for example, colorimetric, its complexation can be followed exclusively by absorption spectroscopy).

These spectroscopies complement each other, in the sense that, by recording the absorption spectrum of a given compound, it is possible to determine the wavelength region where it is to be excited (which usually is in absorption maxima), in order to measure the fluorescence spectrum.

In a typical cation sensing experiment, the chemosensor is dissolved in an adequate solvent, of spectroscopic grade, with a concentration that permits a linearity in Beer's law (if a solution is too concentrated, most of the light will be absorbed at the surface facing the light source, and few will reach the detector, for what the relationship between absorbance intensity and concentration is lost). A stock solution of the metal cation to be studied is also prepared, and after recording the absorption and emission spectra of the free ligand, small volume increments of metal solution are added (the ligand concentration is kept constant). Between each addition, both absorption and emission spectra are recorded, in order to observe the differences produced during the titration in function of the cation concentration.

For DNA binding experiments, these techniques were also used, but in order to determine the changes on the properties of Ru(II) complexes after binding to DNA. The general procedure was to dissolve the complex to be studied and measure absorption, emission and luminescence lifetime (see section I.8.2). A DNA stock solution was prepared, which was then progressively added to the Ru(II) solution (between each addition the solution was allowed to equilibrate for about 30 minutes). Differences in absorbance upon binding to DNA are commonly hypochromism and bathochromism of its MLCT absorption band (see section I.5). Fluorescence emission usually is enhanced, for the reasons mentioned in section I.5.

I.8.2 Time-resolved fluorescence spectroscopy: Single Photon Timing (SPT)

This technique has been used in the DNA binding experiments of Ru(II) complexes. It is very useful to access information that is not given by steady-state fluorescence emission spectroscopy, namely through measurement of fluorescence lifetime decays. While in steady-state measurements the sample is being continuously irradiated, in SPT the radiation source is pulsed, and the pulse is normally shorter than the decay time of the sample.[10]

Usually, macromolecules can exist in more than one conformation, and the decay time of a bound probe may depend on conformation. While in steady-state measurements, it would be impossible to distinguish between the fluorescence of the different conformations, measuring a fluorescence decay can give two different decay times, each one assignable to a different conformation.

In the DNA binding experiments, after measuring absorption and steady-state emission upon each DNA concentration increment, luminescence lifetimes were measured. The interaction of the complexes with the biopolymer could be observed by an increase in their mean luminescence lifetime, which can be attributed to the same reason that causes an enhancement of fluorescence intensity (section I.5).

I.8.3 Synthetic techniques

Alongside with conventional synthetic methodologies, some of the syntheses included in this thesis were performed either via microwave irradiation or ultrasonication, which contributed to a more sustainable approach and diminished the reaction times, with satisfactory yields.

I.8.3.1 Microwave irradiation

Microwave-assisted reactions have gained popularity among synthetic chemists due to the drastic reduction in reaction times and minimization of secondary reactions.[82] For a synthetic chemist, a reaction with high yields and minimal secondary products is highly desirable. From a sustainable viewpoint, minimizing the use of toxic solvents is also extremely important (in some cases, it is even possible to perform solvent-free reactions). Polar compounds with relatively high boiling points are usually chosen as solvents (e.g. water, ethylene glycol or dimethylformamide) and the volume of solvent is, in general, significantly reduced when compared to conventional synthesis.

The synthesis of all the Ru(II) complexes presented in this thesis were performed via microwave-assisted reactions, in 5 mL of ethylene glycol, for two minute periods. The solvent was then distilled at reduced pressure and recovered, and the yields were quite satisfactory in general.

I.8.3.2 Ultrasounds

Ultrasound-assisted synthesis is also a powerful tool in terms of reducing reaction times and performing clean synthesis. The correct term for the application of ultrasounds in synthesis is sonochemistry, and it is a subject that attracted more

attention is the last two decades of the twentieth century, due to the more easily available ultrasonic cleaning baths. The power of this technique results from the formation of the so-called cavitation bubbles, which after collapsing release very high pressures and temperatures.[83]

Two of the quinoline derived compounds presented in chapter VI of this thesis were obtained via ultrasound-assisted synthesis, in 5 mL of ethanol or methanol, for periods of one hour.

I.9 References

[1] A. Hulanicki, S. Glab and F. Ingman, *Pure Appl. Chem.*, 1991, **63**, 1247-1250.

[2] L. Prodi, F. Bolletta, M. Montalti and N. Zaccheroni, *Coord. Chem. Rev.*, 2000, **205**, 59-83.

[3] R. A. Bissell, A. P. de Silva, H. Q. N. Gunaratne, P. L. M. Lynch, G. E. M. Maguire and K. R. A. S. Sandanayake, *Chem. Soc. Rev.*, 1992, **21**, 187-195.

[4] A. P. de Silva, H. Q. N. Gunaratne, T. Gunnlaugsson, A. J. M. Huxley, C. P. McCoy, J. T. Rademacher and T. E. Rice, *Chem. Rev.*, 1997, **97**, 1515-1566.

[5] B. Valeur and I. Leray, *Coord. Chem. Rev.*, 2000, **205**, 3-40.

[6] A. W. Czarnik, *Acc. Chem. Res.*, 1994, **27**, 302-308.

[7] M. H. Keefe, K. D. Benkstein and J. T. Hupp, *Coord. Chem. Rev.*, 2000, **205**, 201-228.

[8] B. Valeur, *Molecular Fluorescence: Principles and Applications*, Wiley VCH, Weinheim, Germany, 2001.

[9] A. P. Demchenko, *Introduction to Fluorescence Sensing*, Springer, 2009.

[10] J. R. Lakowicz, *Principles of Fluorescence Spectroscopy*, 3rd ed., Springer, 2006.

[11] B. Wardle, *Principles and Applications of Photochemistry*, Wiley, Chichester, England, 2009.

[12] N. J. Turro, *Modern Molecular Photochemistry*, University Science Books, California, USA, 1991.

[13] C. Lodeiro, J. L. Capelo, J. C. Mejuto, E. Oliveira, H. M. Santos, B. Pedras and C. Nuñez, *Chem. Soc. Rev.*, 2010, **39**, 2948-2976.

[14] C. Lodeiro and F. Pina, *Coord. Chem. Rev.*, 2009, **253**, 1353-1383.

[15] J. L. Atwood and J. W. Steed, *Encyclopedia of Supramolecular Chemistry*, Taylor and Francis, New York, Boca Raton, 2004, vol. 1.

[16] J. W. Steed and J. L. Atwood, *Supramolecular Chemistry*, Wiley, Chichester, England, 2005.

[17] C. J. Pedersen, *J. Am. Chem. Soc.*, 1967, **89**, 2495-2496.

[18] P. D. Beer, P. A. Gale and D. K. Smith, *Supramolecular Chemistry*, Oxford University Press, Oxford, England, 1999.

[19] R. G. Pearson, *J. Am. Chem. Soc.*, 1963, **85**, 3533-3539.

[20] A.P. de Silva and S. A. de Silva, *J. Chem Soc., Chem. Commun.*, 1986, 1709-1710.

[21] J. Bourson and B. Valeur, *J. Phys. Chem.*, 1989, **93**, 3871-3876.

[22] G. W. Gokel, W. M. Leevy and M. E. Weber, *Chem. Rev.*, 2004, **104**, 2723-2750.

[23] S. Fery-Forgues and F. Al-Ali, *J. Phot. Photobiol. C. Photochem. Revs.*, 2004, **5**, 139-153.

[24] E. Karapinar and E. Özcan, *J. Incl. Phen. Mac. Chem.*, 2003, **47**, 59-63.

[25] J-E. Jee, M. C. Chang and C-H. Kwak, *Inorg. Chem. Commun.*, 2004, **7**, 614-617.

[26] K. M-C. Wong, W-P. Li, K-K. Cheung and V. W-W. Yam, *New J. Chem.*, 2005, **29**, 165-172.

[27] J. Arias, M. Bardají and P. Espinet, *J. Organomet. Chem.*, 2006, **691**, 4990-4999.

[28] E. Biron, F. Otis, J. C. Meillon, M. Robitaille, J. Lamothe, P. Van Hove, M. E. Cormier and N. Voyer, *Bioorg. Med. Chem.*, 2004, **12**, 1279-1290.

[29] S. Yagai and A. Kitamura, *Chem. Soc. Rev.*, 2008, **37**, 1520-1529.

[30] K. Kinbara and T. Aida, *Chem. Rev.*, 2005, **105**, 1377-1400.

[31] M. Kralj, L. Tusek-Bozic and L. Frkanec, *ChemMedChem*, 2008, **3**, 1478-1492.

[32] P. G. Cozzi, *Chem. Soc. Rev.*, 2004, **33**, 410-421.

[33] W. Radecka-Paryzek, V. Patroniak and J. Lisowski, *Coord. Chem. Rev.*, 2005, **249**, 2156-2175.

[34] P. A. Vigato and S. Tamburini, *Coord. Chem. Rev.*, 2004, **248**, 1717-2128.

[35] S. R. Collinson and D. E. Fenton, *Coord. Chem. Rev.*, 1996, **148**, 19-40.

[36] D. E. Fenton, *Chem. Soc. Rev.*, 1988, **17**, 69-90.

[37] V. Alexander, *Chem. Rev.*, 1995, **95**, 273-342.

[38] M. Fondo, A. M. García-Deibe, N. Ocampo, J. Sanmartín, M. R. Bermejo, E. Oliveira and C. Lodeiro, *New J. Chem.*, 2008, **32**, 247-257.

[39] C. Lodeiro, J. C. Lima, A. J. Parola, J. S. Seixas de Melo, J. L. Capelo, B. Covelo, A. Tamayo and B. Pedras, *Sens. Actuators B*, 2006, **115**, 276-286.

[40] C. Nuñez, R. Bastida, A. Macías, E. Bértolo, L. Fernandes, J. L. Capelo and C. Lodeiro, *Tetrahedron*, 2009, **65**, 6179-6188.

[41] Y. Zhou, H. N. Kim and J. Yoon, *Bioorg. Med. Chem. Lett.*, 2010, **20**, 125-128.

[42] Z. Xu, J. Yoon and D. Spring, *Chem. Soc. Rev.*, 2010, **39**, 1996-2006.

[43] R. Krämer, *Angew. Chem. Int. Ed.*, 1998, **37**, 772-773.

[44] L. Fabrizzi, M. Lichelli, P. Pallavicini, A. Perotti, A. Taglietti and D. Sacchi, *Chem. Eur. J.*, 1996, **2**, 75-82.

[45] C. Lodeiro and J. L. Capelo, *J. Incl. Phen. Mac. Chem.*, 2004, **49**, 249-258.

[46] G. Barbarella, M. Melucci and G. Sotgiu, *Adv. Mater.*, 2005, **17**, 1581-1593.

[47] G. Barbarella, L. Favaretto, G. Sotgiu, M. Zambianchi, A. Bongini, C. Arbizzani, M. Mastragostino, M. Anni, G. Gigli and R. Cingolani, *J. Am. Chem. Soc.*, 2000, **122**, 11971-11978.

[48] H-A. Ho and M. Leclerc, *J. Am. Chem. Soc.*, 2004, **126**, 1384-1387.

[49] F. Faridbod, M. R. Ganjali, R. Dinarvand and P. Norouzi, *Comb. Chem. High Throughput Screen.*, 2007, **10**, 527-546.

[50] E. M. Kober and T. J. Meyer, *Inorg. Chem.*, 1982, **21**, 3967-3977.

[51] J. N. Demas and G. A. Crosby, *J. Am. Chem. Soc.*, 1971, **93**, 2841-2847.

[52] C. Moucheron, A. Kirsch-De Mesmaeker and J. M. Kelly, *Struct. Bonding*, 1998, **92**, 163-216.

[53] V. Balzani and S. Campagna, *Topics in Current Chemistry: Photochemistry and Photophysics of Coordination Compounds*, vol. 1, Springer-Verlag, Berlin, Germany, 2007.

[54] M. E. Jiménez-Hernández, F. Manjón, D. García-Fresnadillo and G. Orellana, *Solar Energy*, 2006, **80**, 1382-1387.

[55] P. Ashton, R. Ballardini, V. Balzani, A. Credi, K. R. Dress, E. Ishow, C. J. Kleverlaan, O. Kocian, J. A. Preece, N. Spencer, J. F. Stoddart, M. Venturi and S. Wenger, *Chem. Eur. J.*, 2000, **6,** 3558-3574.

[56] V. Balzani, G. Bergamini, F. Marchioni and P. Ceroni, *Coord. Chem. Rev.*, 2006, **250**, 1254-1266.

[57] L. Tormo, N. Bustamante, G. Colmenarejo and G. Orellana, *Anal. Chem.*, 2010, **82**, 5195-5204.

[58] J.G. Vos and J.M. Kelly, *Dalton Trans.*, 2006, **41**, 4869-4883.

[59] E. R. Carraway, J. N. Demas, B. A. DeGraff and J. R. Bacon, *Anal. Chem.*, 1991, **63**, 337-342.

[60] G. Orellana, M. C. Moreno-Bondi, E. Segovia and M. D. Marazuela, *Anal. Chem.*, 1992, **64**, 2210-2215.

[61] C. Malins, H. G. Glever, T. E. Keyes, J. G. Vos, W. J. Dressick and B. D. MacCraith, *Sens. Actuators B*, 2000, **67**, 89-95.

[62] M. S. Vickers, K. S. Martindale and P. D. Beer, *J. Mater. Chem.*, 2005, **15**, 2784-2790.

[63] P. D. Beer, F. Szemes, P. Passaniti and M. Maestri, *Inorg. Chem.*, 2004, **43**, 3965-3975.

[64] C. Lodeiro, F. Pina, A. J. Parola, A. Bencini, A. Bianchi, C. Bazzicalupi, S. Ciattini, C. Giorgi, A. Masotti, B. Valtancoli and J. Seixas de Melo, *Inorg. Chem.*, 2001, **40**, 6813-6819.

[65] K. E. Erkkila, D. T. Odom and J. K. Barton, *Chem. Rev.*, 1999, **99**, 2777-2795.

[66] L. N. Ji, X. H. Zou and J. G. Liu, *Coord. Chem. Rev.*, 2001, **216**, 513-536.

[67] C. Metcalfe and J. A. Thomas, *Chem. Soc. Rev.*, 2003, **32**, 215-224.

[68] M. J. Clarke, *Coord. Chem. Rev.*, 2002, **232**, 69-93.

[69] H. Chao and L. N. Ji, *Bioinorg. Chem. Appl.*, 2005, **3**, 15-28.

[70] A. M. Pyle, J. P. Rehmann, R. Meshoyrer, C. V. Kumar, N. J. Turro and J. K. Barton, *J. Am. Chem. Soc.*, 1989, **111**, 3051-3058.

[71] C. V. Kumar, J. K. Barton and N. J. Turro, *J. Am. Chem. Soc.*, 1985, **107**, 5518-5523.

[72] A. Kirsch-De Mesmaeker, G. Orellana, J. K. Barton and N. J. Turro, *Photochem. Photobiol.*, 1990, **52**, 461-472.

[73] A. E. Friedman, J. C. Chambron, J. P. Sauvage, N. J. Turro and J. K. Barton, *J. Am. Chem. Soc.*, 1990, **112**, 4960-4962.

[74] E. J. C. Olson, D. Hu, A. Hörmann, A. M. Jonkman, M. R. Arkin, E. D. A. Stemp, J. K. Barton and P. F. Barbara, *J. Am. Chem. Soc.*, 1997, **119**, 11458-11467.

[75] F. Westerlund, F. Pierard, M. P. Eng, B. Nordén and P. Lincoln, *J. Phys. Chem. B*, 2005, **109**, 17327-17332.

[76] F. Westerlund, M. P. Eng, M. U. Winters and P. Lincoln, *J. Phys. Chem. B*, 2007, **111**, 310-317.

[77] M. Li and P. Lincoln, *J. Inorg. Biochem.*, 2009, **103**, 963-970.

[78] M. R. Gill, J. Garcia-Lara, S. J. Foster, C. Smythe, G. Battaglia and J. A. Thomas, *Nature Chemistry*, 2009, **1**, 662-667.

[79] E. C. Long and J. K. Barton, *Acc. Chem. Res.*, 1990, **23**, 271-273.

[80] J. P. Sauvage, *Perspectives in Supramolecular Chemistry, vol. 5: Transition Metals in Supramolecular Chemistry*, John Wiley & Sons, Chichester, England, 1999.

[81] D. L. Nelson and M. M. Cox, *Lehninger Principles of Biochemistry*, 5th ed., W. H. Freeman and Company, New York, USA, 2008.

[82] N. E. Leadbeater, *Microwave Heating as a Tool for Sustainable Chemistry*, CRC Press, Boca Raton, Florida, USA, 2011.

[83] T. J. Mason and J. P. Lorimer, *Applied Sonochemistry*, Wiley-VCH, Weinheim, Germany, 2002.

Chapter II

Synthesis, characterization and spectroscopic studies of two new Schiff-base bithienyl pendant-armed 15-crown-5 molecular probes.

Published in:

B. Pedras; L. Fernandes; E. Oliveira; L. Rodríguez; M. M. M. Raposo; J. L. Capelo; C. Lodeiro.

Inorg. Chem. Commun., **2009**, *12*, 79-85.

Resumo

Dois novos ligandos constituídos por um éter 15-coroa-5 como unidade receptora e uma unidade de bitiofeno como sonda emissiva foram sintetizados e caracterizados de modo a avaliar as suas capacidades de coordenação, bem como o seu efeito sensor. O ligando **L1** apresenta uma unidade de éter-coroa aromático que está directamente ligada ao sistema π–conjugado imina-2,2'-bitiofeno, e o ligando **L2** é formado por uma unidade de éter coroa alifático ligada ao mesmo sistema imina-2,2'-bitiofeno através de um espaçador metileno. Complexos metálicos sólidos de Ni(II), Pd(II), Hg(II) e Na(I) foram sintetizados com ambos os sistemas macrocíclicos, e os ligandos foram estudados em solução na presença dos mesmos iões metálicos. Todos os compostos sólidos foram caracterizados através de técnicas analíticas e espectroscópicas correntes. O efeito sensorial foi averiguado usando espectroscopias de absorção, emissão e MALDI-TOF-MS.

A minha contribuição para este trabalho consistiu na síntese e caracterização de ambos os ligandos e de alguns dos complexos sólidos, bem como parte do estudo do efeito sensorial realizado por espectroscopias de absorção e emissão.

Abstract

Two new ligands provided with a 15-crown-5 as a receptor unit and bithiophene unit as an emissive probe have been synthesized and characterized in order to evaluate their coordination capabilities and sensor effect. Ligand **L1** presents an aromatic crown ether moiety that is directly linked to the imine-2,2´-bithiophene π–conjugated system, and ligand **L2** is constituted by an aliphatic crown ether moiety that is linked to the same imine-2,2´-bithiophene system through a methylene unit. Solid metal complexes of Ni(II), Pd(II), Hg(II) and Na(I) have been synthesized using both macrocyclic compounds, and have been studied in solution in the presence of the same metal ions. All solid compounds have been characterized by common analytical and spectroscopic techniques. The sensorial effect has been studied using absorption, emission and MALDI-TOF-MS spectroscopies.

My contribution to this work was the synthesis and characterization of both ligands and some of the solid complexes, as well as part of the sensorial effect studies by absorption and emission spectroscopies.

Very recently G. W. Gokel and coworkers [1] and S. Fery-Forgues and coworker [2] have reviewed the importance of crown ethers as molecular sensors for ions, as molecular scaffolds and as complexing agents. Many of these systems are provided with rigid binding units, molecular tweezers, butterfly structures, molecular rods, etc., presenting two well defined coordination units.

These compounds are very appealing due to their potential applications for simultaneous recognition of a transition metal ion and an alkaline or alkaline-earth metal ion [3-6]. The interaction with two metal ions normally modulates several interesting properties, as it has been reported previously. For example in compound I [3] (Scheme II.1) the complexation capability was modulated by the alkaline Na(I), in compounds II and III the redox behavior of the Ni(II) and Re(I) complexes, respectively, was modulated by the alkaline and alkaline earth metals [4, 5]. Finally, the liquid crystal property in compound IV has been also modulated in the presence of Na(I) [6]. Recently, we have synthesized and characterized several heterocyclic compounds functionalized with (oligo)thiophene π-conjugated systems for sensor applications [7]. Tertiary amines functionalized with a methylene crown ether moiety and two (oligo)thiophene pendants are one of the most recent examples of new heterocyclic sensors reported by us. In this case Na(I) or H^+ modulated the intensity of the emission shown by the Pd(II) complexes [7d].

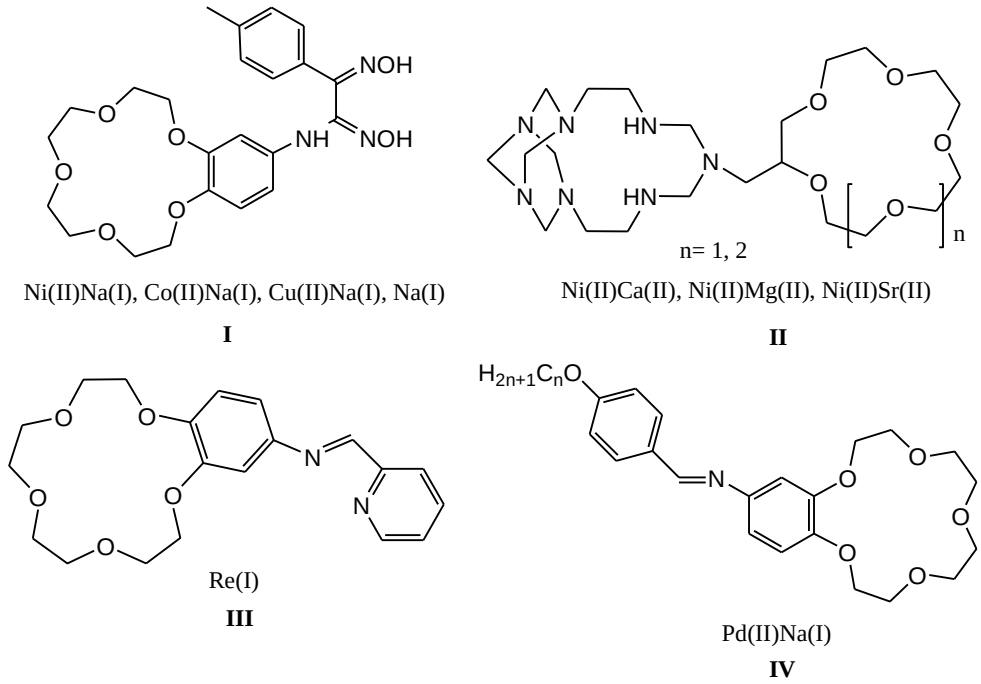

Ni(II)Na(I), Co(II)Na(I), Cu(II)Na(I), Na(I)

I

Ni(II)Ca(II), Ni(II)Mg(II), Ni(II)Sr(II)

II

III

IV

Scheme II.1.- Examples of crown ether ligands used for transition metal-alkaline metal combinations.

Active molecules that interact with analytes through the enhancement of any particular property are very appealing for analytical applications; particularly active molecules to be detected and used by spectrometry techniques are very interesting for their further use as MS-active matrices [8].

As part of our research project in multifunctional/multisensorial molecular probes and keeping this alkaline/alkaline-earth modulation properties idea in mind, we report here two new compounds**, L1** and **L2** (Scheme II.2), that are provided with a bithiophene emissive unit covalently linked through an imine bond to a 15-crown-5 chelating unit (Scheme II.2) [9]. We were particularly interested in exploring the effect of the flexibility of the chemical spacer between the bithiophene heterocyclic system and the crown ether moiety, and the influence of Na(I) on the spectroscopic properties. Moreover, solid metal complexes have been obtained by direct reaction between ligands **L1** and **L2** and nickel(II) perchlorate, palladium(II) tetrafluoroborate and mercury(II) triflate salts, respectively [10]. In all cases, mononuclear complexes have been isolated except when sodium(I) was added to the palladium(II) complexes, where dinuclear compounds Na(I)Pd(II) were obtained in both cases. The synthesis and characterization have been performed as reported [11].

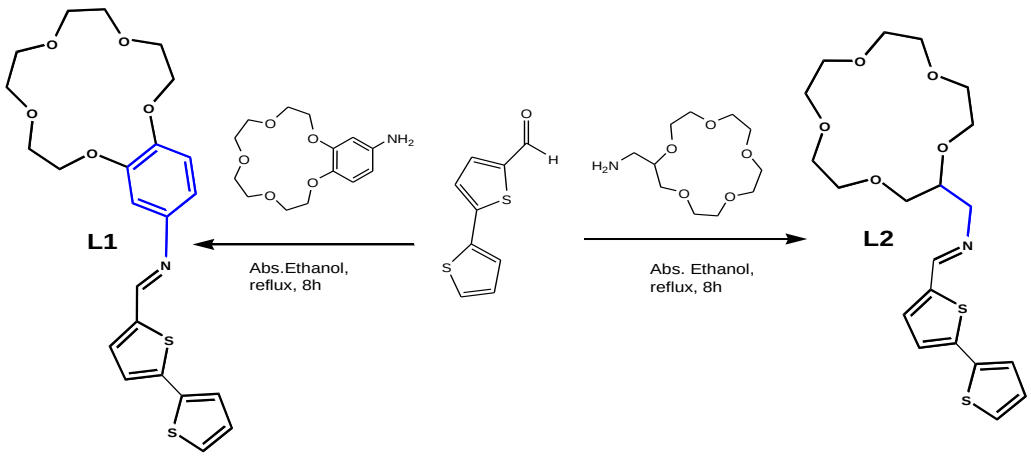

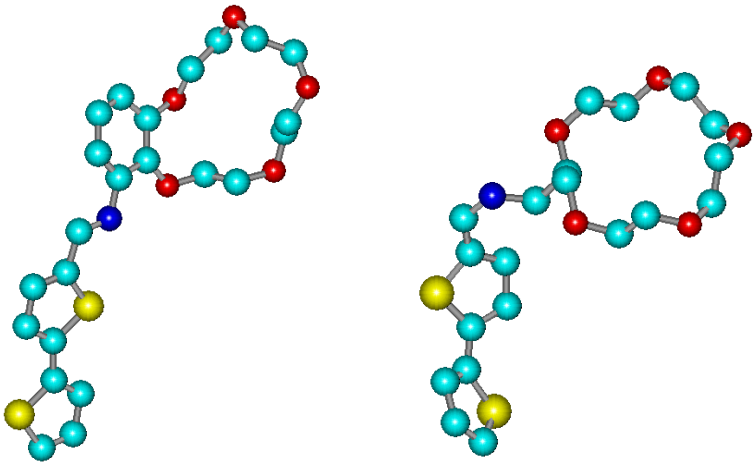

L1 **L2**

Scheme II.2.- Synthesis of **L1** and **L2** receptors, and computer drawn structures for both ligands produced with HYPERCHEM version 7.0, for illustration purposes only (bottom).

The electronic absorption characterizations of **L1** and **L2** were performed in acetonitrile solution and are shown in Figure II.1A. The absorption spectrum of **L1** shows two bands centered at 380 nm and 250 nm with molar absorption coefficients of 34.8 x 10^3 and 16.8 x 10^3 $M^{-1}cm^{-1}$, respectively.

Semi-empirical ZINDO/S electronic structure calculations indicated that these low energy transitions are predominantly π-π^* from the imine-bithiophene units

directly linked to the crown-ether and also with some contribution of the benzene group in **L1**.

L2 shows the most intense absorption band blue shifted with respect to **L1** with a maximum centered at 340 nm (11.3 x 10^3 $M^{-1}cm^{-1}$) and appears in the same region for the bithiophene precursor band (Figure II.1B).

Excitation of ligand **L1** at 380 and 402 nm does not show any fluorescence emission. On the other hand, excitation of **L2** at 340 nm shows a very low emission centered at 405 nm with a Stokes shift of 65 nm (Figure II.1). This emission is very similar in shape to the emission observed for the 2,2´-bithiophene precursor (Figure II.1B), but with a red-shift of 50 nm due to the electronic delocalization imposed by the imine bond.

The fluorescence quantum yield of **L2** in acetonitrile was found to be 0.028, and it was determined using a solution of quinine sulphate in H_2SO_4 0.5M as standard reference (ϕ = 0.546). [12]

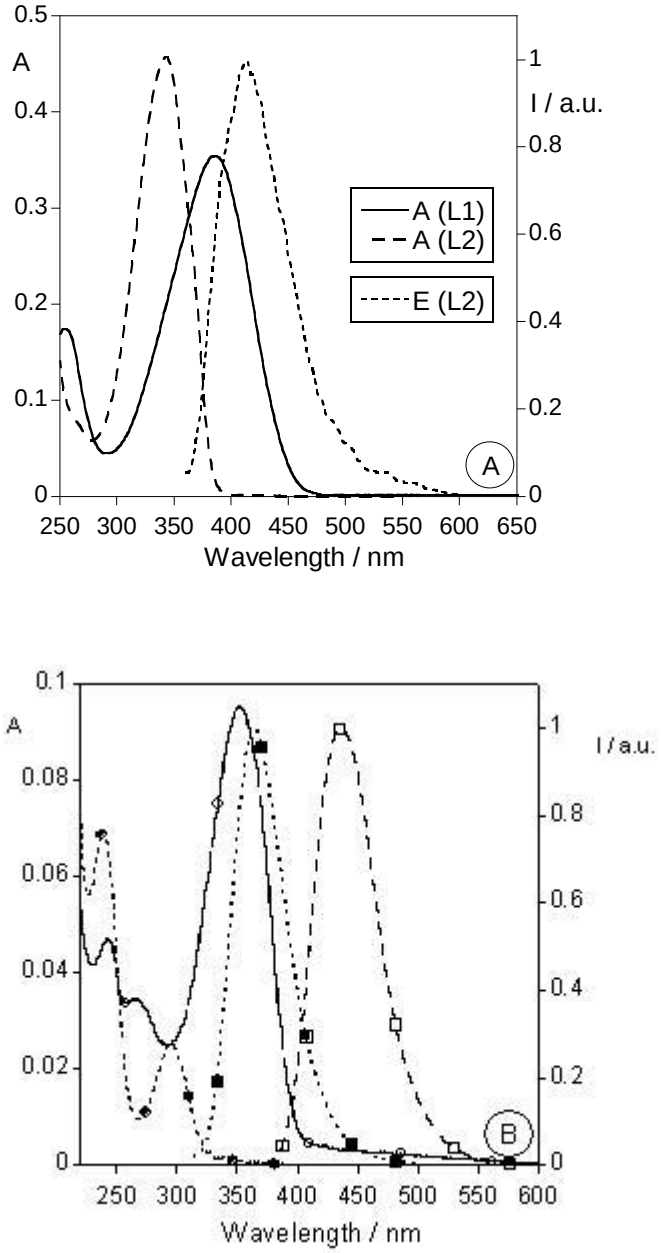

Figure II.1.- A) Absorption spectrum of **L1** and absorption and emission spectra of **L2** in acetonitrile solution ([**L1**] = 1.04 x 10^{-5}M; [**L2**] = 4.02 x 10^{-5}M, λ_{exc}= 361nm). B) Absorption (○) and emission (□) spectra of the organic precursor 2,2'-bithiophene-5-carbaldehyde. ([BTP] = 4.65x10^{-6}M, λ_{exc} = 354nm) and absorption (●) and emission (■) spectra of the precursor 4'-aminobenzo-15-crown-5 [4AMC] = 8.82 x10^{-6}M, λ_{exc}= 298nm) in acetonitrile.

The effect of Ni(II), Pd(II) and Hg(II) complexation on absorption, fluorescence and MALDI-TOF-MS spectra was studied by dissolving both ligands in acetonitrile and titrating with the metal ions.

The absorption spectra of **L1** in the presence of Pd(II) shows a small red-shift after the addition of one equivalent of metal. The bands are shifted from 250 to 270 nm, and from 380 to 405 nm. For the other studied metals no change was observed. On excitation of the complexes of **L1** at 380 or 405 nm, no emission was observed in all cases.

Ligand **L2** proves to be useful as absorption and fluorescence molecular probe for Ni(II), Pd(II) and Hg(II). Addition of Ni(II) and Hg(II) induced a red-shift of *ca.* 15 nm in the absorption spectra while Pd(II) showed a *ca.* 45 nm red-shift. (See Figure II.2A). At the same time, a very strong emission was observed upon Pd(II) complexation. The intensity of emission observed upon Ni(II) and Hg(II) addition was very small when compared with the Pd(II) complex. This emission is not affected after the addition of an excess of Na(I) (up to 100 equivalents).

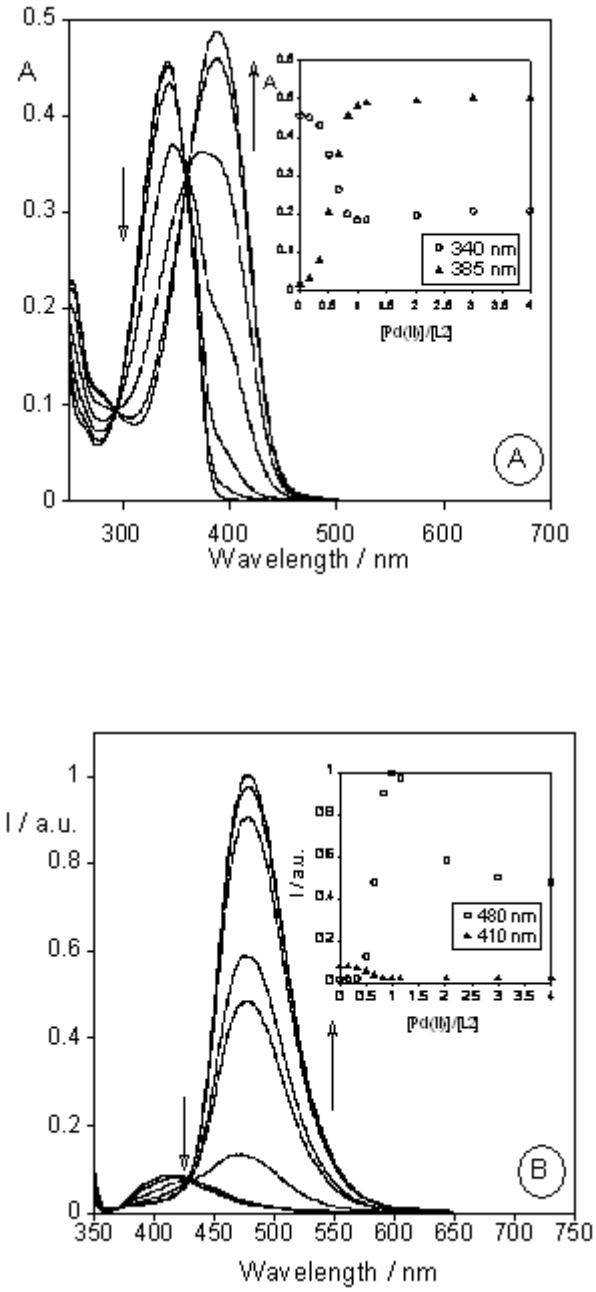

Figure II.2.- Absorption (A) and Emission (B) titration of **L2** in the presence of Pd(II) after addition of one initial equivalent of Na(I) in acetonitrile solution ([**L2**] = 4.02 x 10^{-5}M, λ_{exc}= 361nm). The insets show the absorption at λ_{abs} = 341 and 385 nm (Pd(II) complex) and fluorescence emission at 410 and 481 nm (Pd(II) complex).

Figure II.2A shows the absorption titration of ligand **L2** at different concentrations of Pd(II) after the addition of one equivalent of Na(I). Isosbestic points were observed at 296 and 362 nm, suggesting at least two species in solution, the complex L2-Na(I) and the Pd(II)Na(I) complex. The inset shows the absorption

maxima for the bands corresponding to these two species; changes in absorbance finished after addition of one equivalent of metal ion. These results are in agreement with the mononuclear complexes obtained by direct synthesis [10].

Fluorescence titration is represented in Figure II.2B upon excitation in the isosbestic point at 360 nm. The stoichiometry was also confirmed from this titration, panel B figure II.2; significant enhancement of the fluorescence intensity and a strong red shift were observed upon addition of one equivalent of Pd(II). Addition of the second equivalent of Pd(II) produced a partial quenching of the emission. The inset of Figure II.2B depicts the emission at 410 nm (ligand band) and at 480 nm (complex band); this effect could be attributed to a conformational change in the position and involvement of the bithiophene chromophore with the metal center, where the S-donor atoms have some interaction with the Pd(II).

Similar effect was reported recently by us with a family of tertiary amines bearing (oligo)thiophene and crown ether moieties. [7d]. This result suggests that ligand **L2** could be used as a new active emissive probe to detect Pd(II) by fluorescence spectroscopy in organic solvents, and points out the future application of **L2** as a probe for Pd(II) detection during organic synthesis with Pd(II) as a catalyst. It is also very important to mention that due to the open-shell electronic property of Pd(II) (d^8 element), a positive probe for Pd(II) detection is not common [13,7] because normally Pd(II) complexation produces a quenching in the fluorescence intensity.

A MALDI-TOF-MS study was performed using ligands **L1** and **L2**. The samples were dissolved in acetonitrile (1-2μg/μL) and no matrix was added to obtain the mass spectra [11].

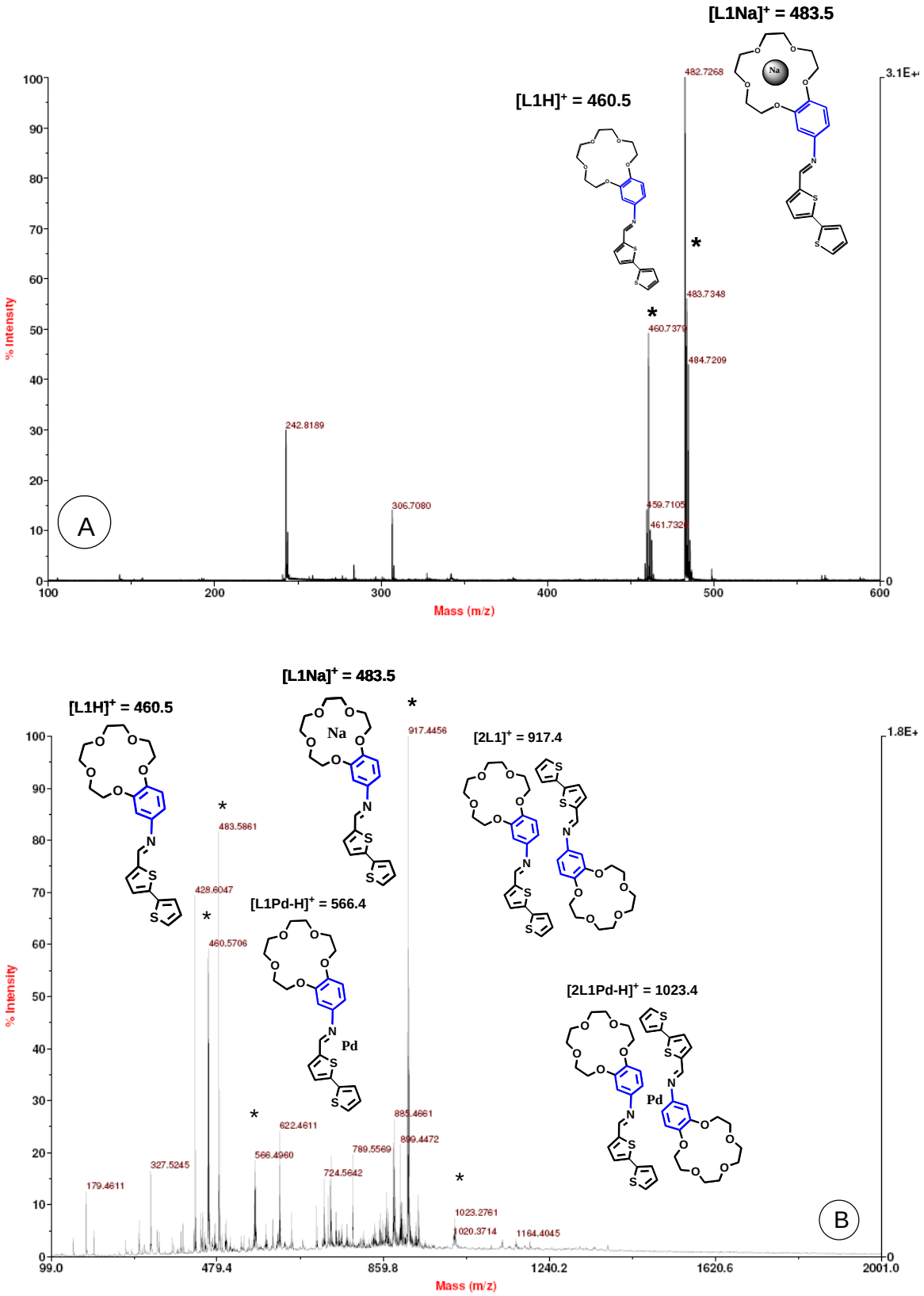

Figure II.3.- A) MALDI-TOF-MS spectra of **L1** in the presence of one equivalent of Na(I) without matrix in acetonitrile solution. B) MALDI-TOF-MS spectra of **L1**Na after the addition of one equivalent of Pd(II).

Figure II.3A shows the MALDI-TOF-MS spectrum without matrix of ligand **L1** after the addition of one equivalent of Na(I) metal ion. The spectrum shows strong peaks at 483.5 and 460.5 *m/z* that are attributable to the fragments [**L1**Na]$^+$ and [**L1**H]$^+$ respectively. Two small fragmentation peaks at 306.7 and 242.8 *m/z* can also be observed due to the fragmentation of the ligand.

Figure II.3B presents the bimetallic titration with Na(I) and Pd(II) by MALDI-TOF-MS spectrometry. The spectrum of ligand **L1** after the Na(I) and Pd(II) addition shows strong peaks at 460.5, 483.5 and 566.4 *m/z* that are attributable to the fragments [**L1**H]$^+$, [**L1**Na]$^+$ and [**L1**PdH]$^+$. Other peaks are observed due to fragmentation. At higher mass values, two peaks at 917.4 and 1023.4 *m/z* attributable to the association fragments of two ligands [2**L1**]$^+$ and metal complex [2**L1**Pd]$^\bullet$ are also observed.

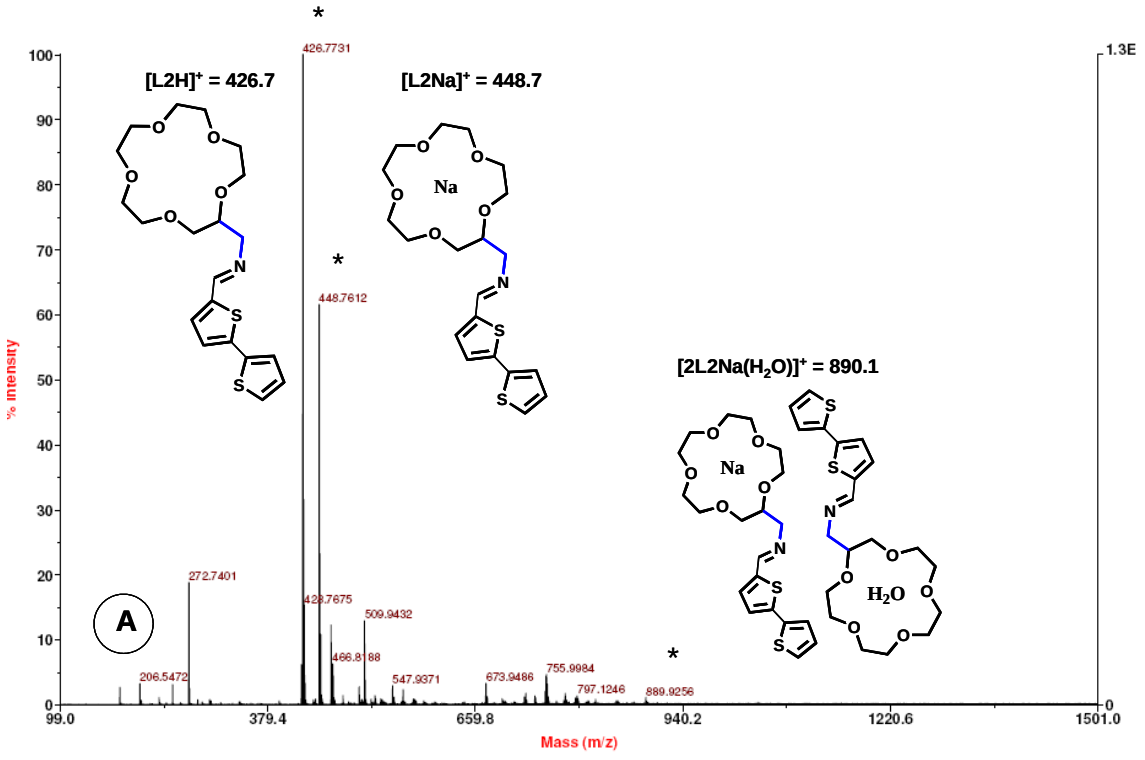

Figure II.4.- A) MALDI-TOF-MS spectra of **L2** in the presence of one equivalent of Na(I) without matrix in acetonitrile solution.

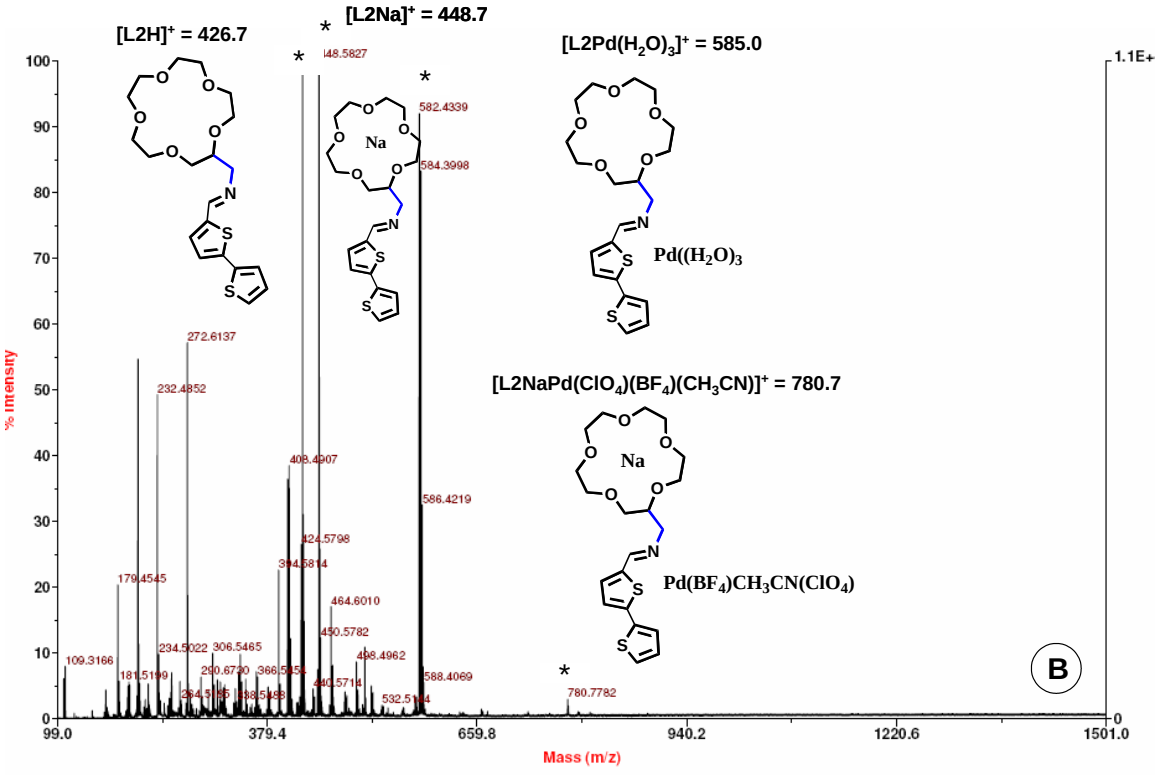

Figure II.4.- B) MALDI-TOF-MS spectra of **L2**Na after titration with one equivalent of Pd(II).

The same experiments have been carried out with ligand **L2**. Figure II.4A and B shows the MALDI-TOF-MS spectra of **L2** after sodium(I) addition and after sodium(I) and palladium(II) titration. In both experiments the ligand acts as chemosensor and as MALDI-TOF-MS active matrix.

Figure II.4A shows the most intense peaks at 426.7 and 448.7 *m/z* that are attributable to the [**L2**H]$^+$ and [**L2**Na]$^+$ fragments. At higher values, a peak at 890.1 *m/z* was observed. This peak is attributable to the species containing two ligands, one sodium atom and one water molecule.

Peaks at 585.0 and 780.7 corresponding to the species [**L2**Pd$(H_2O)_3$]$^+$ and [**L2**NaPd$(ClO_4)(BF_4)(CH_3CN)$]$^+$ can also be observed (see Figure II.4B).

Upon titration of **L2** with Ni(II), a peak at 583.5 *m/z*, attributed to the species [**L2**Ni(ClO_4)]$^+$, appears in the spectrum as the most intense one. In the presence of Hg(II), three peaks at 426.6, 448.6 and 662.2 *m/z* have been observed; these peaks can be attributed to the fragments [**L2**H]$^+$, [**L2**Na]$^+$ and [**L2**Hg$(H_2O)_2$]$^+$, respectively.

In order to compare these results with the solid complexes synthesized, all the metal complexes have been characterized by MALDI-TOF-MS spectrometry using the same procedure, and their results are summarized in the experimental section.

In conclusion, two new molecular probes containing a 15-crown-5 as receptor unit and a bithiophene unit as emissive chromophore have been synthesized and characterized. Their coordination and sensor capabilities using absorption, emission and MALDI-TOF-MS spectroscopies were explored.

All results show that ligands **L1** and **L2** can be used as new active probes for Pd(II), Pd(II)Na(I), Hg(II) and Ni(II) by absorption (**L1** and **L2**), fluorescence emission (**L2**) and MALDI-TOF-MS (**L1** and **L2**).

Acknowledgments

We thank Fundação para a Ciência e a Tecnologia (FCT) / FEDER (Portugal/EU) (Project PDTC/QUI/66250/2006 FCT-FEDER). B. Pedras and E. Oliveira acknowledge the FCT/Portugal for the PhD grants references SFRH/BD/27786/2006 and SFRH/BD/38909/2007.

References

[1] G. W. Gokel, W. M. Leevy, M. E. Weber, Chem. Rev. 104 (2004) 2723.

[2] S. Fery-Forgues, F. Al-ali, J. Phot. Photobiol. C. Photochem. Revs. 5 (2004) 139.

[3] (a) E. Karapinar, E. Özcan, J. Incl. Phen. Mac. Chem., 47 (2003) 59.

[4] (b) J-E. Jee, M. C. Chang, C-H. Kwak, Inorg. Chem. Commun., 7 (2004) 614.

[5] (c) K. M-C. Wong, W-P. Li, K. K-K. Cheung, V. W-W. Yam, New. J. Chem., 29 (2005) 165.

[6] (d) J. Arias, M. Bardají, P. Espinet, J. Organomet. Chem., 691 (2006) 4990.

[7] (a) R. M. F. Batista, E. Oliveira, S. P. G. Costa, C. Lodeiro, M. M. M. Raposo, Org. Lett. 9 (2007), 3201; (b) S. P. G. Costa, E. Oliveira, C. Lodeiro, M. M. M. Raposo, Sensors 7 (2007) 2096; (c) S. P. G. Costa, E. Oliveira, C. Lodeiro, M. M. M. Raposo, Tetrahedron Lett. 49 (2008) 5258; (d) R. M. F. Batista, E. Oliveira, S. P. G. Costa, C. Lodeiro, M. M.M. Raposo, Tetrahedron Letters 49 (2008) 6575. (e) R. M. F. Batista, E. Oliveira, C. Nunez, S. P. G. Costa, C. Lodeiro, M. M. M. Raposo, J. Phys. Org. Chem. 22 (2009) 362.

[8] B. Pedras, H. M. Santos, L. Fernandes, B. Covelo, A. Tamayo, E. Bértolo, T. Avilés, J. L. Capelo, C. Lodeiro, *Inorg. Chem. Commun*.,10 (2007) 925.

[9] Ligands **L1** and **L2** were prepared as follows. A solution of 4'-aminobenzo-15-crown-5 (**L1**) (1 mmol) or 2-(aminomethyl)-15-crown-5 (**L2**) (0.5 mmol) in absolute ethanol (30 mL) was added dropwise to a solution of 2,2'-bithiophene-5-carbaldehyde (1.0 (**L1**) or 0.5 (**L2**) mmol) in the same solvent (30 mL).
The resulting solution was gently refluxed with magnetic stirring for ca. 8 h. As no changes were observed, the solution was cooled to room temperature and kept under stirring 24h. A yellow solution was obtained in both cases, which after solvent removal rendered compounds **L1** and **L2** as a solid powder and an oil, respectively.

Both compounds were washed twice with diethyl ether (10 mL) and dried under vacuum.

L1: Color: Yellow. Yield 0.429 g (94 %). Anal. Calcd for $C_{23}H_{25}NO_5S_2 \cdot 2EtOH$: C, 58.78; H, 6.75; N, 2.55; S, 11.62. Found: C, 58.32; H, 6.20; N, 2.90; S, 11.54. IR (cm^{-1}): $\nu_{(C=Nimine)}$, 1610. ^1H NMR (400 MHz, CD_3CN): δ = 8.62 (s, 1H)$_{imine}$. δ = 7.70-6.70 (m, 8H), δ = 4.40-3.54 (m, 16H). MS (EI) *m/z*: 459.10 [**L1**]$^+$; 460.50 [**L1**H]$^+$

L2: Color: Orange. Yield 0.179 g (84%). Anal. Calcd for $C_{20}H_{27}NO_5S_2 \cdot 1.5H_2O$: C, 53.10; H, 6.68; N, 3.10; S, 14.17. Found: C, 53.00; H, 6.30; N, 2.90; S, 14.28. IR (cm^{-1}): $\nu_{(C=Nimine)}$, 1628. ^1H NMR (400 MHz, CD_3CN): δ = 8.24 (s, 1H) $_{imine}$, δ = 7.34 (d, 1H), δ = 7.27 (d, 1H), δ = 7.22 (d, 1H), δ = 7.15 (d, 1H), δ = 7.02-7.00 (m, 1H), δ = 3.70-3.40 (m, 21H). MS (EI) *m/z*: 425.13 [**L2**]$^+$; (MALDI-TOF-MS): 426.61 [**L2**H]$^+$

[10] **Metal complexes. General Procedure.**

L1: A solution of the corresponding metal salt (0.1 mmol, 25 mL) in acetonitrile was added to a solution of **L1** (0.1 mmol, 20 mL) in the same solvent. On the addition of the metal salt the solution changed from yellow to orange for Ni(II), yellow to red for Pd(II), and yellow to orange for Hg(II). The reaction mixture was stirred overnight at room temperature. In the case of the heterodinuclear compound of Pd(II)Na(II) after half an hour of the Pd(II) addition a solution of $NaClO_4.H_2O$ (0.1 mmol) in acetonitrile was added.

As no further changes were observed, the solvent was evaporated and a solid was obtained. All compounds were washed twice with cold diethyl ether (10 mL) and dried under vacuum.

L1Ni(BF$_4$)$_2$·H$_2$O: Color: Brown/red. Yield 0.063 g (81%). Anal. Calcd for $C_{23}H_{27}B_2F_8NNiO_6S_2$: C, 38.91; H, 3.83; N, 1.97; S, 9.03; Ni, 8.27. Found: C, 39.20; H, 3.81; N, 1.66; S, 8.93; Ni, 8.37. IR (cm^{-1}): $\nu_{(C=Nimine)}$, 1634; MS (MALDI-TOF-MS): 460.10 [**L1**H]$^+$; 623.09 [**L1**NiBF$_4$(H$_2$O)]$^+$.

L1Pd(CH$_3$CN)$_2$(BF$_4$)$_2$·5H$_2$O: Color: Red. Yield 0.068 g (68%). Anal. Calcd for $C_{27}H_{41}B_2F_8N_3O_{10}PdS_2$: C, 35.57; H, 4.53; N, 4.61; S, 7.03. Found: C, 35.14; H, 4.30;

N, 4.02; S, 7.29. IR (cm^{-1}): $\nu_{(C=Nimine)}$, 1650. MS (MALDI-TOF-MS): 653.80 [**L1**$PdBF_4$]$^+$.

L1Hg(CF_3SO_3)$_2$·H_2O: Color: Brown. Yield 0.056 g (53%). Anal. Calcd for $C_{25}H_{27}F_6HgNO_{12}S_4$: C, 30.75; H, 2.79; N, 1.43; S, 13.14; Hg, 20.55. Found: C, 31.06; H, 2.58; N, 1.25; S, 13.02; Hg, 20.75 IR (cm^{-1}): $\nu_{(C=Nimine)}$,1652. MS (MALDI-TOF-MS): 847.70 [**L1**Hg(CF_3SO_3).2H_2O]$^+$.

L1Pd(CH_3CN)$_2$(BF_4)$_2$$NaClO_4$·4$H_2O$: Color: Dark red. Yield 0.099 g (85%). Anal. Calcd for $C_{27}H_{39}B_2ClF_8N_3NaO_{13}PdS_2$: C, 31.90; H, 3.87; N, 4.13; S, 6.31. Found: C, 30.86; H, 3.30; N, 3.95; S, 6.38. IR (cm^{-1}): $\nu_{(C=Nimine)}$,1650. MS (MALDI-TOF): 804.65 [**L1**PdNa(BF_4)$_2$(CH_3CN)]$^+$.

L2: A solution of the corresponding metal salt (0.1 mmol, 25 mL) in acetonitrile or absolute ethanol was added to a solution of **L2** (0.1 mmol, 20 mL) in the same solvent. In the case of Ni(II) and Hg(II) absolute ethanol was used, while for Pd(II) acetonitrile was used, in order to avoid the palladium(II) reduction. On the addition of the metal salt the solution changed from yellow to red-orange for Pd(II), and did not change in the cases of Ni(II) and Hg(II). The reaction mixture was stirred overnight at room temperature.

As no further changes were observed, the solvent was evaporated and a solid was obtained. All compounds were washed twice with cold diethyl ether (10 mL) and dried under vacuum.

L2Ni(ClO_4)$_2$·5H_2O: Color: Yellow. Yield 0.116 g (44%). Anal. Calcd for $C_{20}H_{37}Cl_2NNiO_{18}S_2$: C, 31.10; H, 4.82; N, 1.80; S, 8.29; Ni, 7.59. Found: C, 31.53; H, 5.15; N, 1.79; S, 8.55; Ni, 7.80. IR (cm^{-1}): $\nu_{(C=Nimine)}$, 1654. MS (MALDI-TOF-MS): 426.61 [**L2**H]$^+$; 583.5 [**L2**Ni(ClO_4)]$^+$.

L2Pd(CH_3CN)$_4$(BF_4)$_2$: Color: Red. Yield 0.049 g (55%). Anal. Calcd for $C_{28}H_{39}B_2F_8N_5O_5PdS_2$: C, 38.66; H, 4.52; N, 8.05; S, 7.37. Found: C, 38.25; H, 4.87; N, 7.75; S, 7.75. IR (cm^{-1}): $\nu_{(C=Nimine)}$, 1650. MS (MALDI-TOF-MS): 426.76 [**L2**H]$^+$; 702.10 [**L2**Pd(CH_3CN)$_2$(BF_4)]$^+$.

L2Hg(CF_3SO_3)$_2$·H_2O: Color: Green. Yield 0.090 g (95%). Anal. Calcd for $C_{22}H_{29}F_6HgNO_{12}S_4$: C, 28.05; H, 3.10; N, 1.49; S, 13.61; Hg, 21.29. Found: C, 28.41; H, 3.26; N, 1.62; S, 13.47; Hg, 21.60. IR (cm^{-1}): $\nu_{(C=Nimine)}$, 1663. MS (MALDI-TOF-MS): 426.68 [**L2**H]$^+$; 776.53 [**L2**Hg(CF_3SO_3)]$^+$.

L2Pd(CH_3CN)$_2$(BF_4)$_2$$NaClO_4$: Color: Red. Yield 0.100 g (98 %). Anal. Calcd for $C_{24}H_{33}B_2ClF_8N_3NaO_9PdS_2$: C, 31.67; H, 3.65; N, 4.62; S, 7.05. Found: C, 31.32; H, 3.90; N,4.99; S, 6.74. IR (cm^{-1}): $\nu_{(C=Nimine)}$, 1656. MS (MALDI-TOF-MS): 426.75 [**L2**H]$^+$; 730.63 [**L2**PdNa(BF_4)$_2$]$^+$;742.10 [**L2**PdNa(ClO_4)(BF_4)]$^+$.

[11] **Chemicals and Starting materials**

4'-aminobenzo-15-crown-5, 2-(aminomethyl)-15-crown-5, 2,2'-bithiophene-5-carbaldehyde, and Ni(ClO_4)$_2$6H_2O, Ni(BF_4)$_2$6H_2O, Pd(BF_4)$_2$.4(CH_3CN) and $NaClO_4$ were commercial products from Aldrich used without further purification. Hg(CF_3SO_3)$_2$ was a commercial product from Strem-Chemicals. Solvents were of reagent grade purified by the usual methods.

Instrumentation

Elemental analyses were carried out by the REQUIMTE DQ, Universidade Nova de Lisboa Service on a Thermo Finnigan-CE Flash-EA 1112-CHNS Instrument. Infrared spectra were recorded as KBr discs or in Nujol using Bio-Rad FTS 175-C spectrophotometer. Proton NMR spectra were recorded using a Bruker WM-450 spectrometer. Electronic Impact spectra were determined on a Micromass GCT-TOF7000 and the MALDI-TOF-MS analysis have been performed in a MALDI-TOF-MS model voyager DE-PRO biospectrometry workstation equipped with a nitrogen laser radiating at 337 nm from Applied Biosystems (Foster City, United States) at the REQUIMTE, Chemistry Department, Universidade Nova de Lisboa. The acceleration voltage was 2.0 x 10^4 kV with a delayed extraction (DE) time of 200 ns. The spectra represent accumulations of 5 x 100 laser shots. The reflectron mode was used. The ion source and flight tube pressures were less than 1.80 x 10^{-7} and 5.60 x 10^{-8} Torr, respectively. The MALDI mass spectra of the soluble samples (1 or 2 μg/μL) such as the metal salts were recorded using the conventional sample preparation method for MALDI-MS. One microliter was put on the sample holder on which the chelating ligand had been previously spotted. The sample holder was inserted in the ion source. Chemical reaction between the ligand and metal salts occurred in the holder and complexed species were produced.

Absorption spectra were recorded on a Perkin Elmer lambda 35 spectrophotometer and fluorescence emission on a Perkin Elmer LS45. The linearity of the fluorescence emission *vs.* concentration was checked in the concentration range used (10^{-4}-10^{-6} M). A correction for the absorbed light was performed when necessary. All spectrofluorimetric titrations were performed as follows: the stock solutions of the ligand (*ca.* 1.00 x 10^{-3} M) were prepared by dissolving an appropriate amount of the ligand in a 50 mL volumetric flask and diluting to the mark with absolute EtOH or acetonitrile UVA-sol. The titration solutions ([**L**] = 1.00 x 10^{-6} and 1.00 x 10^{-5} M) were prepared by appropriate dilution of the stock solutions. Titrations of both ligands were carried out by addition of microliter amounts of standard solutions of the ions in absolute ethanol or acetonitrile.

Semi-empirical molecular orbital calculations were carried out using HYPERCHEM version 7.0. Hypercube Inv., 1115 NW 4th St., Gainsville, FL. 32601-4256, USA.

Nickel(II) was measured with a Varian (Cambridge, UK) atomic absorption spectrometry model Spectra AA 20 plus equipped with a 10 cm burner head. Hollow-cathode lamps operated at 4 mA were used as radiation source. The wavelength (nm) and slit width (nm) used were 352.4 and 0.5.

Mercury(II) was determined in a Flow Injection System consisting of: a four channels Gilson (Villiers le Bel, France) Minipuls 2 peristaltic pump, a four channels Ismatec (Glattbrugg, Switzerland) programmable peristaltic pump model Reglo Digital MS-4/12; a Perkin-Elmer (Uberlingen, Germany) membrane gas-liquid separator; a six-port injection valve (Supelco, Bellefonte, PA) with a 500-µL loop, and a Fisher and Porter (Warminster, PA) flow meter (0–100% N_2, 200 ml min^{-1}). Ismatec tygon tubing type R3607 of different internal diameters (2.06 and 3.15 mm id), was used for carrying the reducing agent, carrier solution, and waste solution. The initial conditions for cold vapour generation using $SnCl_2$ as a reducing agent were established in a previous works [14] and were: a 5% mass v^{-1} $SnCl_2$ solution in 10% v.v^{-1} HCl was used as reducing stream with a 3 mL min^{-1} flow rate; a 3% v.v^{-1} HCl solution was used as carrier with a 10 mL min^{-1} flow rate. A 200 mL min^{-1} flow-rate of carrier gas (N_2) was used. Mercury atomic absorbance was measured with a Thermo (Cambridge, UK) atomic absorption spectrometer model Solar S2 equipped with a homemade quartz tube. The quartz tube was kept at room temperature during operation. A mercury hollow-cathode lamp (Thermo) operated at 4 mA was used as a

radiation source. The mercury line at 253.7 nm and a slit width of 0.5 nm were used for measurements. An inorganic mercury stock standard solution (Merck, Darmstat, Germany, 1 $g.L^{-1}$) was used. All stock standard solutions were stored in a refrigerator at 4 ˚C and protected from light. Working standard solutions were prepared just before use by appropriate dilution of the stock standard solution. Sn(II) chloride used as reducing agent was prepared by dissolving the appropriate mass of Sn(II) chloride dehydrate (Panreac, Barcelona, Spain) in concentrated hydrochloric acid and diluted with ultrapure water. Diluted hydrochloric acid (Merck) was used as carrier.

[12] M. Montalti, A. Credi, L. Prodi, M. T.Gandolfi, “Handbook of Photochemistry”, 3th Ed. CRC Press, Taylor & Francis Group, Boca Raton, New York (2006).

[13] (a) Q. E. Cao, Z. D. Hu, Ind. J. Chem. A 11 (1998) 1029; (b) Q. E. Cao, Y. K. Zhao, X. J. Yao, Z. D. Hu, Q. H. Xu, Spectrochim. Acta A 56 (2000) 1319

[14] (a) J.L. Capelo, G. M. Rivas, L. G. Oliveira, C. Villena, A. C. Santos, T. Valada, M. Galesio, P. Oliveira, M. D. R. Gomes de Silva, E. Gaspar, S. Alves, C. Fernandez,; Vaz, C.; Talanta, 68 (2006) 813. (b) A. Tamayo, B. Pedras, C. Lodeiro, L. Escriche, J. Casabo, J. L. Capelo, B. Covelo, R. Kivekäs, R. Sillampää, Inorg. Chem., 46 (2007) 7818.

Chapter III

Sensing Metal Ions with Two New Azomethine-Thiophene Pincer ligands (NSN): Fluorescence and MALDI-TOF MS applications.

Published in:

B. Pedras; H. M. Santos; L. Fernandes; B. Covelo; A. Tamayo; E. Bértolo; J. L. Capelo; T. Avilés; C. Lodeiro.
Inorg. Chem. Commun., **2007**, *10*, 925-929.

Resumo

Neste trabalho apresentam-se dois novos ligandos do tipo pinça azometino-tiofeno **L1** e **L2**, bem como os seus estudos espectroscópicos por absorção, fluorescência e MALDI-TOF-MS. Os dois novos sistemas sintetizados combinam as sondas emissivas pireno e naftaleno com as boas propriedades quelantes de um sistema doador tridentado do tipo SN_2 apresentadas por um ligando do tipo tiofeno – base de Schiff. Ambos os ligandos originaram complexos sólidos analiticamente puros com sais de Ni(II) e Pd(II). O derivado bicromofórico de pireno, **L2**, apresenta duas bandas de emissão em solução, uma correspondente à espécie monomérica e outra desviada para o vermelho, atribuível ao excímero intramolecular. A complexação com Ni(II) e Pd(II) afecta a conformação em solução, aumentando a emissão do monómero em detrimento da banda do excímero; este efeito poderia ser explorado em sensoriamento de metais. O sistema **L1** exibe um comportamento não-emissivo. Foram também efectuadas reacções de complexação *in situ* seguidas por espectrometria de MALDI-TOF-MS sem matriz; estas experiências demonstram que **L1** pode ser um potencial sensor químico de Ni(II) e Pd(II).

A minha contribuição para este trabalho consistiu na síntese e caracterização de **L1, L2** e dos seus complexos metálicos sólidos, bem como os estudos de absorção e emissão com ambos os ligandos na presença de sais metálicos.

Abstract

The two new pincer azomethine-thiophene ligands **L1** and **L2**, their absorption, fluorescence and MALDI-TOF-MS spectroscopic studies are described. The two synthesized systems combine the emissive probes pyrene and naphthyl with the good chelating properties of a tridentate SN_2 donor-set from a thiophene Schiff-base ligand. Both ligands gave analytically pure solid complexes with Ni(II) and Pd(II) salts. The bichromophoric pyrene derivative **L2** presents two emission bands in solution, one corresponding to the monomer species and a red-shifted band attributable to the intramolecular excimer. Ni(II) and Pd(II) complexation affects the conformation in solution, increasing the monomer emission at the expense of the excimer band; this effect could be explored in metal ion sensing. System **L1** behaves as a non emissive probe. *In situ* complexation reactions followed by MALDI-TOF-MS spectrometry without matrix support have also been performed; these experiments show that **L1** could be a potential chemosensor for Ni(II) and Pd(II).

My contribution to this work was the synthesis and characterization of **L1, L2** and its solid metal complexes, as well as the absorption and emission studies of both ligands in the presence of metal salts.

Fluorescence is a widely used method to study chemical sensors, and its applications are rapidly expanding; fluorescence studies offer various possibilities to study the behavior of a sensor, based upon changes in the signal intensity, the formation of excimer/exciplex compounds, energy or electron transfer processes, wavelength modification (excitation and emission), and lifetime. Other techniques such as absorption spectroscopy, electro and magneto chemical measurements, and MALDI-TOF-MS spectrometry can be also used for the study of chemical sensors. In particular, MALDI-TOF-MS spectrometry is a strong analytical tool which has been used to study proteins and other compounds with high molecular weights; however, its use to study small molecules and for the analysis of inorganic complexes is less documented [1].

Selective detection of metal ions and anions by using self-organized Schiff-base host molecules has attracted much attention [2]. Several conjugate macrocyclic and acyclic Schiff-base chemosensors based on polyoxa and/or oxa-aza [3], polyaza [4], and azathia [5] as receptor units, can be found in the scientific bibliography. In many of them coordinative aromatic units are employed to modulate the sensorial properties [6]. Thiophene is a heterocyclic ring often employed in materials such as conjugated polymers [7], conductivity-based sensory devices [8], novel drugs [9], optoelectronic devices [10], bio-diagnostics devices [11], and nonlinear optical compounds [12]. Thiophene is chemically stable and easy to process, which explains its successful application in such varied fields [13], however, it has been considerably less used in single molecular chemosensors.

In recent years we have studied a number of polyaza and polyoxa aza systems as potential chemosensors for the recognition of metal ions and anions, as temperature sensors, and as elemental molecular machines, studying their dynamics/energetic effects and using the excimer formation/detachment as our analysis tool [14b]. As part of our research in multifunctional/multisensorial molecular probes, we present herein two systems that combine the emissive probes pyrene and naphthyl with the good chelating properties of a tridentate SN_2 donor-set from a thiophene Schiff-base ligand. We were particularly interested on the effect of the thiophene ring as aromatic spacer and/or its potential involvement in sensitive effects via excimer formation. The two multifunctional probes presented here could be used

to detect metal ions in solution, by following the sensorial effect based on the emitted light (fluorescence) or the changes observed in the MALDI-TOF-MS spectra due to the formation of complexated species.

Both bichromophoric systems have been synthesized by direct reaction between thiophene-2,5-dicarbaldehyde (1) and the appropriate pyrene or naphthalene amine [15] following the reaction scheme presented in Figure III.1. Moreover, solid metal complexes have been obtained by direct reaction between ligands **L1** and **L2** and the $Ni(ClO_4)_2 \cdot 6H_2O$ and $Pd(CH_3CN)_4(BF_4)_2$ metal salts. In all cases, mononuclear complexes have been isolated and characterized [16]. The synthesis was also attempted using the perchlorates of Ag(I), Cu(I), Hg(II), Cd(II), Cu(II) and Zn(II); however, under the experimental conditions employed, no analytically pure products were recovered.

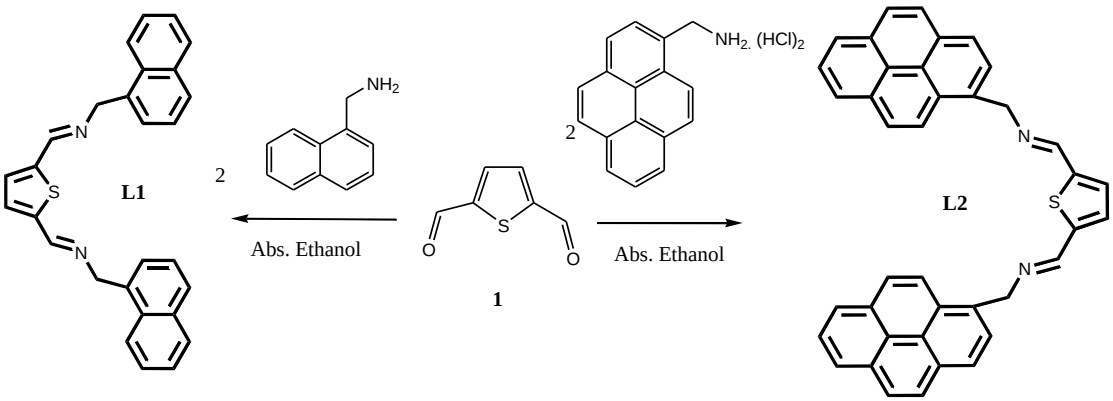

Figure III.1.- Synthesis of L1 and L2 receptors.

Spectroscopic characterization of **L1** and **L2** in dichloromethane solution is shown in Figure SM III.1. The absorption spectrum of **L1** shows a band centered at 300 nm, typical for naphthalene-containing compounds [17]. **L2** shows a band characteristic of pyrene derivatives, which has a vibrational fine structure with five maxima at 266, 277, 317, 331 and 348 nm [18]. Excitation of ligand **L1** at 300 and 340 nm reveals that both naphthalene units are totally quenched. However, excitation of ligand **L2** at 350 nm shows the characteristic pyrene emission bands attributable to a monomer at 400 nm, and an excimer at 525 nm (Figure III.2) [18]. In the solid state, the monomer band disappears and the red-shifted and less structured excimer band appears at ca. 580 nm.

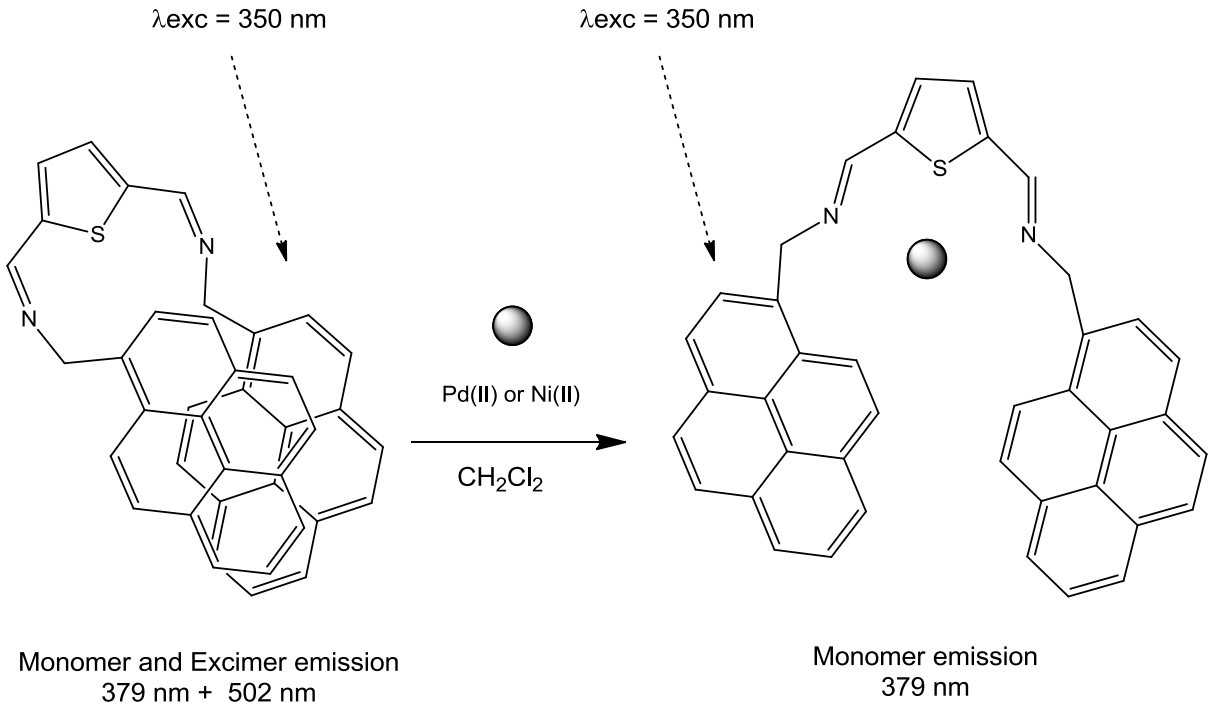

Figure III.2.- Excimer-monomer emissions in ligand **L2** upon metal complexation.

The effect of Ni(II) and Pd(II) complexation on absorption, fluorescence and MALDI-TOF-MS were studied dissolving both probes in dichloromethane. **L1** proved to be a useful molecular device using absorption and MALDI-TOF-MS techniques, while **L2** proved to be useful as absorption and fluorescence molecular chemosensor. Figure III.3 shows the absorption titration of ligand **L1** at different concentrations of Ni(II) and Pd(II). Isosbestic points are observed in both cases at 335 and 329 nm, respectively, suggesting at least two species in solution, the free ligand and the metal complex. The insets show the absorption maxima for both ligands; changes in absorbance finished after addition of one equivalent of each metal ion.

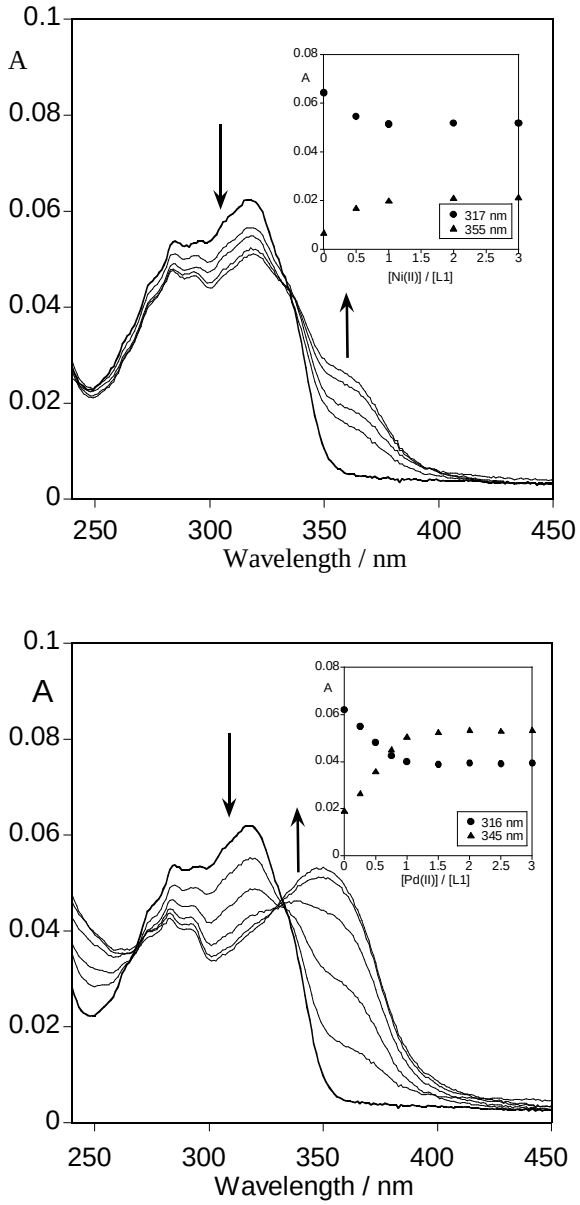

Figure III.3.- Absorption spectra of **L1** in the presence of Ni(II) (up) and Pd(II) (down) in the concentration range of 0 - 3 equivalents, in dichloromethane solution ([**L1**] = 1 x 10^{-5}M.). The insets show the absorption at λ_{abs} = 317 and 355 nm (Ni(II) complex) and absorption at 316 and 345 nm (Pd(II) complex).

A MALDI-TOF-MS study in dichloromethane was performed using ligand **L1**. The samples were dissolved in dichloromethane (1-2μg/μL) and no matrix was added to obtain the mass spectra. Figure III.4 presents the MALDI-TOF-MS spectra of ligand **L1** and the respective Ni(II) and Pd(II) complexation in dichloromethane. The spectrum of ligand **L1** shows strong peaks at 419 [**L1**H]$^+$, and fragmentation peaks at

279 and 141 *m/z*, attributable to the fragments $[\mathbf{L1}\text{-}C_{11}H_9]^+$ and $[C_{11}H_9]^+$. A peak corresponding to the species $[2\mathbf{L1}]^+$ at 835.6 *m/z* can also be observed (see fragmentations in Figure SM III.2). Upon complexation with Ni(II), a peak at 478.7 *m/z*, attributed to the species $[\mathbf{L1}Ni]^+$, appears in the spectrum. In the presence of Pd(II), three peaks at 523.6, 649.5 and 941.6 *m/z* have been observed; these peaks can be attributed to the fragments $[\mathbf{L1}Pd]^+$, $[\mathbf{L1}Pd(CH_3CN)_3]^+$ and $[2\mathbf{L1}+Pd]^+$, respectively. These results indicate that compound **L1** can be used as a new active complexed probe by absorption and MALDI-TOF-MS. The recorded spectra agree with the MALDI-TOF-MS results for the synthesized solid samples (see Figure SM III.3).

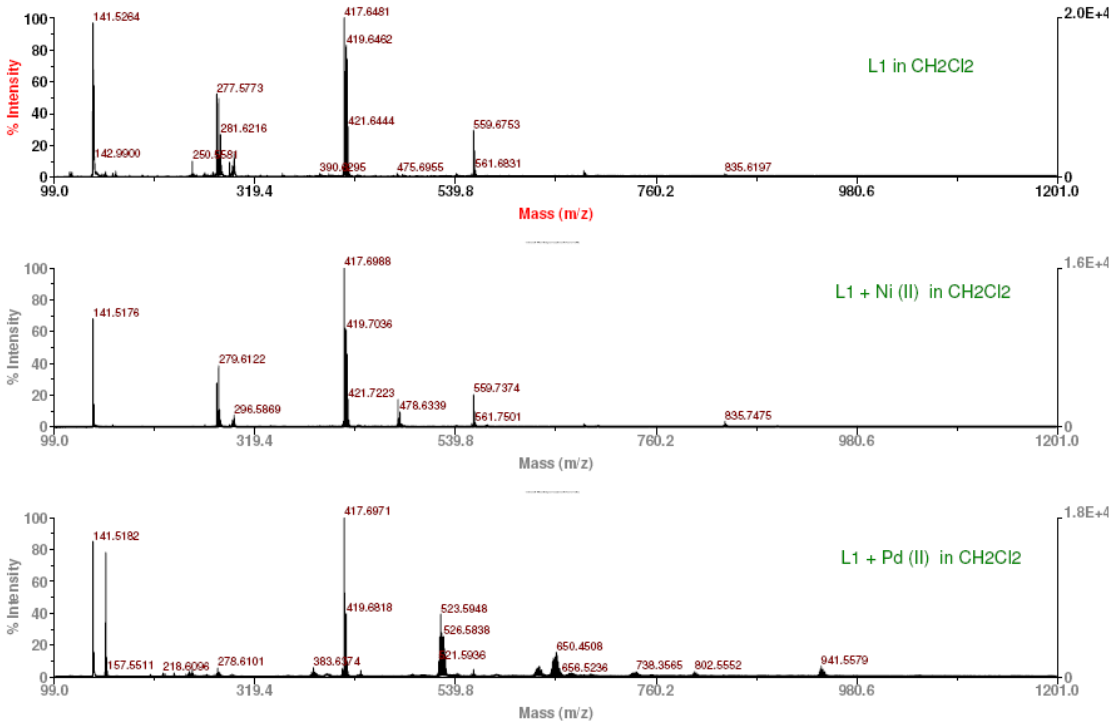

Figure III.4.- MALDI-TOF-MS spectra of free ligand **L1** (top), and **L1** in the presence of one equivalent of Ni(II) (middle) and Pd(II) (bottom), in dichloromethane.

Coordination of Ni(II) and Pd(II) to ligand **L2** was followed by absorption and fluorescence emission spectroscopies. Figure III.5 shows the Ni(II) metal titration in dichloromethane. Titration with Pd(II) gave similar results and is given in Figure SM III.4, supplementary material. Panel A of Figure III.5 shows the absorption titration of **L2** with $Ni(ClO_4)_2$. As it can be seen in this figure, the addition of Ni(II) to a dichloromethane solution of **L2** causes a red shift of the pyrene bands, and a decrease of their extinction coefficients. Such changes can be attributed to metal ion

complexation by the ligand. These changes were complete upon addition of one equivalent of Ni(II) ion, which suggests that each molecule of **L2** interacts with one Ni(II) ion.

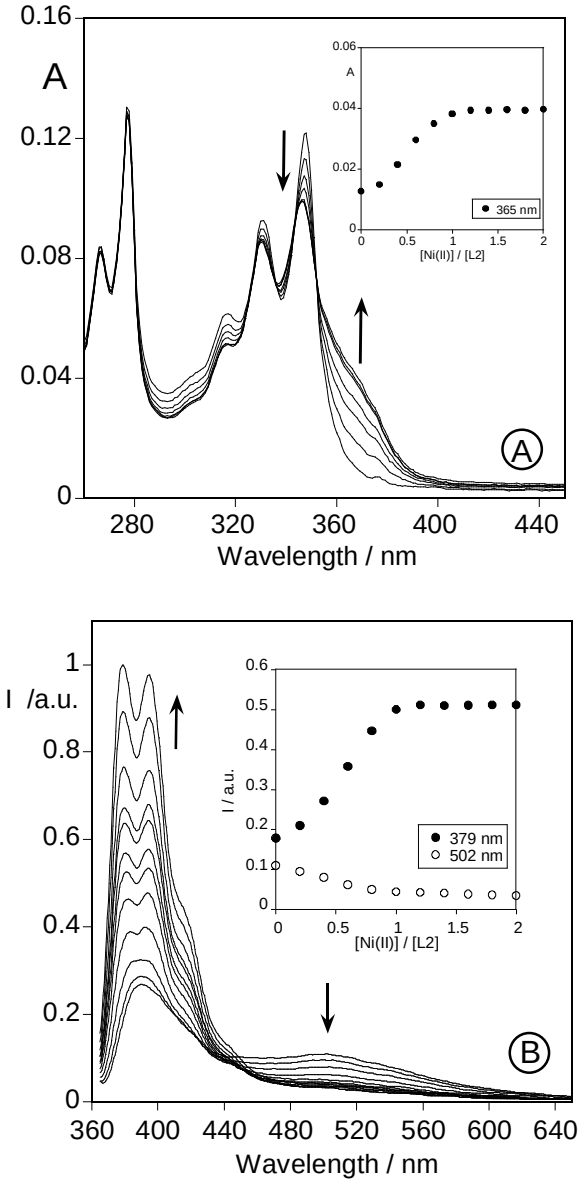

Figure III.5.- Absorption (A) and fluorescence (B) spectra of **L2** in the presence of Ni(II) in the concentration range of 0 - 2 equivalents, in dichloromethane solution ([**L2**] = 1 x 10^{-6}M. λ_{exc} = 350 nm). Inset shows (A) absorption at 365 nm and (B) intensity of emission as a function of [Ni(II)]/[**L2**] at λ_{em} = 379 nm (monomer) and 502 nm (excimer).

Such stoichiometry was also determined from the fluorescence titrations, Panel B of Figure III.5; significant enhancement of the fluorescence intensity of the monomer band, and simultaneous decrease in the intramolecular excimer band was observed upon the addition of Ni(II). The inset of Figure III.5B depicts the emission at 379 nm (monomer band) and at 502 nm (excimer band); this effect is attributed to a conformational change in the position of both chromophores in the metal complex [18]. These results suggest that ligand **L2** could be used as a new active emissive probe to detect Ni(II) and Pd(II) by absorption and fluorescence spectroscopies.

Acknowledgments

We are indebted to Fundação para a Ciência e a Tecnologia (FCT) / FEDER (Portugal/EU) (Project POCI/QUI/55519/2004 FCT-FEDER), and Canterbury Christ Church University Research Fund for financial support. E.B, J.L.C. and C. L also thank bilateral program “Acções integradas Luso-Británicas 2006” for the bilateral agreement numbers B-16/06 and B-61/07. B.P acknowledges the FCT/Portugal for the PhD grant SFRH/BD/27786/2006.

References

[1] (a) K. Matsumoto, H. Ajiro, S. Habaue, Y. Okamoto, Rapid Commun. Mass Spectrom. 17 (2003) 678. (b) R. Lobinski, D. Schaumloffel, J. Szpunar, Mass Spectrometry Reviews, 25 (2006) 255-289. (c) A. V. Hirner, Anal. Bioana. Chem. 385 (2006) 555.

[2] (a) B. Linton, A. D. Hamilton, Chem. Rev., 97 (1997)1669. (b) M. S. Godman, J. Weiss, A. D. Hamilton, V. Jubian, B. Linton, A. D. Hamilton, J. Am. Chem. Soc., 117, (1995) 11610. (c) M. Al-Sayah, N. R. Branda, Angew. Chem. Int. Ed. 39 (2000) 945. (d) T. Moriuchi, M. Nishiyama, T. Hirao, Eur. J. Inorg. Chem., (2002) 447, and references therein. (e) T. F. Jiao, M. H. Liui, J. Phys. Chem., B, 109 (2005) 2532. (f) O. Ramstrom, J. M. Lehn, Nature Rev. Drug Disc. 1 (2002) 26.

[3] (a) C. Lodeiro, J. L. Capelo, J. Incl. Phen. Macro. Chem., 49 (2004) 249. (b) Z. Ma, R. D. Yang, L. Yan, Chin. Chem. Let. 10 (1999) 995. (c) Z. Ma, R. D. Yang, L. Yan, J. Chem. Res. S., 21 (1999) 712.

[4] (a) W. Radecka-Paryzek, V. Patroniak, J. Lisowski, Coord. Chem. Rev., 249 (2005) 2156. (b) A. M. Herrera, G. V. Kalayda, J. S. Disch, R. P. Wilstrom, I. V. Korendovych, R. J. Staples, C. F. Campana, Q. Y. Nazarenko, T. E. Haas, E. V. Rybak-Akimova, Dalton Trans., 23 (2003) 4482. (c) S. C. Menon, A. Panda, H. B. Singh, R. J. Butcher, Chem. Commun., 2 (2000) 143.

[5] (a) A. T. Chaviara, P. J. Cox, K. H. Repana, A. A. Pantazaki, K. t. Papazisis, A. H. Kortsaris, D. A. Kyriakidis, G. St Nikolov, C. A. Bolos, J. Inorg. Biochem., 99 (2005) 467. (b) D. Habibi, A. E. Movahhed, Rus. J. Inorg. Chem., 48 (2003) 844. (c) D. H. Won, C. H. Lee, Tetrahedron Letters, 42 (2001) 1969. (d) H. Adams, M. R. J. Elsegood, D. E. Fenton, S. L. Heath, S. J. Ryan, Inorg. Chem. Commun., 2 (1999) 139. (e) H. Adams, D. E. Fenton, S. J. Ryan, Inorg. Chem. Commun., 2 (1999) 52. (f) H. Adams, N. A. Bailey, S. R. Collinson, D. E. Fenton, J. C. Hawley, S. J. Kitchen, J. Organometal. Chem., 550 81998) 7. (g) P. Dias, A. Domenech, E. García-España, C. Soriano, Polyhedron, 21 (2002) 1523.

[6] (a) D. Esteban, D. Bañobre, R. Bastida, A. de Blas, A. Macías, T. Rodríguez-Blás, D. E. Fenton, H. Adams, J. Mahía, Inorg. Chem., 38 (1999) 1937. (b) M. D. Fernández-Fernández, R. Bastida, A. Macías, P. Perez-Lourido, L. Valencia., Inorg. Chem., 45 (2006) 2266. (c) A. Tamayo, L. Escriche, C. Lodeiro, J. Ribas-Ariño, J. Ribas, B. Covelo, J. Casabo, Inorg. Chem., 45 (2006) 7621. (d) A. Tamayo, J. Casabo, C. Lodeiro, B. Covelo, C. D. Brondino, R. Kivekas, R. Sillampaa, Inorg. Chem., 45 (2006) 1140. (e) C. Lodeiro, R. Bastida, E. Bértolo, A. Rodríguez, Can. J. Chem., 82 (2004) 437.

[7] (a) D. T. McQuade, A. E. Pullen, T.M. Swager, Chem. Rev., 100 (2000) 2537. ; (b) Y. Coskun, A. Cirpan, L. Toppare, J. Mat. Science, 42 (2007) 368
(c) M. Sebastian, M. Hissler, C. Fave, J. Rault-Berthelot, C. Odin, R. Reau, Angew. Chem. Int. Ed., 45 (2006) 6152.

[8] D. M. Vriezema, J. Hoogboom, K. Velonia, K. Takazawa, P. C. M. Christianen, J. C. Maan, A. E. Rowan, R. J. M. Nolte, Angew. Chem. Int. Ed. 42 (2003) 772.

[9] C. Wu, E. R. Decker, N. Blok, H. Bui, T. J. You, J. Wang, A. R. Bougoyne, V. Knowles, K. L. Berens, G. W. Holland, T. A. Brock, R. A. F. Dixon, J. Med. Chem. 47 (2004) 1969.

[10] (a) M. Halik, H. Klauk, U. Zschieschang, G. Schimd, S. Ponomarenko, S. Kirchmeyer, W. Weber, Adv. Mater. 15 (2003) 917. (b) Y. M. Sun, Y. W. Ma, Y. Q. Liu, Y. Y. Lin, Z. Y. Wang, Y. Wang,C. G. Di, K. Xiao, X. M. Chen, W. F. Qiu, B. Zhang, G. yu, W. P. Hu, D. B. Zhu, Adv. Func. Mat., 16 (2006) 426.

[11] (a) K. Dore, M. Leclerc, D. Boudreau, J. Fluorescence, 16 (2006) 259. (b) K. Dore, S. Dubus, H. A. Ho, I. Levesque, M. Brunette, G. Corbeil, M. Boissinot, G. Boivin, M.G. Bergeron, D. Boudreau, M. Leclerc, J. Am. Chem. Soc., 126 (2004) 4240.

[12] (a) M. M. M. Raposo, A. M. R. C. Sousa, G. Kirsch, P. Cardoso, M. Belsey, E. D. Gomes, A. M. C. Fonseca, Org. Lett. 8 (2006) 3681.

[13] G. Barbarella, M. Melucci, G. Sotgiu, Avd. Mat. 17 (2005) 1581.

[14] (a) J. Pina, J. S. De Melo, F. Pina, C. Lodeiro, J. C. Lima, A. J. Parola, C. Soriano, M. P. Clares, M. T. Albelda, R. Aucejo, E. García-España, Inorg. Chem., 44 (2005) 7449. (b) J. S. de Melo, J. Pina. F. Pina, C. Lodeiro, A. J. Parola, J. C. Lima, M. T. Albelda, M. P. Clares, E. García-España, C. Soriano, J. Phys. Chem. A, 107 (2003) 11307. (c) M. T. Albelda, E. García-España, L. Gil, J. C. Lima, C. Lodeiro, J. S. de Melo, A. J. Parola, F. Pina, C. Soriano, J. Phys. Chem. B., 107 (2003) 6573.

[15] Ligands **L1** and **L2** were prepared as follows. A solution of 1-(aminomethyl)-naphthalene (**L1**) or 1-pyrenemethyl amine hydrochloride (**L2**) (2 mmol) in ethanol (10 mL) was added drop wise to a solution of 2,5-thiophenedicarboxaldehyde (1 mmol) in the same solvent (35 mL). A few drops of triethylamine were added. The resulting solution was gently refluxed with magnetic stirring for ca. 4 h. As no changes were observed, the pale yellow solution was cooled to room temperature and kept under stirring for 48 h. A powder precipitate formed, which was then filtered off, washed with cold absolute ethanol and diethyl ether, and dried under vacuum.

L1: Colour: White. Yield 0.336 g (80%). Anal. Calcd for $C_{28}H_{22}N_2S \cdot 1.5H_2O$: C, 75.48; H, 5.66; N, 6.29; S, 7.20. Found: C, 75.57; H, 4.97; N, 6.14; S, 7.19. M.P.: 165-170ºC. IR (cm^{-1}): ν, 1627 (C=N). ^1H NMR (400 MHz, $CDCl_3$): δ = 8.36 (s, 2H); δ = 8.09-8.07 (d, 2H); δ = 7.89-7.79 (dd, 4H); δ = 7.55-7.43 (m, 8H); δ = 7.20 (s, 2H); δ = 5.31-5.20 (s, 4H). MS (EI): 418 [**L1**H]$^+$.

L2: Colour: Yellow. Yield 0.238 g (84%). Anal. Calcd for $C_{40}H_{26}N_2S \cdot 0.5H_2O$: C, 83.45; H, 4.73; N, 4.87; S, 5.57. Found: C, 83.56; H, 4.66; N, 64.90; S, 5.47. M.P.: 195-215ºC. IR (cm^{-1}): ν, 1622 (C=N). ^1H NMR (400 MHz, $CDCl_3$): δ = 8.70 (s, 2H); δ = 8.43-8.03 (m, 18H); δ = 7.49 (s, 2H); δ = 5.55 (s, 4H) . MS (EI): 567 [**L2**H]$^+$; 590 [**L2**+Na]$^+$.

[16] *Metal complexes. General Procedure*. Work was performed under argon atmosphere using Schlenk tubes and vacuum line techniques, as well as dried solvents. To a solution of **L1** or **L2** (0.25 mmol) in dichloromethane or acetonitrile, depending on the metal salt used, was added a solution of $Pd(CH_3CN)_4(BF_4)_2$ (0.25 mmol) in acetonitrile (10 mL) or $Ni(ClO_4)_2 \cdot 6H_2O$ in dichloromethane (10 mL). The resulting mixture was kept stirred overnight at room temperature. A precipitate was formed, which was then filtered off, washed with dichloromethane or acetonitrile and dried under vacuum.

$PdL1(CH_3CN)_2(BF_4)_2 \cdot 1.5\ H_2O$

Colour: Red-orange. Yield 0.090 g (42%). Anal. Calcd for $C_{32}H_{31}B_2F_8N_4O_{1.5}PdS$: C, 54.85; H, 3.30; N, 7.99; S, 4.56. Found: C, 54.61; H, 3.70; N, 7.60; S, 4.51. ^1H NMR (400 MHz, CD_3CN): δ = 8.61 (s, 2H)$_{imine}$; IR (cm^{-1}): ν, 1669.48. MS (MALDI-TOF) = 417.65 [**L1**]; 542.56 [**L1**Pd + H_2O]; 649.1 [**L1**Pd + 3CH_3CN]; 942.4 [2**L1**+Pd]$^+$.

$NiL1(ClO_4)_2 \cdot 3H_2O$

Colour: Yellow. Yield: 0.088 g (52%). Anal. Calcd for $C_{28}H_{28}Cl_2N_2NiO_{11}S$: C, 46.13; H, 3.85; N, 3.84; S, 4.39; Ni, 8.05 Found: C, 46.02; H, 4.18; N, 3.80; S, 4.29; Ni,7.89 IR (cm^{-1}): ν, 1660.80. MS (MALDI-TOF) = 418.69 [**L1**]; 559.74 [**L1**Ni + 2 CH_3CN];

$PdL2(CH_3CN)_2(BF_4)_2$

Colour: Pale orange. Yield 0.090 g (33%). Anal. Calcd for $C_{44}H_{32}B_2F_8N_4PdS$: C, 56.90; H, 3.22; N, 6.03; S, 3.45. Found: C, 56.63; H, 3.61; N, 5.95; S, 2.91.

^{1}H NMR (400 MHz, CD_3CN): δ = 8.85 (s, 2H)$_{imine}$; IR (cm^{-1}): v, 1630. MS (MALDI-TOF) = 565 [**L2**H]$^{+}$; 671.5 [**L2**Pd]$^{+}$.

NiL2$(ClO_4)_2 \cdot H_2O$

Color: Yellow. Yield: 0.090 g (21%). Anal. Calcd for $C_{40}H_{28}Cl_2N_2NiO_9S$: C, 57.12; H, 3.32; N, 3.32; S, 3.80; Ni, 6.98,. Found: C, 57.02; H, 3.18; N, 3.80; S, 4.29; Ni, 7.05 IR (cm^{-1}): v, 1660.80. MS (MALDI-TOF) = 565.7 [**L2**H]$^{+}$.

[17] (a) J. S. de Melo, M. T. Albelda, P. Díaz, E. García-España, C. Lodeiro, M. A. Bernardo, J. C. Lima, F. Pina, C. Soriano. J. Chem. Soc., Perkin Trans *2* (2002) 991. (b) F. Pina, J. C. Lima, C. Lodeiro, J. S. de Melo, P. Diaz, M. T. Albelda, E. García-España, J. Phys. Chem., A., 106 (2002) 8207.

[18] C. Lodeiro, J. C. Lima, J. Parola, J. S. de Melo, J. L. Capelo, A. Tamayo, B. Covelo, B. Pedras, Sensors. Act. B. Chem., 115 (2006) 276.

Supplementary material

Chemicals and starting materials:

1-(aminomethyl)-naphthalene, 1-pyrenemethyl amine hydrochloride, 2,5-thiophenedicarboxaldehyde, $Ni(ClO_4)_2 6H_2O$ and $Pd(BF_4).4(CH_3CN)$ were commercial products from Aldrich used without further purification. Solvents were of reagent grade purified by the usual methods.

Instrumentation

Elemental analyses were carried out by the REQUIMTE DQ, Universidade Nova de Lisboa Service on a Thermo Finnigan-CE Flash-EA 1112-CHNS Instrument. Infrared spectra were recorded as KBr discs or in Nujol using Bio-Rad FTS 175-C spectrophotometer. Proton NMR spectra were recorded using a Bruker WM-450 spectrometer. Electronic Impact spectra were determined on a Micromass GCT-TOF7000 and the MALDI-TOF-MS analysis have been performed in a MALDI-TOF-MS model voyager DE-PRO biospectrometry workstation equipped with a nitrogen laser radiating at 337 nm from Applied Biosystems (Foster City, United States) at the REQUIMTE, Chemistry Department, Universidade Nova de Lisboa. The acceleration voltage was 2.0×10^4 kV with a delayed extraction (DE) time of 200 ns. The spectra represent accumulations of 5 x 100 laser shots. The reflectron mode was used. The ion source and flight tube pressures were less than 1.80×10^{-7} and 5.60×10^{-8} Torr, respectively.

Absorption spectra were recorded on a Perkin Elmer lambda 35 spectrophotometer and fluorescence emission spectra on a Perkin Elmer LS45 spectrofluorometer. The linearity of the fluorescence emission *vs.* concentration was checked in the concentration range used (10^{-4}-10^{-6} M). A correction for the absorbed light was performed when necessary. All spectrofluorimetric titrations were performed as follows: the stock solutions of the ligand (*ca.* 1×10^{-3} M) were prepared by dissolving an appropriate amount of the ligand in a 50 mL volumetric flask and diluting to the mark with absolute EtOH UVA-sol. The titration solutions ([**L**] = 1.00×10^{-6} and 1.00×10^{-5} M) were prepared by appropriate dilution of the stock solutions. Titrations of both ligands were carried out by addition of microliter amounts of standard solutions of the ions in absolute ethanol.

Nickel(II) was measured with a Varian (Cambridge, UK) atomic absorption spectrometry model Spectra AA 20 plus equipped with a 10 cm burner head. Hollow-cathode lamps operated at 4 mA were used as radiation source. The wavelength (nm) and slit width (nm) used were 352.4 and 0.5.

Procedure for MALDI-TOF-MS sample preparation.

The MALDI mass spectra of the soluble samples (1 or 2 μg/μL) such as the metal salts were recorded using the conventional sample preparation method for MALDI-MS. 1μL was put on the sample holder on which the chelating ligand had been previously spotted. The sample holder was inserted in the ion source. Chemical reaction between the ligand and metal salts occurred in the holder and complexed species were produced.

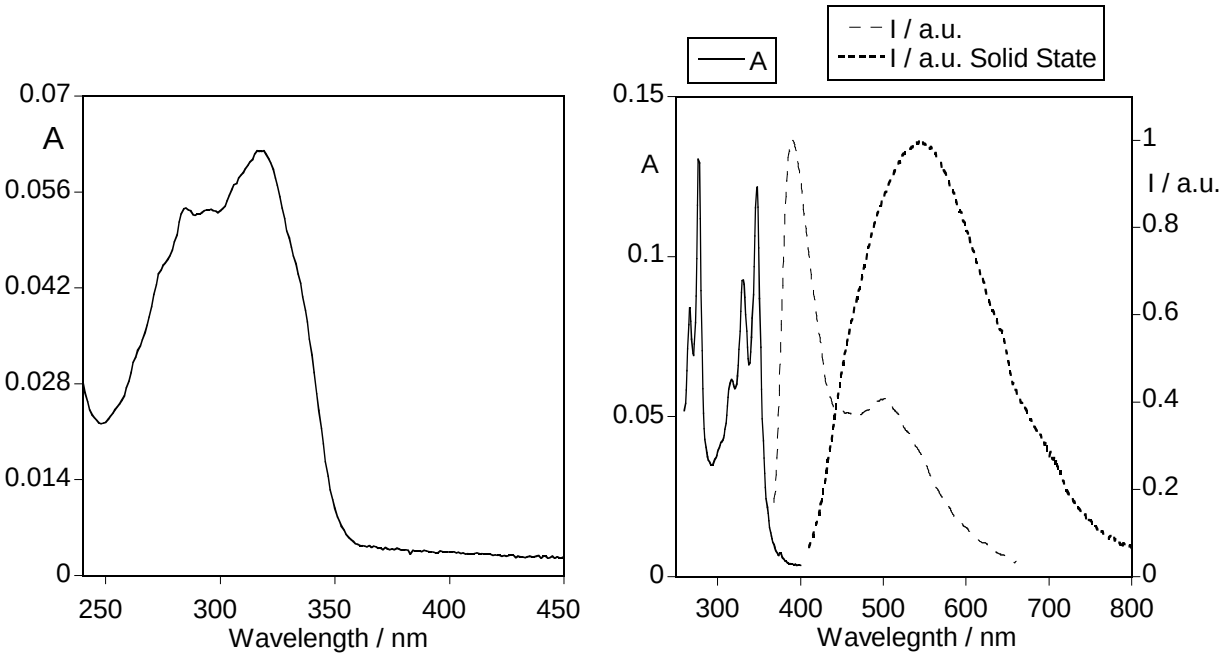

Figure SM III.1.- Absorption spectrum of **L1** (left) and absorption, emission and solid state fluorescence spectra of **L2** (right). ([**L1**] = 1 x 10^{-5}M; [**L2**] = 1 x 10^{-6}M. λ_{exc} = 350 nm).

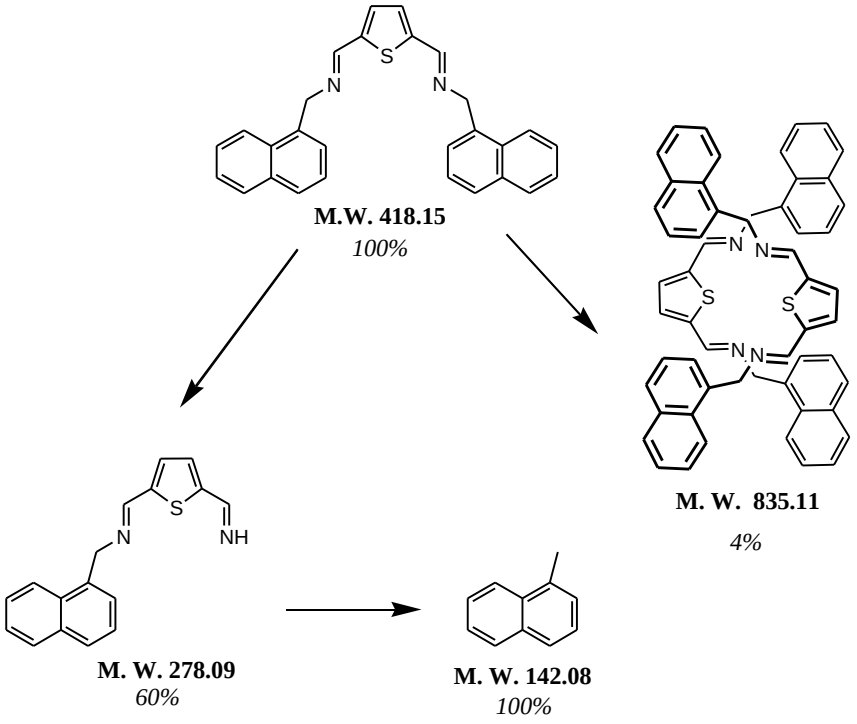

Figure SM III.2. MALDI-TOF-MS fragmentation of **L1.**

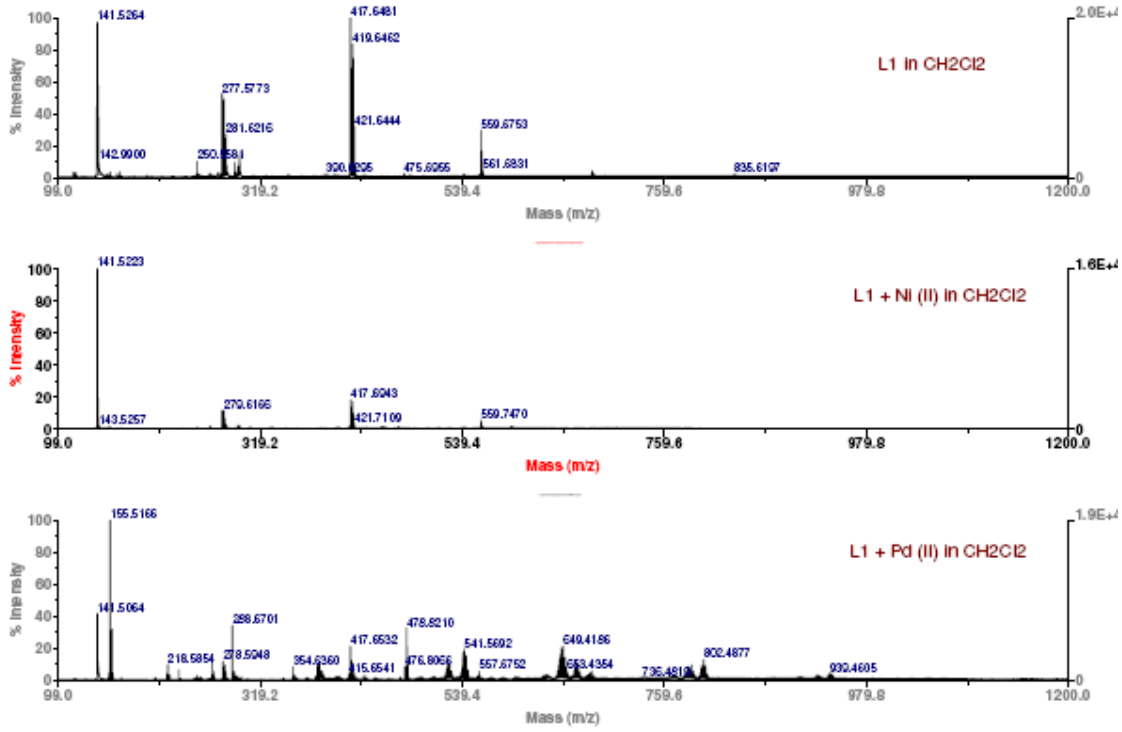

Figure SM III.3.- MALDI-TOF-MS spectra of the ligand **L1** and its corresponding solid complexes with Ni(II) and Pd(II) in dichloromethane.

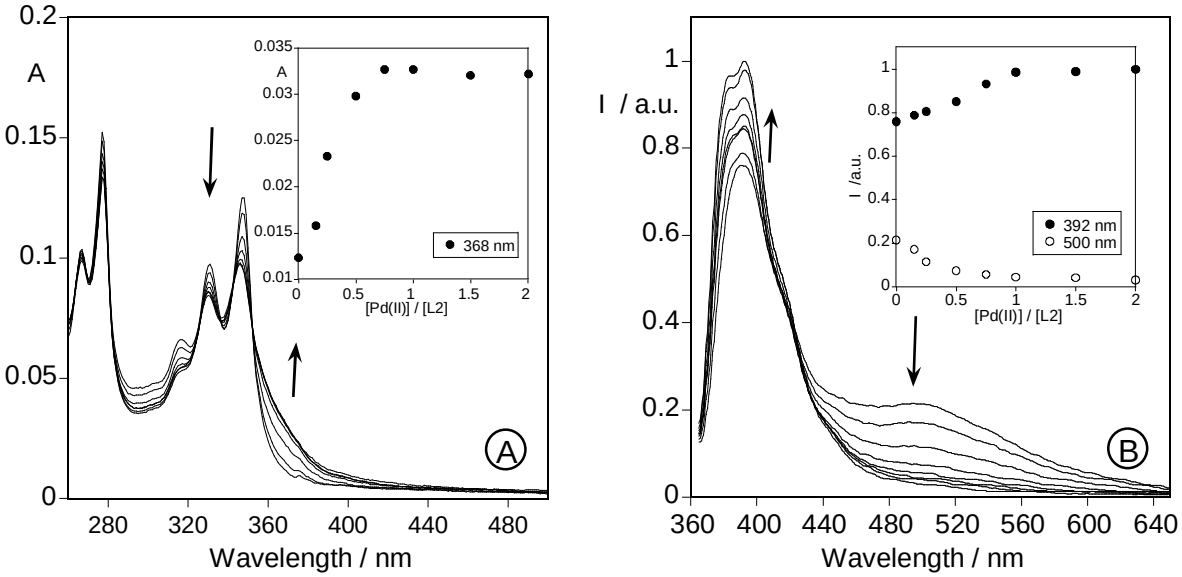

Figure SM III.4.- Absorption (A) and fluorescence (B) spectra of **L2** in the presence of Pd(II) in the concentration range 0 to 2 equivalents, in dichloromethane solution ([**L2**] = 1 x 10^{-6}M. λ_{exc} = 350 nm). Inset shows (A) absorption a 368 nm and (B) intensity of emission as function of [Pd(II)]/[**L2**] at λ_{em} = 392 nm (monomer) and 500 nm (excimer).

Chapter IV

A new tripodal poly-imine indole-containing ligand: Synthesis, complexation, spectroscopic and theoretical studies.

Published in:

B. Pedras; E. Oliveira; H. Santos; L. Rodríguez; R. Crehuet; T. Avilés; J. L. Capelo; C. Lodeiro.

Inorg. Chim. Acta, **2009**, *362*, 2627-2635.

IV.1 Resumo

Neste capítulo são descritos um novo ligado tripodal flexível derivado do 3-metilindol, ("InTREN" **L**) e os seus complexos mononucleares de Zn(II), Cu(II), Ni(II), Hg(II) e Pd(II). Todos os compostos foram obtidos sob a forma de amostras sólidas analiticamente puras. A caracterização dos compostos foi efectuada por espectroscopias de ^{1}H-RMN, IV e absorção Uv-Vis, espectrometria de massa MALDI-TOF-MS e análise elementar e a sua geometria foi optimizada utilizando a teoria do funcional da densidade (DFT).

Foram efectuados cálculos baseados na teoria do funcional da densidade dependente do tempo, de modo a atribuir as bandas de absorção de menor energia do ligando livre e do respectivo complexo de Zn(II). O sistema é um excelente candidato para experiências de reconhecimento/coordenação *in situ* por MALDI-TOF-MS e por espectroscopia de absorção. A presença de três grupos indol no ligando InTREN torna possível a síntese de novas estruturas supramoleculares tridimensionais por automontagem.

A minha contribuição para este trabalho consistiu na síntese e caracterização do ligando InTREN, **L**, e de parte dos respectivos complexos metálicos, bem como a realização de parte dos estudos fotofísicos por espectroscopia de absorção na presença de catiões metálicos.

IV.2 Abstract

A novel flexible tripodal ligand derived from 3-methylindole, ("InTREN" **L**), and its mononuclear Zn(II), Cu(II), Ni(II), Hg(II) and Pd(II) complexes are described. All compounds gave analytically pure solid samples. Characterization of the compounds was accomplished by ^{1}H-NMR, IR and absorption spectroscopies, matrix assisted laser desorption/ionization time-of-flight mass spectrometry (MALDI-TOF-MS) and elemental analysis and their geometry optimized using Density Functional Theory (DFT).

Time-dependent-density functional theory (TD-DFT) calculations have been used to assign the lowest energy absorption bands of the free ligand and the Zn(II) complex. The system is a very good candidate for *in situ* recognition/coordination effects by MALDI-TOF-MS spectrometry and absorption spectroscopy. The presence of three indole groups in InTREN opens up the possibility to synthesize new three-dimensional self-assembled supramolecular structures.

My contribution to this work was the synthesis and characterization of the ligand InTREN, **L**, and of some of its metal complexes, as well as part of the photophysical studies by absorption spectroscopy in the presence of metal ions.

IV.3 Introduction

Chemosensors containing polyamine groups are well-studied receptors capable of interacting with metal ions and anionic species [1-3]. In most cases they clearly show changes on their intrinsic optical properties such as emission signal intensity, wavelength modification, formation of excimer or exciplex [4]. Several studies have been developed by us, in this field, using linear polyamine chains linked to fluorescent units [5].

Tripodal polyamines possess a more flexible structure than their analogue linear compounds, and they are also being explored in recognition processes [6]. On the other hand, Schiff-base host molecules have also attracted much attention in recent years due to selective detection of metal ions and anions [7]. For this reason, the construction of new tripodal compounds that also contain Schiff-base systems seems promising in a research project focused on ions detection.

The synthesis of new TREN-derivatives (TREN = tris(2-aminoethyl)amine) as multifunctional supramolecular devices is still in vogue due to this tripodal tetraamine that has been described to be a very versatile platform for the allosteric control of the activity of rather different synthetic systems ranging from HIV-1 protease inhibitors [8] to membrane permeability effectors [9].

Moreover, indole is a very interesting chromophore which is present in the aminoacid tryptophan [10]. It has attracted a considerable amount of attention due to being an important source of emission in proteins. This fact is commonly used by biological chemists, because it can offer an intrinsic fluorescent probe of the different photophysical processes involved within this molecule in different environments [11].

We have taken into consideration all these facts in order to design a new tripodal ligand (named by us “InTREN”) provided with three indole groups linked to each of the three N-amine terminal groups of TREN, and we report here the synthesis and complexation studies conducted with it. This ligand presents a very wide range of potentially interesting properties to be explored. A first insight has been recently reported by us, where the synthesis and supramolecular studies of new gold metallosupramolecular structures used for recognition effects have been studied [12]. These studies have been developed using the flexible poly-imine InTREN chemosensor as a starting synthon.

IV.4 Results and Discussion

IV.4.1 Synthesis and characterization. Complexation Studies.

Ligand InTREN (**L**) has been synthesized by direct reaction of 5-methylindole-3-carboxaldehyde and TREN amine in refluxed acetonitrile following the reaction procedure presented in Scheme IV.1.

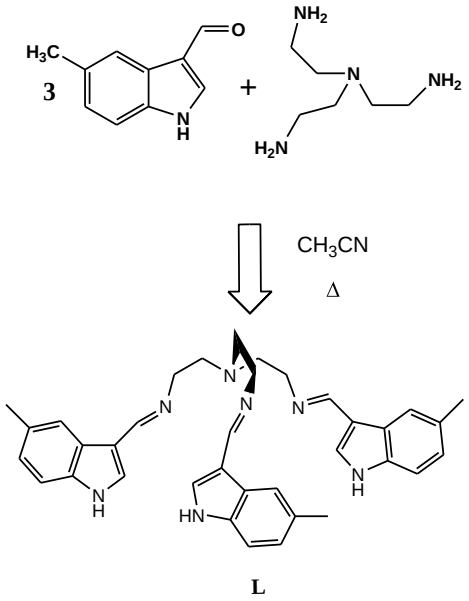

Scheme IV.1. Synthesis of ligand InTREN (**L**).

Solid metal complexes have been obtained by the direct reaction between ligand **L** and the $Ni(BF_4)_2{\cdot}6H_2O$, $Cu(CF_3SO_3)_2$, $Zn(CF_3SO_3)_2$, $Hg(CF_3SO_3)_2$ and $Pd(CH_3CN)_4(BF_4)_2$ salts by addition of the metal salt dissolved in acetonitrile to a hot stirring solution of ligand **L** in the same solvent. In all cases pure mononuclear complexes have been characterized. The number of metal ions in each complex has been determined by atomic absorption spectrometry following several methods as was reported previously [13]. The synthesis was also attempted using the perchlorate salt of Hg(I); however, until now non analytically pure product was recovered.

The absorption spectrum of **L** shows two bands at 262 and 288 nm assigned to the π-π^* transitions in the ligand (below, theoretical calculations section). The band centered at *ca.* 288 nm presents the characteristic shape of the indole group, and is attributed to the two close low-lying $\pi\pi^*$ excited states ^1L_a and ^1L_b (see figure SM IV.1) [14].

Protonation of the ligand leads to a decrease in both absorption bands at 262 and 288 nm, and a new one centered at 337 nm appears. Titration with an HBF_4 acidified ethanolic solution shows that two equivalents of protons are enough to achieve a plateau (See Figure IV.1). This result suggests that the four nitrogen atoms present in the TREN moiety must share both protons in order to minimize the electrostatic repulsions.

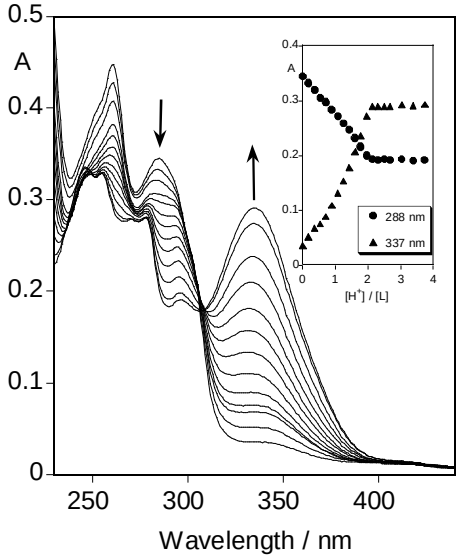

Figure IV.1. Absorption titration of **L** with HBF_4 in absolute ethanol solution, in the concentration range 0-4 equivalents ([**L**] = 9.35 x 10^{-6}M. Room temperature).

Molecular recognition of metal cations constitutes a potential application for this kind of compounds. With this goal in mind, metal titrations of **L** with Zn(II), Ni(II), Cu(II) Pd(II) and Hg(II) salts were undertaken in absolute ethanol solution, and changes in their electronic spectra were recorded.

Addition of increasing amounts of the corresponding triflate or tetrafluoroborate salts to a 9.35 x 10^{-6} M solution of the InTREN compound leads to a decrease of the highest energy absorption bands at 262 and 288 nm and the formation of a new band at higher wavelengths (*ca.* 325 nm for Zn(II); *ca* 325 nm for Cu(II); *ca*. 320 nm for Ni(II); *ca*. 323 nm for Pd(II) and *ca.* 315 nm for Hg(II); see Figure IV.2). Representation of the variation maxima as a function of the number of metal equivalents added to the solution leads us to attribute the formation of a 1:1 complex between the InTREN ligand and the metal atom (inset Figures IV.2A-C). The metal titrations with Pd(II) and Hg(II) salts are similar to the Ni(II) titration and not shown.

The changes in absorption intensity with metal ion concentration yield good correlation fits for a 1:1 stoichiometry, and all the association constants are similar and very high, with a log K = 6.9-6.8 value.

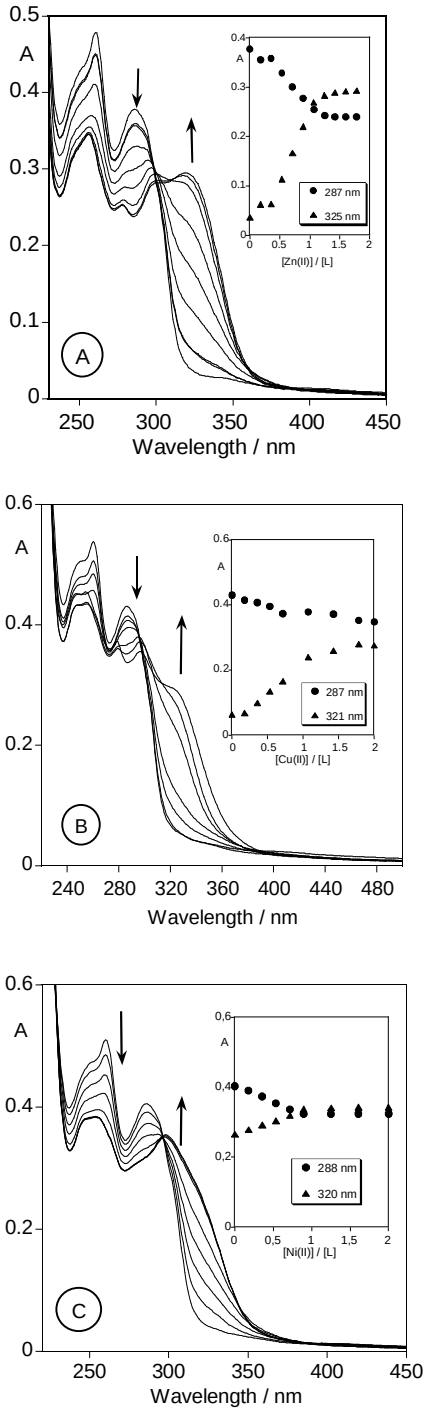

Figure IV.2. Absorption titrations of **L** with $Zn(CF_3SO_3)_2$ (A), $Cu(CF_3SO_3)_2$ (B) and $Ni(BF_4)_2 \cdot 6H_2O$ (C) salts in absolute ethanol solution, in the concentration range 0-2 equivalents ([**L**] = 9.35 x 10^{-6} M. Room temperature).

Taking into account the affinity of these metals to coordinate with tertiary amine nitrogen atoms and imine nitrogen atoms, and due to the presence of a proton in the nitrogen of the indole groups, which prevents their involvement in coordination, we could expect that the metal atom could coordinate to the imine nitrogen atoms of the InTREN ligand. DFT studies also suggest the involvement of the central tertiary amine in the coordination (below, section IV.4.2). This fact is supported by the results observed in the IR spectrum, which clearly indicates that the coordination takes place by these groups. The IR spectrum of the Schiff-base **L** shows a vibrational band at 1633 cm^{-1} corresponding to the band assigned to v(C=N) bond. In general, this band is shifted to lower wavenumbers (1616 to 1610 cm^{-1}), due to the metal coordination to the imine nitrogen as observed for other similar compounds [4a, 15]. The band at 1100-1200 cm^{-1} assigned to v(C-N) bond is also shifted to lower wavenumbers. ^{1}H-NMR spectra are also in agreement with this coordination, since the imine protons are shifted *ca*. 1.5 ppm downfield. Moreover, X-ray crystal structures of other similar tripodal compounds recently published by Brewer and co-workers show the coordination with metal atoms by the imines and imidazole N atoms [16]. In our case, the introduction of indoles instead of imidazoles provides the molecule a different conformation that seems to be reflected in the additional participation of the tertiary amine in the metal coordination. Although the ligand coordinated with all the metals studied (Zn(II), Cu(II), Ni(II), Hg(II) and Pd(II)), unfortunately, a selective recognition from the ligand towards each metal ion in the presence of other metals was not observed.

The synthesis of new organic matrices to be used in MS-spectrometry as active probes is a goal in future applications based on recognition phenomena in solid state. With this purpose in mind, a MALDI-TOF-MS study was performed using ligand **L** dissolved in absolute ethanol, acetonitrile or dichloromethane (Figure SM IV.2). The samples were dissolved in the corresponding solvent (1-2 µg/µL), and no matrix was added to obtain the mass spectra. A thin film was then formed after drying the small solvent spot on the MALDI plate.

In all cases, peaks were observed attributable to the protonated ligand at *ca*. 570 *m/z* and several fragmentations with different intensities. In acetonitrile, the molecular ion peak at 570.7 *m/z* appears with 100% intensity (see Figure IV.3 for main important fragmentation peaks A, B and C).

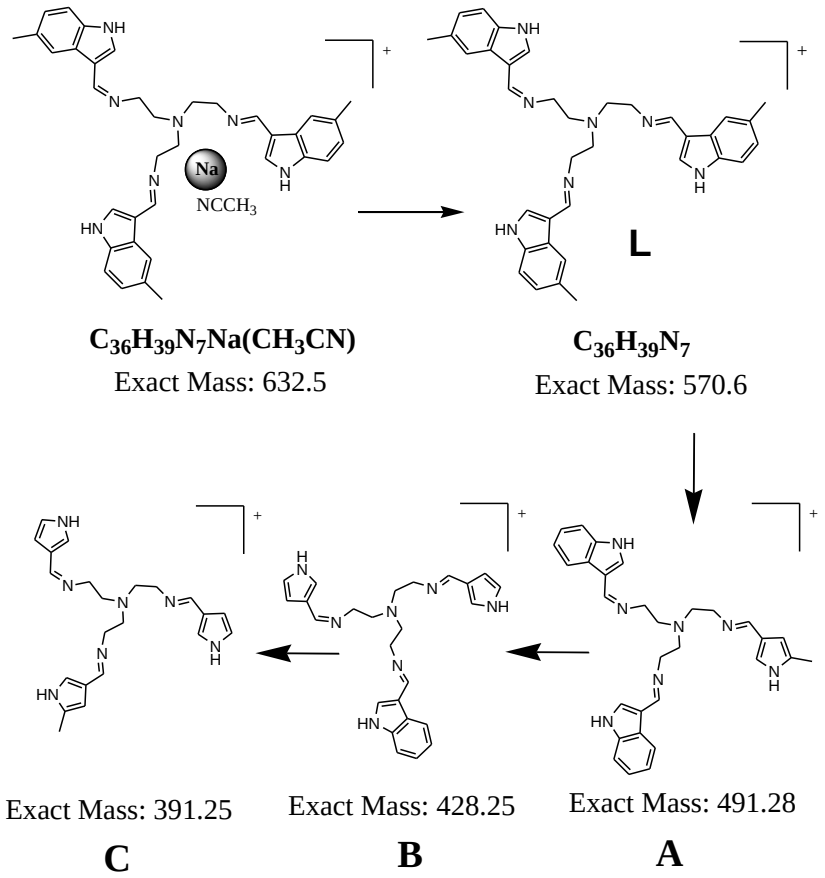

Figure IV.3. Main fragmentation peaks observed in the MALDI-TOF-MS spectra of **L** in different solvents without matrix.

Addition of an acetonitrile solution of the metal ions over the dried ligand spot in the MALDI-TOF-MS plate, and drying again the sample, allows us to follow *in situ* metal ion coordinations. Figure IV.4 presents the MALDI-TOF-MS spectra of the ligand **L** after *in situ* titration with Zn(II), Cu(II), Ni(II), Hg(II) and Pd(II) without matrix. The spectra show peaks corresponding to the species $[\mathbf{L}M]^+$, $[\mathbf{L}M(H_2O)]^+$ or $[\mathbf{L}M(X)]^+$ (X= counterion or solvent) confirming the complexation reaction. Also for Pd(II) and Hg(II) complexes, peaks corresponding to the fragment B of the ligand complexed by the metal ions were observed.

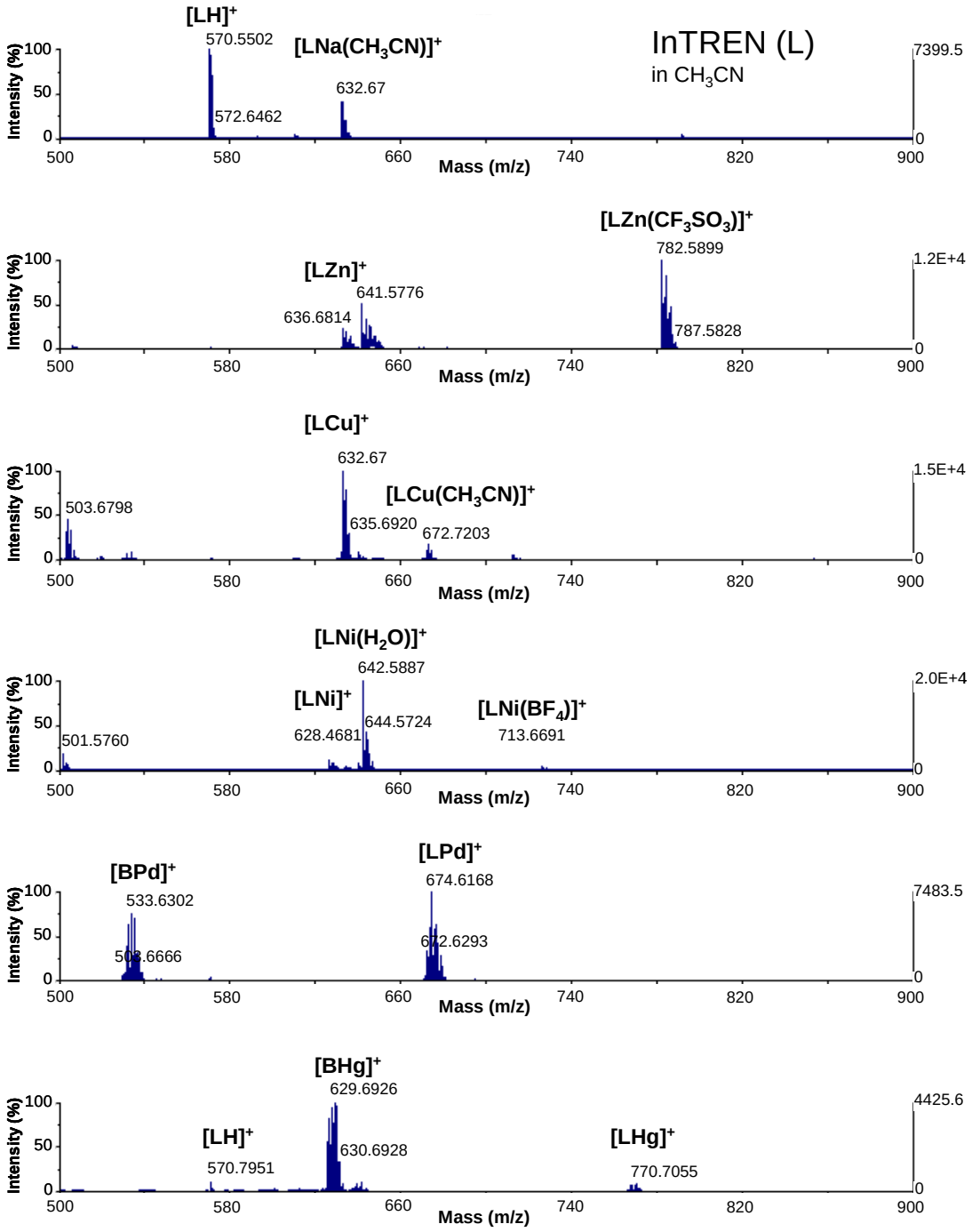

Figure IV.4. MALDI-TOF-MS spectra of ligand **L** in acetonitrile and its metal complexes of Zn(II), Cu(II), Ni(II), Pd(II) and Hg(II).

These results show that compound **L** can be used as a new active complexed probe to detect metal ions by absorption and MALDI-TOF-MS. All MALDI-TOF-MS titration experiments are coincident with the MALDI-TOF-MS spectra of the synthesized and isolated solid complexes.

IV.4.2 Conformational Study

Because the InTREN ligand is highly flexible, with many rotable bonds, we have performed an automatic conformational search with molecular mechanics (see section IV.6.3). This search gave an occluded conformation for the InTREN as the lowest energy one, with many similar structures at less than 2 kcal mol^{-1}. The lowest energy structure (named **1a**) is reported in Figure IV.5.

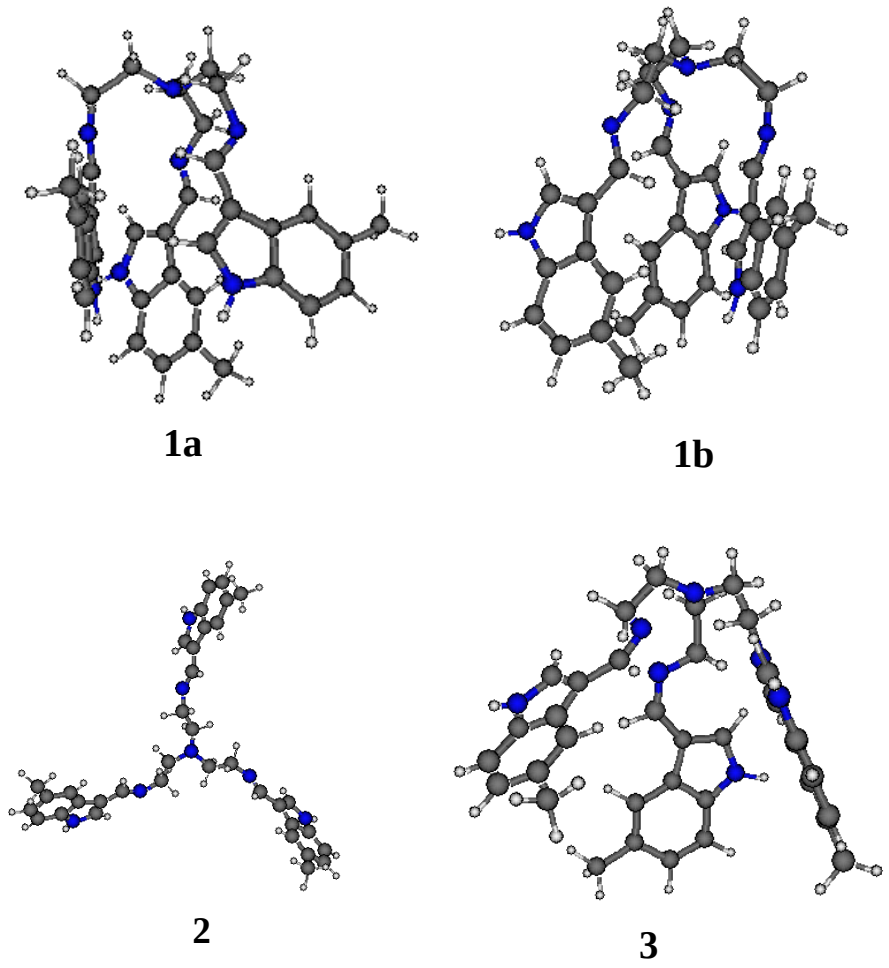

Figure IV.5. Minimized energy molecular structures for **L** in its different possible conformations.

A manual search for open conformations gave an extended conformation **2**. Although at gas-phase this conformation is 7.9 kcal mol^{-1} more unstable than **1a**, solvation effects at the density functional theory/polarizable continuum model (DFT/PCM) level turn conformation **2**, 10.2 kcal more stable (see Table IV.1). We have also considered the possibility of the imine bond having a *Z* conformation. We have found several conformers but here we will only report conformer **3**, because of

its importance in zinc coordination (below). Compound **3** is more than 20 kcal mol^{-1} more unstable than **2** in ethanol, so that if equilibrium effects prevail, its population will be negligible.

Because of its conformation, **2** cannot coordinate metal ions through its iminic nitrogens. Therefore, one should expect a conformational change upon coordination. The most stable structure that we have found is the one originating from conformer **3**. Within the occluded conformations, conformation **1b** is the most stable one, 1.0 kcal mol^{-1} more stable than **1a** (see Figures IV.6 and IV.7 for the geometry of these complexes and Table IV.1 for their calculated free energies in solution). Compound **1b** without zinc coordination was 0.9 kcal mol^{-1} more unstable than **1a**.

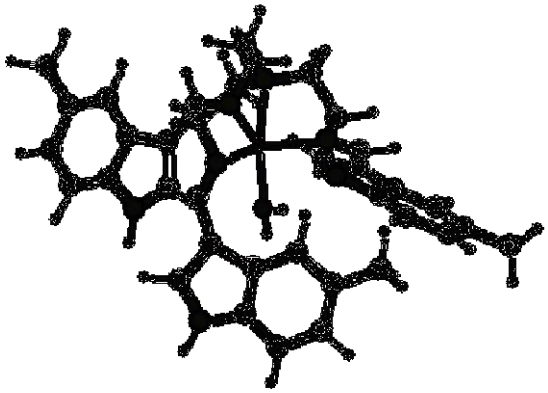

Figure IV.6. Minimized energy molecular structure of $[Zn{\cdot}\mathbf{1b}]^{2+}$ complex.

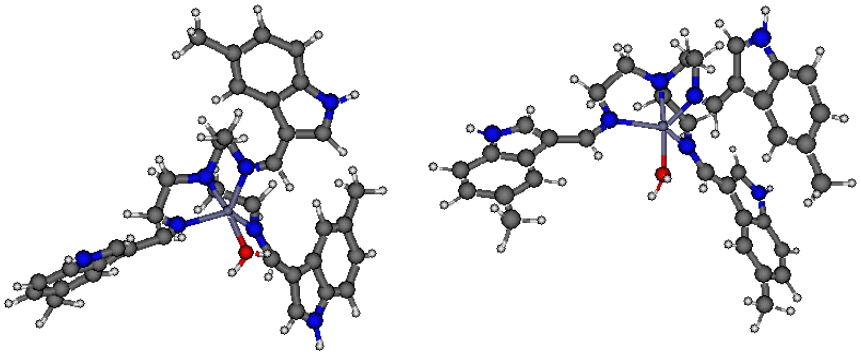

$\mathbf{Zn^{2+}{\cdot}1a}$ $\mathbf{Zn^{2+}{\cdot}3}$

Figure IV.7. Minimized energy molecular structure of $[Zn\mathbf{L}]^{2+}$ complex (**L** = **1a**, left and **3**, right).

Compound	ΔG	ΔG complexed with Zn and H_2O
1a	0.0	0.0
1b	0.9	–1.0
2	–10.2	——
3	10.3	–10.4

Table IV.1. Calculated relative free energies in solution for the different conformers discussed in the text.

Two points deserve further details. First, coordination through the central amine, and second *Z*-*E* rotamers. Complexation with conformer **3** shows that the zinc ion is penta-coordinated, with one position occupied by a water molecule and another by the central nitrogen. When **1** coordinates to the metal atom, it shows the same coordination number and ligands. The same can be said of other conformations we have located but not reported in this text. In all the cases, the water molecule is tightly bound, with binding energies of 18.0 and 20.3 kcal mol^{-1} for **1a** and **3**, respectively, and similar for other compounds. All attempts to locate a conformer where the central amine was not coordinating the metal were unsuccessful. This result contrasts with the previously reported for similar compounds [17], but as already mentioned, the imine and indole ligands favour this coordination geometry. The coordination through the imines can be seen experimentally from the IR spectrum (see section IV.6). The computed spectrum agrees with the red-shift of the imines, from 1689 cm^{-1} in **2** to 1746 cm^{-1} in $[Zn{\cdot}\mathbf{3}]^{2+}$. There is also a shift in the amine stretching from 936 to 910 cm^{-1}, but the calculated and the experimental intensity for this band is much weaker, and this explains why its coordination cannot be distinguished from the IR spectrum.

We address now the *Z*-*E* equilibrium of the imines. We have seen that the most stable free InTREN has *E* conformation (**2**) while the most stable InTREN coordinating zinc (**3**) is *Z*. If the *Z*-*E* equilibrium is fast, the titration with Zn(II) will gradually favour the conformation of **3** as it binds. In some cases the rotameric equilibrium of imines can be slow, and the two conformers can be isolated. If the *Z*-*E* equilibration takes place in a longer time scale than the Zn(II) titration, then **3** could not be the conformer responsible for the spectrum in Figure IV.2A because the most

stable free InTREN is **2** and complexation would lead to a complex in the *E* conformation.

In such a case, **3** cannot be the conformer responsible for the spectrum in Fig. IV.2A. In the following section we will see that the calculated spectrum can help to elucidate which conformer is responsible for the spectrum.

IV.4.3 TD-DFT Calculations

We have performed time-dependent-density functional theory (TD-DFT) calculations for the free InTREN **2** and for the zinc complexes [Zn**1a**]$^{2+}$, [Zn**1b**]$^{2+}$, and [Zn**3**]$^{2+}$ (see Figures IV.6-8).

[Zn**1a**]$^{2+}$ and [Zn**1b**]$^{2+}$ have similar peak number and positions, but their relative intensity can have a considerable variation. The best fit with the experimental spectra is obtained with [Zn**1b**]$^{2+}$, in agreement with DFT calculations. For the free InTREN, **2** also gives a good agreement with the experiment (see Fig. SM IV.3), but this agreement could be improved by locating similar structures of **2** that could potentially have slightly different relative intensities and similar energies. On the other hand, **3** has a very different spectrum, which does not match the experimental results. This points to a *Z-E* equilibrium that is too slow to take place during the titration. Therefore in the remaining discussion we will only consider the spectra of the free InTREN **2** and the complexed form [Zn**1b**]$^{2+}$ (Figure IV.6).

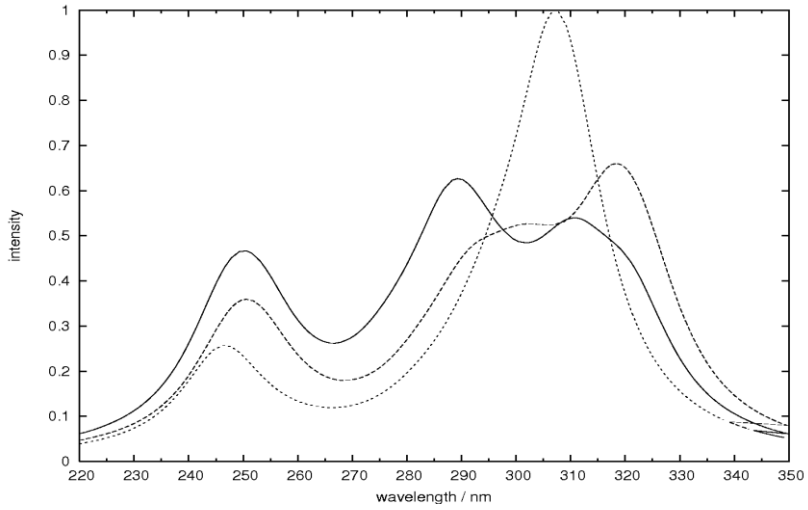

Figure IV.8. Simulated spectra from the TD-DFT calculations for the zinc complexes of **1a** (solid line), **1b** (dashed line) and **3** (dotted line).

DFT calculations have been carried out in order to know the geometry of the frontier orbitals of the compounds. These calculations have been done with the free InTREN ligand and with one of the metal complexes (Zn(II)-derivative). The highest energy occupied orbitals are mainly localized at the indole groups with some contribution of the imines and in the case of the free organic ligand, some contribution of the central tertiary amine is also observed. The lowest energy unoccupied orbitals are mainly located at the imines with some contribution of the indoles. For the metal derivative, significant contribution of the zinc atom is also observed in the LUMO with an antibonding character for the Zn-imine bond. A contribution of the indole groups is also present in both cases.

TD-DFT studies have been very useful in order to assign the electronic absorption transitions of the compounds. The most stable conformation **2** has been used for the calculations of the free InTREN ligand, and the most relevant electronic transitions are presented in Table IV.2.

Transition	E/nm	E/eV	λ_{max}/nm	OS
H-1 → L (40%), H → L (38%), H → L+2 (15%)	290	4.28	288	1.030
H-3 → L+2 (34%), H-1 → L+2 (18%), H-1 → L (15%), H → L (13%)	276	4.49		0.041
H-4 → L (28%), H-3 → L (25%), H-4 → L (18%), H-4 → L+2 (15%)	267	4.64		0.076
H-1 → L (45%), H-4 → L (25%), H-4 → L+2 (10%)	257	4.83	262	0.813

Table IV.2. Calculated TD-DFT low-energy singlet excitation energies, wavelengths and oscillator strengths (OS) and experimental data for **L**.

The low energy excitations obtained by this method are in good agreement with the experimental results, and are in the range 257-290 nm including ethanol effects. The band at 290 nm (experimental value: 288 nm) is assigned to a mixed transition from the highest occupied molecular (HOMO, 38%) and HOMO-1 orbitals (40%) to the LUMO and from the HOMO to the LUMO+2 (15%). The second observed band with high oscillator strength value (calculated value: 257 nm and experimental value: 262 nm) is a mixed transition from the HOMO-1 (45%) and HOMO-4 (25%) orbitals to the LUMO and from the HOMO-4 to the LUMO+2 (10%). The involved orbitals in these transitions are represented in Figure IV.9.

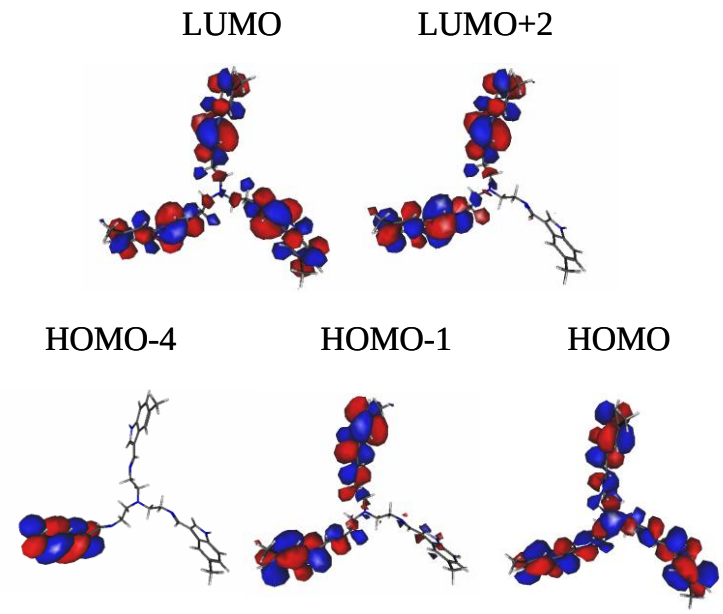

Figure IV.9. Isodensity representation of the orbitals of InTREN ligand involved in the lowest energy transitions.

This figure clearly shows that the indole groups are mainly involved in the HOMO-1 and HOMO-4 orbitals, and the tertiary amine seems only to concentrate its electronic density at the HOMO orbital. Although LUMO orbitals are also partially located at the indoles, more significant contribution of the imine groups is observed. So, the electronic transitions are intraligand π-π^* transitions (LLCT), mainly indole → imine in nature (where the p orbital of the tertiary amine is partially involved) mixed with LLCT (indole → indole) transitions.

Similar studies have been carried out with the Zn(II) derivative [Zn**1b**]$^{2+}$. Since the hydration of the complex is highly favourable, TD-DFT studies have been carried out for the hydrated molecule (TD-DFT studies for the non-hydrated complex have also been calculated and are presented in Supplementary Material).

The lowest energy transitions with higher oscillator strengths are presented in Table IV.3.

Transition	*E/nm*	*E/eV*	λ_{max}/*nm*	*OS*
H → L (98%)	323	3.83	325	0.601
H-1 → L (75%), H → L (21%)	300	4.13	300	0.264
H-1 → L (95%)	291	4.25		0.287
H → L+3 (57%), H → L (40%)	253	4.90	255	0.342

Table IV.3. Calculated TD-DFT low-energy singlet excitation energies, wavelengths and oscillator strengths (OS) and experimental data for $[Zn\mathbf{L}]^{2+}\cdot H_2O$.

The calculated lowest energy band for the Zn(II) complex (323 nm; experimental value: 325 nm) is red-shifted in comparison with the corresponding absorption of the free ligand, as observed in the experimental data. This band is an almost net HOMO → LUMO transition.

The second observed transition (see Table IV.3) with a high oscillator strength value is assigned to a HOMO-1 → LUMO mixed with H → L (300 nm; experimental value: 300 nm), and the highest calculated energy band is constituted by HOMO to LUMO and LUMO+3 transitions (253 nm; experimental value: 255 nm). The orbitals involved in these transitions are shown in Figure IV.10.

Figure IV.10 shows that the HOMO and HOMO-1 orbitals are mainly centered at the indole, and some electronic density is also observed at the imine groups. The LUMO has an important contribution of the metal atom and presents a decrease of the electronic density of the indole. So, the HOMO → LUMO and HOMO-1 → LUMO transitions could be attributed to a LMCT (indole → Zn) probably mixed with some LMCT (imine → Zn).

The highest energy calculated transition with high oscillator strength value involves the HOMO, LUMO and LUMO+3 orbitals. The latter is quite purely located at the indole group. Therefore, the corresponding lowest energy band is a LMCT transition mixed with LLCT (indole → indole).

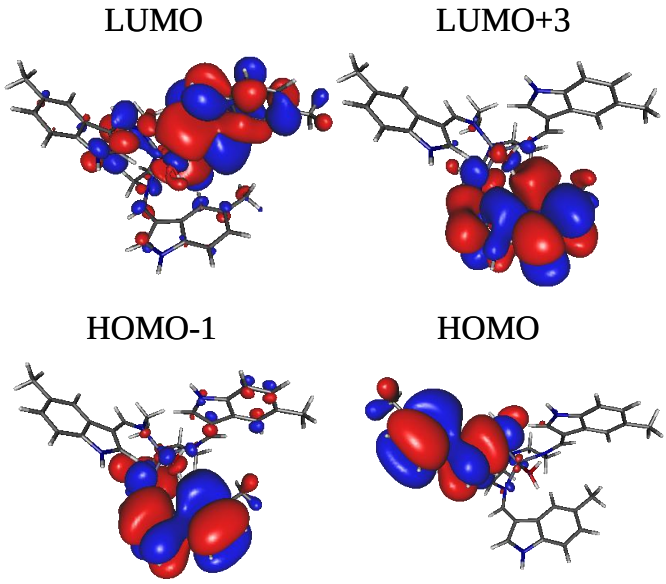

Figure IV.10. Isodensity representation of the orbitals of the $[Zn\mathbf{L}]^{2+}\cdot H_2O$ complex involved in the lowest energy transitions.

IV.5 Conclusions

A new tripodal ligand "InTREN" containing three methyl-indole groups, and its mononuclear Zn(II), Cu(II), Ni(II), Hg(II) and Pd(II) complexes have been prepared. All compounds have been fully characterized by elemental analyses, MALDI-TOF-MS spectrometry, IR, UV-vis, and ^{1}H NMR spectroscopies when applied.

Absorption and MALDI-TOF-MS spectrometry results obtained show that ligand **L** can be used as a new active probe to detect metal ions by both techniques.

DFT and TD-DFT studies lead us to assign the minimum energy conformation for the InTREN ligand and for their Zn(II) metal complexes. Although different possible conformations have been obtained, the comparison with experimental data has been very useful to identify the expected geometry for the species present in solution.

TD-DFT studies have also been used to assign the electronic absorption transitions of the compounds. Thus, intraligand π-π^* transitions (LLCT) are attributed to the free ligand, while LMCT (indole → Zn) probably mixed with some LMCT (imine → Zn) are the responsible for the main electronic transitions of the metal complexes.

IV.6 Experimental

IV.6.1 Chemicals and Starting materials

5-Methylindole-3-carboxaldehyde, TREN amine and $Ni(BF_4)_2{\cdot}6H_2O$, $Cu(CF_3SO_3)_2$, $Zn(CF_3SO_3)_2$, $Hg(CF_3SO_3)_2$ and $Pd(CH_3CN)_4(BF_4)_2$ were commercial products from Aldrich used without further purification. Solvents were of reagent grade purified by the usual methods.

IV.6.2 Instrumentation

Elemental analyses were carried out by the REQUIMTE DQ, Universidade Nova de Lisboa Service on a Thermo Finnigan-CE Flash-EA 1112-CHNS Instrument. Infrared spectra were recorded as KBr discs or in Nujol using a Bio-Rad FTS 175-C spectrophotometer. Proton NMR spectra were recorded using a Bruker WM-450 spectrometer.

MALDI-TOF-MS spectra have been performed in a MALDI-TOF-MS model Voyager DE-PRO Biospectrometry Workstation equipped with a nitrogen laser radiating at 337 nm from Applied Biosystems (Foster City, United States) from the MALDI-TOF-MS Service of the REQUIMTE, Chemistry Department, Universidade Nova de Lisboa. The acceleration voltage was 2.0×10^4 kV with a delayed extraction (DE) time of 200 ns. The spectra represent accumulations of 5 x 100 laser shots. The reflection mode was used. The ion source and flight tube pressures were less than 1.80×10^{-7} and 5.60×10^{-8} Torr, respectively.

The MALDI mass spectra of the soluble samples (1 or 2 μg/μL) such as the ligand and metal complexes were recorded using the conventional sample preparation method for MALDI-MS. In the metal titrations by MALDI, 1 μL of the metal sample was put on the sample holder on which the chelating ligand **L** had been previously spotted. The sample holder was inserted in the ion source. Chemical reaction between the ligand and metal salts occurred in the holder and complexed species were produced in the gas phase.

Absorption spectra were recorded on a Perkin Elmer lambda 35 spectrophotometer. All spectroscopic titrations were performed as follows: the stock solutions of the ligand (*ca.* 1×10^{-3} M) were prepared by dissolving an appropriate

amount of the ligand in a 50 mL volumetric flask and diluting to the mark with absolute EtOH or CH_3CN UVA-sol. The titration solutions ([**L**] = 9.35 x 10^{-6} M) were prepared by appropriate dilution of the stock solutions. Proton and metal titrations were carried out by addition of microliter amounts of standard solutions of the corresponding ions in absolute ethanol. The association constants of the ligand with the metal cations were obtained from the fit of the absorption titration data with the equation derived by Lehn [18].

Copper(II) determinations were performed on a Varian model Zeeman spectraA300 plus atomic absorption spectrometer in combination with an autosampler; pyrolitic graphite-coated graphite tubes with platform were used [13a]. For the determination of copper concentration, 20 µL of solution was injected into the graphite furnace, where it was dried, ashed and atomized. The signal was measured in the peak area mode. Each completed determination was followed by a 2 s clean-up cycle of the graphite furnace at 2800 ºC. During the drying, ashing, and cleanup cycles, the internal argon gas was passed through the graphite furnace at 300 mL/min. The internal argon gas flow was interrupted during the atomization cycle, but was restored for the cleanup cycle. The relative standard deviation among replicate was typically < 5%.

Nickel(II) was measured with a Varian (Cambridge, UK) atomic absorption spectrometry model Spectra AA 20 plus equipped with a 10 cm burner head. Hollow-cathode lamps operated at 4 mA were used as radiation source. The wavelength (nm) and slit width (nm) used were 352.4 and 0.5.

Mercury(II) was determined in a Flow Injection System consisting of a four channels Gilson (Villiers le Bel, France) Minipuls 2 peristaltic pump, a four channels Ismatec (Glattbrugg, Switzerland) programmable peristaltic pump model Reglo Digital MS-4/12; a Perkin-Elmer (Uberlingen, Germany) membrane gas-liquid separator; a six-port injection valve (Supelco, Bellefonte, PA) with a 500-µL loop, and a Fisher and Porter (Warminster, PA) flow meter (0–100% N_2, 200 ml min^{-1}). Ismatec tygon tubing type R3607 of different internal diameters (2.06 and 3.15 mm id), was used for carrying the reducing agent, carrier solution, and waste solution. The initial conditions for cold vapour generation using $SnCl_2$ as reducing agent were established in a previous work [13b], and were a 5% mass v^{-1} $SnCl_2$ solution in 10% v v^{-1}. HCl was used as reducing stream with a 3 mL min^{-1} flow rate; a 3% v v^{-1} HCl solution was used as carrier with a 10 mL min^{-1} flow rate. A 200 mL min^{-1} flow-rate of carrier gas

(N_2) was used. Mercury atomic absorbance was measured with a Thermo (Cambridge, UK) atomic absorption spectrometer model Solar S2 equipped with a homemade quartz tube. The quartz tube was kept at room temperature during operation. A mercury hollow-cathode lamp (Thermo) operated at 4 mA was used as radiation source. The mercury line at 253.7 nm and a slit width of 0.5 nm were used for measurements. An inorganic mercury stock standard solution (Merck, Darmstat, Germany, 1 g L^{-1}) was used. All stock standard solutions were stored in a refrigerator at 4 °C and protected from light. Working standard solutions were prepared just before use by appropriate dilution of the stock standard solution. Sn(II) chloride used as reducing agent was prepared by dissolving the appropriate mass of Sn(II) chloride dehydrate (Panreac, Barcelona, Spain) in concentrated hydrochloric acid and diluted with ultrapure water. Diluted hydrochloric acid (Merck) was used as carrier.

Zinc(II) was determined by Inductively coupled plasma atomic emission spectroscopy (ICP-AES, Model Ultima, Jobin–Yvon, France). The measurements were made with the following instrument parameters: plasma power 1200 kW, and plasma gas flow 12 L min^{-1}. The wavelength used was 213.856 nm.

IV.6.3 Computational Details

The conformational analysis of the InTREN ligand was performed with the Molecular Operating Environment (MOE) software (Chemical Computing Group), using the MMFF94x force field and a Born solvation model with the dielectric constant of ethanol.

We have chosen the PBE0 functional (named PBE1PBE in Gaussian) to perform all geometry optimizations and TD-DFT calculations. This functional has shown to give accurate spectroscopic results for different organic aromatic molecules [19]. These authors also pinpointed the importance of using a large basis set, with triple-zeta, polarization and diffuse functions. The large size of the molecules in this work limits the size of the affordable basis sets. We performed a test with one conformation of the InTREN ligand and the 6-31G(d), 6-311G(d), 6-311G(2d), 6-311+G(d), and 6-311+G(2d) and found that the diffuse functions had a much crucial effect on the position of the absorption band than the doubling the polarization functions (see Fig. SM IV.4). Therefore, all the TD-DFT calculations presented in this work used the 6-311+G(d) basis set. With this basis set, the calculation of the InTREN ligand involved 1063 basis functions and the ligand with hydrated zinc ion

1149 basis functions. Twenty five excited states have been calculated with the TD-DFT method. Geometries of all compounds were optimized with the 6-311G(d) basis set. The description of the solvent effect has been accounted with the Polarizable Continuum model PCM [20] using ethanol as a solvent. All the energies reported in the text correspond to PCM free energy values determined at PBE0/6-311+G(d)/PBE0/6311G(d). All calculations have been performed with the Gaussian 03 software. [21] Gabedit was used to generate the graphical three-dimensional representations of the orbitals. [22]

IV.6.4 Synthesis of L

InTREN ligand **L** was prepared as follows. A solution of 5-methylindole-3-carboxaldehyde (3 mmol) in acetonitrile (25 mL) was added dropwise to a solution of Tris(2-aminoethyl)amine, TREN (1 mmol) in the same solvent (50 mL). The resulting solution was gently refluxed with magnetic stirring for *ca*. 4 h. As no changes were observed, the pale orange solution was cooled to room temperature, and the orange powder precipitate formed was then filtered off, washed with cold absolute ethanol and diethyl ether, and dried under vacuum.

Colour: White. Yield 0.55 g (95.5%). Anal. Calcd for $C_{36}H_{39}N_7 \cdot 2H_2O$: C, 71.40; H, 7.15; N, 16.19; Found: C, 71.50; H, 7.10; N, 16.35. M.p.: 165-170ºC. IR (cm^{-1}): ν, 1633 (C=N). ^1H NMR (400 MHz, $CDCl_3$): δ = 9.98 (s, 3H)$_{NH\ indole}$; δ = 8.43 (s, 3H)$_{imine}$; δ = 8.26-6.80 (m, 12H); δ = 2.44-2.40 (dd, 12H); δ = 2.38 (s, 9H). UV-Vis (λ (nm); ε (M^{-1} cm^{-1}): (262; 48297), (288; 30621). MS (MALDI-TOF-MS) m/z: 571.5 [**L**H]$^+$; 633.5 [**L**+Na+CH_3CN]$^+$.

IV.6.5 Synthesis of the metal complexes. General Procedure.

Synthetic manipulations were performed under argon atmosphere using a bottom round flask and vacuum line techniques. A solution of the metal(II) salts $Ni(BF_4)_2 \cdot 6H_2O$, $Cu(CF_3SO_3)_2$, $Zn(CF_3SO_3)_2$, $Hg(CF_3SO_3)_2$ and $Pd(CH_3CN)_4(BF_4)_2$ (0.08 mmol) in hot acetonitrile (50 mL) was added to a refluxing solution of **L** (InTREN) (0.08 mmol) in the same solvent (15 mL). The solution was magnetically stirred and heated. Refluxing continued for *ca*. 4-5 h. The resulting mixture was allowed to stir overnight at room temperature, and the stirring was kept for 48h. After that a precipitated was formed, the solid was separated by filtration, washed with cold

absolute ethanol or acetonitrile, and dried under vacuum. In some cases, the mother solution was concentrated in a rotary evaporator to *ca.* 10-15 mL. A small volume of diethyl ether (*ca.* 2-5 mL) was slowly infused into the solution producing powdery precipitates. The products were then separated by filtration, washed with cold ethanol or methanol, then cold diethyl ether and dried under vacuum.

The compounds are air stable, soluble in acetonitrile, methanol, dimethylformamide, dimethylsulfoxide, dichloromethane and nitromethane and insoluble in diethyl ether, water and cyclohexane.

Yields obtained are from 60% to 80%.

$ZnL(CF_3SO_3)_2 \cdot 1.5H_2O$

Colour: orange. Yield 0.063 g (80%). Anal. Calcd for $C_{38}H_{42}F_6N_7O_{7.5}S_2Zn$: C, 47.53; H,4.41; N, 10.20; S, 6.68; Zn, 6.80 (Found: C, 47.67; H, 4.60; N, 10.12; S, 6.92; Zn, 7.05 IR (cm^{-1}): v, 1610.66. ^1H NMR (400 MHz, CD_3CN): δ = 10.54 (s, 3H)$_{indole}$ (9.92 (s, 3H)$_{imine}$; MS (MALDI-TOF-MS) *m/z* = 570.6 [**L**H]$^+$; 636.6 [**L**Zn]$^+$; 782.6 [**L**Zn(CF_3SO_3)]$^+$.

$CuL(CF_3SO_3)_2 \cdot 3H_2O$

Colour: Dark green. Yield: 0.052 g (67%). Anal. Calcd for $C_{38}H_{45}CuF_6N_7O_9S_2$: C, 46.31; H, 4.60; N, 9.95; S, 6.51; Cu, 6.45. Found: C, 46.48; H, 4.44; N, 9.99; S, 6.55; Cu, 6.55. IR (cm^{-1}): v, 1615.85. MS (MALDI-TOF-MS) *m/z* = 570.0 [**L**H]$^+$: 633.5 [**L**Cu]$^+$; 672.7 [**L**Cu(CH_3CN)]$^+$

$NiL(BF_4)_2 \cdot 3.5H_2O$

Colour: Pale yellow. Yield: 0.062 g (21%). Anal. Calcd for $C_{36}H_{46}B_2F_8N_7NiO_{3.5}$: C, 49.98; H, 5.36; N, 11.33; Ni, 6.78. Found: C, 49.51; H, 11.31; N, 5.10; Ni, 6.65. IR (cm^{-1}): v, 1616.80. MS (MALDI-TOF-MS) *m/z* = 570.0 [**L**H]$^+$; 628.4 [**L**Ni]$^+$; 642.6 [**L**Ni(H_2O)]$^+$; 713.6 [**L**Ni(BF_4)]$^+$

$PdL(BF_4)_2 \cdot 3H_2O$

Colour: Red-orange. Yield 0.070 g (97%). Anal. Calcd for $C_{36}H_{45}B_2F_8N_7O_3Pd$: C, 47.84; H, 5.02; N, 10.85. Found: C, 47.75; H, 5.53; N, 10.98. IR (cm^{-1}): v, 1628.47. MS (MALDI-TOF-MS) *m/z* = 533.6 [**B**Pd]$^+$; 676.6 [**L**Pd]$^+$.

$HgL(CF_3SO_3)_2 \cdot CH_3CN$

Colour: Orange brownish. Yield: 0.047 g (53%). Anal. Calcd for $C_{40}H_{42}F_6HgN_8O_6S_2$: C, 43.30; H, 3.82; N, 10.10; S, 5.78; Hg, 18.08. Found: C, 43.69; H, 4.31; N, 10.73; S, 5.80; Hg, 17.98. IR (cm^{-1}): v, 1647.27. MS (MALDI-TOF-MS) *m/z* = 570.7 $[LH]^+$; 629.6 $[\mathbf{B}Hg]^+$; 770.71 $[\mathbf{L}Hg]^+$.

IV.7 Acknowledgements

We are indebted to *Fundação para a Ciência e a Tecnologia* (FCT)/ FEDER (Portugal/EU) (Projects PTDC/QUI/66250/2006 and PTDC/QUI/66440/2006 FCT-FEDER). E.O, B.P, H.S. and L.R acknowledge the FCT/Portugal PhD grants SFRH/BD/35905/2007, SFRH/BD/27786/2006, SFRH/BD/38509/2007 and postdoctoral grant SFRH/BPD/26882/2006, respectively. This work has been partly performed using the CESCA resources. R. C. would like to thank the Ramón y Cajal program.

IV.8 References

[1] (a) F. Pina, J.C. Lima, C. Lodeiro, J.S. de Melo, P. Díaz, M.T. Albelda, E. García-España, J. Phys. Chem. A, 106 (2002) 8207; (b) J.S. de Melo, J. Pina, F. Pina, C. Lodeiro, A.J. Parola, J.C. Lima, M.T. Albelda, M.P. Clares, E. García-España, C. Soriano, J. Phys. Chem. A, 107 (2003) 11307; (d) F. Pina, M.A. Bernardo, E. García-España, Eur. J. Inorg. Chem. 10 (2000) 2143; (e) A. Tamayo, L. Escriche, J. Casabo, B. Covelo, C. Lodeiro, Eur. J. Inorg. Chem. 15 (2006) 2997.

[2] (a) L. Fabbrizzi, M. Licchelli, G. Rabaioli, A. Taglietti, Coord. Chem. Rev. 205 (2000) 85; (b) L. Fabbrizzi, M. Licchelli, F. Mancin, M. Pizzeqhello, G. Rabaioli, A. Taglietti, P. Tecilla, U. Tonellato, Chem. A. Eur. J. 8 (2002) 94; (c) K. Ghoso, G. Masanta, Chem. Lett. 35 (2006) 414.

[3] (a) D.C. Magri, J.F. Callan, A.P. de Silva, D.B. Fox, N.D. McClenaghan, K.R.A.S. Sandanayake, J. Fluoresc. 15 (2005) 769; (b) K. Kubo, A. Mori, J. Mater. Chem., 15 (2005) 2902; (c) N.J. Youn, S.K. Chang, Tetrahedron Lett. 46 (2005) 125; (e) T. Gunnlaugsson, T.C. Lee, R. Parkesh, Org. Lett. 5 (2003) 4065; (d) K. Kubo, T. Sakurai, A. Mori, Talanta 50 (1999) 73.

[4] (a) A. Bencini, A. Bianchi, C. Lodeiro, A. Masotti, A. J. Parola, F. Pina, J. S. Melo, B. Valtancoli, Chem. Commun. (2000) 1639; (b) B. Pedras, H. M. Santos, L. Fernandes, B. Covelo, A. Tamayo, E. Bértolo, T. Avilés, J. L. Capelo, C. Lodeiro, Inorg. Chem. Commun. 10 (2007) 925; (c) C. Lodeiro, J. C. Lima, J. Parola, J. S. Seixas de Melo, J. L. Capelo, A. Tamayo, B. Covelo, B. Pedras, Sensor. Actuat. B: Chem. 115 (2006) 276.

[5] (a) J. Pina, J. S. De Melo, F. Pina, C. Lodeiro, J. C. Lima, A. J. Parola, C. Soriano, M. P. Clares, M. T. Albelda, R. Aucejo, E. García-España, Inorg. Chem. 44 (2005) 7449; (b) M. T. Albelda, E. García-España, L. Gil, J. C. Lima, C. Lodeiro, J. S. de Melo, A. J. Parola, F. Pina, C. Soriano, J. Phys. Chem. B. 107 (2003) 6573.

[6] (a) A. Scarso, G. Zaupa, F. B. Houillon, L. J. Prins, P. Scrimin, J. Org. Chem. 72 (2007) 376; (b) S. L. Tobey, E. V. Ansyln, J. Am. Chem. Soc. 125 (2003) 14807; (c) C. J. Jocher, E. G. Moore, J. Xu, S. Avedano, M. Botta, S. Aime, K. N. Raymond, Inorg. Chem. 46 (2007) 9182; (d) L. Prodi, F. Bolletta, M. Montalti, N. Zaccheroni, Eur. J. Inorg. Chem. (1999) 455; (e) L. Fabbrizzi, M. Lichelli, L. Parodi, A. Poggi, A. Taglietti, Eur. J. Inorg.Chem. (1999) 35.

[7] (a) B. Linton, A. D. Hamilton, Chem. Rev. 97 (1997) 1669; (b) M. S. Godman, J. Wei, A. D. Hamilton, V. Jubian, B. Linton, A. D. Hamilton, J. Am. Chem. Soc. 117 (1995) 11610; (c) M. Al-Sayah, N. R. Branda, Angew. Chem., Int. Ed. 39 (2000) 945; (d) T. Moriuchi, M. Nishiyama, T. Hirao, Eur. J. Inorg. Chem. (2002) 447; (e) T. F. Jiao, M. H. Liui, J. Phys. Chem. B 109 (2005) 2532; (f) O. Ramstrom, J. M. Lehn, Nature Rev. Drug Disc., 1 (2002) 26.

[8] S. Valente, M. Gobbo, G. Licini, A. Scarso, P. Scrimin, Angew. Chem., Int. Ed. 40 (2001) 3899.

[9] (a) P. Scrimin, A. Veronese, P. Tecilla, U. Tonellato, V. Monaco, F. Formaggio, M. Crisma, C. Toniolo, J. Am. Chem. Soc. 118 (1996) 2505; (b) P. Scrimin, P. Tecilla, U. Tonellato, A. Veronese, M. Crisma, F. Formaggio, C. Toniolo, Chem. Eur. J. 8 (2002) 2753.

[10] (a) A. Homer, Biochemical Journal, 7 (1913) 101; (b) J. V. Kostir, Nature 160 (1947) 266.

[11] (a) S. Koenig, L. Müller, D. K. Smith, Chem. Eur. J. 7 (2001) 979; (b) S. Sinha, R. De, T. Ganguly, Spectrochimica Acta A 54 (1998) 145; (c) C. A. M. Portugal, J. G. Crespo, J. C. Lima, J. Memb. Sci. 300 (2007) 211.

[12] L. Rodríguez, C. Lodeiro, J. C. Lima, R. Crehuet, Inorg. Chem. 47 (2008) 4952.

[13] (a) J.L. Capelo, A. V. Filgueiras, I. Lavilla and C. Bendicho. Talanta. 50 (1999) 905; (b) C. Fernandez, A, C. L. Conceição, R. Rial-Otero, C. Vaz, J. L. Capelo, Anal. Chem., 78 (2006) 2494; (c) A. Tamayo; B. Pedras; C. Lodeiro; L. Escriche; J. Casabó; J. L. Capelo; B. Covelo; R. Sillanpää; R. Kivekäs, Inorg. Chem. 46 (2007) 7818.

[14] (a) L. Serrano-Andrés, B. O., Roos, J. Am. Chem. Soc. 118 (1996) 185; (b) A. C. Borin, L. Serrano-Andrés, Chem. Phys. 262 (2000) 253.

[15] (a) C. Lodeiro, R. Bastida, E. Bértolo, A. Rodríguez, Can. J. Chem. 82 (2004) 437; (b) M. Vicente, C. Lodeiro, H. Adans, R. Bastida, A. De Blás, D. E. Fenton, A. Macías, A. Rodríguez, T. Rodríguez-Blás, Eur. J. Inorg. Chem. 5 (2000) 1015.

[16] G. Brewer, C. Brewer, R. J. Butcher, E. E. Carpenter, Inorg. Chim. Acta 359 (2006) 1263.

[17] H. Nakamura, M. Fujii, Y. Sunatsuki, M. Kojima, N. Matsumoto, Eur. J. Inorg. Chem. (2008) 1258.

[18] P. Čudić, M. Žinić, V. Tomišić, V. Simeon, J.-P. Vigneron, J.-M. Lehn, J. Chem. Soc., Chem. Commun. (1995) 1073.

[19] (a) J. Preat, D. Jacquemin, V. Wathelet, J.-M. André, E. A. Perpète J. Phys. Chem. A 110 (2006) 8144; (b) D. Jacquemin, E. A. Perpète, G. E. Scuseria, I. Ciofini, C. Adamo, J. Chem. Theory Comput. 4 (2008) 123.

[20] J. Tomasi, B. Mennucci, R. Cammi, Chem. Rev. 105 (2005) 2999.

[21] M. J. T. Frisch, G. W. Trucks, H. B. Schlegel, G. E. Scuseria, M. A. Robb, J. R. Cheeseman, J. A. Montgomery, Jr., T. Vreven, K. N. Kudin, J. C. Burant, J. M. Millam, S. S. Iyengar, J. Tomasi, V. Barone, B. Mennucci, M. Cossi, G. Scalmani, N. Rega, G. A. Petersson, H. Nakatsuji, M. Hada, M. Ehara, K. Toyota, R. Fukuda, J. Hasegawa, M. Ishida, T. Nakajima, Y. Honda, O. Kitao, H. Nakai, M. Klene, X. Li, J. E. Knox, H. P. Hratchian, J. B. Cross, V. Bakken, C. Adamo, J. Jaramillo, R. Gomperts, R. E. Stratmann, O. Yazyev, A. J. Austin, R. Cammi, C. Pomelli, J. W. Ochterski, P. Y. Ayala, K. Morokuma, G. A. Voth, P. Salvador, J. J. Dannenberg, V. G. Zakrzewski,; S. Dapprich, A. D. Daniels, M. C. Strain, O. Farkas, D. K. Malick, A. D. Rabuck, K. Raghavachari, J. B. Foresman, J. V. Ortiz, Q. Cui, A. G. Baboul, S. Clifford, J. Cioslowski, B. B. Stefanov, G. Liu, A. Liashenko, P. Piskorz, I. Komaromi, R. L. Martin, D. J. Fox, T. Keith, M. A. Al-Laham, C. Y. Peng, A. Nanayakkara, M. Challacombe, P. M. W. Gill, B. Johnson, W. Chen, M. W. Wong, C. Gonzalez, and J. A. Pople, *Gaussian 03, (Revision C.02);* Gaussian, Inc., Wallingford CT, 2004.

[22] A.R. Allouche, Gabedit is a free Graphical User Interface for computational chemistry packages. It is available from http://gabedit.sourceforge.net/home.htm.

IV.9 Supplementary material

Electronic absorption spectrum of **L**, MALDI-TOF-MS spectra of **L** in different solvents. Table with calculated TD-DFT low-energy singlet excitation energies wavelengths and oscillator strengths for $[Zn\mathbf{L}]^{2+}$ complex and isodensity representation of the orbitals of the same complex involved in the lowest energy transitions; simulated spectra of conformer **1a** with different basis sets and Cartesian coordinates of all the structures calculated in this work and simulated spectra from the TD-DFT calculations for **2**.

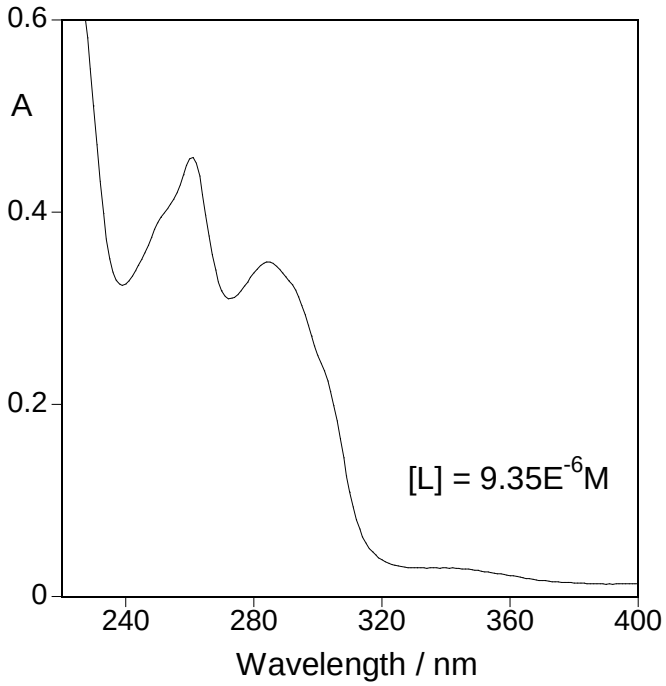

Figure SM IV.1.- Absorption spectrum of **L** in absolute ethanol solution ([**L**] = 9.35 x 10^{-6}M; room temperature).

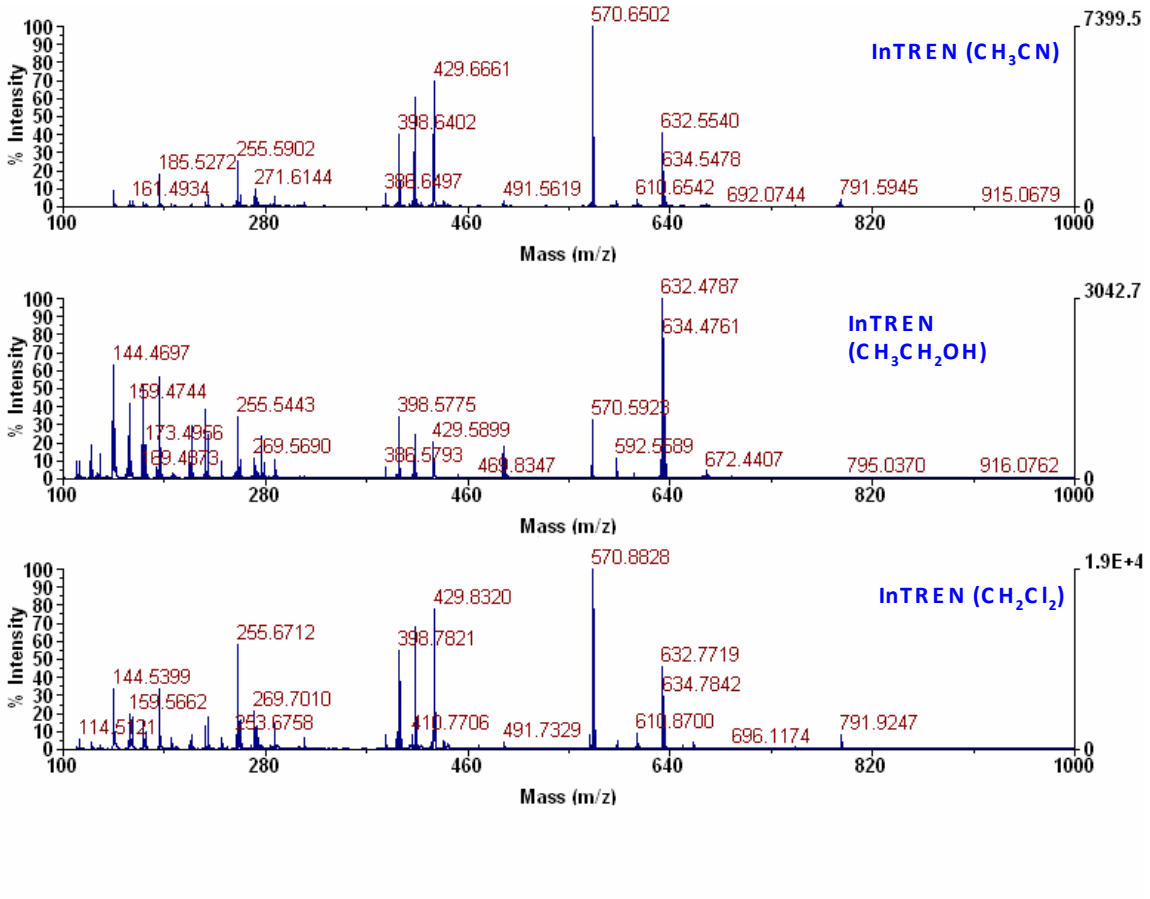

Figure SM IV.2.- MALDI-TOF-MS spectra of ligand **L** in different solvents without matrix.

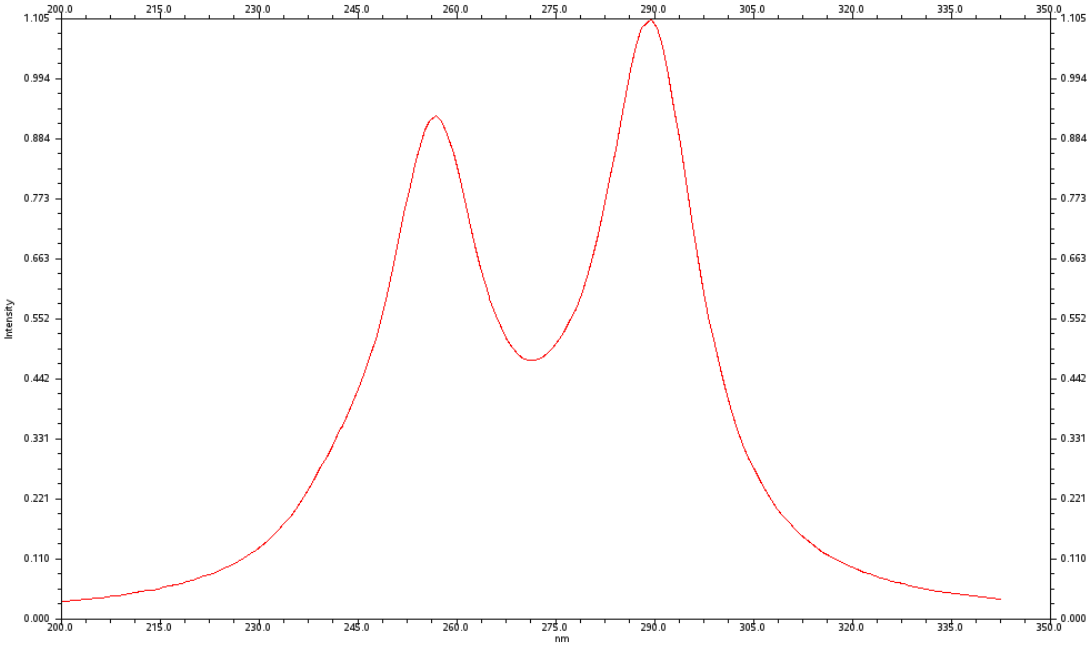

Figure SM IV.3. Simulated spectra from the TD-DFT calculations for **2.**

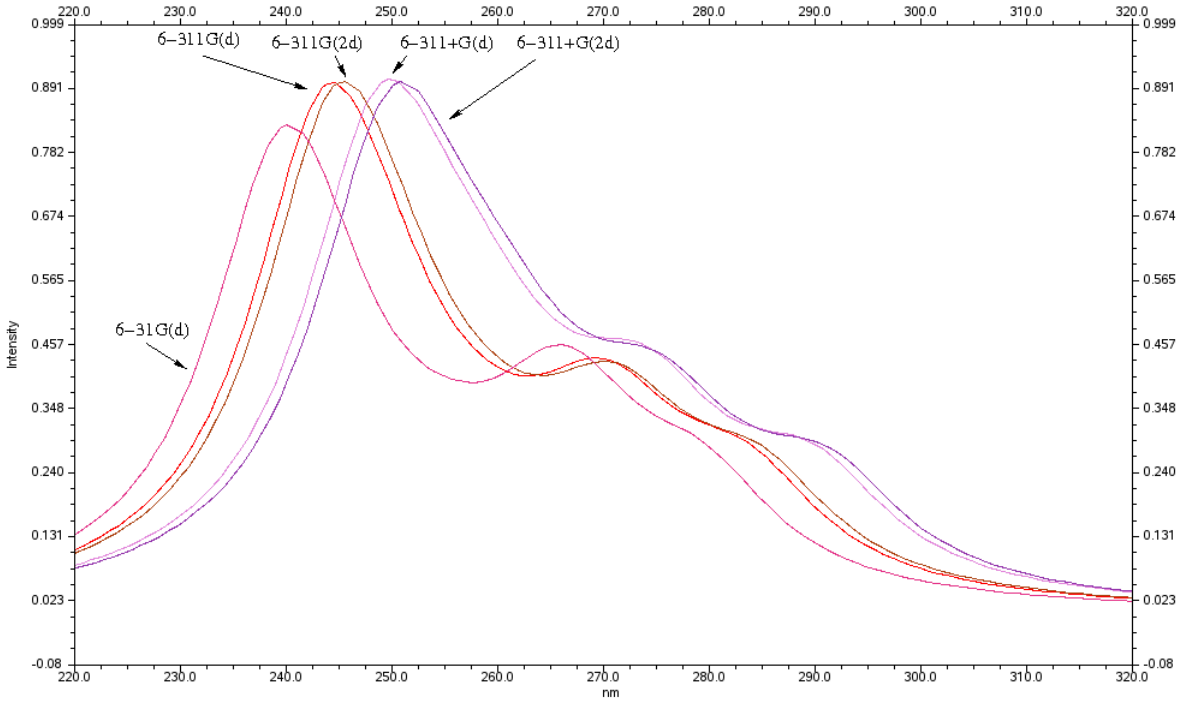

Figure SM IV.4. Simulated spectra of conformer **1a** with different basis sets.

Transition	*E/nm*	*E/eV*	λ_{max}/*nm*	*OS*
H → L (98%)	305	4.07	320	1.418
H → L (75%), H-3 → L (25%)	294	4.22		0.014
H → L (64%), H-3 → L (20%)	282	4.39	280	0.181
H → L+3 (61%), H-3 → L+3 (37%)	249	4.98	255	0.906

Table SM IV.1. Calculated TD-DFT low-energy singlet excitation energies, wavelengths and oscillator strengths (OS) and experimental data for [Zn**L**]$^{2+}$.

Chapter V

Novel Ru(II) Thienyl-imidazo-phenanthroline polypyridyl complexes: synthesis, characterization, photophysical studies and interaction with DNA.

B. Pedras; R. M. F. Batista; L. Tormo; S. P. G. Costa; M. M. M. Raposo; J. L. Capelo; C. Lodeiro.

Submitted, **2010**.

V.1 Resumo

Uma nova família de complexos de Ru(II) polipiridilo (**C1** a **C6**) contendo ligandos furil- ou tienil-imidazo-fenantrolina foi sintetizada utilizando radiação microondas e caracterizada por análise elementar, ^{1}H-RMN, espectroscopias de absorção Uv-vis e de fluorescência, e espectrometrias de massa FAB, EI-MS e MALDI-TOF-MS. A interacção com ADN de timo de vitela na ausência e na presença de diferentes supressores de emissão (brometo de etídio, hexacianoferrato de potássio(II) e metilviologénio) foi estudada por espectroscopia de absorção, medidas de luminescência em estado estacionário e temporização de fotões únicos. Os seus espectros electrónicos apresentam picos de absorção no visível a 457-463 nm, com luminescência vermelha a 603-613 nm. Os rendimentos quânticos de emissão destes complexos situam-se entre 0.006-0.016 em solução de DMSO não-desarejada. Os tempos de vida de luminescência em água estão situados no intervalo de 0.4 a 1.0 μs, com um comportamento não-exponencial devido à formação de agregados por parte da sonda. Os complexos de Ru(II) **C3**, **C4**, **C5** e **C6** apresentam constantes intrínsecas de associação com DNA de 2.74 x 10^5, 3.02 x 10^5, 1.32 x 10^5 e 1.63 x 10^5 M^{-1}, respectivamente. A longa estrutura planar dos ligandos imidazo-fenantrolina e os dados espectroscópicos obtidos sugerem um modo de união parcialmente intercalativo das novas sondas metálicas ao ADN de dupla cadeia.

A minha contribuição para este trabalho consistiu na síntese e caracterização de todos os novos complexos de ruténio(II), bem como os estudos fotofísicos da sua interacção com ADN e supressores de emissão seleccionados.

V.2 Abstract

A new family of Ru(II) polypyridyl complexes (**C1** to **C6**) containing furyl- or thienyl-imidazo-phenanthroline ligands were synthesized using microwave irradiation and characterized by elemental analysis, ^{1}H-NMR, UV-vis absorption and fluorescence spectroscopy, FAB, EI-MS and MALDI-TOF-MS spectrometry. The interaction with calf thymus DNA in the absence and in the presence of different quenchers (ethidium bromide, potassium hexacyanoferrate(II) and methylviologen) has been studied by absorption spectroscopy, steady-state and single-photon timing luminescence measurements. Their electronic spectra show visible absorption peaks at 457-463 nm, with red luminescence at 603-613 nm. The emission quantum yields of these complexes are between 0.006–0.016 in air-equilibrated DMSO solution. Luminescence lifetimes in water lie within the 0.4 to 1.0 μs range, with a non-exponential behavior due to aggregation of the probe. Ru(II) complexes **C3**, **C4**, **C5** and **C6** show intrinsic dsDNA-binding constants of 2.74 x 10^5, 3.02 x 10^5, 1.32 x 10^5 and 1.63 x 10^5 M^{-1}, respectively. The planar extended structure of the imidazo-phenanthroline ligands and the collected spectroscopic data suggest a partial intercalative binding mode of the novel metal probes to double-stranded DNA.

My contribution to this work was the synthesis and characterization of all the ruthenium(II) complexes, and the photophysical studies of their interaction with DNA and selected quenchers.

V.3 Introduction

Among the multiple application fields of ruthenium(II) polypyridyl complexes,[1] its interaction with nucleic acids has been one of the most thoroughly studied over more than two decades.[2] Featuring a wide range of extraordinary properties such as chemical stability, excited-state reactivity, redox potentials,[3] luminescence emission and excited-state lifetimes, these complexes have attracted considerable attention from a great number of researchers, finding applications in areas such as photophysics, photochemistry, supramolecular chemistry, bioinorganic chemistry and catalysis.

Concerning their interaction with biological structures, Ru(II) polyazaheteroaromatic compounds have been used as probes of the biopolymer tertiary structure, photocleavage agents and, in recent times, as inhibitors of biological functions.[4,1a] One of the most extensively studied metal complexes used as luminescent probe is $[Ru(bpy)_2(dppz)]^{2+}$ (bpy = 2,2'-bipyridine, dppz = dipyrido[3,2-a:2',3'-c]phenazine).[5] This complex functions as a molecular "light switch" for DNA because of the dramatic emission enhancement experienced by this probe and related phenazine complexes in the presence of double-stranded nucleic acids, being otherwise weakly emissive in aqueous solution. The reason for this behaviour is the peculiar electronic nature of the phenazine ligand and the lowest-lying excited state swap that occurs in protic solvents,[6] together with the intercalative binding mode to double-stranded DNA of Ru(II)-dppz and related complexes.[7] For all ruthenium(II) polypyridyl complexes, non-radiative vibrational deactivation with the water molecules can be minimized by a close interaction with a hydrophobic negatively charged surface,[8] and the intimate contact (e.g. DNA intercalation) with the biopolymer protects the triplet excited state of the probe from the O_2 quenching,[9] overall leading to a substantial increase in the ^{3}MLCT excited state lifetime.

Very recently these complexes have been applied as multifunctional biological agents for direct imaging of DNA in living cells.[10] By varying the ligands that constitute the complexes, it is possible to modify the nature and strength of their binding to nucleic acids. As mentioned above, all positively charged complexes are expected to be attracted to the anionic DNA, and those containing at least one extended heteroaromatic ligand in the coordination sphere may insert such ligand between adjacent base-pairs of double-stranded DNA (i.e. binding by intercalation).[2a,7,9a,11] Indeed, it has been observed that while $[Ru(bpy)_3]^{2+}$ binds in a

relatively weak manner to DNA (mostly through electrostatic interaction in one of the grooves), the interaction of $[Ru(phen)_3]^{2+}$ is stronger.[12]

Therefore, in order to study the factors that influence the DNA-binding mode of Ru(II) complexes with extended and ancillary ligands, the structural diversity of the metal chelating structures must be taken into account. Moreover, a further tuning of the probe photophysical and DNA binding properties might be achieved when new extended conjugation systems are composed by different heterocyclic nuclei (molecular *meccano* concept).

Following our ongoing projects on fluorescent reporters and their sensing applications,[13] we have tackled the synthesis and characterization of novel (oligo)thienyl-[14] and arylthienyl-imidazo-phenanthrolines[15] due to their interesting emissive properties (see below). Taking also into account that furans exhibit high fluorescence quantum yields[16] and the recent studies concerning the DNA binding and photocleavage of Ru(II) complexes of a 2-(5-methyl-furan-2-yl)imidazo[4,5-f][1,10]phenanthroline ligand,[17] suggesting that these complexes bind to DNA through intercalation and, when irradiated at 400 nm, promote the photocleavage of the DNA, we set out to synthesize Ru(II) furyl-imidazo-phenanthroline complexes that were hitherto unknown.

In this way, four new ligands and six Ru(II) polypyridyl complexes, **C1** to **C6**, are photochemically characterized in this work, and the interaction of the latter with calf-thymus DNA has been followed by steady-state and single-photon timing luminescence measurements. The effect of three different quenchers on the emission properties of the DNA-bound complexes has also been studied, in an attempt to reveal the possible binding modes of the complexes to the nucleic acid.[18]

V.4 Experimental Section

V.4.1 Materials

All reagents used in the present work were commercially available and used without further purification, unless otherwise stated. Progress of the reactions was monitored by thin layer chromatography (0.25 mm thick pre-coated Merck

Fertigplatten Kieselgel 60F_{254} silica plates), while purification was carried out by silica gel column chromatography (Merck Kieselgel 60; 230-400 mesh). Calf thymus DNA was obtained from Pharmacia GE Healthcare and purified by extensive dialysis against TRIS buffer. The concentration of stock solutions was determined spectrophotometrically using the molar absorption coefficient per base pair (12800 M^{-1} cm^{-1}) at 258 nm[9a] and found to be 2.82 mM (for the stock solution used with **C1** to **C3**) and 2.02 mM (for the stock solution used with **C4** to **C6**) in base pairs. All the experiments with DNA were carried out in pH-7.0 3-mM Tris buffer.

V.4.2 Instrumentation

NMR spectra of the ligands were obtained on a Varian Unity Plus spectrometer at 300 MHz for ^{1}H NMR and 75.4 MHz for ^{13}C NMR or a Bruker Avance III 400 at 400 MHz for ^{1}H NMR and 100 MHz for ^{13}C NMR, using the solvent residual peak as internal reference. The solvents are indicated in parenthesis before the chemical shift values (δ in ppm relative to TMS). NMR spectra of the complexes were recorded on a Bruker AVANCE II at 400 MHz for ^{1}H NMR, and processed with the TOPSPIN 2.0 software (Bruker). Melting points were determined on a Gallenkamp apparatus and are uncorrected. Infrared spectra were recorded on a BOMEM MB 104 spectrophotometer. UV-vis absorption spectra of the ligands (200–800 nm) were measured with a Shimadzu UV/2501PC apparatus and those of the complexes on a Varian Cary 3Bio spectrophotometer.

Mass spectrometry analyses of the ligands were performed at the C.A.C.T.I. - Unidad de Espectrometria de Masas of the University of Vigo, Spain, and the mass spectrometry analyses of the Ruthenium(II) complexes were performed at the Analytical Services of the Laboratory of REQUIMTE-Departamento de Química, Universidade Nova de Lisboa. Elemental analyses were performed at the Analytical Services of the Laboratory of REQUIMTE-Departamento de Química, Universidade Nova de Lisboa, on a Thermo Finnigan-CE Flash-EA 1112-CHNS Instrument.

The steady-state luminescence measurements were carried out with a Perkin-Elmer LS-5 spectrofluorometer. Luminescence lifetimes were determined at 25 ± 1 ºC using ca. 10^{-5} M solutions of the Ru(II) complexes by the single-photon timing (SPT) technique with an Edinburgh Analytical Instruments LP900 kinetic spectrometer. Excitation of the samples was carried out with a Horiba NanoLED-07N 405-nm pulsed laser diode (<700 ps). A wide band-pass 405-nm interference filter

(Edmund Scientific) was placed in front of the laser source and cut-off filters (590 nm, Lambda Research Optics) were used in the emission path to avoid distortions from the laser light scattering. The luminescence decay profiles were fit either to a single exponential function or to a sum of 2-3 exponential functions with the original Marquardt algorithm-based EAI decay analysis software. Satisfactory fits were obtained in all cases, as judged from the weighted residuals, the goodness-of-the-fit χ^2 parameter and the autocorrelation function. No oxygen outgassing was performed. The accuracy in the measured lifetimes for the multi-exponential decay fits is estimated to be ±3% (1% for the single-exponential decays) and 10% for the relative weights. The pre-exponential weighted emission lifetime (τ_m) is defined according to Eq. 1, where τ_i is the emission lifetime for each component of the multi-exponential fit whose relative weight is $(\%)_i$.

$$\tau_m = \sum_i \frac{(\%)_i}{100} \tau_i \qquad (1)$$

For the preliminary studies of complexes C1 to C3 in the presence of DNA, a solution of the metal complex in TRIS buffer with a concentration of *ca*. 10^{-5} M was obtained by dilution of a concentrated DMSO stock solution of each complex. Each solution was mixed with DNA in different proportions, and their spectra recorded both in the presence and in the absence of the biopolymer. The mixtures were allowed to equilibrate for at least half an hour between each addition and the respective measurement. For the subsequent studies with DNA the same procedure was adopted, by measuring at different [DNA]/[Ru] ratios and choosing the ratio after which no significant changes in the emission spectrum and lifetime were observed to be studied with the selected quenchers (ethidium bromide, potassium hexacyanoferrate(II) and methyl viologen).

V.4.3 Synthesis

The precursor complex, namely *cis*-$[Ru(bpy)_2Cl_2]$, was synthesized according to literature methods.[19] The syntheses of ligands 4a and 4b have been previously reported.[14a]

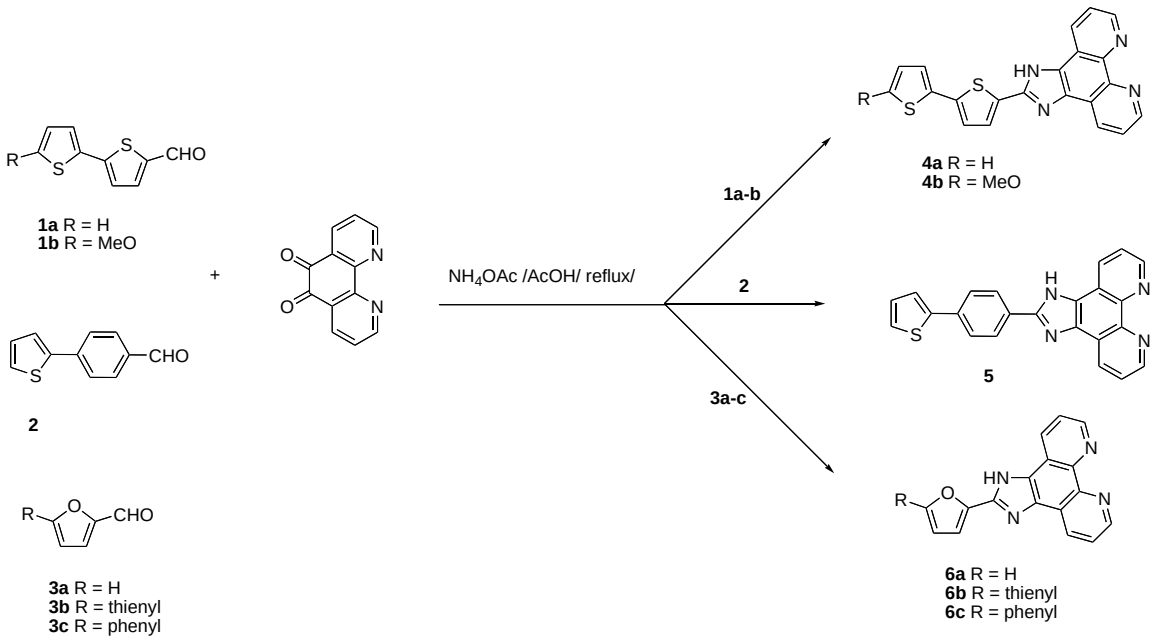

Scheme V.1. Synthesis of phenanthroline-derived ligands.

V.4.3.1. General procedure for the synthesis of imidazo[4,5-*f*][1,10]phenanthrolines 5 and 6

A mixture of the corresponding aldehyde (1.2 mmol), NH_4OAc (20 mmol) and 1,10-phenanthroline-5,6-dione (1 mmol) in glacial acetic acid (10 mL) was stirred and heated at reflux for 5 h. The mixture was then cooled to room temperature and the product precipitated during neutralization with NH_4OH 5 M. The precipitate was filtered out, washed with water and diethyl ether, recrystallized from absolute ethanol and dried under vacuum to give the expected product.

2-(4'-(thien-2''-yl)phen-2'-yl)-1*H*-imidazo[4,5-*f*][1,10]phenanthroline (5). Yellow solid (0.139 g, 82%). ^{1}H NMR (300 MHz, DMSO-d_6): δ 7.18-7.21 (m, 1H, 4´´-H), 7.62 (d, 1H, *J*= 5.1 Hz, 3´´-H), 7.66 (d, 1H, *J*= 3.6 Hz, 5´´-H), 7.81-7.85 (m, 2H, 5-H and 10-H), 7.90 (d, 2H, *J*= 8.7 Hz, 2´-H and 6´-H), 8.31 (d, 2H, *J*= 8.4 Hz, 3´-H and 5´-H), 8.92 (dd, 2H, *J*= 8.1 and 1.5 Hz, 4-H and 11-H), 9.03 (dd, 2H, *J*= 4.5 and 1.8 Hz, 6-H and 9-H), 13.79 (s, 1H, N*H*) ppm. ^{13}C NMR (75.4 MHz, DMSO-d_6): δ 123.4, 124.5, 125.8, 126.5, 126.9, 128.7, 128.8, 129.8, 134.7, 135.9, 142.6, 146.4, 147.8, 150.1 ppm. MS (FAB): *m/z* (%) 379 ([M+H]$^+$, 100). HRMS (FAB): *m/z* calcd. for $C_{23}H_{15}N_4S$ 379.1017; found 379.1015. IR (KBr, ν /cm^{-1}): 3439, 2950, 1605, 1562, 1531, 1479,

1451, 1429, 1395, 1351, 1312, 1296, 1259, 1212, 1190, 1119, 1069, 1029, 957, 844, 803, 740. Decomposition at T > 320 ºC. UV (ethanol, nm): λ_{max} (log ε) = 345 (4.16).

2-(furan-2'-yl)-1*H*-imidazo[4,5-*f*][1,10]phenanthroline (6a). The compound was isolated as an orange solid (0.114 g, 85%). ^{1}H RMN (300 MHz, DMSO-d_6): δ 6.76-6.79 (m, 1H, 4'-H), 7.25 (d, 1H, *J* = 3.0 Hz, 3'-H), 7.78-7.82 (m, 2H, 5-H + 10-H), 7.99 (d, 1H, *J* = 1.2 Hz, 5'-H), 8.90 (d, 2H, *J* = 7.8 Hz, 4-H + 11-H), 9.02 (d, 2H, *J* = 1.8 Hz, 6-H + 9-H), 13.93 (br s, 1H, N*H*) ppm. ^{13}C NMR (75.4 MHz, DMSO-d_6): δ 109.9, 112.5, 123.3, 129.6, 143.0, 143.6, 144.4, 145.4, 147.9 ppm. MS (FAB): *m/z* (%) 287 ([M+H]$^+$, 100), 226 (5). HRMS (FAB): *m/z* calcd. for $C_{17}H_{11}N_4O$ 287.09389; found 287.09274. IR (Nujol, ν /cm^{-1}): 3396, 2923, 2853, 1644, 1565, 1538, 1507, 1463, 1397, 1377, 1350, 1228, 1191, 1116, 1073, 1017, 976, 897, 885, 807, 739. Mp = 122.3–124.5 ºC. UV/Vis (ethanol, nm): λ_{max} (log ε) = 318 (4.14).

2-(5'-(thien-2''-yl)furan-2'-yl)-1*H*-imidazo[4,5-*f*][1,10]phenanthroline (6b). The compound was isolated as a dark yellow solid (0.110 g, 79 %). ^{1}H RMN (400 MHz, DMSO-d_6): δ 7.03 (d, 1H, *J* = 3.6 Hz, 3'-H), 7.20-7.22 (m, 1H, 4''-H), 7.33 (d, 1H, *J* = 4.0 Hz, 4'-H), 7.60 (dd, 1H, *J* = 3.6 and 1.2 Hz, 3''-H), 7.66 (dd, 1H, *J* = 5.2 and 0.8 Hz, 5''-H), 7.79-7.86 (m, 2H, 5-H + 10-H), 8.89-8.94 (m, 2H, 4-H + 11-H), 9.03 (dd, 2H, *J* = 4.0 and 2.0 Hz, 6-H + 9-H), 13.89 (s, 1H, N*H*) ppm. ^{13}C NMR (100.6 MHz, DMSO-d_6): δ 108.0, 112.3, 119.2, 123.1, 123.4, 123.5, 124.4, 125.9, 126.4, 128.3, 129.7, 131.9, 135.8, 142.5, 143.6, 143.7, 144.3, 147.9, 147.9, 149.8 ppm. MS (FAB): *m/z* (%) 369 ([M+H]$^+$, 100), 226 (4). HRMS (FAB): *m/z* calcd. for $C_{21}H_{12}N_4OS$ 369.08048; found 369.08046. IR (Liquid film, ν /cm^{-1}): 3436, 1567, 1498, 1444, 1421, 1265, 1072, 1017, 896, 738, 704. Mp = 241.0-242.2 ºC. UV/Vis (ethanol, nm): λ_{max} (log ε) = 364 (4.20).

2-(5'-phenylfuran-2'-yl)-1*H*-imidazo[4,5-*f*][1,10]phenanthroline (6c). The compound was isolated as a yellow solid (0.061 g, 60 %). ^{1}H RMN (400 MHz, DMSO-d_6): δ 7.23 (d, 1H, *J* = 3.6 Hz, 3'-H), 7.34-7.38 (m, 2H, 4''-H + 4'-H), 7.49 (t, 2H, *J* = 8.0 and 7.6 Hz, 3''-H + 5''-H), 7.80-7.83 (m, 2H, 5-H + 10-H), 7.91 (d, 2H, *J* = 7.6 Hz, 2''-H + 6''-H), 8.93 (dd, 2H, *J* = 8.4 and 1.6 Hz, 4-H + 11-H), 9.02 (dd, 2H, *J* = 6.0 and 1.6 Hz, 6-H + 9-H) ppm. ^{13}C NMR (100.6 MHz, DMSO-d_6): δ 108.4, 111.9, 121.6, 123.3, 123.9, 128.1, 128.9, 131.3, 131.3, 143.2, 143.6, 145.3, 147.8, 153.9 ppm. MS (FAB): *m/z* (%) 363 ([M+H]$^+$, 100). HRMS (FAB): *m/z* calcd. for $C_{23}H_{15}N_4O$

363.12380; found 363.12404. IR (Nujol, ν /cm^{-1}): 3371, 2911, 2853, 1619, 1565, 1490, 1397, 1299, 1277, 1190, 1150, 1124, 1073, 1027, 924, 803, 758, 688. Mp = 243.4-244.9. UV/Vis (ethanol, nm): λ_{max} (log ε) = 353 (4.48).

V.4.3.2. Synthesis of the Ru(II) Complexes

In 5 mL of ethylene glycol, the corresponding quantity of imidazo-phenanthroline ligand and the $Ru(bpy)_2Cl_2$ complex were dissolved. The mixture was heated in a Milestone microwave oven (450 W) for 30 s, which led to a color change from violet to deep orange, and then allowed to cool for a while. The mixture was heated for three more periods of 30 s. The solvent was removed by distillation at low pressure, the residue was dissolved in 2 mL of water, and a saturated NH_4PF_6 aqueous solution was added. The precipitate formed was then filtered through a frit, washed with water (3 x 10 mL) and diethyl ether (3 x 10 mL), and dried under vacuum.

C1: 30.2 mg (7.85 x 10^{-5} mol) of **4a** and 42.7 mg (8.2 x 10^{-5} mol) of $Ru(bpy)_2Cl_2$ were used. Colour: Deep orange. Yield: 73.9 mg (87%). Anal. Calcd for $C_{41}H_{28}F_{12}N_8P_2RuS_2$: C, 45.30; H, 2.60; N, 10.30; S, 5.90. Found: C, 45.40; H, 2.80; N, 10.05; S, 5.85. ^{1}H NMR (CD_3CN): δ = 8.69 (s, 1H); 8.56 (t, 4H); 8.36 (d, 2H); 8.11 (m, 4H); 7.85 (m, 7H); 7.47 (m, 7H); 7.13 (m, 3H) ppm. FD-MS: *m/z* 943.06 ([M-PF_6]$^+$), 797.08 ([M-2PF_6-H]$^+$), 399.04 ([M-2PF_6]$^{2+}$). ESI-MS: *m/z* 943.2 ([M-PF_6]$^+$), 797.2 ([M-2PF_6-H]$^+$), 399.1 ([M-2PF_6]$^{2+}$). MALDI-TOF MS: *m/z* 797.6 ([M-2PF_6-H]$^+$), 641.6 ([M-2PF_6-bpy-H]$^+$).

C2: 24.3 mg (5.85 x 10^{-5} mol) of **4b** and 32.0 mg (6.15 x 10^{-5} mol) of $Ru(bpy)_2Cl_2$ were used. A few drops of ethanol were added in order to increase solubilization of the ligand. Colour: Deep orange. Yield: 29.3 mg (45%). Anal. Calcd for $C_{42}H_{30}F_{12}N_8OP_2RuS_2 \cdot 1.5C_2H_5OH$: C, 45.55; H, 3.30; N, 9.45; S, 5.40. Found: C, 45.88; H, 3.40; N, 9.70; S, 5.85. ^{1}H NMR (CD_3CN): δ = 8.80 (d, 2H); 8.53 (m, 4H); 8.10 (t, 2H); 7.99 (t, 2H); 7.87 (m, 4H); 7.66 (d, 3H); 7.56 (m, 2H); 7.44 (t, 2H); 7.25 (t, 2H); 7.02 (d, 1H); 6.91 (d, 1H); 6.24 (d, 1H); 3.92 (s, 3H) ppm. FD-MS: *m/z* 973.03 ([M-PF_6]$^+$), 827.07 ([M-2PF_6-H]$^+$). ESI-MS: *m/z* 973.2 ([M-PF_6]$^+$), 827.2 ([M-2PF_6-H]$^+$), 414.1 ([M-Ru(bpy)$_2$(PF_6)$_2$]$^{\bullet}$. MALDI-TOF MS: *m/z* 827.6 ([M-2PF_6-H]$^+$).

C3: 30.5 mg (8.06 x 10^{-5} mol) of **5** and 44.1 mg (8.47 x10^{-5} mol) of $Ru(bpy)_2Cl_2$ were used. Colour: Deep orange. Yield: 26.3 mg (30%). Anal. Calcd for $C_{43}H_{30}F_{12}N_8P_2RuS{\cdot}6H_2O$: C, 43.40; H, 3.55; N, 9.40; S, 2.70. Found: C, 43.35; H, 3.25; N, 9.40; S, 2.55. ^{1}H NMR ($(CD_3)_2CO$): δ = 9.21 (d, 2H); 8.89 (dd, 4H); 8.50 (d, 2H); 8.31 (m, 4H); 8.20 (m, 4H); 7.99 (d, 2H); 7.91 (dd, 2H); 7.83 (d, 2H); 7.66 (m, 3H); 7.55 (d, 1H); 7.42 (t, 2H); 7.20 (m, 1H) ppm. FD-MS: *m/z* 790.82 ($[M\text{-}2PF_6\text{-}H]^+$). ESI-MS: *m/z* 937.3 ($[M\text{-}PF_6]^+$), 791.3 ($[M\text{-}2PF_6\text{-}H]^+$), 396.1 ($[M\text{-}Ru(bpy)_2(PF_6)_2]^{\bullet}$). MALDI-TOF-MS: *m/z* 791.28 ($[M\text{-}2PF_6\text{-}H]^+$).

C4: 27.2 mg (7.99 x 10^{-5} mol) of **6a** and 44 mg (8.39 x 10^{-5} mol) of $Ru(bpy)_2Cl_2$ were used. An orange solid was obtained. Yield: 72.2 mg (91%). Anal. Calcd for $C_{37}H_{26}F_{12}N_8OP_2Ru$: C, 44.90; H, 2.65; N, 11.30. Found: C, 44.35; H, 2.85; N, 11.30. ^{1}H NMR ($(CD_3)_2CO$): δ = 9.07 (d, 2H); 8.86 (dd, 4H); 8.35 (m, 2H); 8.25 (t, 3H); 8.16 (m, 4H); 7.91 (m, 4H); 7.64 (m, 2H); 7.40 (m, 2H); 7.33 (s, 1H); 6.76 (s, 1H) ppm. MALDI-TOF-MS: *m/z* 699.73 ($[M\text{-}2PF_6\text{-}H]^+$), 543.71 ($[M\text{-}2PF_6\text{-bpy-}H]^+$)

C5: 25 mg (6.18 x 10^{-5} mol) of **6b** and 33.8 mg (6.49 x 10^{-5} mol) of $Ru(bpy)_2Cl_2$ were used. An orange solid was obtained. Yield: 60.0 mg (91%). Anal. Calcd for $C_{41}H_{28}F_{12}N_8OP_2RuS$: C, 45.95; H, 2.65; N, 10.45; S, 3.00. Found: C, 45.90; H, 2.65; N, 10.60; S, 2.60. ^{1}H NMR ($(CD_3)_2CO$): δ = 8.82 (m, 5H); 8.40 (m, 1H); 8.23-8.16 (m, 8H); 7.96 (m, 2H); 7.64-7.40 (m, 8H); 7.15 (s, 1H); 6.95 (s, 1H) ppm. MALDI-TOF-MS: *m/z* 781.79 ($[M\text{-}2PF_6\text{-}H]^+$), 625.73 ($[M\text{-}2PF_6\text{-bpy-}H]^+$), 368.73 ($[M\text{-}Ru(bpy)_2(PF_6)_2]^{\bullet}$

C6: 23.5 mg (5.64E-05 mol) of **6c** and 30.8 mg (5.93E-05 mol) of $Ru(bpy)_2Cl_2$ were used. An orange solid was obtained. Yield: 57.8 mg (96%). Anal. Calcd for $C_{43}H_{30}F_{12}N_8OP_2Ru$: C, 48.45; H, 2.85; N, 10.50. Found: C, 48.35; H, 3.00; N, 9.90. ^{1}H NMR ($(CD_3)_2CO$): δ = 8.83 (m, 5H); 8.40 (m, 1H); 8.25-8.16 (m, 8H); 8.02 (m, 3H); 7.79 (s, 3H); 7.72 (s, 2H); 7.45-7.38 (m, 5H); 7.12 (s, 1H) ppm. MALDI-TOF-MS: *m/z* 775.65 ($[M\text{-}2PF_6\text{-}H]^+$), 619.62 ($[M\text{-}2PF_6\text{-bpy-}H]^+$), 463.57 ($[M\text{-}(bpy)_2\text{-}2PF_6\text{-}H]^+$), 362.67 ($[M\text{-}Ru(bpy)_2(PF_6)_2]^{\bullet}$)

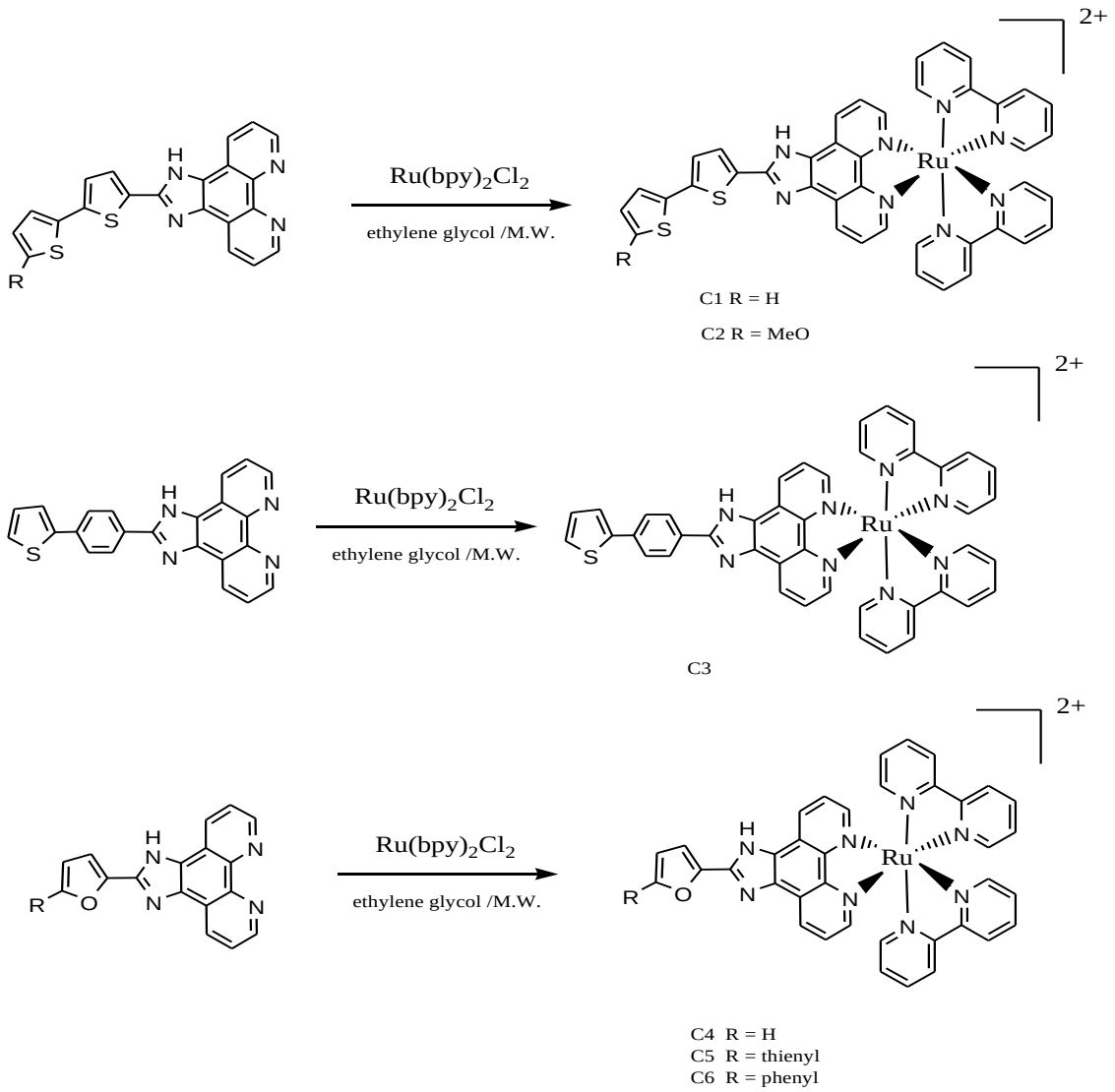

Scheme V.2. Ruthenium(II) Complexes.

V.5. Results and Discussion

V.5.1 Synthesis

In order to compare the effect of the electronic nature of aryl and heteroaryl moieties on the optical properties of linear imidazo-phenanthrolines **4-6**, formyl-derivatives containing bithienyl **1a**-**b**, arylthienyl **2**, furyl **3a**, thienylfuryl **3b** and arylfuryl **3c** π-conjugated bridges were used as precursors of phenanthrolines **4**-**6**.

Compounds **1a**, **2**, **3a** and **3c** were commercially available. The synthesis of 5'-formyl-2-methoxy-2,2'-bithiophene **1b** has been reported.[20]

Therefore, heterocyclic ligands **4**-**6** with either bithienyl, arylthienyl, furyl, thienylfuryl and arylfuryl moieties (unsubstituted or bearing a methoxy donor group) linked to the chelating imidazo-phenanthroline system, were synthesized in good to excellent yields (60-85%, Table V.1) through the Radziszewski reaction,[21] using 5,6-phenanthroline-dione, formyl precursors **1**-**2** and ammonium acetate in refluxing glacial acetic acid for 15 h (Scheme V.1).

In the ^{1}H NMR spectra of most imidazo-phenanthroline derivatives, a peak at about 13.8-13.9 ppm was detected as a broad singlet that was attributed to the N-H in the imidazole moiety. The NH was also identified by IR spectroscopy as a sharp band within the spectral region of 3371-3439 cm^{-1}.

Formyl derivative	Phenanthroline product	R	Yield (%)	IR ν_{N-H} (cm^{-1})	δ_H (imidazole) (ppm)
2	**5**	-	82	3439	13.8
3a	**6a**	H	85	3396	13.9
3b	**6b**	thienyl	79	3436	13.9
3c	**6c**	phenyl	60	3371	*

* Not observed.

Table V.1. Ligand characterization data.

The complexes were obtained by direct reaction of the ligands with $Ru(bpy)_2Cl_2$ in ethylene glycol, under microwave irradiation for 2 min (Scheme V.2). Their purity was confirmed by elemental analysis, ^{1}H NMR and MALDI-TOF MS (see Experimental section).

V.5.2 Spectroscopic characterization

The absorption spectra of the Ru(II) complexes consist mainly of three resolved bands in the 200-600 nm region. The bands around 280 nm are attributed to ligand-centered (LC) π-π^* transitions; the bands around 350 nm are due to the n-π^* transitions and the lowest energy bands at around 460 nm are assigned to the metal-to-ligand charge transfer (MLCT) transitions. The emission spectra are all centered above 600 nm according to what is expected for Ru(II) polypyridyl complexes (see Figures SM V.1 and SM V.2, Supplementary material). Table V.2 summarizes all the spectroscopic data.

Complex	λ_{max}^{abs} / nm	$\varepsilon_{max} / M^{-1}cm^{-1}$	λ_{max}^{em} / nm	Φ_F
C1	463	12719	608	0.006
C2	459	17778	607	0.015
C3	460	11947	603	0.016
C4	459	15873	613	0.009
C5	458	14341	613	0.008
C6	457	12016	611	0.008

Table V.2 – MLCT (d-π*) absorption and emission maxima, molar absorption coefficients (in Tris buffer) and fluorescence quantum yields (in air-equilibrated DMSO) of complexes **C1** to **C6**.

V.5.3 Interaction of Ru(II) complexes with DNA

Electronic absorption spectroscopy is a very useful technique in DNA-binding studies, since binding to double stranded (ds) DNA through intercalation normally results in hypochromism and bathochromism of the MLCT visible absorption band of the complex.[22] The extent of the hypochromism usually parallels the intercalative binding strength.[22] On the other hand, luminescence studies usually show the enhancement of both the luminescence intensity and lifetime of the Ru(II) complexes

upon binding to the DNA. This indicates that the complexes can interact with DNA and are protected by this polynucleotide to some extent from quenching by molecular oxygen and the solvent molecules. Emission quenching experiments may provide further information, since the Stern-Volmer quenching constants can be used as a measure of the binding affinity.

In this way, preliminary studies were performed with complexes **C1**, **C2** and **C3** to compare the interaction of these complexes with DNA in a qualitative way. All the preliminary results obtained with **C1** to **C3** in the presence of DNA are reported in the Supplementary material.

The interaction of the stronger emissive **C3** to **C6** complexes was studied quantitatively; Figure V.1 shows in more detail the spectroscopic study of complex **C3** bearing a thienyl-aryl substituent in the presence of increasing amounts of DNA. Panel A indicates that there is a hypochromicity in the MLCT band upon addition of DNA, suggesting the intercalation of **C3** into the double DNA helix. At the same time the emission intensity (Panel B) and lifetime (Table SM V.1 in Supplementary Material) of the bound luminophore are enhanced due to a combination of a more hydrophobic microenvironment around the metal complex after binding (the O-H oscillators help to deactivate the emissive ^{3}MLCT state) and the protection from quenching by dissolved molecular oxygen imparted by the polynucleotide strand. Figure V.1B shows the increases observed both in the steady state spectra and in the luminescence lifetime in the presence of DNA.

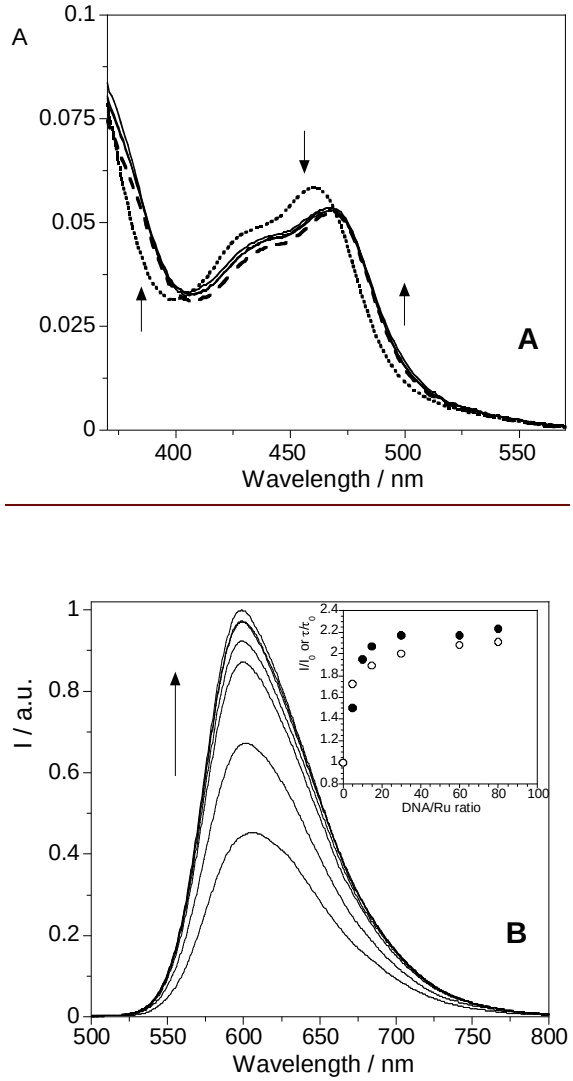

Figure V.1 – (A) Absorption spectra of **C3**, 4.9 μM in TRIS buffer, in the absence (···), and presence of CT-DNA in ratios of 5 (---) and 10 to 30 (**—**).
(B) Emission spectra of C3, 4.9 μM in TRIS buffer, in the presence of increasing amounts of CT-DNA (DNA/Ru ratio of 0 – 80, in base pairs). λ_{exc} = 465 nm. Inset: changes in the emission intensity, I/I_0 (●), and emission lifetime, τ/τ_0 (○), of C3 as a function of DNA/Ru ratio.

A similar behavior was found for the other imidazo-phenanthroline complexes, as can be seen for complex **C5** in Figure V.2 and Table SM V.2 in Supplementary Material. All the results for the remaining complexes are reported in Figures SM V.3 to SM V.6, and Tables SM V.3 and SM V.4, Supplementary Material.

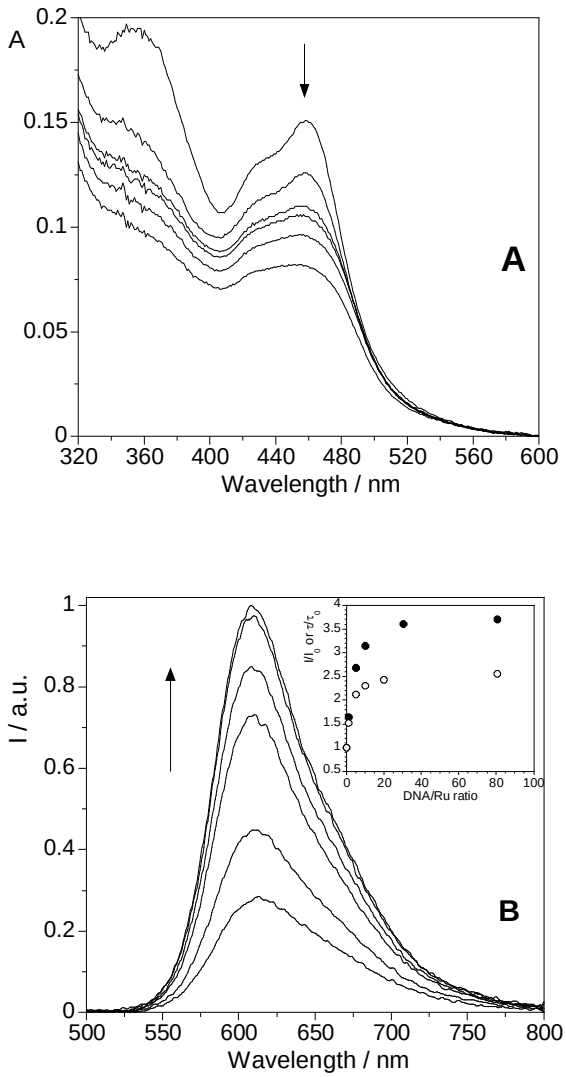

Figure V.2 – (A) Absorption spectra of C5, 10.5 μM in TRIS buffer, in the presence of increasing amounts of CT-DNA (DNA/Ru ratio of 0 – 80, in base pairs). **(B)** Emission spectra of C5, 10.5 μM in TRIS buffer, in the presence of increasing amounts of CT-DNA (DNA/Ru ratio of 0 – 80, in base pairs). λ_{exc} = 460 nm. Inset: changes in the emission intensity, I/I_0 (●), and emission lifetime, τ/τ_0 (○), of C5 as a function of DNA/Ru ratio.

The intrinsic DNA binding constants (K_b), which provide a measure of the interaction strength, were obtained by monitoring the changes in absorbance at 460 nm with increasing concentrations of DNA. The experimental data were fit to the simple Scatchard eq (2),[23] that is only valid for low binder-to-DNA ratios (i.e., far from the DNA saturation) and assumes no binding cooperativity:

$$[DNA]/(\varepsilon_a - \varepsilon_f) = [DNA]/(\varepsilon_b - \varepsilon_f) + 1/[K_b(\varepsilon_b - \varepsilon_f)] \quad (2)$$

where [DNA] is the concentration of the nucleic acid in base pairs, ε_a is the apparent absorption coefficient obtained by calculating A_{obs}/[Ru], and ε_f and ε_b are the absorption coefficients for the free and the fully bound ruthenium complex, respectively.

In the [DNA]/(ε_a- ε_f) vs. [DNA] plot, K_b is given by the ratio of the slope to the intercept. The binding constants obtained thereof for complexes **C3**, **C4**, **C5** and **C6** were, respectively, 2.74 x 10^5, 3.02 x 10^5, 1.32 x 10^5 and 1.63 x 10^5 M^{-1} (see Figures SM V.7 to SM V.10, Supplementary Material). These values are larger than those of the DNA (minor) groove binding Ru(II) complexes such as tris(1,10-phenanthroline)ruthenium(II) and related structures (1.1 x 10^4 – 4.8 x 10^4 M^{-1}),[23,24,25] but smaller than those observed for the $[Ru(bpy)_2(dppz)]^{2+}$ DNA intercalator and other complexes containing an extended phenazine ligand (10^7 to 10^9 M^{-1}).[4c] This result would indicate a more intimate binding of the imidazo-phenanthroline complex to the polynucleotide double strand than that of the simple tris-phenanthroline complex although not as efficient as those bearing a fused polycyclic (hetero)aromatic system that can be inserted between adjacent base pairs of the DNA ladder.

It is interesting to note that the MLCT absorption band of complexes **C4-C6** centered at ca. 455 nm undergoes a more pronounced hypochromic effect upon binding to ds-DNA than the MLCT band at ca. 430 nm. This observation would indicate that the former corresponds to the electronic transition involving the chelating ligand that interacts more closely with the polynucleotide base-pair strand, presumably the intercalated **6a-c** imidazo-phenanthrolines (the small bpy ligands are unable to intercalate into the double helix[26]). Surprisingly enough, the same difference is not observed for the Ru(II) complex **C3** that contains the imidazo-phenanthroline **5**. In the absence of molecular modeling studies, we can hypothesize that the crescent-shaped ligands 6a-c intercalate more efficiently than the long, linear, twisted phenyl-substituted imidazo-phenanthroline **5**.

Except for **C3**, the emission profile of the luminophoric complexes in buffer solution can only be fit to a double exponential function (Tables SM V.1 to SM V.4, Supplementary Material). This fact may be attributed to aggregation of the hydrophobic dyes; the observation of just two components is a consequence of the strong fitting power of the bi-exponential function which does not require introduction of additional components. However, a variety of self-aggregates displaying different

stoichiometries is to be expected, the emission lifetime of which cannot be fully resolved. In the presence of just a 5-fold (molar) concentration of DNA the luminescence decay slows down for the same reasons outlined above for the emission intensity and, although the individual lifetimes of the observed components remain almost the same for higher DNA concentrations, τ_m increases as a consequence of the rise of the contribution of the long lifetime component to the overall decay (except for **C3** where the individual components remain unchanged). These results indicate that the Ru(II) complexes in buffer solution are already fully bound to the DNA under the used experimental conditions even at a $[DNA]_{bp}$/Ru ratio as low as 5. Further addition of the polynucleotide would just make the luminescent probes shift their binding mode, e.g. from aggregated on the double helix to individually bound, as they become "diluted" with larger amounts of DNA. The longest emission lifetime would correspond to the isolated Ru(II) complexes while the shortest one is the signature of the aggregates.

The lack of change in the relative contribution of the short and long lifetimes in the case of the DNA-bound complex **C3**, and the preeminence of the fast component of the decay even at large $[DNA]_{bp}$/Ru ratios might be a consequence of its different interaction mode with the polynucleotide (see above) and a more difficult self-aggregation (unlike the other imidazo-phenanthroline complexes, a single-exponential decay is observed for the photoexcited **C3** in the absence of DNA).

V.5.4 Emission quenching studies

After having studied the interaction of all the complexes with DNA, it was observed that in all cases no significant changes occurred, neither in the emission spectra nor in the luminescence lifetimes, for DNA/Ru ratios in excess of 30. Therefore, this ratio was chosen for subsequent studies with selected excited state quenchers (ethidium bromide, potassium hexacyanoferrate(II) and methyl viologen).[27] It is well established that those quenchers deactivate the excited state of most Ru(II) polypyridyls by photoinduced electron transfer with rate constants in excess of 10^9 L mol^{-1} s^{-1}. Starting with **C3**, it was found out that the addition of increasing amounts of ethidium bromide to a mixture of **C3**+DNA (ratio 1:30) promoted an enhancement of the absorption values in the region corresponding to the MLCT absorption band (Figure SM V.11, Supplementary Material). However, since the intrinsic absorption of ethidium takes place in the same wavelength range,

this absorption increase had to be discarded. A similar effect occurred with the emission spectra (Figure SM V.11, Supplementary Material) and luminescence lifetime measurements (Table SM V.5, Supplementary Material), since both compounds emit in the same region, and the lifetime values for ethidium are significantly shorter, thus masking the true τ_m values.

In the case of potassium hexacyanoferrate(II) quencher, no changes in the luminescence lifetime were observed for the photoexcited **C3** bound to DNA (See Figure SM V.12 and Table SM V.6, Supplementary Material). These results suggest that the complex is fully bound to DNA as the positively charged complex should be easily quenched by this highly anionic quencher if both species were free in solution,[27] while the negative DNA phosphate backbone hinders quenching of the bound complex emission. However, total luminescence quenching is observed for the DNA-bound **C3** complex, both in steady-state and time-resolved emission, in the presence of methyl viologen (MV^{2+}) (Figure V.3 and Table V.3).

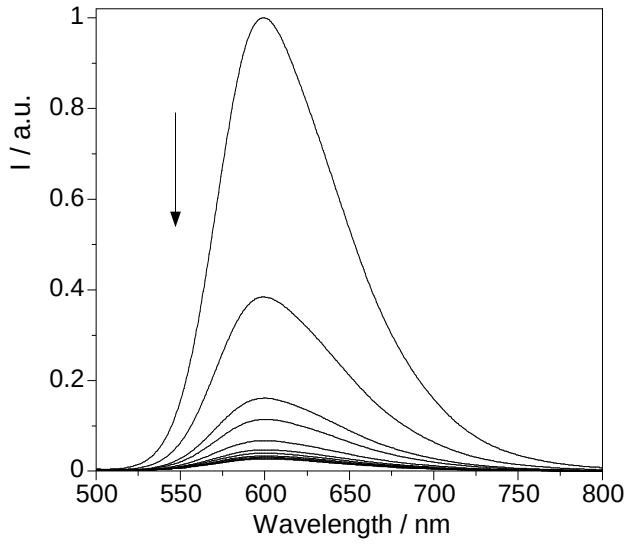

Figure V.3 – Emission spectra of CT-DNA + **C3** (Ratio 30/1) in the presence of increasing amounts of methyl viologen (0 – 200 μM). [C3] = 4.90 μM. $[DNA]_{stock}$ = 2.82 mM. $[MV^{2+}]_{stock}$ = 5 mM. λ_{exc} = 465 nm.

$[MV^{2+}]$ / μM	τ_1/μs	(%)	τ_2/μs	(%)	τ_3/μs	(%)	τ_m / μs	χ^2
0	-		**0.74**	**67**	**1.34**	**33**	**0.94**	**1.10**
5	**0.14**	**21**	**0.43**	**60**	**0.84**	**19**	**0.45**	**1.04**
15	**0.08**	**37**	**0.22**	**50**	**0.54**	**13**	**0.21**	**1.03**
25	**0.08**	**56**	**0.21**	**37**	**0.55**	**10**	**0.17**	**1.10**
50	**0.04**	**54**	**0.13**	**41**	**0.40**	**5**	**0.10**	**1.04**
75	**0.03**	**62**	**0.10**	**35**	**0.38**	**3**	**0.07**	**1.05**
100	**0.03**	**69**	**0.09**	**30**	**0.44**	**1**	**0.05**	**0.91**
125	**0.02**	**66**	**0.08**	**32**	**0.40**	**2**	**0.05**	**1.04**
150	**0.02**	**70**	**0.07**	**29**	**0.40**	**1**	**0.04**	**0.95**
175	**0.02**	**73**	**0.07**	**25**	**0.41**	**2**	**0.04**	**0.98**
200	**0.02**	**77**	**0.07**	**22**	**0.47**	**1**	**0.04**	**0.98**

Table V.3 – Luminescence lifetimes of 1:30 C3:DNA at different MV^{2+} concentrations. [C3] = 4.90 μM. λ_{exc} = 405 nm. λ_{em} = 610 nm. [DNA] = 2.82 mM. $[MV^{2+}]$ = 10 mM.

Emission quenching experiments for complexes **C4**, **C5** and **C6** have also been performed using methyl viologen as a quencher, and the results are comparable to those obtained for **C3**. Steady-state emission spectra and luminescence lifetime decays for **C5** are represented on Figure V.4 and Table V.4, respectively (See absorption spectra in Figure SM V.13, Supplementary Material). All the results for the remaining complexes are reported in Figures SM V.14 and SM V.15 and Tables SM V.7 and SM V.8, Supplementary Material. The slight enhancement of the lifetime values for the last methyl viologen additions (Tables SM V.7 and SM V.8) suggests a partial displacement of the DNA bound Ru(II) complexes to the bulk solution under these conditions.

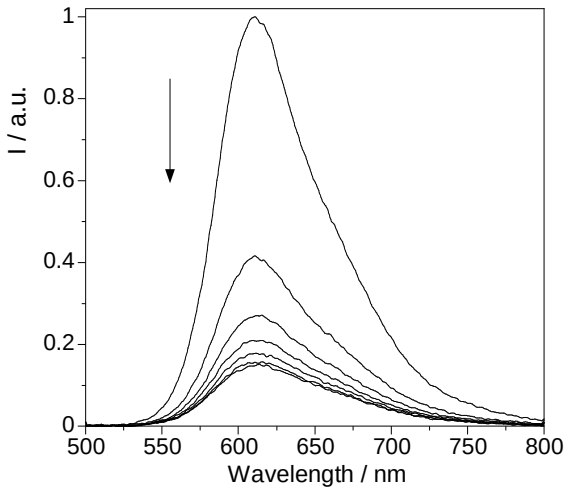

Figure V.4 – Emission spectra of CT-DNA + **C5** (Ratio 30/1) in the presence of increasing amounts of methyl viologen (0 – 200 μM). λ_{exc} = 465 nm. [C5] = 10.5 μM.

$[MV^{2+}]$ / μM	τ_1/μs	(%)	τ_2/μs	(%)	τ_3/μs	(%)	τ_m / μs	χ^2
0	-		**0.50**	**47**	**1.51**	**53**	**1.04**	**1.03**
25	**0.18**	**32**	**0.49**	**61**	**1.09**	**7**	**0.43**	**1.12**
50	**0.13**	**32**	**0.31**	**55**	**0.67**	**13**	**0.30**	**1.19**
75	**0.12**	**57**	**0.36**	**40**	**0.85**	**3**	**0.24**	**1.11**
100	**0.07**	**40**	**0.21**	**43**	**0.55**	**17**	**0.21**	**1.12**
150	**0.07**	**57**	**0.31**	**34**	**0.65**	**9**	**0.20**	**1.09**
200	**0.05**	**55**	**0.28**	**27**	**0.57**	**18**	**0.21**	**1.06**

Table V.4 – Luminescence lifetimes of 1:30 **C5**:DNA at different MV^{2+} concentrations. [C5] = 10.5 μM. λ_{exc} = 405 nm. λ_{em} = 613 nm.

From the complexes **C3-C6** emission quenching studies with methyl viologen the Stern-Volmer constants, K_{SV}, and the corresponding quenching rate constants, k_q, were determined. Whenever non-linear Stern-Volmer plots were obtained, the rate constant data refer to the initial slope. The k_q values obtained from each lifetime component (fast and slow, respectively) of each complex, were: 1.7 x 10^{11} and 1.0 x 10^{11} $M^{-1}s^{-1}$ (**C3**); 9.4 x 10^9 and 1.9 x 10^{10} $M^{-1}s^{-1}$ (**C4**); 3.9 x 10^9 and 7.6 x 10^9 $M^{-1}s^{-1}$ (**C5**); 2.0 x 10^{10} and 2.1 x 10^{10} $M^{-1}s^{-1}$ (**C6)**. These values exceed by one or two orders of magnitude those commonly obtained for Ru(II) complexes with MV^{2+} (ca. 10^9 $M^{-1}s^{-1}$).[27] Such acceleration of the photoinduced electron transfer might be due to several

factors, one of them being the increase of the local concentration (closer average distance) of donor and acceptor species on the nucleic acid (since both the ruthenium (II) complex and the quencher are bound to the DNA). Considering this effect, the calculated values for the quenching rate constants represent only apparent values, since the quencher concentration values on the abscissa correspond to different local quencher concentrations on the polynucleotide.

The results for **C3**+DNA in the presence of methyl viologen are represented in Figure V.5. All the other results, including the data for C3 with ethidium bromide, are represented in Figures SM V.16 to SM V.19, Supplementary Material).

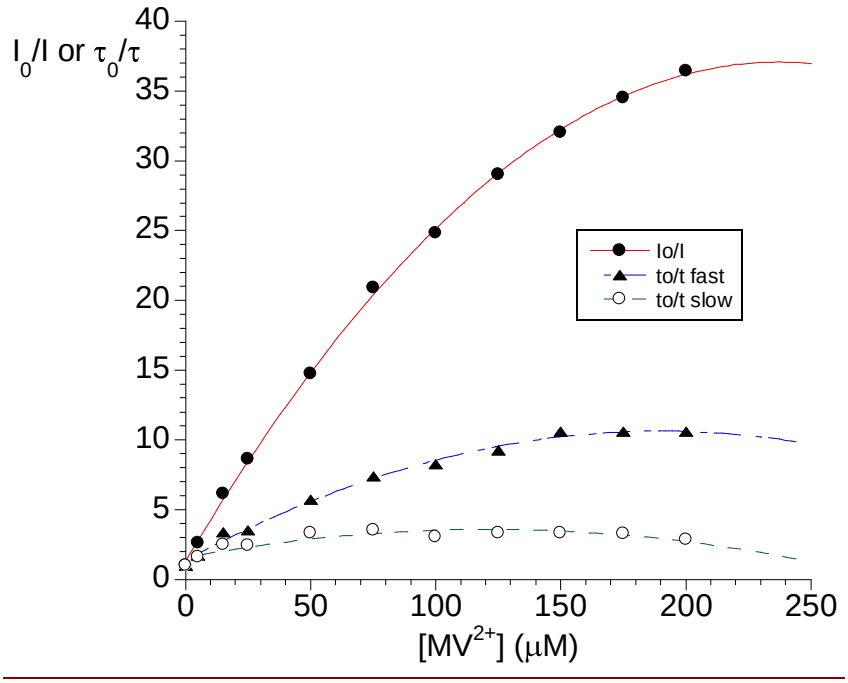

Figure V.5 – Stern-Volmer emission intensity (●) and lifetime quenching plot for C3+DNA (ratio 1:30) in the presence of increasing amounts of methyl viologen (MV^{2+}). Both fast (short) (▲) and slow (long) (○) components of the emission decay are represented. λ_{exc} = 405 nm. Emission collected at 610 nm.

V.6 Conclusions

Four new ligands and six Ru(II) polypyridyl complexes have been synthesized, the latter through microwave-assisted reactions, which considerably reduces the reaction times from hours to minutes, with satisfactory yields. Studies of their interaction with calf thymus DNA have suggested a partial intercalation of the probes

into the nucleic acid double strand. According to the structural features of the complexes and the obtained values for the binding constants, it is possible that the crescent-shaped complexes C4, C5 and C6 have a more intimate binding to the polynucleotide double strand than the phenyl-substituted C3. Luminescence quenching studies further support this hypothesis, since in the case of potassium hexacyanoferrate(II) no quenching was observed (which indicates that all the complex was bound to the DNA) and with methyl viologen the quenching was accompanied by partial displacement of the complexes to the bulk solution at high quencher concentrations. All these results illustrate the feasibility of fine tuning the DNA interaction mode of luminescent Ru(II) complexes containing extended imidazo-phenanthroline ligands by molecular engineering of their aryl substituents. Such feature might be used in the future to design tailored molecular probes of the polynucleotide features.

V.7 Acknowledgments

We are indebted to InOU Uvigo for project K914 122P 64702 (Spain), Xunta de Galicia (Spain) for project 09CSA043383PR and FCT-Portugal for project PTDC/QUI/66250/2006 for financial support. The NMR spectrometers are part of the National NMR Network and were purchased in the framework of the National Programme for Scientific Re-equipment, contract REDE/1517/RMN/2005, with funds from POCI 2010 (FEDER) and FCT-Portugal.
J. L. C. and C. L. thank Xunta de Galicia, Spain, for the Isidro Parga Pondal Research Program. B. P. and R. B. thank FC-MCTES (Portugal) for their PhD grants SFRH/BD/27786/2006 and SFRH/BD/36396/2007, respectively.
We are grateful to Dr. A. Jorge Parola from the REQUIMTE, Universidade NOVA de Lisboa, Portugal for his help with the synthesis of the $Ru(bpy)_2Cl_2$ precursor.

V.8 References

(1) (*a*) J.G. Vos and J.M. Kelly, *Dalton Trans.*, 2006, **41**, 4869-4883; (*b*) D.A. Jose, P. Kar, D. Koley, B. Ganguly, W. Thiel, H. N. Ghosh and A. Das, *Inorg. Chem.*, 2007,

46, 5576-5584. (*c*) V. Balzani, G. Bergamini, F. Marchioni and P. Ceroni, *Coord. Chem. Rev.*, 2006, **250**, 1254-1266.

(2) (*a*) B. Norden, P. Lincoln, B. Akerman and E. Tuite, *Met. Ions Biol. Syst.*, 1996, **33**, 177-252; (*b*) E. D. A. Stemp and J. K. Barton, *Met. Ions Biol. Syst.*, 1996, **33**, 325-365; (*c*) C. Moucheron, A. Kirsch-De Mesmaeker and J. M. Kelly, *Struct. Bonding*, 1998, **92**, 163-216; (*d*) K. E. Erkkila, D. T. Odom and J. K. Barton, *Chem. Rev.*, 1999, **99**, 2777-2795; (*e*) L. N. Ji, X. H. Zou and J. G. Liu, *Coord. Chem. Rev.*, 2001, **216**, 513-536; (*f*) C. Metcalfe and J. A. Thomas, *Chem. Soc. Rev.*, 2003, **32**, 215-224; (*g*) M. J. Clarke, *Coord. Chem. Rev.*, 2002, **232**, 69-93; (*h*) H. Chao and L.N. Ji, *Bioinorg. Chem. Appl.*, 2005, **3**, 15-28.

(3) B. T. Farrer and H. H. Thorp, *Inorg. Chem*., 2000, **39**, 44-49.

(4) (*a*) A. Kirsch-De Mesmaeker, J. P. Lecomte and J. M. Kelly, *Top. Curr. Chem.*, 1996, **177***,* 25-76; (*b*) Y. Jenkins, A. E. Friedman, N. J. Turro and J. K. Barton, *Biochemistry*, 1992, **31**, 10809-10816; (*c*) A. E. Friedman, J. C. Chambron, J. P. Sauvage, N. J. Turro and J. K. Barton, *J. Am. Chem. Soc.*, 1990, **112**, 4960-4962; (*d*) A. B. Tossi and J. M. Kelly, *Photochem. Photobiol.,* 1989, **49**, 545-556; (*e*) I. Ortmans, C. Moucheron and A. Kirsch-De Mesmaeker, *Coord. Chem. Rev.*, 1998, **168***,* 233-271; (*f*) J. M. Kelly, M. Feeney, L. Jacquet, A. Kirsch-De Mesmeaker and J. P. Lecomte, *Pure Appl. Chem.*, 1997, **69**, 767-772; (*g*) F. Piérard, A. Del Guerzo, A. Kirsch-De Mesmaeker, M. Demeunynck and J. Lhomme, *Phys. Chem. Chem. Phys.*, 2001, **3**, 2911-2920.

(5) (*a*) E. Amouyal, A. Homsi, J. C. Chambron and J. P. Sauvage, *J. Chem. Soc. Dalton Trans.*, 1990, 1841-1845; (*b*) R. B. Nair, B. M. Cullum and C. J. Murphy, *Inorg. Chem*., 1997, **36***,* 962-965; (*c*) L. Ujj, C. G. Coates, J. M. Kelly, P. Kruger, J. J. McGarvey and G. H. Atkinson, *J. Phys. Chem. B.*, 2002, **106**, 4854-4862; (*d*) C. G. Coates, P. L. Callaghan, J. J. McGarvey, J. M. Kelly, P. Kruger and M. E. Higgins, *J. Raman Spectrosc.*, 2000, **31**, 283-288; (*e*) C. Turro, S.H. Bossman, Y. Jenkins, J. K. Barton and N. J. Turro, *J. Am. Chem. Soc.*, 1995, **117**, 9026-9032; (*f*) E. Sabatini, H. D. Nikol, H. B. Gray and F. C. Anson, *J. Am. Chem. Soc.*, 1996, **118**, 1158-1163; (*g*)

X. Q. Guo, F. N. Castellano, L. Li and J. R. Lakowicz, *Biophys. Chem.,* 1998, **71**, 51-62; (*h*) M. K. Brennaman, J. H. Alstrum-Acevedo, C. N. Fleming, P. Jang, T. J. Meyer and J. M. Papanikolas, *J. Am. Chem. Soc.,* 2002, **124**, 15094-15098; (*i*) G. Pourtois, D. Beljonne, C. Moucheron, S. Schumm, A. Kirsch-De Mesmaeker, R. Lazzaroni and J. L. Brédas, *J. Am. Chem. Soc.*, 2004, **126**, 683-692.

(6) E. J. C. Olson, D. Hu, A. Hormann, A. M. Jonkman, M. R. Arkin, E. D. A. Stemp, J. K. Barton and P. F. Barbara, *J. Am. Chem. Soc.*, 1997, **119**, 11458-11467.

(7) (*a*) E. Tuite, P. Lincoln and B. Nordén, *J. Am. Chem. Soc.,* 1997, **119**, 239-240; (*b*) C. Hiort, P. Lincoln and B. Nordén, *J. Am. Chem. Soc.*, 1993, **115**, 3448-3454; (*c*) P. Lincoln, A. Broo and B. Nordén, *J. Am. Chem. Soc.*, 1996, **118***,* 2644-2653; (*d*) P. Nordell, F. Westerlund, M. Wilhelmsson, B. Nordén and P. Lincoln, *Angew. Chem. Int. Ed.*, 2007, **46**, 2203-2206; (*e*) P. Nordell and P. Lincoln, *J. Am. Chem. Soc.*, 2005, **127**, 9670-9671; (*f*) B. Önfelt, J. Olofsson, P. Lincoln and B. Nordén, *J. Phys. Chem. A*, 2003, **107**, 1000-1009; (*g*) J. Olofsson, B. Önfelt and P. Lincoln, *J. Phys. Chem. A*, 2004, **108**, 4391-4398; (*h*) F. Westerlund, F. Pierard, M. P. Eng, P. Nordén and P. Lincoln, *J. Phys. Chem. B*, 2005, **109**, 17327-17332; (*i*) F. Westerlund, M. P. Eng, M. U. Winters and P. Lincoln, *J. Phys. Chem. B*, 2007, **111**, 310-317; (*j*) F. Westerlund, P. Nordell, J. Blechinger, T. M. Santos, B. Nordén and P. Lincoln, *J. Phys. Chem. B*, 2008, **112**, 6688-6694; (*k*) C. G. Coates, J. Olofsson, M. Coletti, J. J. McGarvey, B. Önfelt, P. Lincoln, B. Norden, E. Tuite, P. Matousek, A. W. Parker, *J. Phys. Chem. B*, 2001, **105**, 12653-12664; (*l*) M. Li and P. Lincoln, *J. Inorg. Biochem.* 2009, **103**, 963-970.

(8) (*a*) D. García-Fresnadillo and G. Orellana, *Helv. Chim. Acta*, 2001, **84**, 2708-2730; (*b*) S. W. Snyder, S. L. Buell, J. N. Demas and B. A. DeGraff, *J. Phys. Chem.* 1989, **93**, 5265-5271.

(9) (*a*) A. Hergueta-Bravo, M. E. Jiménez-Hernández, F. Montero, E. Oliveros and G. Orellana, *J. Phys. Chem. B*, 2002, **106***,* 4010-4017; (*b*) M. F. Ottaviani, N. D. Ghatlia, S. H. Bossmann, J. K. Barton, H. Durr and N. J. Turro, *J. Am. Chem. Soc.*, 1992, **114***,* 8946-8952.

(10) M. R. Gill, J. Garcia-Lara, S. J. Foster, C. Smythe, G. Battaglia and J. A. Thomas, *Nature Chemistry,* 2009, **1**, 662-667.

(11) A. Kirsch-De Mesmaeker, G. Orellana, J. K. Barton and N. J. Turro, *Photochem. Photobiol.,* 1990, **52**, 461-472.

(12) J. M. Kelly, A. B. Tossi, D. J. McConnell and C. OhUigin, *Nucl. Acids Res.*, 1985, **13**, 6017-6034.

(13) (*a*) C. Lodeiro, J. L. Capelo, J. C. Mejuto, E. Oliveira, H. M. Santos, B. Pedras and C. Nuñez, *Chem. Soc. Rev.* 2010, **39**, 2948-2976; (*b*) C. Lodeiro and F. Pina, *Coord. Chem. Rev.*, 2009, **253**, 1353-1383; (*c*) B. Pedras, H. M. Santos, L. Fernandes, B. Covelo, A. Tamayo, E. Bértolo, J. L. Capelo, T. Avilés, C. Lodeiro, *Inorg. Chem. Comm.*, 2007, **10***,* 925-929; (*d*) J. Lopez-Gejo, A. Arranz, A. Navarro, C. Palácio, E. Munoz and G. Orellana, *J. Am. Chem. Soc.*, 2010, **132**, 1746-1747; (*e*) J. Lopez-Gejo, D. Haigh and G. Orellana, *Langmuir*, 2010, **26**, 2144-2150.

(14) (*a*) R. M. F. Batista, S. P. G. Costa, C. Lodeiro, M. Belsley and M. M. M. Raposo, *Tetrahedron,* 2008, **64**, 9230-9238. (*b*) R. M. F. Batista, S. P. G. Costa, C. Lodeiro, M. Belsley, E. de Matos Gomes and M. M. M. Raposo, *Adv. Mat. Forum IV,* 2008*,* **263***,* 587-588.

(15) R. M. F. Batista, S. P. G. Costa, M. Belsley and M. M. M. Raposo, *Dyes Pigments,* 2009, **80**, 329-336.

(16) A. Kobori, J. Morita, M. Ikeda, A. Yamayoshi and A. Murakami, *Biorg. Med. Chem. Lett.,* 2009, **19**, 3657-3660.

(17) L. F. Tan, S. Zhang, X. H. Liu and Y.Xiao, *Australian J. Chem.*, 2008, **9**, 725-731.

(18) G. Orellana, A. Kirsch-De Mesmaeker, J. K. Barton and N. J. Turro, *Photochemistry and Photobiology,* 1991, **54***,* 499-509.

(19) B. P. Sullivan, D. J. Salmon, T. J. Meyer, *Inorg. Chem.* 1978, **17**, 3334-3341.

(20) M. M. M. Raposo and G. Kirsch, *Tetrahedron*, 2003, **59**, 4891-4899.

(21) D. Davidson, M. Weiss and M. J. Jelling, *J. Org. Chem*., 1937, **2**, 319-327.

(22) E. C. Long and J. K. Barton, *Acc. Chem. Res.*, 1990, **23**, 271–273.

(23) A. Wolf, G. H. Shimer Jr. and T. Meehan, *Biochemistry*, 1987, **26**, 6392-6396.

(24) A. M. Pyle, J. P. Rehmann, R. Meshoyrer, C. V. Kumar, N. J. Turro and J. K. Barton, *J. Am. Chem. Soc.*, 1989, **111***,* 3051-3058.

(25) J. L. Morgan, D. P. Buck, A. G. Turley, J. G. Collins and F. R. Keene, *Inorg. Chim. Acta*, 2006, **359***,* 888-898.

(26) I. D. Vladescu, M. J. McCauley, M. E. Nuñez, I. Rouzina and M. C. Williams, *Nature Methods*, 2007, **4**, 517-522.

(27) M. Z. Hoffman, F. Bolletta, L. Moggi and G. L. Hug, *J. Phys. Chem. Ref. Data*, 1989, **18**, 219-544.

V.9 Supplementary Material

Absorption spectra of complexes **C1** to **C6**; luminescence lifetimes for **C3** to **C6** at different Ru:DNA ratios; Absorption and emission spectra of **C4** and **C6** with CT-DNA; Ethidium bromide, methyl viologen and potassium ferrocyanide experiments and Stern-Volmer experiments with DNA. This material is available free of charge via the Internet at http://pubs.acs.org.

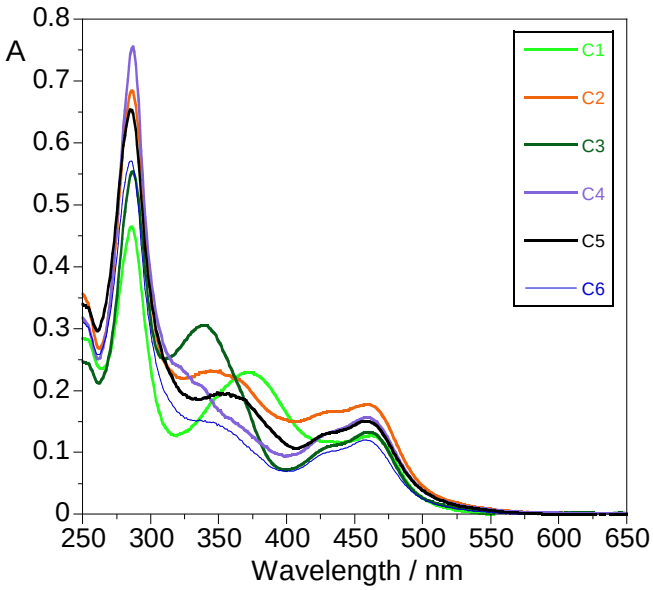

Figure SM V.1 – Absorption spectra of **C1** to **C6** in TRIS buffer. (Room temperature, pH = 7. [C1] = [C6] = 10 μM. [C3] = 9.43 μM. [C4] = 9.85 μM. [C2] = [C5] = 10.5 μM).

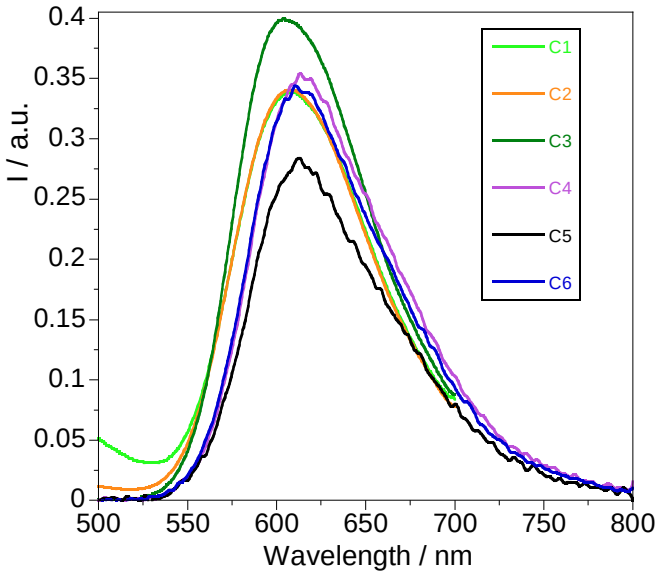

Figure SM V.2 – Emission spectra at room temperature of **C1** to **C6** in TRIS buffer. (pH = 7. [C1] = [C6] = 10 μM. [C3] = 9.43 μM. [C4] = 9.85 μM. [C2] = [C5] = 10.5 μM. λ_{exc} = 370 nm for C1, C2 and C3; 460 nm for C4, C5 and C6).

$[DNA]_{bp}/[C3]$	τ_1/μs	(%)	τ_2/μs	(%)	τ_m / μs	χ^2
0	0.47	100	-		-	1.08
5	0.62	61	1.10	39	0.81	0.99
15	0.68	57	1.17	43	0.89	1.22
30	0.74	67	1.34	33	0.94	1.10
60	0.77	66	1.37	34	0.98	1.08
80	0.79	67	1.41	33	0.99	1.02

Table SM V.1 – Luminescence lifetimes of C3 at different Ru:DNA ratios. [C3] = 4.90 μM; λ_{exc} = 405 nm; λ_{em} = 610 nm. $[DNA]_{bp}$ = 2.82 mM.

$[DNA]_{bp}/[C5]$	$\tau_1/\mu s$	(%)	$\tau_2/\mu s$	(%)	τ_m / µs	χ^2
0	0.35	67	0.61	33	0.43	1.03
1	0.43	78	1.40	22	0.65	1.09
5	0.49	57	1.46	43	0.91	1.13
10	0.52	53	1.52	47	0.99	1.11
20	0.51	46	1.49	54	1.04	1.06
80	0.51	41	1.51	59	1.10	1.05

Table SM V.2 – Luminescence lifetimes of C5 at different Ru:DNA ratios. [C5] = 10.5 µM. λ_{exc} = 405 nm. λ_{em} = 613 nm. $[DNA]_{bp}$ = 2.02 mM.

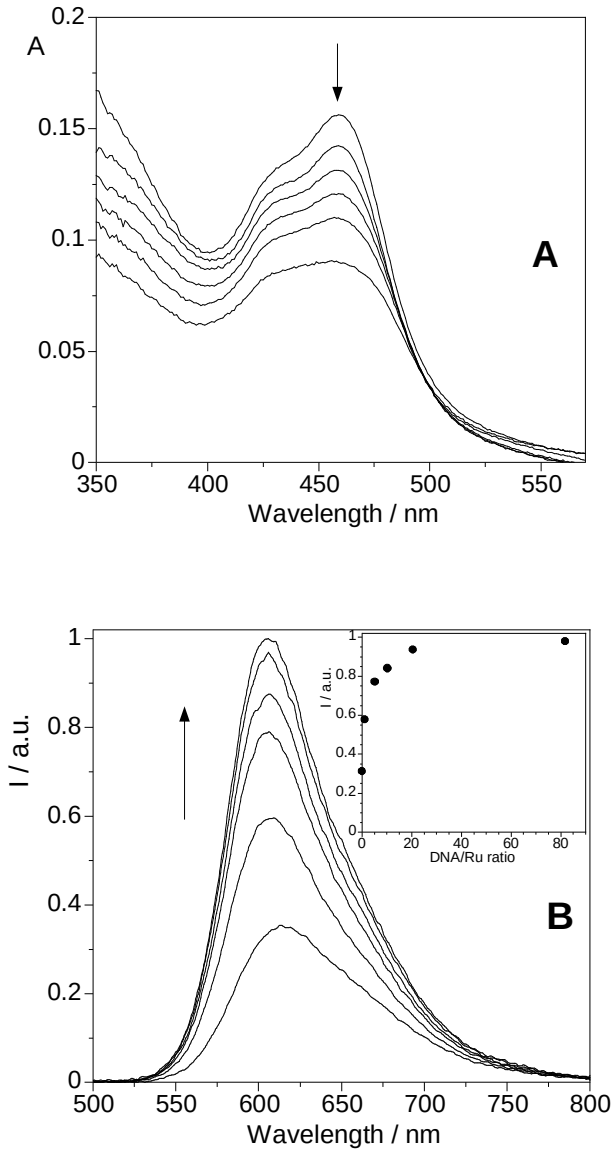

Figure SM V.3 – (A) Absorption spectra of C4, 9.85 μM in TRIS buffer, in the presence of increasing amounts of CT-DNA (DNA/Ru ratio of 0 – 80, in base pairs). **(B)** Emission spectra of C4, 9.85 μM in TRIS buffer, in the presence of increasing amounts of CT-DNA (DNA/Ru ratio of 0 – 80, in base pairs). λ_{exc} = 460 nm. Inset: changes in the emission of C4 at λ = 600 nm as a function of DNA/Ru ratio.

$[DNA]_{bp}/[C4]$	$\tau_1/\mu s$	(%)	$\tau_2/\mu s$	(%)	τ_m / µs	χ^2
0	0.29	67	0.52	33	0.37	1.00
1	0.41	62	1.36	38	0.77	1.11
5	0.46	45	1.36	55	0.95	1.08
10	0.55	45	1.42	55	1.03	1.02
30	0.60	42	1.47	58	1.11	1.09
80	0.66	40	1.51	60	1.17	1.00

Table SM V.3 – Luminescence lifetimes of C4 at different Ru:DNA ratios. [C4] = 9.85 µM. λ_{exc} = 405 nm. λ_{em} = 613 nm. $[DNA]_{bp}$ = 2.02 mM.

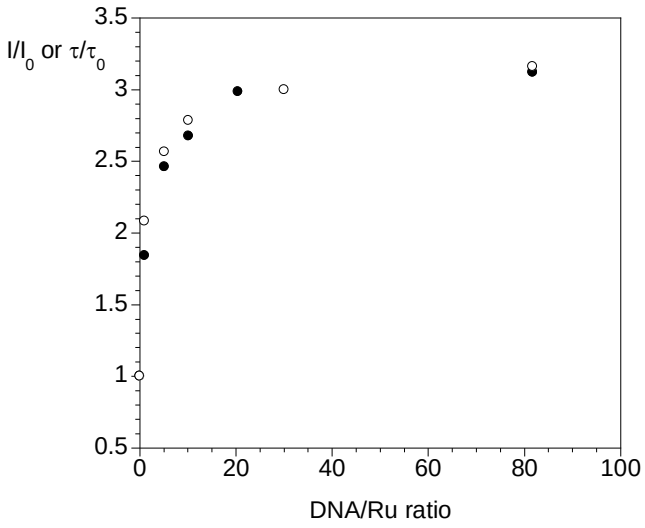

Figure SM V.4 – Changes in the emission intensity, I/I_0 (●), and emission lifetime, τ/τ_0 (○), of C4 in the presence of increasing amounts of CT-DNA.

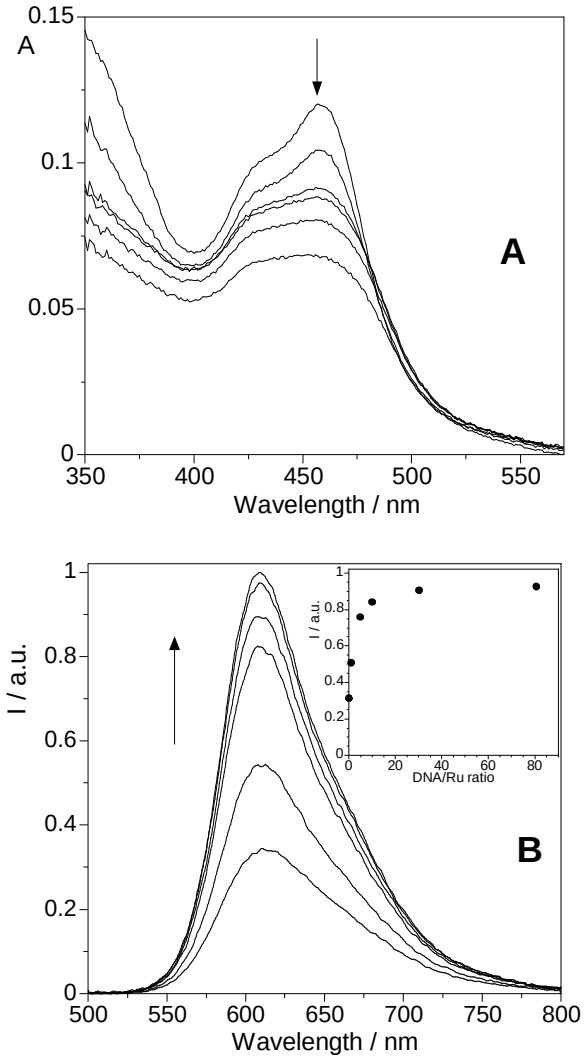

Figure SM V.5 – (A) Absorption spectra of C6, 10.0 μM in TRIS buffer, in the presence of increasing amounts of CT-DNA (DNA/Ru ratio of 0 – 80, in base pairs). **(B)** Emission spectra of C6, 10.0 μM in TRIS buffer, in the presence of increasing amounts of CT-DNA (DNA/Ru ratio of 0 – 80, in base pairs). λ_{exc} = 460 nm. Inset: changes in the emission of C5 at λ = 600 nm as a function of DNA/Ru ratio.

$[DNA]_{bp}/[C6]$	$\tau_1/\mu s$	(%)	$\tau_2/\mu s$	(%)	τ_m / µs	χ^2
0	**0.30**	**45**	**0.51**	**55**	**0.42**	**1.09**
1	**0.43**	**78**	**1.41**	**22**	**0.65**	**1.13**
5	**0.48**	**51**	**1.43**	**49**	**0.94**	**1.09**
10	**0.52**	**48**	**1.50**	**52**	**1.03**	**1.02**
20	**0.49**	**40**	**1.48**	**60**	**1.08**	**1.05**
30	**0.54**	**40**	**1.50**	**60**	**1.12**	**1.09**
80	**0.59**	**41**	**1.55**	**59**	**1.16**	**1.02**

Table SM V.4 – Luminescence lifetimes of C6 at different Ru:DNA ratios. [C6] = 10.0 µM. λ_{exc} = 405 nm. λ_{em} = 613 nm. $[DNA]_{bp}$ = 2.02 mM.

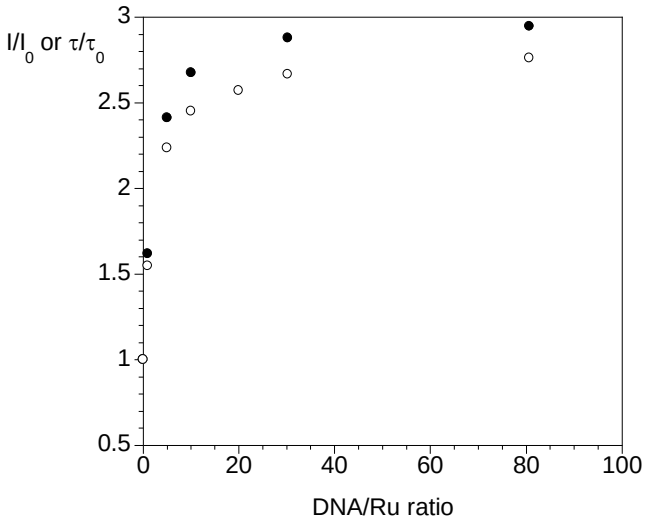

Figure SM V.6 – Changes in the emission intensity, I/I_0 (●), and emission lifetime, τ/τ_0 (○), of C6 in the presence of increasing amounts of CT-DNA.

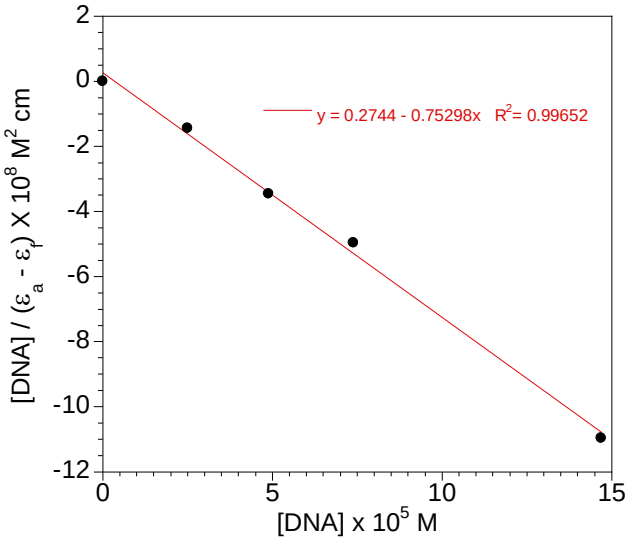

Figure SM V.7 – Plot of [DNA]/(ε_a- ε_b) vs. [DNA] for the absorption titration of C3 with DNA. [C3] = 4.90 μM. $[DNA]_{stock}$ = 2.82 mM. K_b = 2.74 x 10^5 M^{-1}.

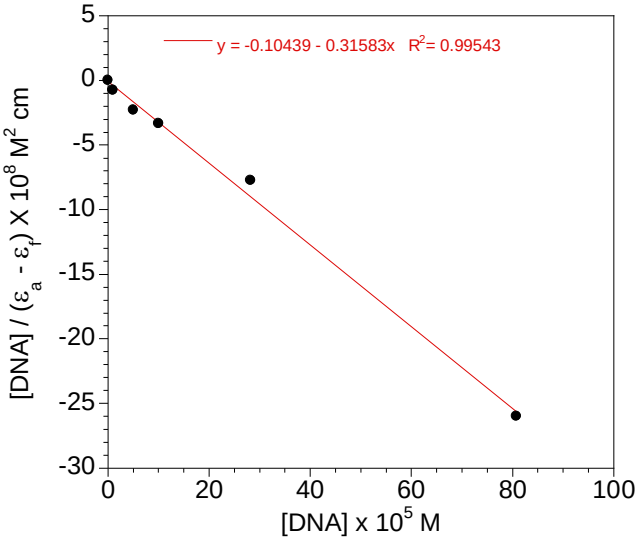

Figure SM V.8 – Plot of [DNA]/(ε_a- ε_b) vs. [DNA] for the absorption titration of C4 with DNA. [C4] = 9.85 μM. $[DNA]_{stock}$ = 2.82 mM. K_b = 3.02 x 10^5 M^{-1}.

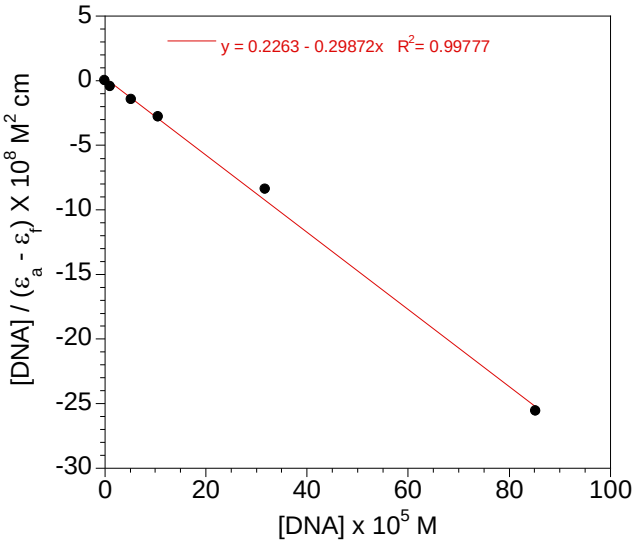

Figure SM V.9 – Plot of [DNA]/(ε_a- ε_b) vs. [DNA] for the absorption titration of C5 with DNA. [C5] = 10.5 μM. $[DNA]_{stock}$ = 2.82 mM. K_b = 1.32 x 10^5 M^{-1}.

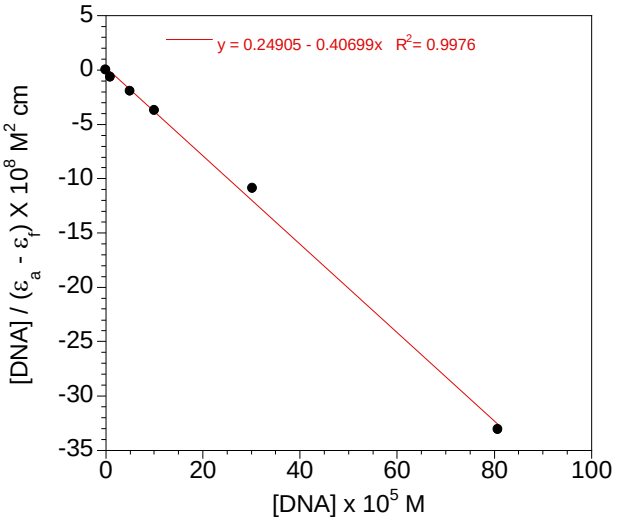

Figure SM V.10 – Plot of [DNA]/(ε_a- ε_b) vs. [DNA] for the absorption titration of C6 with DNA. [C6] = 10.0 μM. $[DNA]_{stock}$ = 2.82 mM. K_b = 1.63 x 10^5 M^{-1}.

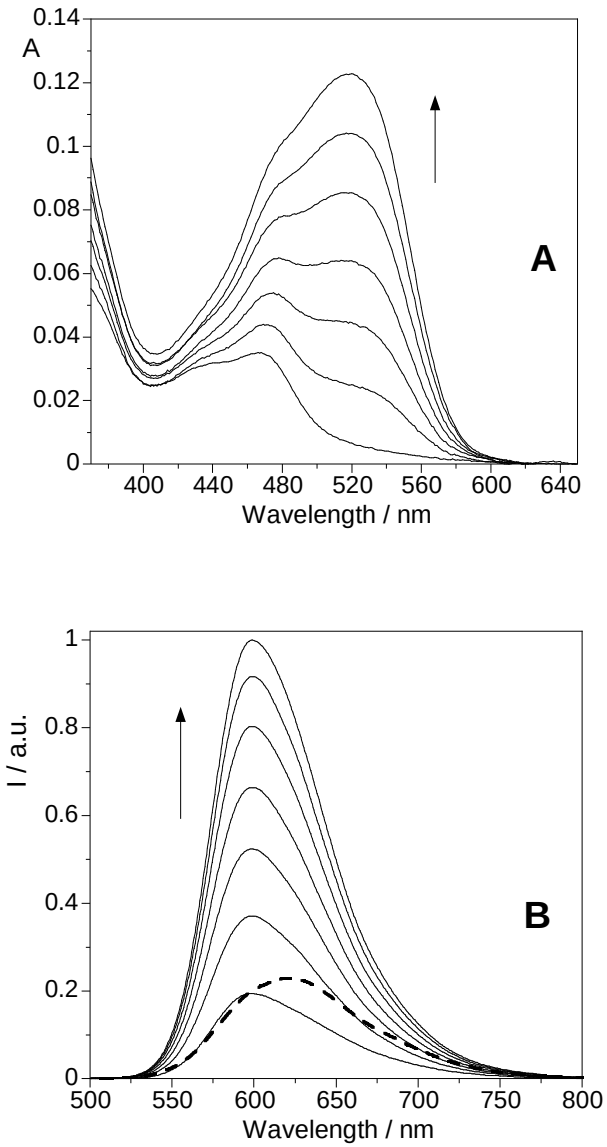

Figure SM V.11 – (A) Absorption spectra of CT-DNA + C3 (Ratio 30/1) in the presence of increasing amounts of ethidium bromide (0 – 30 μM). [C3] = 4.90 μM. $[DNA]_{stock}$ = 2.82 mM. $[ETBr]_{stock}$ = 1mM. **(B)** Emission spectra of ethidium bromide (---) and of CT-DNA + C3 (Ratio 30/1) in the presence of increasing amounts of ethidium bromide (0 – 30 μM). [C3] = 4.90 μM. $[DNA]_{stock}$ = 2.82 mM. $[ETBr]_{stock}$ = 1 mM. λ_{exc} = 465 nm.

[EtBr] / μM	τ_1/μs	(%)	τ_2/μs	(%)	τ_3/μs	(%)	τ_m / μs	χ^2
0			**0.74**	**67**	**1.34**	**33**	**0.94**	**1.10**
5	**0.03**	**80**	**0.53**	**11**	**1.09**	**9**	**0.18**	**1.10**
10	**0.03**	**85**	**0.46**	**7**	**0.97**	**8**	**0.13**	**1.08**
15	**0.03**	**88**	**0.35**	**6**	**0.84**	**6**	**0.10**	**1.16**
20	**0.03**	**89**	**0.30**	**5**	**0.74**	**6**	**0.08**	**1.09**
25	**0.03**	**90**	**0.32**	**6**	**0.75**	**4**	**0.07**	**1.17**
30	**0.03**	**91**	**0.24**	**4**	**0.60**	**5**	**0.06**	**1.10**

Table SM V.5 – Luminescence lifetimes of 1:30 C3:DNA at different ETBr concentrations. [C3] = 4.90 μM. λ_{exc} = 405 nm. λ_{em} = 610 nm. [DNA] = 2.82 mM. [ETBr] = 1 mM.

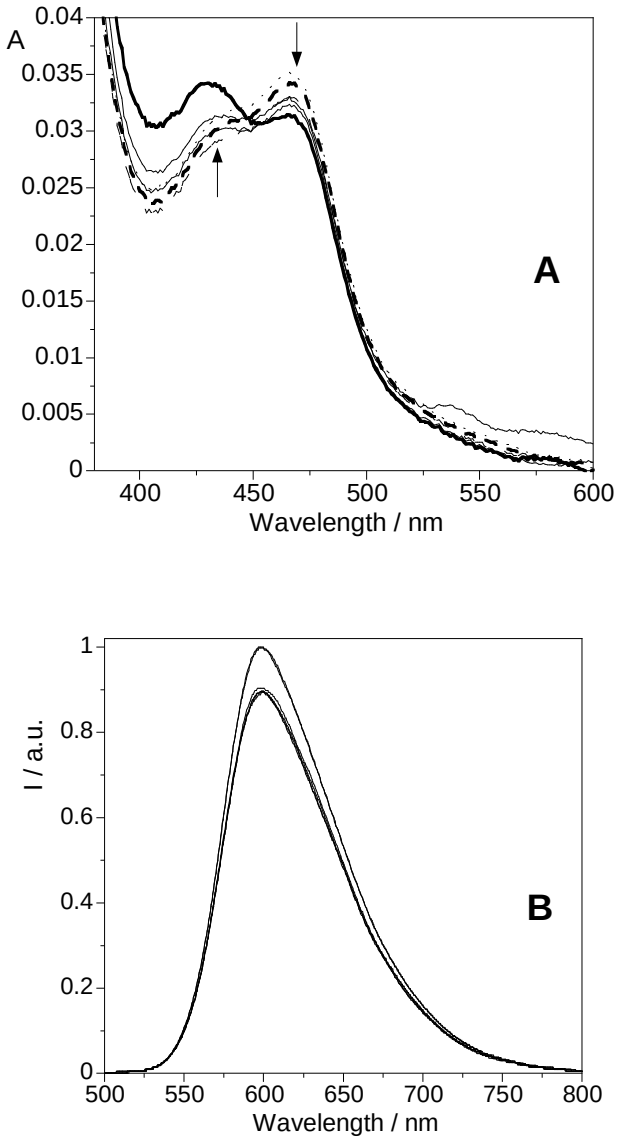

Figure SM V.12 – (A) Absorption spectra of CT-DNA + C3 (Ratio 30/1) in the presence of increasing amounts of potassium ferrocyanide (0 – 400 μM). [C3] = 4.90 μM. **(B)** Emission spectra of CT-DNA + C3 (Ratio 30/1) in the presence of increasing amounts of potassium ferrocyanide (0 – 400 μM). [C3] = 4.90 μM. λ_{exc} = 465 nm.

$[Fe(CN)_6]/\mu M$	$\tau_1/\mu s$	(%)	$\tau_2/\mu s$	(%)	τ_m / µs	χ^2
0	**0.74**	**67**	**1.34**	**33**	**0.94**	**1.10**
50	**0.74**	**65**	**1.33**	**35**	**0.95**	**1.12**
100	**0.80**	**72**	**1.44**	**28**	**0.98**	**1.00**
200	**0.78**	**67**	**1.37**	**33**	**0.97**	**0.98**
400	**0.80**	**69**	**1.44**	**31**	**1.00**	**1.09**

Table SM V.6 – Luminescence lifetimes of 1:30 C3:DNA at different $K_4Fe(CN)_6$ concentrations. [C3] = 4.90 µM. λ_{exc} = 405 nm. λ_{em} = 610 nm. [DNA] = 2.82 mM. $[K_4Fe(CN)_6]$ = 10 mM.

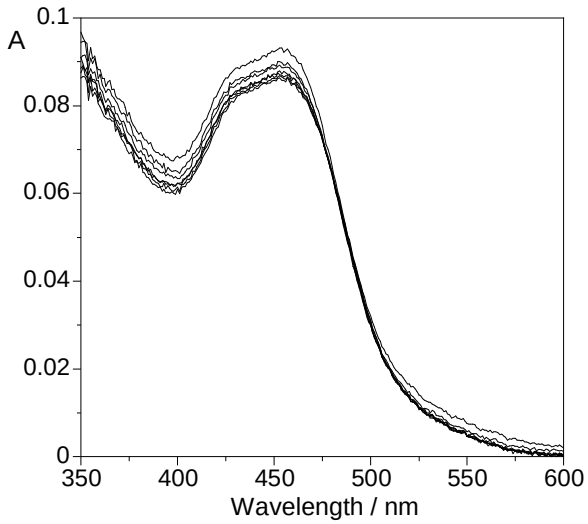

Figure SM V.13 – Absorption spectra of CT-DNA + C5 (Ratio 30/1) in the presence of increasing amounts of methyl viologen (0 – 200 µM). [C5] = 10.5 µM. $[DNA]_{stock}$ = 2.02 mM. $[MV^{2+}]_{stock}$ = 5 mM.

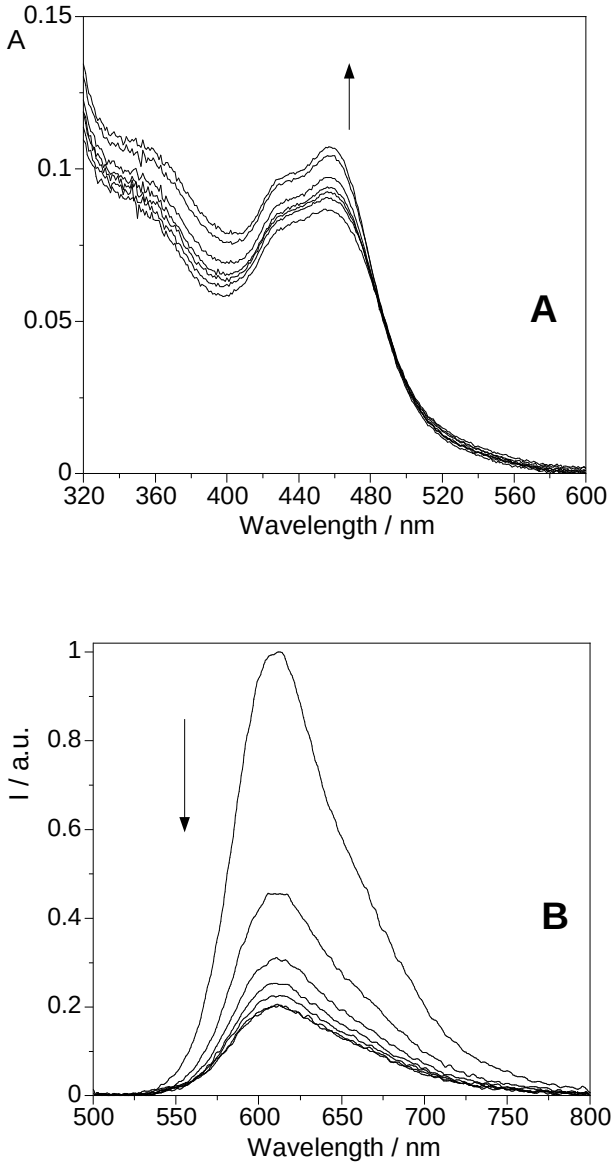

Figure SM V.14 – (A) Absorption spectra of CT-DNA + C4 (Ratio 30/1) in the presence of increasing amounts of methyl viologen (0 – 200 μM). [C4] = 9.85 μM. $[DNA]_{stock}$ = 2.02 mM. $[MV^{2+}]_{stock}$ = 5 mM. **(B)** Emission spectra of CT-DNA + C4 (Ratio 30/1) in the presence of increasing amounts of methyl viologen (0 – 200 μM). λ_{exc} = 465 nm. [C4] = 9.85 μM. $[DNA]_{stock}$ = 2.02 mM. $[MV^{2+}]_{stock}$ = 5 mM.

$[MV^{2+}]$ / μM	τ_1/μs	(%)	τ_2/μs	(%)	τ_3/μs	(%)	τ_m / μs	χ^2
0	**0.51**	**50**	**1.52**	**50**	**-**		**1.02**	**1.08**
25	**0.44**	**66**	**1.01**	**11**	**1.29**	**23**	**0.70**	**1.17**
50	**0.10**	**31**	**0.33**	**61**	**0.76**	**8**	**0.29**	**1.15**
75	**0.09**	**43**	**0.30**	**48**	**0.63**	**9**	**0.24**	**1.01**
100	**0.08**	**44**	**0.24**	**35**	**0.51**	**21**	**0.22**	**1.03**
150	**0.06**	**48**	**0.28**	**35**	**0.56**	**17**	**0.22**	**1.11**
200	**0.05**	**44**	**0.30**	**38**	**0.57**	**18**	**0.24**	**1.11**

Table SM V.7 – Luminescence lifetimes of 1:30 C4:DNA at different MV^{2+} concentrations. [C4] = 9.85 μM. λ_{exc} = 405 nm. λ_{em} = 613 nm. [DNA] = 2.02 mM. $[MV^{2+}]_{stock}$ = 5 mM.

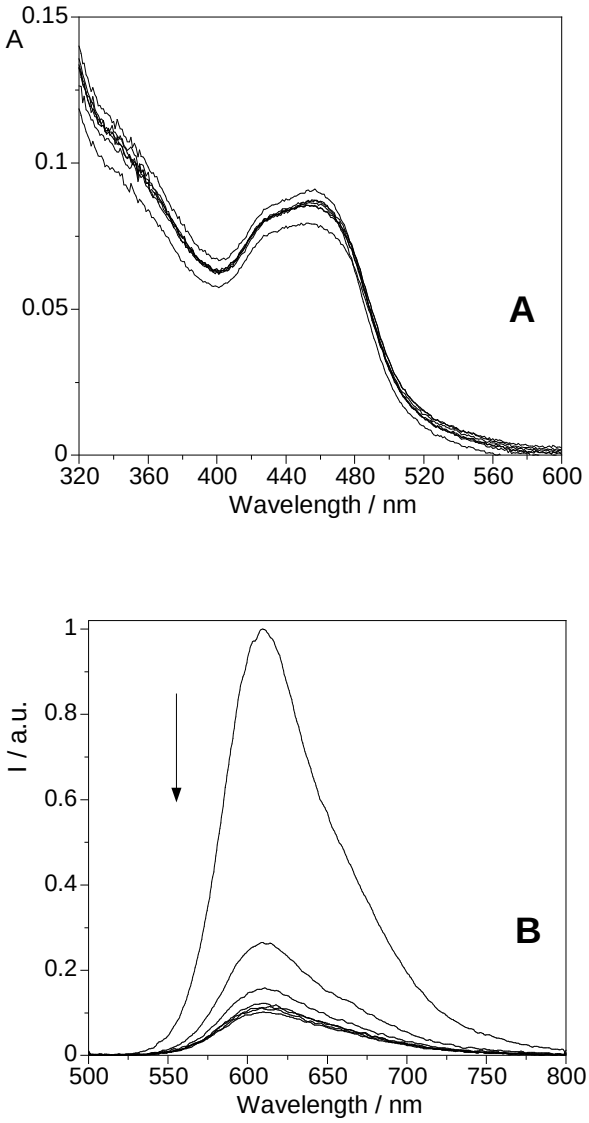

Figure SM V.15 – (A) Absorption spectra of CT-DNA + C6 (Ratio 30/1) in the presence of increasing amounts of methyl viologen (0 – 200 μM). [C6] = 10.0 μM. $[DNA]_{stock}$ = 2.02 mM. $[MV^{2+}]_{stock}$ = 5 mM. **(B)** Emission spectra of CT-DNA + C6 (Ratio 30/1) in the presence of increasing amounts of methyl viologen (0 – 200 μM). λ_{exc} = 465 nm. [C6] = 10.0 μM. $[DNA]_{stock}$ = 2.02 mM. $[MV^{2+}]_{stock}$ = 5 mM.

[MV^{2+}] / μM	τ_1/μs	(%)	τ_2/μs	(%)	τ_3/μs	(%)	τ_m / μs	χ^2
0	-		0.54	40	1.50	60	1.12	1.09
25	0.10	25	0.32	56	0.68	19	0.33	1.18
50	0.10	48	0.29	46	0.70	6	0.23	1.04
75	0.07	45	0.20	43	0.53	12	0.18	1.16
100	0.06	51	0.20	34	0.54	15	0.18	1.01
150	0.04	52	0.14	27	0.49	21	0.16	0.94
200	0.06	50	0.38	45	0.75	5	0.24	1.08

Table SM V.8 – Luminescence lifetimes of 1:30 C6:DNA at different MV^{2+} concentrations. [C6] = 10.0 μM. λ_{exc} = 405 nm. λ_{em} = 613 nm. [DNA] = 2.02 mM. [MV^{2+}] = 5 mM.

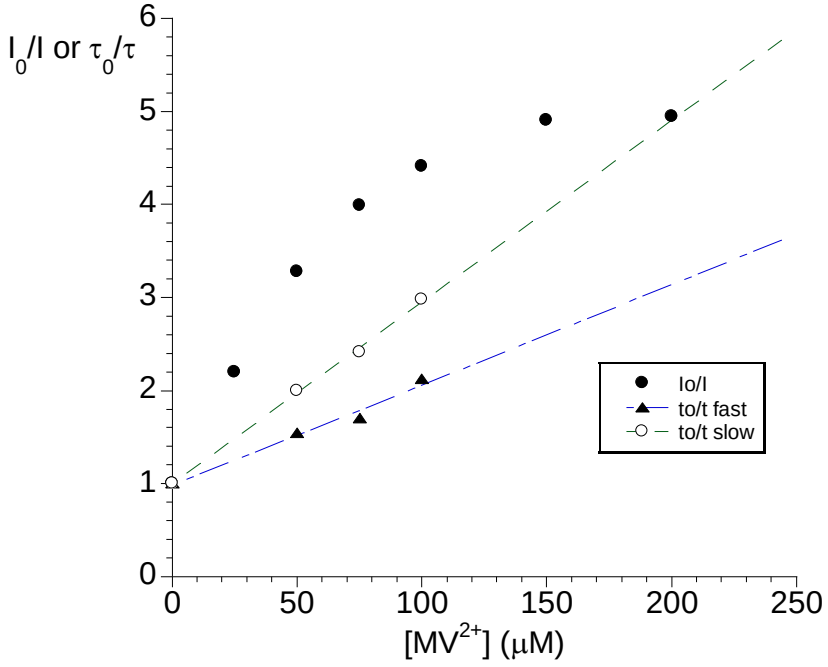

Figure SM V.16 – Stern-Volmer emission intensity (●) and lifetime quenching plot for C4+DNA (ratio 1:30) in the presence of increasing amounts of methyl viologen (MV^{2+}). Both fast (short) (▲) and slow (long) (○) components of the emission decay are represented. λ_{exc} = 405 nm. Emission collected at 613 nm.

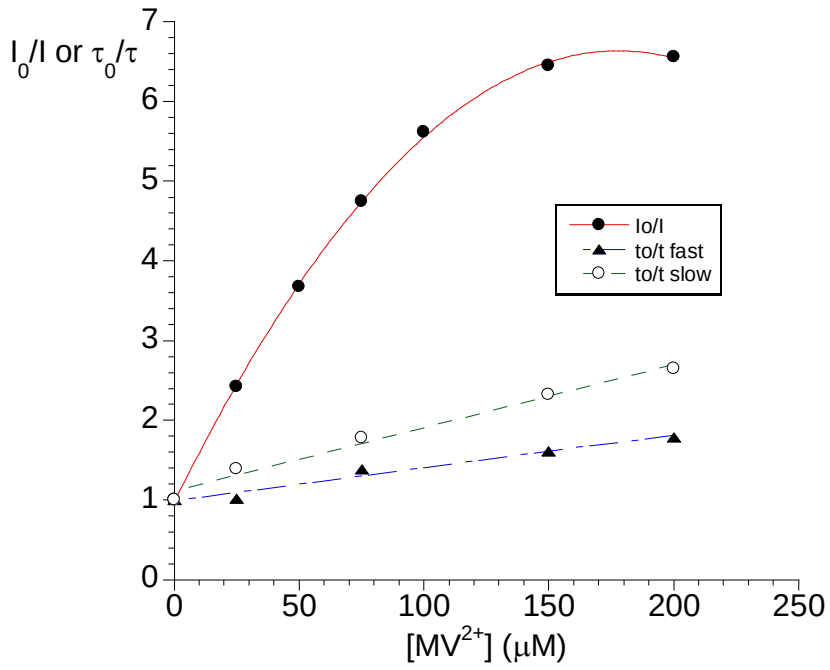

Figure SM V.17 – Stern-Volmer emission intensity (●) and lifetime quenching plot for C5+DNA (ratio 1:30) in the presence of increasing amounts of methyl viologen (MV^{2+}). Both fast (short) (▲) and slow (long) (○) components of the emission decay are represented. λ_{exc} = 405 nm. Emission collected at 613 nm.

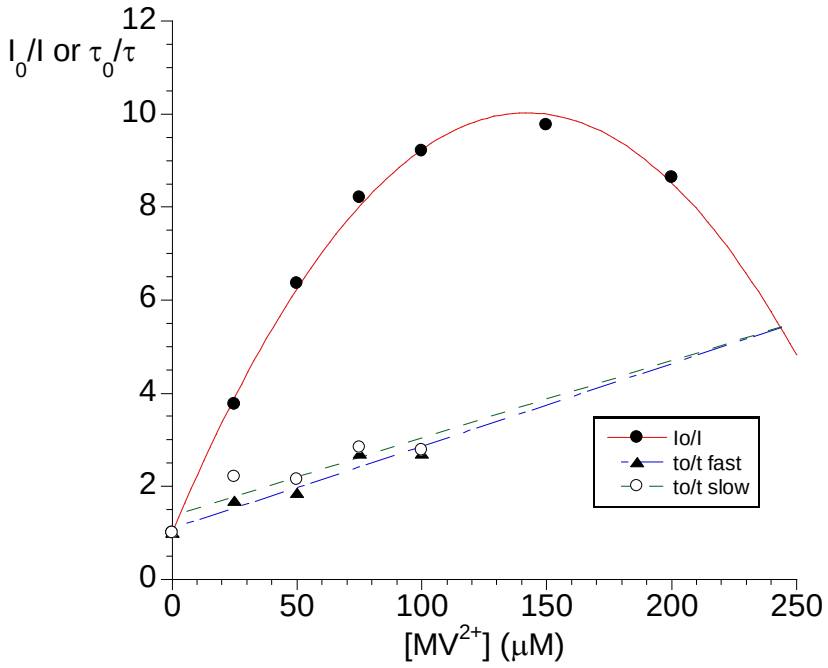

Figure SM V.18 – Stern-Volmer emission intensity (●) and lifetime quenching plot for C6+DNA (ratio 1:30) in the presence of increasing amounts of methyl viologen (MV^{2+}). Both fast (short) (▲) and slow (long) (○) components of the emission decay are represented. λ_{exc} = 405 nm. Emission collected at 613 nm.

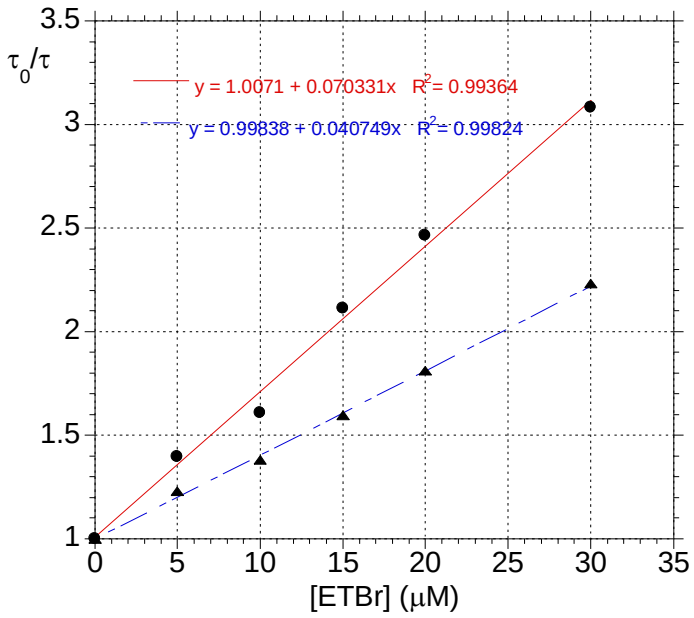

Figure SM V.19 – Stern-Volmer lifetime quenching plot for C3+DNA (ratio 1:30) in the presence of increasing amounts of ethidium bromide (ETBr). Both fast (short) (●) and slow (long) (▲) components of the emission decay are represented. λ_{exc} = 405 nm. Emission collected at 610 nm.

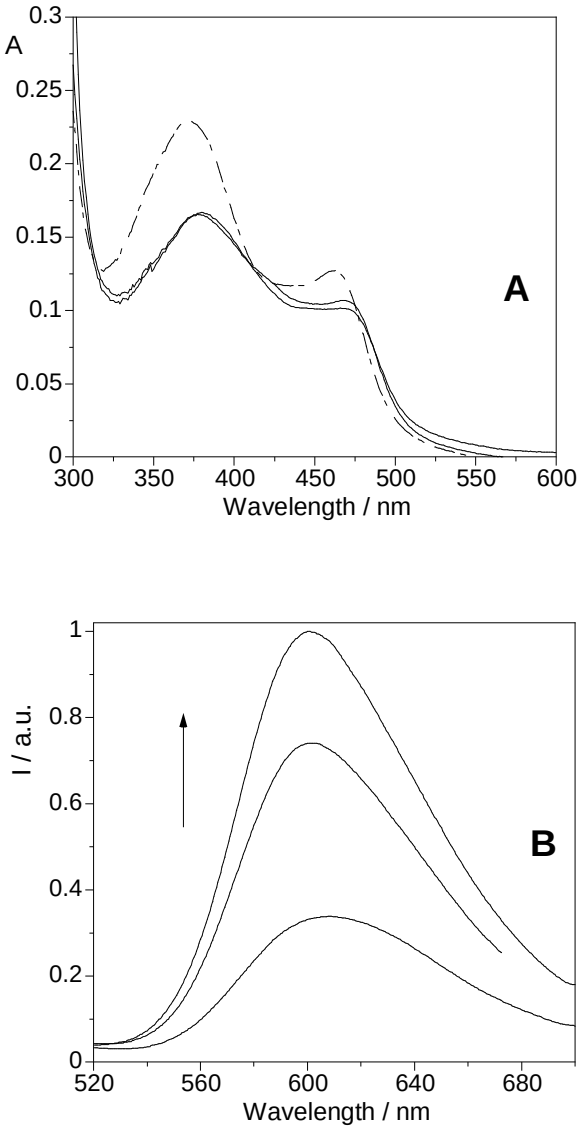

Figure SM V.20 – (A) Absorption spectra of C1, 10 μM in TRIS buffer, in the absence (---) and presence (—) of increasing amounts of CT-DNA (ratio DNA/Ru: 0 – 10, in base pairs). [DNA] = 2.82 mM. **(B)** Emission spectra of C1, 10 μM in TRIS buffer, in the presence of increasing amounts of CT-DNA (ratio DNA/Ru: 0 – 10, in base pairs). λ_{exc} = 370 nm. [DNA] = 2.82 mM.

Medium	τ_1/µs	(%)	τ_2/µs	(%)	τ_m / µs	χ^2
TRIS	0.41	81	1.48	19	0.62	1.07
1:30 DNA	0.53	54	1.71	46	1.07	1.00

Table SM V.9 – Luminescence lifetimes of C1 in TRIS buffer in the absence and presence of CT-DNA (ratio 1:30). [C1] = 10 µM. λ_{exc} = 371 nm. λ_{em} = 610 nm.

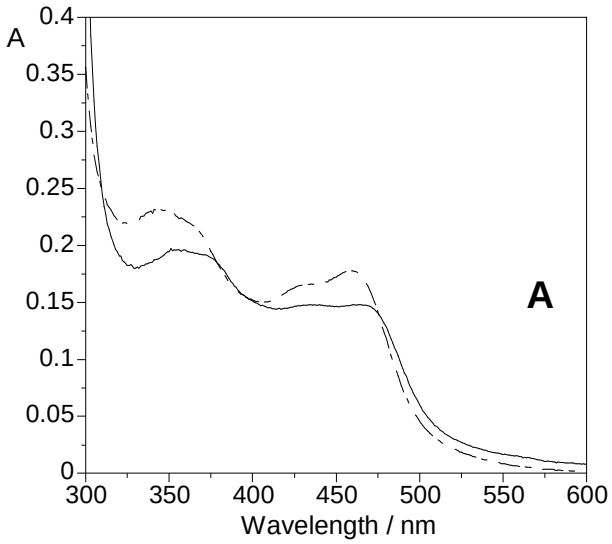

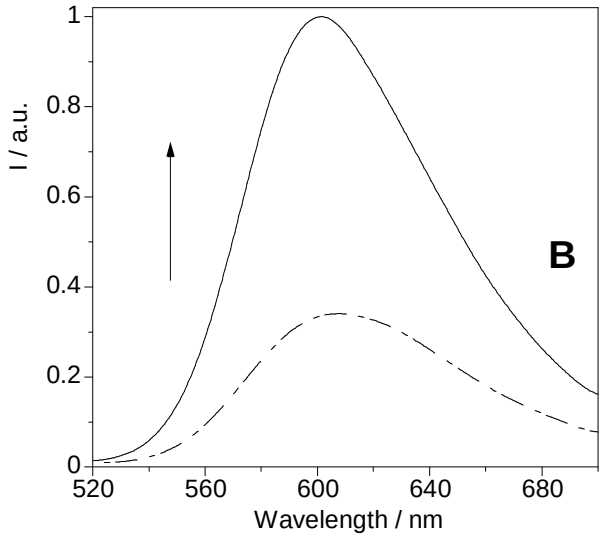

Figure SM V.21 – (A) Absorption spectra of C2, 10.5 µM in TRIS buffer, in the absence (---) and presence (—) of CT-DNA (ratio DNA/Ru = 30, in base pairs). **(B)** Emission spectra of C2, 10.5 µM in TRIS buffer, in the absence (---) and presence (—) of CT-DNA (ratio DNA/Ru = 30, in base pairs). λ_{exc} = 370 nm. [DNA] = 2.82 mM.

Medium	τ_1/μs (%)	τ_2/μs (%)	τ_m / μs	χ^2
TRIS	**0.30 22**	**0.52 78**	**0.47**	**1.19**
1:30 DNA	**0.39 28**	**1.31 72**	**1.05**	**1.04**

Table SM V.10 – Luminescence lifetimes of C2 in different media. [C2] = 10 μM. λ_{exc} = 371 nm. λ_{em} = 610 nm.

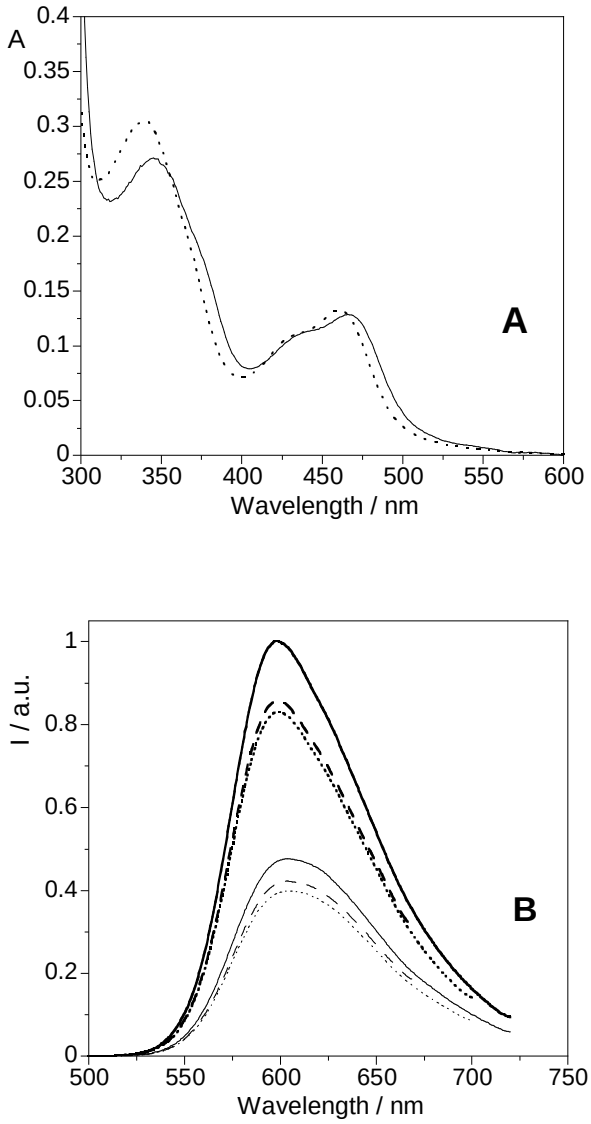

Figure SM V.22 – (A) Absorption spectra of C3, 9.43 μM, in TRIS buffer (···) and with DNA 1:30 (—). **(B)** Emission spectra of C3, 9.43 μM, in TRIS buffer, pH = 7 (normal lines) and with CT-DNA 1:30 (bold lines). λ_{exc} = 340 nm (---), 370 nm (···) and 465 nm (—).

Medium	τ_1/μs (%)	τ_2/μs (%)	τ_m / μs	χ^2
TRIS	**0.50 100**	**-**	**-**	**1.02**
1:30 DNA	**0.73 59**	**1.25 41**	**0.94**	**1.09**

Table SM V.11 – Luminescence lifetimes of C3 in different media. [C3] = 9.43 μM. λ_{exc} = 371 nm. λ_{em} = 610 nm.

Chapter VI

New quinoline α-diimine ligands as fluorescent probes for metal ions: ultrasound-assisted and conventional synthetic methods.

B. Pedras; V. Rosa; R. Welter; T. Avilés; C. Lodeiro.

To be submitted.

VI.1 Resumo

Três novos quimiossensores para Zn(II) e Cu(II) derivados da 8-aminoquinolina (**1** a **3**), e um complexo de Zn(II) dinuclear (**4**) com potencial aplicação como sensor de água, foram sintetizados e completamente caracterizados. Os seus espectros de absorção apresentam máximos a 310-336 nm, e a sua emissão de fluorescência varia entre 456-498 nm. O composto **1** foi também caracterizado por difracção de raios-X de monocristal. O efeito da coordenação de metais aos compostos **1** a **3** foi estudado através da variação nos espectros de fluorescência, e complementada através do cálculo de constantes de estabilidade metal-ligando. Os resultados obtidos indicam que o composto **3** é o que possui a geometria mais favorável para coordenar dois catiões, facto que é confirmado pela síntese do complexo dinuclear **4**, que possui uma geometria similar.

A minha contribuição para este trabalho consistiu na síntese e caracterização espectroscópica de todos os compostos, bem como a realização de todos os estudos fotofísicos.

VI.2 Abstract

Three new 8-aminoquinoline derived chemosensors (**1** to **3**) for Zn(II) and Cu(II), and one dinuclear Zn(II) complex (**4**) with potential application as water sensor, were synthesized and fully characterized. Their absorption spectra show maxima at 310-336 nm, and fluorescence emission varies between 456-498 nm. Compound **1** was also characterized by single monocrystal X-ray diffraction. The effect upon metal coordination to compounds **1** to **3** was studied by monitoring the changes in fluorescence spectra, and complemented by calculation of metal-ligand stability constants. The results indicate that compound **3** is the one that has the most favorable geometry for coordinating two cations, fact that is confirmed by the synthesis of the dinuclear complex **4**, which has a similar geometry.

My contribution to this work was the synthesis and spectroscopic characterization of all the compounds, as well as the performing of all the photophysical studies.

VI.3 Introduction

Many natural products include the quinoline molecule as a building block in their architecture, of which alkaloids[1] are an example. Numerous quinolines exhibit physiological activities that opened the door to applications in pharmaceuticals (e.g. primaquine, an 8-aminoquinoline, and some of its derivatives are strong drugs used to treat malaria and other parasitic diseases, such as leishmaniasis[2-9]) and they are also widely used in synthetic chemistry.[10]

In 1971, Zatka *et al.* reported the synthesis of a tetradentate β-diketiminate ligand that contained quinoline pendant arms.[11] UV-vis spectroscopy studies showed that this ligand formed 1:1 complexes with Zn and Cd. Work done in the following years confirmed the affinity of quinoline ligands for Zn, producing complexes of high stability and high molar absorptivity values.[12-15]

8-aminoquinoline and 8-hydroxyquinoline (and their derivatives) have found application as fluorogenic sensors for quantitative chemical determinations of Zn(II) and other metal ions.[16-18] These quinolines are non-fluorescent, and the presence of an intramolecular hydrogen bond between the heterocyclic nitrogen atom and the 8-substituted group (i.e. –OH or –NH2)[19-20] allow these compounds to remain unaffected by pH changes.[21] However, when these compounds chelate Zn(II) and other metal ions, they present some intense yellow-greenish fluorescence. Cations like Zn(II), Ca(II) and Al(III) can break hydrogen bonding in these compounds, and therefore enhance fluorescence, which permits their selective detection. Besides its chelating properties (which come from a fusion of pyridine with aniline to form a N,N' chelating motive), 8-aminoquinoline and its derivatives have recently been given credit for their antiprotozal and other medicinal properties.[22] They also have been used to prepare highly conducting co-polymers.[23] Different functionalized molecules of 8-aminoquinoline have been recently reported.[24-26]

As part of our ongoing research project in the design and synthesis of new versatile fluorescent chemosensors[27] (fluorescent probes in solution and active-recognition matrices in gas-phase), we report here the synthesis, characterization and metal ion interaction studies of a new family of fluorescent compounds (**1** to **4**),

containing one or two emissive quinoline units in a Schiff-base skeleton. Classical and ultrasound-assisted synthetic methods will also be discussed.

VI.4 Results and discussion

VI.4.1 Synthesis and characterization of compounds 1 to 4

The initial focus of the synthetic part of this work was the development of an optimized set of reaction conditions, by means of reduction of reaction times without yield decrease, and whenever possible by improving the latter. For such a task, the synthesis of compounds **1** and **2** was ultrasound-assisted, which allowed the reactions to be completed in one-hour periods, and the yields were somehow satisfactory. For compounds **3** and **4** the same procedure could not be used, since the addition of 2,3-butadione in the case of **3** produces a highly exothermic reaction (and therefore the addition has to be made in an ice bath), and for **4** a template synthesis was required, with refluxing glacial acetic acid, and it did not work in the ultrasonic bath. Scheme VI.1 represents the synthesis of the four new compounds.

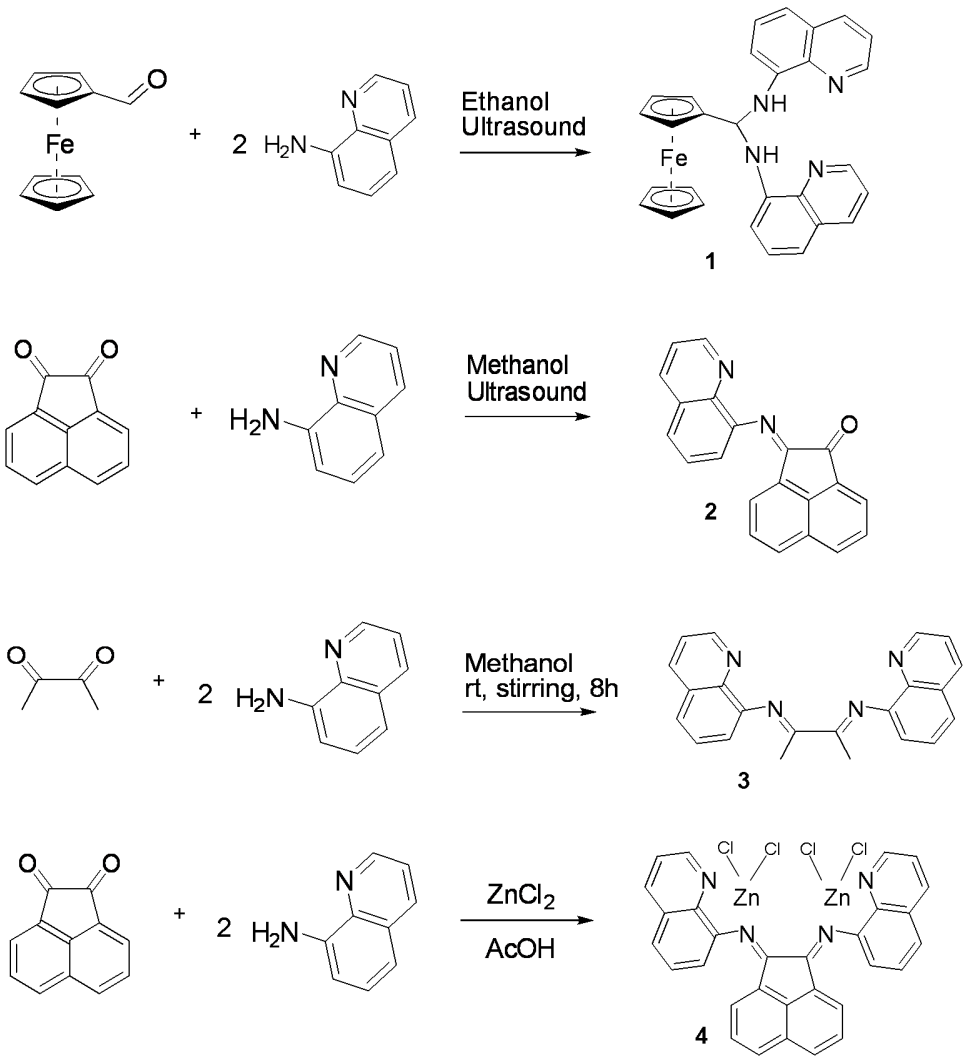

Scheme VI.1 – Synthesis of quinoline-derived compounds.

The four compounds were characterized by elemental analysis, ^{1}H-NMR, IR, UV-vis absorption and fluorescence spectroscopies and MALDI-TOF MS spectrometry. Compound **1** was also characterized by single monocrystal X-ray diffraction. Elemental analyses fit perfectly with the chemical formula suggested and data confirm that the four compounds have been obtained. The infrared spectra (Nujol mulls in NaCl plates) show in the case of **1** the presence of a band at 3382 cm^{-1}, corresponding to the N-H vibration in the secondary amine bond. In addition, the total absence of bands corresponding to imine bonds in **1** confirms that a complete formation of the amine derivative occurred. The usual mechanism for this transformation should be the reductive amination of ferrocenealdehyde, but in our case there is neither a hydride source nor a hydrogen catalyst present to perform the reduction. In this way, what probably occurred was something similar to the mechanism related by Stacy and coworkers,[28] where the initially formed imine is

partially hydrolyzed (in our case, probably with the help of ultrasounds) to the aldehyde and amine precursors, and the latter then attacks the unchanged imine, thus leading to the formation of the diamine product. In the cited example, an electron-withdrawing nitro substituent enhances the electron deficiency on the carbon atom of the C=N bond. In our case, this role must be played by the Fe(II) cation of the ferrocene moiety. In both cases the reaction is favored by the presence of an excess of amine.

For the imine compounds a band at 1623 or 1667 cm^{-1} was observed, corresponding to the C=N vibration of the imine bond. ^{1}H-NMR spectra show all the integrations and chemical shifts corresponding to what is expected. By MALDI-TOF MS it is possible to see the peaks corresponding to the molecular ions, also in some cases the fragmentation patterns, and even polymeric forms in the case of **2**. The UV-visible and luminescence spectroscopic characterization data are collected in Table VI.1, and the emission quantum yields of the compounds in different solvents are presented in Table VI.2.

Compound	λ_{max}^{abs} / *nm*	ε_{max} / $M^{-1}cm^{-1}$	λ_{max}^{em} / *nm*	Stokes shift / nm
1	336	11428	456	120
2	322	9151	498	176
3	313	6344	461	148
4	310	14223	488	178

Table VI.1 – Absorption and emission maxima and molar absorption coefficients of compounds **1** to **4**.

	1	2	3	4
DMSO	0.078	0.022	0.053	0.075
THF	0.005	0.032	0.008	
Acetonitrile	0.002	0.026	0.016	
Ethyl acetate	0.004	0.024	0.016	
Methanol	0.001	0.009	0.006	
Dichloromethane	0.012	0.026	0.011	

Table VI.2 – Fluorescence quantum yields of compounds **1** to **4**, in different solvents. Reference: quinine sulphate in 0.5 M H_2SO_4.

Based on the data of Table VI.2 it is possible to see that all the compounds are more emissive in DMSO, while in methanol (which is the only protic solvent in the list), emission is almost completely quenched in the case of **1**, and reduces dramatically in the remaining compounds as well. It is possible that protonation of the quinoline takes place, while for **1** both amine groups can also be protonated. A comparative test was made with the precursor 8-aminoquinoline (see Supplementary Material) by studying its emission spectra in different solvents, and the results match. According to what was observed, protic solvents were discarded for the performing of titration experiments, because no emission was observed, and DMSO because no quenching could be observed. The chosen solvent was dichloromethane.

VI.4.2. X-ray diffraction characterization of 1

Compound **1** has been obtained in single crystal form ready for X-ray analysis. This complex crystallizes in the centrosymetric space group $P2_1/c$. The asymmetric unit contains two similar molecules corresponding effectively to the compound **1**. An ORTEP view of one molecule of the asymmetric unit is presented in figure VI.1.

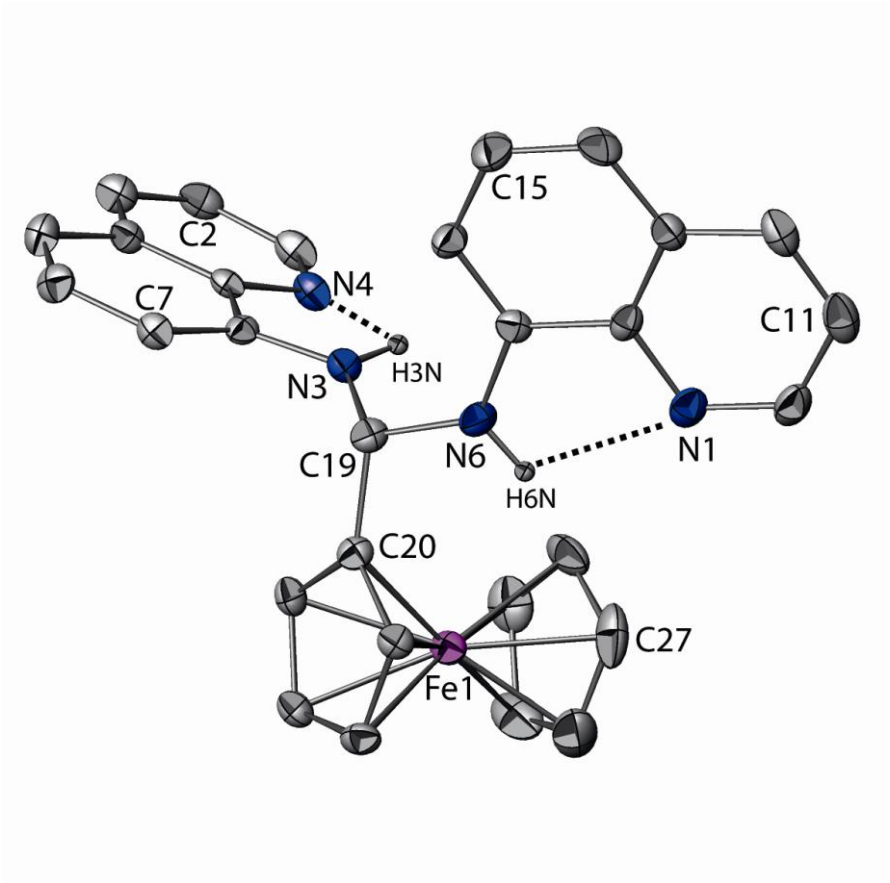

Figure VI.1 - ORTEP view (ATOMS[30]) of compound **1** with partial labeling scheme. Only one molecule of the asymmetric unit is presented, for clarity. The ellipsoids enclose 50% of the electronic density. Dashed lines indicate intramolecular hydrogen bonds.

The angle between both quinoline groups is about 81° (77° for the other molecule), as clearly evidences the packing view in figure VI.2. Specific hydrogen bonds have been detected in this crystal structure. Some are represented in figure VI.1 and also reported in table VI.3. Many non classical hydrogen bonds – CH-π- have also been detected. They occur in numerous directions in the crystal network, giving rise to the stability of the crystalline solid state (a selected crystal packing diagram is presented in figure VI.2).

Donor -- H ..Acceptor	D - H	H...A	D...A	D - H...A
Intramolecular				
N(3) -- H(3N) .. N(4)	0.8802	2.3439	2.688(8)	103.40
N(6) -- H(6N) .. N(1)	0.8795	2.2921	2.676(9)	106.34
N(7) -- H(7N) .. N(2)	0.8793	2.3108	2.681(8)	105.38
N(8) -- H(8) .. N(5)	0.8799	2.3588	2.681(10)	101.78
Intermolecular				
C(22) -- H(22) .. N4_$1	0.9501	2.5787	3.441(11)	151.12
C(52) -- H(52) .. N5_$2	0.9501	2.6078	3.503(9)	157.19

Table VI.3 - Analysis of Hydrogen Bonds in compound **1** with PLATON[31] (Equivalent Position Code: $1 = 1-x,-1-y,-z ; $2 = -x,-2-y,-z).

Crystal Data	
Formula	$C_{29}H_{24}FeN_4$
Formula Weight	484.37
Crystal System	Monoclinic
Space group	$P2_1/c$ (No.14)
a, b, c [Å]	20.9510(10) 11.9890(10) 20.6140(10)
α, β, γ [°]	90 119.22(5) 90
V [$Å^3$]	4519(2)
Z	8
d_{calc} [$g.cm^{-3}$]	1.424
μ(MoKα) [/mm]	0.693
F(000)	2016
Crystal Size [mm]	0.10 x 0.10 x 0.10
Data Collection	
Temperature (K)	173
Theta Min-Max [°]	1.1, 30.0
Dataset	0: 29 ; -16: 0 ; -29: 25
Tot., Uniq. Data, R(int)	13144, 13143, 0.000
Observed data [I >2σ(I)]	7462
Refinement	
Nref, Npar	13143, 613
R, wR2, S	0.1107, 0.2954, 1.05
Max. and Av. Shift/Error	0.00, 0.00
Min. and Max. Resd. Dens. [$e.Å^{-3}$]	-0.95, 1.52

Table VI.4 - Crystal data and details of the structure determination for compound **1**.

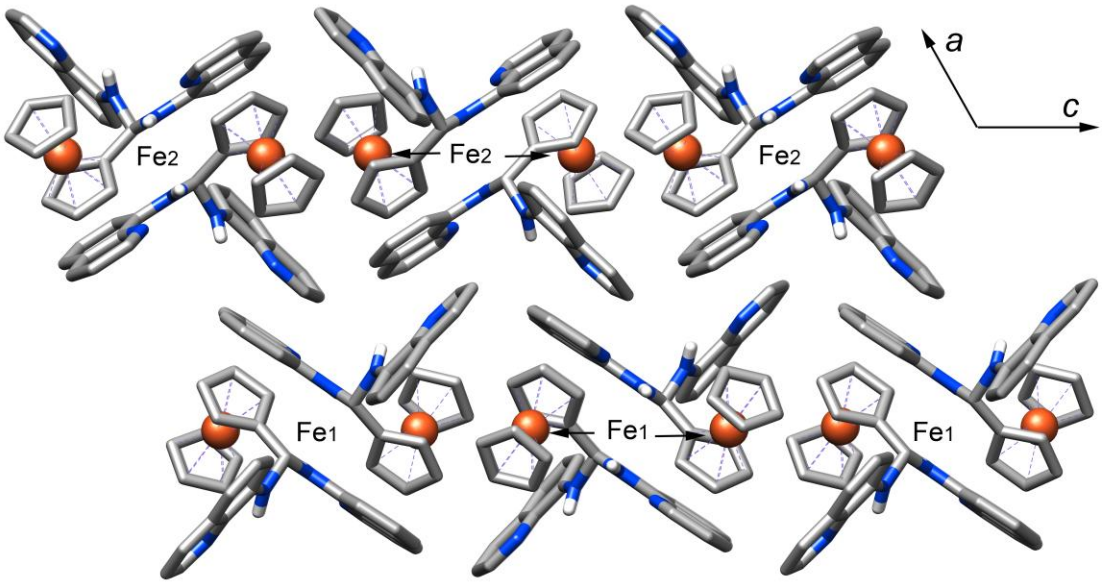

Figure VI.2 – Packing diagram of compound **1** in projection in the (a,c) sheet. Only iron atoms are represented as spheres.

VI.4.3. Spectrophotometric and spectrofluorimetric studies

The affinity of compounds **1**, **2** and **3** for transition metal ions, more specifically for Zn(II) and Cu(II) was the main goal of our work, due to the importance of developing new fluorescence compounds for sensing these metals, given their important role in biochemical processes, among others; whereas for compound **4** a preliminary application as a water sensor was tested.

In Figure VI.3 are represented the absorption and emission spectra resulting from the titration of **1** with Zn(II). The lack of isosbestic points in absorption spectra is an indicator that more than one species might be formed, and the band at ca. 530 nm indicates the formation of a complex. In emission spectra, a quenching of the fluorescence is observed upon addition of Zn(II), which at first sight does not match the expected behaviour for Zn(II) coordination, since it is a d^{10} ion, and therefore should produce a CHEF effect after coordination. As Bazzicalupi et al.[32] reported previously for a macrocyclic ligand, this quenching can be also understood by the presence of a non-coordinated nitrogen atom in the ligand, that quenches the fluorescence emission.

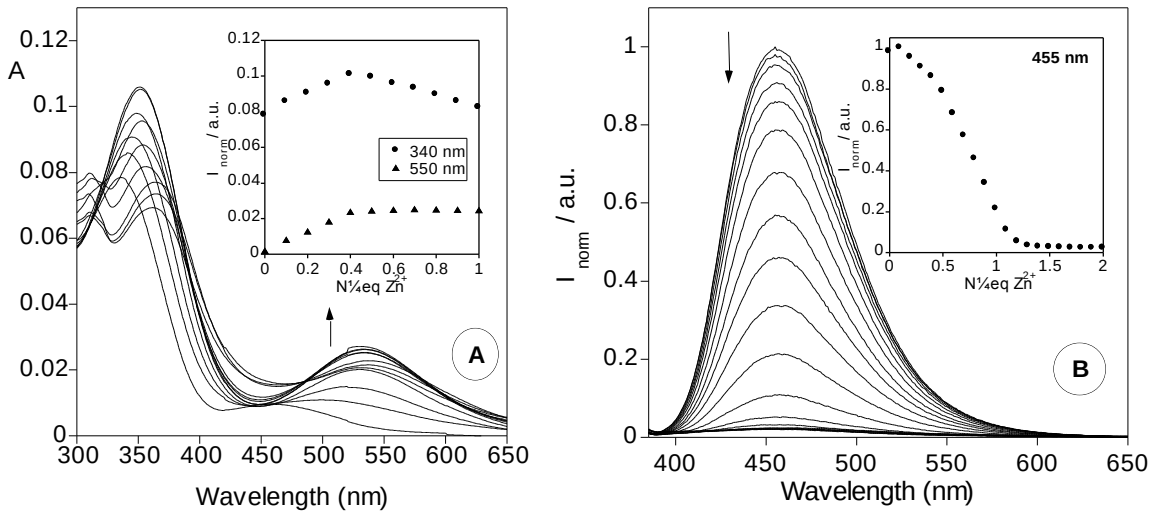

Figure VI.3 – (A) Absorption spectra of compound **1**, 10 μM in CH_2Cl_2, in the presence of increasing amounts of Zn^{2+}. Inset: changes in the absorption of **1** at 340 nm (●) and 550 nm (▲) as a function of the number of Zn^{2+}equivalents. **(B)** Emission spectra of compound **1**, 10 μM in CH_2Cl_2, in the presence of increasing amounts of Zn^{2+}. λ_{exc} = 340 nm. Inset: changes in the emission of **1** at 455 nm, as a function of the number of Zn^{2+}equivalents.

Binding constants were determined with the Hypspec program, and were found to be: for LM, log β = 6.69; for L_2M, log β = 9.01. These results confirm that there are two species in solution, one formed by one ligand and one Zn(II) ion, and the other constituted by two ligands and one Zn(II), the latter species being more stable and preferably formed.

Titration of **1** with Cu(II), represented in Figure VI.4, shows a quenching of the fluorescence emission upon metal coordination. In this case the results are as expected, due to the d^9 configuration of Cu(II), which usually produces a CHEQ effect. In the inset it is possible to see that a total quenching occurs after addition of two equivalents of copper(II), which suggests that two metals are coordinated to the ligand. The stability constant determined for this association was found to be log β = 10.32 for the LM_2 species, and this was the only stoichiometry that could generate an acceptable value by the program. This value can be explained having in mind that 8-aminoquinoline derivatives are highly selective for Cu(II) ions,[33] and the molecule of **1**

is extremely flexible, since it is not a Schiff base and therefore the quinoline moieties can rotate around the N-C-N bond.

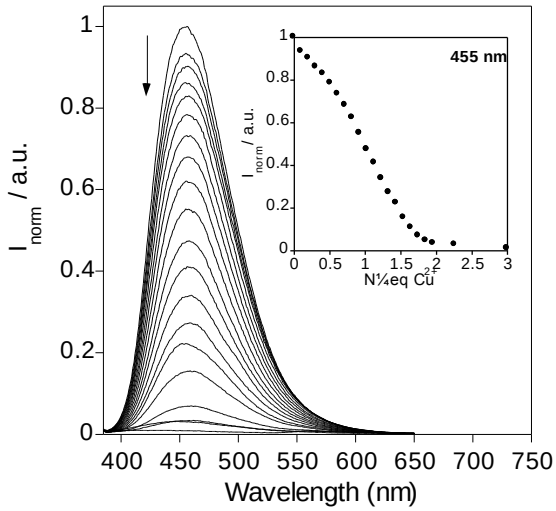

Figure VI.4 – Emission spectra of compound **1**, 10 μM in CH_2Cl_2, in the presence of increasing amounts of Cu^{2+}. λ_{exc} = 340 nm. Inset: changes in the emission of **1** at 455 nm, as a function of the number of Cu^{2+} equivalents.

Titrations of **2** with Zn(II) and Cu(II) resulted in slight enhancement of the fluorescence in both cases (the spectra can be found in Supplementary Material). The values obtained for the binding constants (for Zn(II): log β = 5.14 and 9.84, for LM and L_2M, respectively; for Cu(II): log β = 6.06, for LM) are expected, since this ligand only has one quinoline moiety, and for Zn(II) two ligands are needed to form a stable complex. For Cu(II), only the 1:1 species is formed.

The case of **3** is depicted in Figure VI.5, where for titration with Zn(II) an enhancement of the fluorescence is observed, and Cu(II) produces a quenching of the emission, according to the normally observed behavior for these ions.

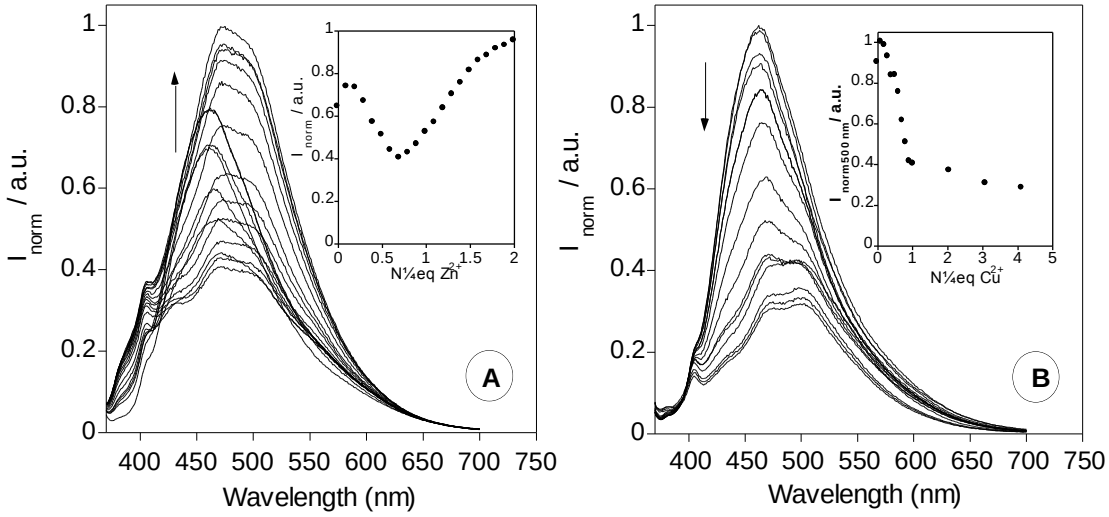

Figure VI.5 – (A) Emission spectra of compound **3**, 10 μM in CH_2Cl_2, in the presence of increasing amounts of Zn^{2+}, λ_{exc} = 360 nm. Inset: changes in the emission of **3** at 475 nm (●), as a function of the number of Zn^{2+} equivalents. **(B)** Emission spectra of **3**, 10 μM in CH_2Cl_2, in the presence of increasing amounts of Cu^{2+}. λ_{exc} = 360 nm. Inset: changes in the emission of **3** at 462 nm (○), and 500 nm (▲) as a function of the number of Cu^{2+} equivalents.

The first quenching observed during the Zn(II) titration (Figure VI.5A) could be due to the partial protonation of the quinoline groups, that produces a quenching via PPT (photoinduced proton transfer). A similar behavior was observed previously in our group[34] when several macrocyclic ligands containing sulphur and nitrogen as donor atoms were titrated with Zn(II) or Pd(II).

The determined binding constants for these two titrations were the following: log β = 9.02 and 16.54, respectively for LM and LM_2 in the case of Zn(II); log β = 13.82 for LM_2 in the case of Cu(II), being stronger for the first metal ion. This is the ligand that has the most favourable geometry of the three that were studied, in order to bind two metal ions. This fact is confirmed by the synthesis of compound **4**, which has a similar disposition of quinoline units, and is a dinuclear Zn(II) complex.

In order to use the distance between both metal ions for sensorial effects, with compound **4**, some preliminary studies were performed in order to investigate its effect as water sensor. In a qualitative manner (because stoichiometries are very

difficult to match in this case) it was observed that this compound, which is initially fluorescent (because Zn(II) prevents PET from the electron-pair located on the Schiff base nitrogens to the fluorophore), experiences a total quenching of its emission as H_2O is increasingly added to the solution (Figure VI.6).

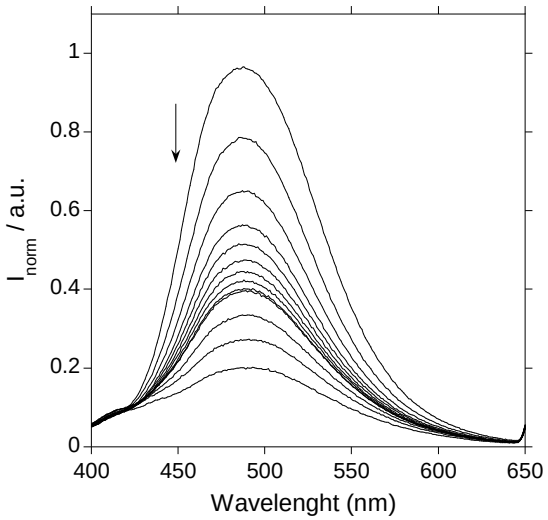

Figure VI.6 – Emission spectra of **4**, 5 μM in DMSO, in the presence of increasing amounts of H_2O. λ_{exc} = 330 nm.

One possible explanation for this result is that the oxygen atoms might donate some electronic density to Zn(II) coordinated ions, thus weakening their bonds to the nitrogen atoms. In this way, the latter can undergo photoinduced electron transfer to the quinoline moiety, quenching its emission.

VI.5 Conclusions

By classical and ultrasound-assisted synthetic methods, a new family of emissive compounds containing two quinoline units (**1, 3** and **4**) or one unit (**2**) was successfully synthesized and characterized. Compound **4** was obtained by template synthesis.

The effect of transition and post-transition metal cations such as Cu^{2+} and Zn^{2+} on the absorption and fluorescence spectra was explored. To conduct

spectrophotometric analyses, the ligand was dissolved in several aprotic and protic solvents and titrated with the analytes. The best results were obtained in dichloromethane, where a remarkable sensing effect was obtained for the aforementioned cations.

The application of compound **4** as potential fluorescence sensor of water was explored. This system can sense water in organic solvents, by emission quenching, although for the moment only qualitative results have been obtained.

VI.6 Experimental section

VI.6.1 General

All reactions and manipulations of solutions were performed under an argon atmosphere using Schlenk techniques, except where noted. Organic reagents and transition-metal salts were purchased from Merck and Aldrich and used as received. Elemental analyses were performed at the Analytical Services of the Laboratory of REQUIMTE, Departamento de Química, Universidade Nova de Lisboa, on a Thermo Finnigan CE Flash-EA 1112-CHNS instrument. IR spectra were recorded as Nujol mulls on NaCl plates using a Mattson Satellite FTIR spectrometer. NMR spectra were recorded using a Bruker AVANCE II at 400 MHz and processed with the TOPSPIN 2.0 software (Bruker). Mass spectrometry analyses were performed at the Analytical Services of the Laboratory of REQUIMTE-Departamento de Química, Universidade Nova de Lisboa, using a MALDI-TOF-MS model voyager DE-PRO Biospectrometry Workstation equipped with a nitrogen laser radiating at 337 nm from Applied Biosystems (Foster City, United States). UV-vis absorption spectra of the compounds were measured with a JASCO-650 UV-vis spectrophotometer. Fluorescence emission spectra were carried out with a HORIBA-JOBIN IVON Spectramax 4 spectrofluorometer.

All spectrophotometric and spectrofluorimetric titrations for compounds **1**, **2** and **3** were performed as follows: stock solutions of the compound (ca. 10^{-3} M) were prepared by dissolving an appropriate amount of the compound in a 20 mL volumetric flask and diluting to the mark with CH_2Cl_2 UVA-sol. All measurements

were performed at 298 K. The titration solutions ([C] = $1.0x10^{-5}$ M) were prepared by appropriate dilution of the stock solutions. Titrations of the compounds were carried out by addition of microliter amounts of standard solutions of zinc(II) in the form of $Zn(BF_4)_2$ salt and copper(II) as $Cu(BF_4)_2$ salt in acetonitrile. For compound **4**, given its poor solubility in most solvents, the stock solution (ca. 10^{-4} M) was prepared in DMSO, and the titration solution ([C] = $5.0x10^{-6}$ M) by dilution of this one. The titration was performed by adding microliter amounts of Milli-Q water. Luminescence quantum yields of all the compounds in different solvents were measured using a solution of quinine sulfate in H_2SO_4 (0.1 M) as a standard (Φ_F = 0.546).[29]

VI.6.2 Synthesis

VI.6.2.1 Synthesis of 1

A mixture of ferrocenaldehyde (100 mg, 0.47 mmol), 8-aminoquinoline (134.7 mg, 0.93 mmol) and 500 mg of silica was added to a Schlenk tube, degassed for 15 minutes and kept under argon atmosphere. Absolute ethanol (5 mL) was degassed and added to the mixture, which was then sonicated in an ultrasonic bath at room temperature for a period of 1 hour. After this period, the suspension was filtered off, and the silica was washed with $CHCl_3$ until a complete extraction was achieved. The red solution obtained was then evaporated to dryness, to render a dark-red oil. The residue was then redissolved in a small volume of $CHCl_3$ and slowly precipitated from petroleum ether. It was then filtered off, washed with petroleum ether and dried under vacuum. The compound was isolated as a grayish-brown solid (100.1 mg, 44%). Anal. Calcd for $C_{29}H_{24}FeN_4$: C, 71.91; H, 4.99; N, 11.57. Found: C, 71.10; H, 5.21; N, 11.31. ^{1}H NMR (CD_2Cl_2): δ = 8.93 (d, 1H); 8.75 (d, 1H); 8.21 (d, 1H); 8.11 (d, 1H); 7.66 (d, 1H); 7.57 (d, 1H); 7.46-7.32 (m, 4H); 7.25 (d, 1H); 7.17 (d, 1H); 6.94 (d, 1H); 5.03 (br s, 2H); 4.88 (s, 1H); 4.55 (d, 3H); 4.39 (s, 5H) ppm. IR (nujol mull/ NaCl plates), cm^{-1}: 3382 [$\nu(N\text{-}H)_{secondary\ amine}$]. MALDI-TOF MS: *m/z* 341.1 [**1**-$C_9H_7N_2$]$^+$ where ($C_9H_7N_2$ = a quinoline pendant arm).

VI.6.2.2 Synthesis of 2

A mixture of acenaphthenequinone (100 mg, 0.55 mmol), 8-aminoquinoline (79.1 mg, 0.55 mmol) and 500 mg of silica was added to a Schlenk tube, degassed for 15 minutes and kept under argon atmosphere. Methanol (5 mL) was degassed and added to the mixture, followed by a few drops (ca. 0.5 mL) of formic acid. The suspension was then sonicated in an ultrasonic bath at room temperature for a period of 1 hour, after which the suspension was filtered off, and washed with MeOH, leaving a greenish solid mixed with the silica. It was then extracted with $CHCl_3$ and evaporated to dryness, rendering a green solid (43.2 mg, 26%). Anal. Calcd for $C_{21}H_{12}N_2O$·MeOH: C, 77.63; H, 4.74; N, 8.23. Found: C, 77.63; H, 4.33; N, 7.89. ^{1}H NMR (DMSO-d_6): δ = 8.40-8.33 (m, 3H); 8.21-8.14 (m, 3H); 8.04-8.02 (d, 2H); 7.89-7.85 (m, 4H) ppm. IR (nujol mull/ NaCl plates), cm^{-1}: 1667 [v(C=N)$_{imine}$]. MALDI-TOF MS: *m/z* 308.1 ([**2**H$^+$]); 617.3 ([2**2**H$^+$]).

VI.6.2.3 Synthesis of 3

This reaction was performed in air-equilibrated conditions. To a solution of 8-aminoquinoline (1.64 g, 11.4 mmol) in methanol (10 mL) was added dropwise and under an ice bath 2,3-butadione (0.5 mL, 5.7 mmol). The temperature was then increased to room temperature, and the mixture was stirred for 8 hours. The solvent was then evaporated to dryness under vacuum, without heating, because the reaction is exothermic. The residue was redissolved in a small volume of dichloromethane, and slowly precipitated from pentane. It was then filtered off, washed with pentane and dried under vacuum. The compound was isolated as a dark-purple solid (804 mg, 42%). Anal. Calcd for $C_{22}H_{18}N_4$: C, 78.08; H, 5.36; N, 16.56. Found: C, 78.01; H, 5.47; N, 16.36. ^{1}H NMR ($CDCl_3$): δ = 8.73-8.63 (d, 2H); 8.04 (s, 2H); 7.33-6.90 (m, 8H); 2.20-2.08 (m, 6H) ppm. IR (nujol mull/ NaCl plates), cm^{-1}: 1644 [v(C=N)$_{imine}$]. MALDI-TOF MS: *m/z* 338.19 ([**3**H$^+$]).

VI.6.2.4. Template synthesis of 4

This reaction was performed in air-equilibrated conditions. A suspension of acenaphthenequinone (300 mg, 1.65 mmol) and $ZnCl_2$ (449 mg, 3.29 mmol) in glacial acetic acid (5 mL) was allowed to stir for 10 minutes, at room temperature. 8-

aminoquinoline (475 mg, 3.29 mmol) was then added, and the mixture was refluxed for 1 hour, after which it was allowed to cool to room temperature. The suspension was then filtered off, washed with glacial acetic acid (3 X 5 mL), dichloromethane (3 X 5 mL), diethyl ether (3 X 5 mL) and dried under vacuum. An orange solid was obtained (1.11 g, 95 %). Solubility: only partially soluble in DMSO and DMF. Anal. Calcd for $C_{30}H_{18}N_4Zn_2Cl_4$: C, 50.96; H, 2.57; N, 7.92. Found: C, 50.84; H, 2.74; N, 7.73. IR (nujol mull/ NaCl plates), cm^{-1}: 1623 [$\nu(C=N)_{imine}$].

VI.6.3 Crystal structure determination

A single crystal of compound **1**, was mounted on a Nonius Kappa-CCD area detector diffractometer (*Mo Kα*λ = 0.71073 Å). The complete conditions of data collection (Denzo software) and structure refinements are given below. The cell parameters were determined from reflections taken from one set of 10 frames (1.0° steps in phi angle), each at 20 s exposure. The structure was solved using direct methods (SHELXS97) and refined against F^2 using the SHELXL97 software.[35] The absorption was not corrected. All non-hydrogen atoms were refined anisotropically. Hydrogen atoms were generated according to stereo-chemistry and refined using a riding model in SHELXL97. Crystallographic data (excluding structure factors) have been deposited in the Cambridge Crystallographic Data Center as Supplementary publication nº CCDC. Copies of the data can be obtained free of charge on application to CCDC, 12 Union Road, Cambridge CB2 1EZ, UK (fax: (+44)1223-336-033; e-mail: deposit@ccdc.cam.ac.uk).

VI.7 Acknowledgments

We thank *Fundação para a Ciência e Tecnologia*, (FCT), Portugal, for funding (Project PTDC/QUI/66440/2006), University of Vigo INOU-ViCou K914 and K915 (Spain) and Scientific PROTEOMASS Association (Ourense-Spain) for financial support. B.P. thanks Fundação para a Ciência e a Tecnologia / FEDER (Portugal/EU) for the PhD Grant ref. SFRH/BD/27786/2006. J.L. and. and C.L. thank Xunta de Galicia for the Isidro Parga Pondal Research programme.

VI.8 References

1. (a) Michael, J. P. *Nat. Prod. Rep.*, **1997**, *14*, 605; (b) Balasubramanian, M.; Keay, J. G. *Comprehensive Heterocyclic Chemistry II*; Katritzky, A. R., Rees, C. W., Scriven, E. F. V., Eds.; Pergamon: Oxford, **1996**; *Vol. 5*, 245–266.

2. White, N. J. *New Engl. J. Med*. **1996**, *335*, 800.

3. Banerjee, G.; Medda, S.; Basu, M. K. *Antimicrob. Agents Chemother*., **1998**, *42*, 348.

4. Rodrigues, J. M., Jr.; Croft, S. L.; Fessi, H.; Bories, C.; Devissaguet, J. P. *Trop. Med. Parasitol*., **1994**, *45*, 223.

5. Olliaro, P. L.; Trigg, P. I. *Bull. W. H. O*., **1995**, *73*, 565.

6. Dietze, R.; Carvalho, S. F.; Valli, L. C.; Berman, J.; Brewer, T.; Milhous, W.; Sanchez, J.; Schuster, B.; Grogl, M. *Am. J. Trop. Med. Hyg*., **2001**, *65*, 685.

7. Shanks, G. D.; Oloo, A. J.; Aleman, G. M.; Ohrt, C.; Klotz, F. W.; Braitman, D.; Horton, J.; Brueckner, R. *Clin. Infect. Dis*., **2001**, *33*, 968.

8. Chen, E. H.; Tanabe, K.; Saggiomo, A. J.; Nodiff, E. A. *J. Med. Chem*., **1987**, *30*, 1193.

9. Carroll, F. I.; Berrang, B. D.; Linn, C. P. *J. Med. Chem*., **1986**, *29*, 1796.

10. (a) Markees, D. G.; Dewey, V. C.; Kidder, G. W. *J. Med. Chem.*, **1970**, *13*, 324; (b) Alhaider, A. A.; Abdelkader, M. A.; Lien, E. J. *J. Med. Chem.*, **1985**, *28*, 1394; (c) Campbell, S. F.; Hardstone, J. D.; Palmer, M. J. *J. Med. Chem.*, **1988**, *31*, 1031; (d) De, S. K.; Gibbs, R. A. *Tetrahedron Lett.*, **2005**, *46*, 1647.

11. Zatka, V.; Holzbecher, J.; Ryan, D. E. *Anal. Chim. Acta*, **1971**, *55*, 273.

12. Furuhashi, A.; Yokota, H. *Bull. Chem. Soc. Jpn.*, **1979**, *52*, 3753.

13. Kerr, M. C.; Preston, H. S.; Ammon, H. L.; Huheey, J. E.; Stewart, J. M. *J. Coord. Chem.*, **1981**, *11*, 111.

14. Pearce, D. A.; Jotterand, N.; Carrico, I. S.; Imperiali, B. *J. Am. Chem. Soc.*, **2001**, *123*, 5160.

15. Nolan, E. M.; Jaworski, J.; Okamoto, K.; Hayashi, Y.; Sheng, M.; Lippard, S. J. *J. Am. Chem. Soc.*, **2005**, *127*, 16812.

16. Fritsch, J.M.; Thoreson, K.A.; McNeill, K. *J. Chem. Soc. Dalton Trans.*, **2006**, 4814.

17. Nowicki, J. L.; Johnson, K.S.; Coale, K.H.; Elord, V.A.; Lieberman, S.H. *Anal. Chem.* **1994**, *66*, 2732.

18. Macias, B.; Garcia, I.; Villa, M.V.; Borras, J.; Casiineiras, A.; Sanz, F. *Z. Anorg. Alleg. Chemie*, **2003**, *629*, 255.

19. Schulman, S.G.; Sanders, L.B. *Anal. Chim. Acta.* **1971**, *56*, 83.

20. Leroux, N.; Goethals, M.; Zeegers-Huyskens, T. *Vib. Spectrosc.* **1995**, *9*, 235.

21. Soroka, K.; Vithanage, R.S.; Phillips, D.A.; Walker, B.; Dasgupta, P.K. *Anal. Chem.* **1987**, *59*, 629.

22. B.L. Tekwami, L.A. Walker, *Curr. Opin. Infect. Dis.,* **2006**, *19*, 623.

23. Li, X.-G.; Hua, Y.-M.; Huang, M.R. *Chem. Eur J.,* **2005**, *11*, 4247.

24. Lim, M.H. ; Wong, B.A. ; Pitcock Jr., W.H. ; Mokshagundam, D. ; Baik, M.-A. ; Lippard, S.J. *J. Am. Chem. Soc.*, **2006**, *128*, 14364.

25. Kim, Y.-H.; Youk, J.S.; Moon, S.Y.; Choe, J.-I.; Chang, S.-K. *Chem. Lett.* **2004**, *33*, 702.

26. Banerjee, D.; Mondal, B.C.; Das, A.K. *J. Indian Chem. Soc.*, **2004**, *81*, 50.

27. Lodeiro, C.; Capelo, J. L.; Mejuto, J. C.; Oliveira, E.; Santos, H. M.; Pedras, B.; Nuñez, C. *Chem. Soc. Rev.* **2010**, *39*, 2948.

28. Stacy, G. W.; Ettling, B. V.; Papa, A. J. *J. Org. Chem.* **1964**, *29*, 1537.

29. Montalti, M.; Credi, A.; Prodi, L.; Gandolfi, M. T. *Handbook of Photochemistry, 3rd ed.*; CRC, Taylor & Francis Group: Boca Raton, New York, NY, **2006**.

30. ATOMS, Software for Crystallography, E. Dowty, Shape Software, 521 HiddenValley Road, Kingsport, TN 37663 USA.

31. Spek, A. L. *PLATON, A Multipurpose Crystallographic Tool*, Utrecht University, The Netherlands, **2004**.

32. Bazzicalupi, C.; Bencini, A.; Bianchi, A.; Giorgi, C.; Fusi, V.; Valtancoli, B.; Bernardo, M. A.; Pina, F. *Inorg. Chem.* **1999**, *38*, 3806.

33. Deraeve, C.; Maraval, A.; Vendier, L.; Faugeroux, V.; Pitié, M; Meunier, B. *Eur. J. Inorg. Chem.* **2008**, 5622.

34. Tamayo, A.; Escriche, L.; Casabó, J.; Covelo, B.; Lodeiro, C. *Eur. J. Inorg. Chem.* **2006**, 2997.

35. Sheldrick, G. M. SHELXL97, University of Göttingen, Germany, **1997**.

VI.9 Supplementary Material

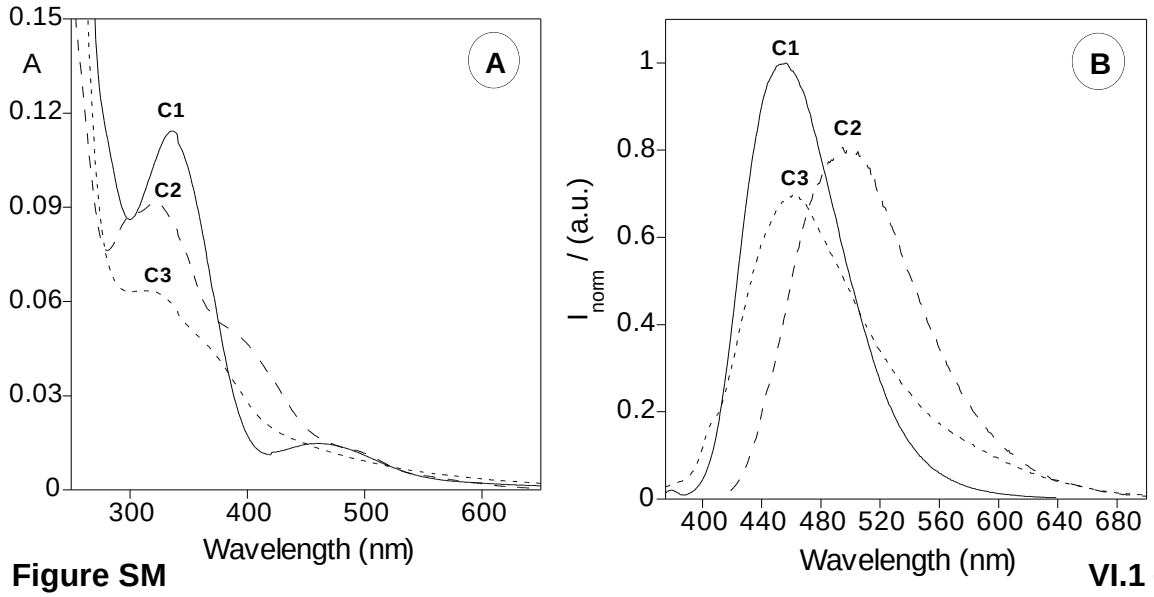

Figure SM VI.1 – Absorption **(A)** and emission **(B)** spectra of **1** (—), **2** (---) and **3** (···) in CH_2Cl_2. [**1**] = [**2**] = [**3**] = 10 μM. λ_{exc} = 340 nm for **1**, 390 nm for **2**, and 360 nm for **3**. Room temperature.

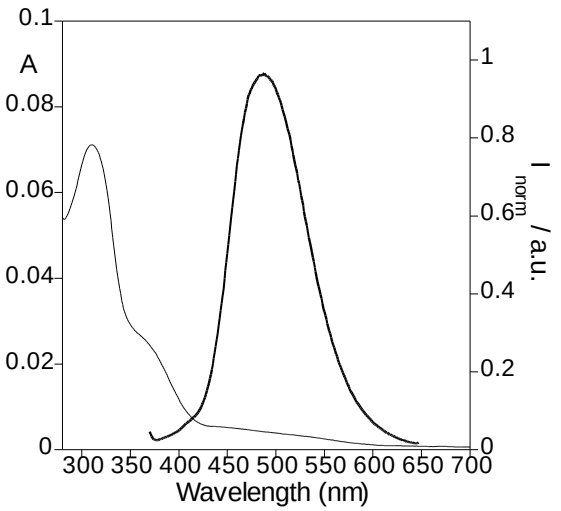

Figure SM VI.2 – Absorption and emission spectra of compound **4**, 5 μM in DMSO. λ_{exc} = 330 nm.

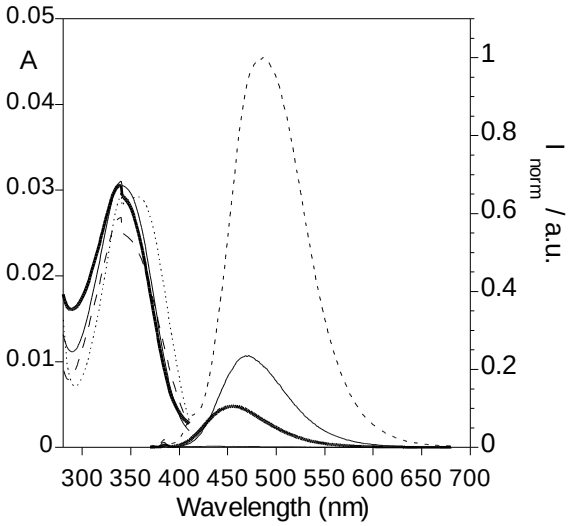

Figure SM VI.3 – Absorption and emission spectra of the precursor 8-aminoquinoline, in different solvents: acetonitrile (—), ethanol (---), DMSO (···), dichloromethane (▬). (λ_{exc} = 345 nm, room temperature).

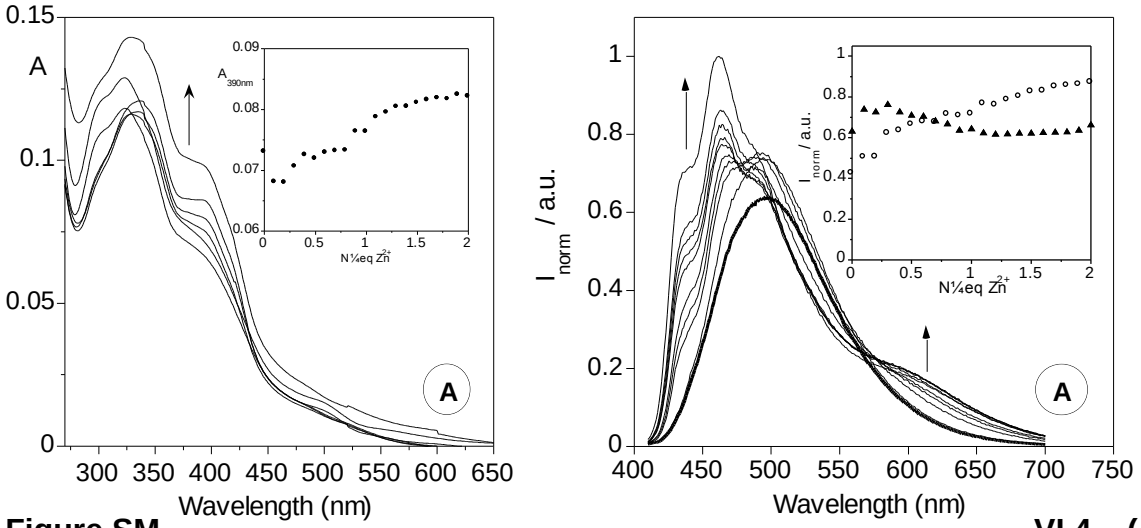

Figure SM VI.4 – (A)

Absorption spectra of compound **2**, 10 μM in CH_2Cl_2, in the presence of increasing amounts of Zn^{2+}. Inset: changes in the absorption of **2** at 390 nm (●) as a function of the number of Zn^{2+} equivalents. **(B)** Emission spectra of **2**, 10 μM in CH_2Cl_2, in the presence of increasing amounts of Zn^{2+}. λ_{exc} = 390 nm. Inset: changes in the emission of compound **2** at 462 nm (○), and 500 nm (▲) as a function of the number of Zn^{2+} equivalents.

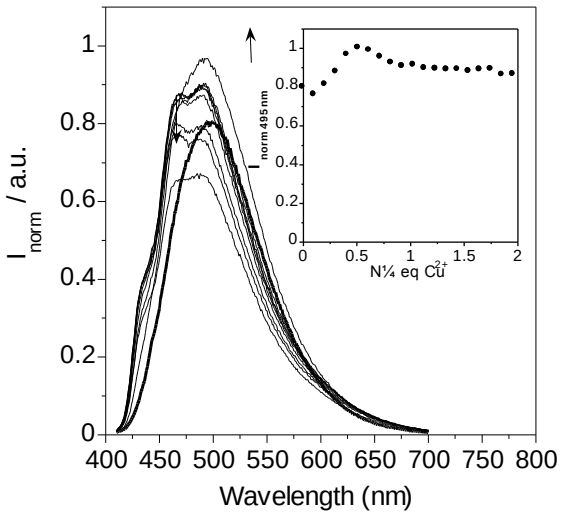

Figure SM VI.5 – Emission spectra of compound **2**, 10 μM in CH_2Cl_2, in the presence of increasing amounts of Cu^{2+}. λ_{exc} = 390 nm. Inset: changes in the emission of compound **2** at 495 nm, as a function of the number of Cu^{2+} equivalents.

Chapter VII

Conclusions

From a global point of view, this thesis was aimed at developing molecules having in mind their structure and their function (which depends on the former) as chemosensors. Only compounds provided with adequate receptors, designed specifically for their target analytes, and combined with the appropriate fluorophores in terms of possible photophysical mechanisms, could successfully perform chemical sensing. This objective has been fulfilled, according to the obtained results for the several designed sensors.

The two chemosensors constituted by a crown ether moiety connected through a Schiff base to a bithiophene unit, were designed to coordinate simultaneously sodium(I) through the crown ether moiety and “soft” transition metal cations through the thiophene sulfur atoms, which at the same time could play a role in the fluorophore emission. The Schiff base nitrogen atom would also help in enhancing the coordinating possibilities. The main result to be highlighted from this chapter is the development of **a CHEF type chemosensor to Pd(II),** which is quite unusual, because this cation normally tends to be sensed by emission quenching.

The pincer-type ligands described in chapter III were applied in Ni(II) and Pd(II) sensing and it was found for both compounds that changes in the absorption spectra occur upon titration with these metal ions. In addition, the compound with pyrene units takes advantage of the photophysical process of **excimer disappearance** after metal binding, which makes it a very useful sensor by absorption and emission spectroscopies. The naphthalene-derived compound found application by **absorption spectroscopy and MALDI-TOF MS**.

In the case of the tripodal poly-imine ligand described in chapter IV, its high flexibility is an advantage when it comes to chelating metal ions through the various nitrogen atoms. Even though no fluorescence was observed, this compound found application in the **sensing of metal ions by absorption spectroscopy and MALDI-TOF MS**.

From the quinoline-derived compounds described in chapter VI, another unusual behavior is found, since one of them senses **Zn(II) by CHEQ effect**, when usually this ion produces an enhancement of the fluorescence emission. Cu(II) sensors behave as expected. It is also worth mentioning the preliminary experience

performed with the dinuclear Zn(II) complex, which allowed the **sensing of water** by emission quenching.

After having seen what happened with the cation sensors, attention is now focused on the luminescent probes for DNA. This family of six Ru(II) complexes presented a common imidazo-phenanthroline unit in all its members, but slight differences in the remaining conjugated structure. By calculating binding constants and performing several quenching studies it was possible to hypothesize that the **crescent-shaped complexes** have a stronger affinity to DNA than its phenyl-substituted analogue. All the studies suggest a **partial intercalation of the probes into the DNA double strand**.

The **sustainable synthetic methods** used to obtain some of the compounds have proved to be an excellent alternative to conventional synthetic pathways. Namely, ultra-sound assisted synthesis of some of the quinoline derivatives allowed the reactions to be complete in one hour periods, and all the ruthenium(II) complexes have been developed with micro-wave assisted synthesis, in two-minute reactions. These methods allow cleaner reactions in shorter reaction times, with very small volumes of solvent, and satisfactory yields.